Optoelectronically active sensitisers for the selective detection of nucleic acid biomarkers

IBRAHIM Q. SAEED

A thesis submitted for the Degree of Doctor of Philosophy

School of Chemistry

Cardiff University

December 2016

DECLARATION

This work has not been submitted in substance for any other degree or award at this or any other university or place of learning, nor is being submitted concurrently in candidature for any degree or other award.

Signed…….. (candidate) Date ...……..…

STATEMENT 1

This thesis is being submitted in partial fulfillment of the requirements for the degree of Doctor of philosophy.

Signed…….. (candidate) Date ...……..…

STATEMENT 2

This thesis is the result of my own independent work/investigation, except where otherwise stated, and the thesis has not been edited by a third party beyond what is permitted by Cardiff University's Policy on the Use of Third Party Editors by Research Degree Students. Other sources are acknowledged by explicit references. The views expressed are my own.

Signed…….. (candidate) Date ...……..…

STATEMENT 3

I hereby give consent for my thesis, if accepted, to be available online in the University's Open Access repository and for inter-library loan, and for the title and summary to be made available to outside organisations.

Signed…….. (candidate) Date ...……..…

STATEMENT 4: PREVIOUSLY APPROVED BAR ON ACCESS

I hereby give consent for my thesis, if accepted, to be available online in the University's Open Access repository and for inter-library loans **after expiry of a bar on access previously approved by the Academic Standards & Quality Committee.**

Signed…….. (candidate) Date ...……..…

Acknowledgements

First and foremost, I would like to express my sincere appreciation to my supervisor Dr. Niek Buurma for all the support and encouragement, for his patience and immense knowledge he gave me during my PhD study. Without his guidance and constant feedback this PhD would not have been accomplishable.

I am also very thankful for my second supervisor Dr. Simon Pope for his continual support and help, for providing most of the ligands during my research.

Many thanks also go to our collaborators (Emily Langdon-Jones, Nick Fletcher, Alaa El-Betany, Richard Wheelhouse), who provided me with a variety of compounds.

I am also very grateful for Dr. Ian Fallis and Dr. James Redman for being as mentor and internal examiner for the annual progress examinations.

Special thanks also goes to Hiwa Ahmad, for all the help kindly offered me in the Laboratory especially during the first year of my study.

I thank my fellow labmates in the POC especially Ammar and Karma for the help and for all the fun we have had during my research.

I greatly appreciate the support and help received throughout my study from Soran Gardy, Zanco Hassan, Hiwa Saeed, Jabbar Gardy, and Mohammed from Cardiff. I also want to thank Kurdistan regional government for being my sponsor.

Finally, and more importantly, I would like to thank my parents; especially my Dad and Mom, my lovely wife Shaduman Sulayman for all of their emotional and financial support they gave me over the period of my degree.

List of abbreviations

DNA	Deoxyribonucleic acid
FSDNA	Fish sperm deoxyribonucleic acid
CTDNA	Calf thymus deoxyribonucleic acid
dsDNA	double-stranded deoxyribonucleic acid
ssDNA	single-stranded deoxyribonucleic acid
MOPS	3-(*N*-morpholino) propanesulfonic acid
DMSO	Dimethyl sulfoxide
TRIS	Tris(hydroxymethyl)aminomethane
UV	Ultra-violet
vis	Visible
A	Absorbance
a.u.	Arbitrary unit
λ_{max}	Lambda max
°C	Degree Celsius
Kcal	Kilocalore
ml	Millilitre
mM	Millimolar
K_b	Binding constant
n	Binding site size in base pairs
K_{agg}	Aggregation constant
ΔH_{agg}	Change in enthalpy of aggregation

Summary

This thesis presents biophysical studies of new optoelecronically active DNA-binders.

Chapter one gives a brief overview of the importance of DNA in medicine, of DNA structure and of the mode of interactions of small molecules with double-stranded DNA, including electrostatic, intercalation and groove interactions. Various examples of small-molecule binding to DNA are discussed. Additionally, this chapter briefly describes the biophysical techniques which can be exploited to quantify the interaction between small-molecules and duplex DNA.

Chapter two describes the results of studies of the interactions of a group of 1,8-naphthalimide derivatives with double-stranded DNA using a variety of techniques viz. spectroscopy, calorimetry, viscosity and molecular docking studies. Additionally, this chapter also presents sequence selectivity studies of this group of compounds for specific sequences $(dAdT)_{12}$●$(dAdT)_{12}$ and $(dGdC)_{12}$●$(dGdC)_{12}$ through UV-visible spectroscopy. The 1,8-napthtalimide unit is shown to be a useful element for inducing DNA-binding.

Chapter three describes studies of the interactions of a family of dendrimeric compounds with double-stranded DNA, again using spectroscopy, calorimetry, viscosity and molecular docking studies. Furthermore, this chapter includes sequence selectivity studies of this group of compounds for $(dAdT)_{12}$●$(dAdT)_{12}$ and $(dGdC)_{12}$●$(dGdC)_{12}$ via UV-visible spectroscopy. The charge and the length of the dendritic structures is shown to strongly affect nucleic acid affinities of this series of molecules.

Chapter four describes the results of studies of the interactions of miscellaneous compounds with double-stranded DNA using variety of techniques viz. spectroscopy, calorimetry, viscosity and molecular docking studies. In addition, this chapter displays sequence selectivity studies of this group of compounds for specific sequences $(dAdT)_{12}$●$(dAdT)_{12}$ and $(dGdC)_{12}$●$(dGdC)_{12}$ via UV-visible spectroscopy.

Chapter five gives an overview and general conclusions about the DNA binding studies presented in Chapters 2, 3 & 4 and finishes with suggestions for future work.

TABLE OF CONTENTS

CHAPTER 2

DNA BINDING STUDIES FOR 1, 8-NAPHTHALIMIDE DERIVATIVES

CHAPTER 3

DNA BINDING STUDIES OF A FAMILY OF DENDRIMERIC COMPOUNDS

CHAPTER 5

EPILOGUE

Chapter 1

INTRODUCTION

Abstract

Since the importance of DNA has been revealed in the field of medicine, binding of a compound with selectivity for a specific DNA sequence is of significant interest in medical and pharmaceutical respects. The first part of Chapter 1 gives a brief overview of the importance of DNA in the medicine, of DNA structure and of the mode of interactions of small molecules with double-stranded DNA, including electrostatic, intercalation and groove interactions. Various examples of small-molecule binding to DNA are discussed. Additionally, this chapter briefly describes the biophysical techniques which can be exploited to quantify the interaction between small-molecules and duplex DNA, such as UV-visible and CD spectroscopy, isothermal titration calorimetry, and viscometry.

1.1 General introduction of the thesis

DNA, the molecule of life, plays an important role in living organisms and it is the long-term storage of hereditary information. Compounds binding to DNA have interested scientists and researchers ever since the importance of DNA has been revealed. The study of small molecules that bind to DNA is a promising field, and could lead to the discovery of new medicines to control genetic and other diseases; the mode of action of several drugs in clinical use for the treatment of diseases is based on their binding to DNA and subsequent modifications of the genetic material. For example, cisplatin, is one of the best-known anticancer drugs that is used to treat various types of cancer.[1] However here we focus on how to exploit DNA-binders as components to enhance DNA detection in genosensors.[2, 3]

Underpinning the use of optoelectronically active compounds in genosensors, is understanding how these compounds interact with DNA. There are several techniques that can be used to study DNA binding and these include UV-visible spectroscopy, isothermal titration calorimetry (ITC), and circular dichroism (CD) spectroscopy. A brief description of these techniques is provided next in the second part of this chapter.

1.2 Deoxyribonucleic acid (DNA)

The discovery of the molecule of life (DNA) in the late 1800_s by the Swiss biochemist Friedrich Miescher inspired many scientists and researchers to study and explore the importance of this molecule in living organisms. DNA is a chemical depository for the genetic information of an organism. The genetic information, stored within DNA in the form of an alphabet consisting of four distinct building blocks, regulates every characteristic of every living species. The mechanisms of DNA functions in the cell cycle, such as replication and transcription, have been fully investigated.[4,5]

According to the "central dogma of molecular biology", the information encoded in DNA in the form of three-letter codons is transferred through RNA to proteins in the cell. This transfer includes several important cellular processes surrounding the DNA such as transcription and translation. Messenger RNA (mRNA) is formed using DNA as a template during the transcription process. The messenger RNA is transferred to the ribosome in the cytoplasm where the proteins are produced through translation. Each of these processes is catalysed by different types of proteins called enzymes.[6]

The interaction of small molecules with DNA can have a great influence on the DNA replication process in the living cell. In the first step DNA transcribed to RNA and usually the transcription involves a particular protein binding to a specific site in the DNA framework. Thus small molecules binding to DNA can emulate or block such binding and lead to stop replication and/or transcription.[7]

1.3 Biosensors (genosensors)

Quantification of biological or biochemical processes is of importance for several applications, including medical and biotechnological applications. However, converting information on biological system into quantitative results is challenging because of the complexity of connecting electronic devices directly to biological environments. A biosensor is defined as an analytical device that converts a biological parameter into a detectable and quantifiable signal.[8] In general, a biosensor consists of two main elements viz. a biological recognition unit (sensing element) that can specifically interact with an analyte and a transducer element which converts a biological response into a measurable electronic signal.[9-12] Biosensors which utilize nucleic acid interactions are referred to as genosensors. The recognition process in genosensors is typically based on DNA hybridization (Figure 1.1), where a short nucleic acid (capture probe) that is immobilized on the sensor forms a receptor and can recognize and interact specifically with its complementary nucleic acid sequence in the analyte sample. Upon hybridization of the capture probe with its target nucleic acid sequence, any changes in optical or electronic properties which occur, can be transduced and amplified using different detectors, including optical and electrochemical detections.[13, 14]

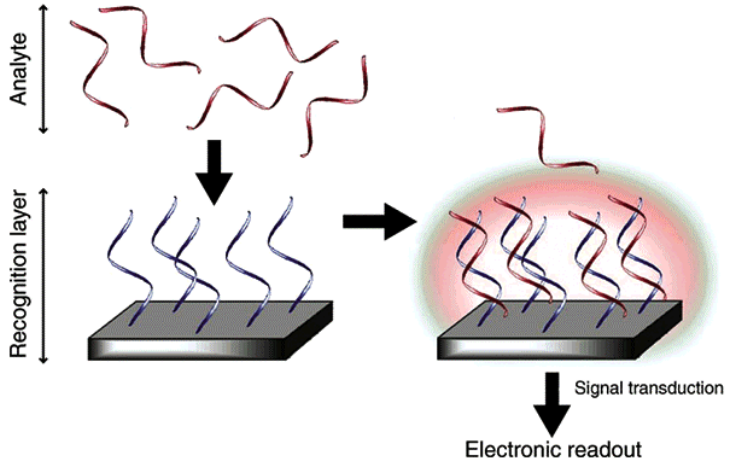

Figure 1.1 General DNA biosensor design.[13]

2.3.1 Detection technologies used for biosensors

2.3.1.1 Electrochemical impedance spectroscopy (EIS)

Electrochemical impedance spectroscopy (EIS) is an important detection technique that is widely used in biosensors, particularly to detect DNA hybridization.[94, 95] A typical DNA sensor using detection through EIS is designed as follows. A single-stranded DNA capture probe is immobilized on an electrode, typically a gold electrode. Upon hybridization of a strand of the target DNA in the sample solution with the single-stranded DNA probe, a change in the impedance of the electrode-solution interface occurs, i.e. the rate of charge transfer between the electrode and a redox indicator $[Fe(CN)_6]^{3-/4-}$ changes resulting from increasing blocking ability of biolayer on the electrode (Scheme 1.1).[96] Thus, any change in the impedance that occurs as a result of the hybridization is detected and measured as a charge transfer resistance (R_{ct}) by electrochemical impedance spectroscopy (EIS).

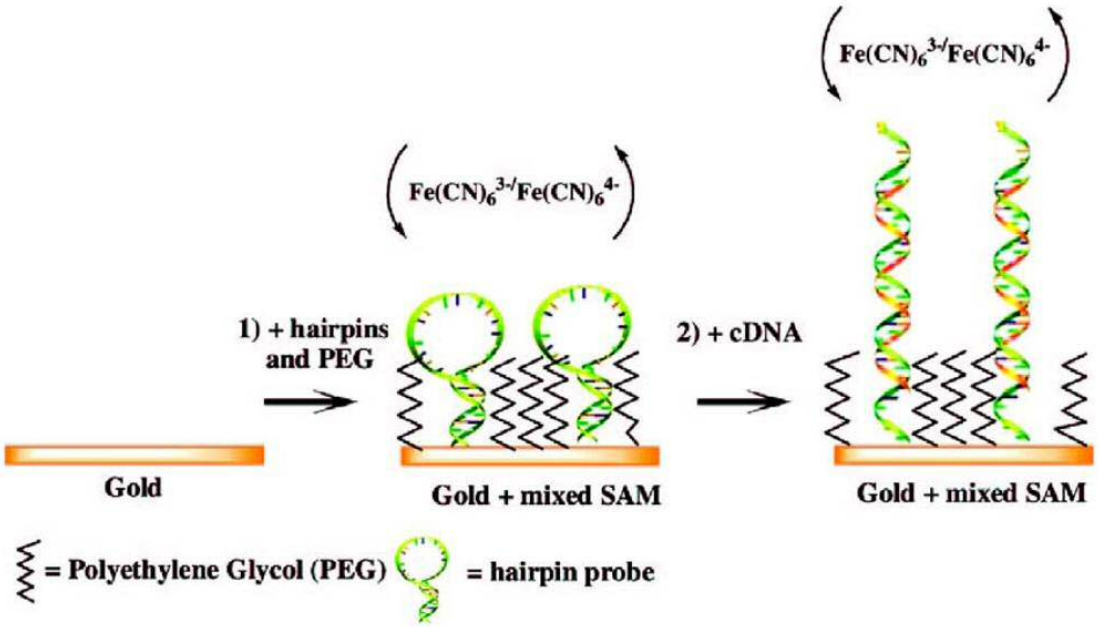

Scheme 1.1 Schematic representation of Biosensor based-EIS detection.[96]

2.3.1.2 Field-effect transistor (Bio-FET)

Typical field-effect transistor based-biosensors consists of a semiconductor transducer, a dielectric layer (SiO_2), a bio-receptor, the analyte, and a gate (Scheme 1.2). The dielectric layer (SiO_2) is used to separate the semiconductor transducer from the analyte solution and electrostatically connects the surface layer to the Bio-FET channel.[93] When the analyte binds to the bio-receptor, changes in the charge distribution at the surface layer happen, leading to a change in the electrostatic potential of the semiconductor, which eventually results in a in the current flowing between the source (S) and the drain (D) of the field effect transistor (FET).[97, 98] Thus, there is a relation between the amount of bound analyte and the current travelling between the source and drain.

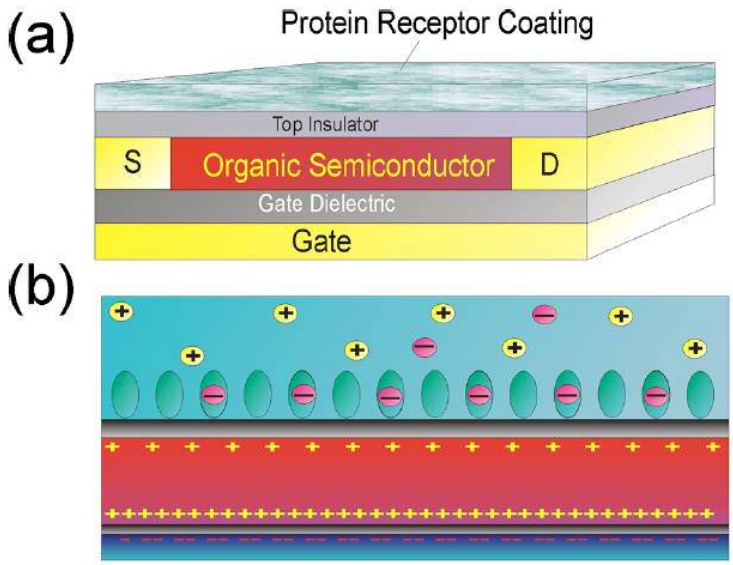

Scheme 1.2 (a) Schematic representation of the Bio-FET. (b) Working principle, including the charge compensation in the semiconductor upon the binding of sulfate ions to the receptor.[98]

2.3.1.3 Coulometry

DNA biosensors-based on coulometry commonly consist of three main components. The first part is an electrode, gold or carbon is often used, the second part is a DNA capture probe, that is attached to the surface of the electrode, and the third part is a redox active label, which are compounds that bind to a hybridized duplex DNA or are attached to a reporter DNA probe via covalent bonds.[99, 100] When the single-stranded DNA capture probe hybridizes with a single-stranded target DNA strand, the redox-active compound binds to that hybridized duplex DNA. This binding event leads to a current between the electrode and redox-active sensitizer and that current will be detected and measured through coulometry (Scheme 1.3).

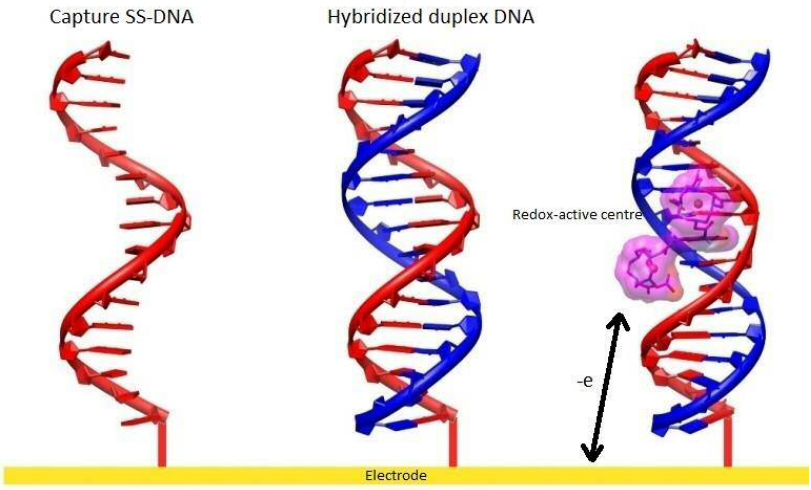

Scheme 1.3 Schematic representation of DNA biosensor based-coulometry.

2.3.1.4 Fluorimetry

DNA sensors using fluorimetry detection are typically constructed from four major components (Scheme 1.4), viz. 1) DNA capture probes that are immobilized on a solid layer, 2) fluorochrome molecules, 3) target DNA molecules in the sample and 4) light sources and detectors.[101, 102] Upon hybridization of the single-stranded DNA capture probe with the single-stranded DNA target, binding of the fluorochrome to the hybridized duplex DNA occurs. Binding of the fluorophore leads to change in its fluorescent properties and converts the biorecognition event into a measurable optical signal.[103]

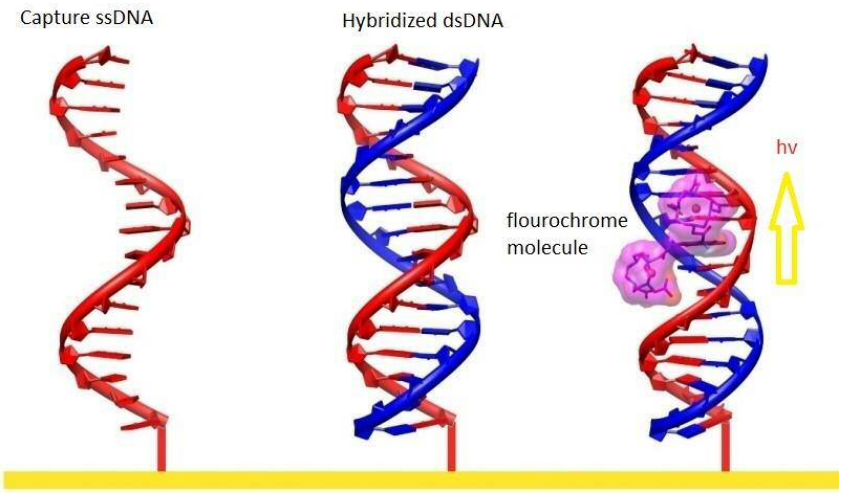

Scheme 1.4 Schematic representation of DNA biosensor-based on fluorimetry.

1.4 DNA structure

The discovery that DNA is the prime molecule carrying all the hereditary information within chromosomes inspired several researchers to focus on its structure. The study of DNA structure reveals how DNA carries the genetic messages that are replicated when chromosomes divide to produce two identical copies of themselves. Some research groups in the United States and in Europe in the late 1940_s and early 1950_s involved in serious efforts, to understand the nature of DNA structure.[15]

In 1953, there appeared three papers in the journal Nature which changed our understanding of life. James Watson and Francis Crick first described the structure of DNA. According to Watson and Crick's model, DNA is a double helix, composed of two antiparallel complementary strands, twisted around each other and held together through hydrogen bonding between the purine derivatives (adenine and guanine) and pyrimidine derivatives (cytosine and thymine) base pairs (Figure 1.2). Each nucleobase in a particular stand is linked via the glycoside bonds to the C1 of the deoxyribose sugar backbone. The sugar units in the backbone are joined together via 3'-hydroxyl and 5'-hydroxyl groups by phosphodiester groups. These linker groups are orientated outside of the double helix to minimize repulsion between the strands, while the nucleotides are inside of the helix, stacking along the direction of the helix axis.[16]

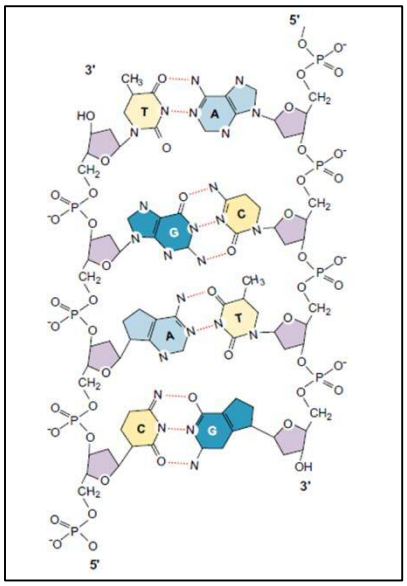

Figure 1.2 Detailed chemical structure of DNA.[15]

There are four nitrogen heterocyclic bases in DNA; these bases are divided into two classes, the purine derivatives adenine (A) and guanine (G), whilst cytosine (C) and thymine (T) are pyrimidine derivatives. The bases are connected to the sugar with a glycosidic bond, through N9 of the purine bases and N1 of the pyrimidine bases (Figure 1.3).

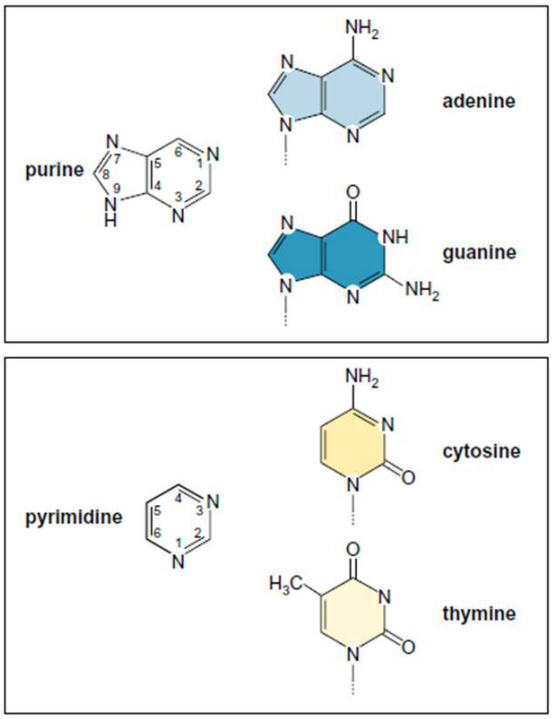

Figure 1.3 purine and pyrimidine derivatives bases.[15]

Base pairing, between adenine (A) and thymine (T) and between guanine (G) and cytosine (C), leads to a complementary relationship between the sequences of bases on the two intertwined chains and gives DNA its self-encoding character.

The pairing between A and T base pairs results in forming two hydrogen bonds, while G and C base pairs form three hydrogen bonds, making G-C base pairs more stable than A-T base pairs. On the other hand, the higher stability of G-C base pairs in DNA is not only due to the presence of additional hydrogen interaction, but instead is due to stronger stacking interactions between the base pairs (i.e. along the helical stack).[17]

In addition, the back bone of DNA (sugar and phosphate groups) can produce various torsional effects on the secondary structure of the nucleic acid, allowing double

stranded DNA to adopt several conformations depending on base-pairs sequences and conditions, viz. A-, B- and Z-DNA (Figure 1.4).[18]

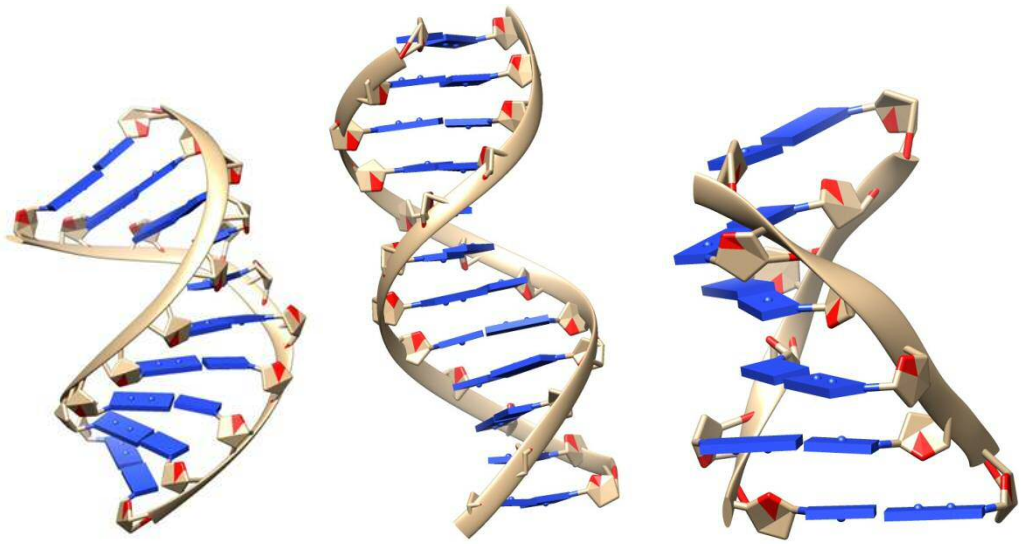

Figure 1.4 The conformations of DNA (from left to right). (a) A-DNA (NDB ID: AD0003), (b) B-DNA (NDB ID: BD0003) and (c) Z-DNA (NDB ID: ZD0008).

Both A- and B-DNA have right-handed helical structures, whereas Z-DNA possesses left-handed helical structure. Each conformation has a different number of base pairs per helical turn. For A-DNA 11 base pairs with C3'-endo conformation for the sugar unit form a helical turn, while B-DNA contains 10.4 base pairs with C2'-endo conformation for the sugar unit per helical turn. One helical turn for the Z-DNA conformation corresponds to 12 base pairs. In addition, there are other DNA conformations which are well known such as G-quadruplex, triplex and i-motif structures (Figure 1.5).

Figure 1.5 Other DNA conformations (from left to right): a) G-quadruplex DNA (PDB: ID 2HY9), b) triplex DNA (NDB ID: BD0017) and c) i-motif (NDB ID: 2N89).

1.5 DNA grooves

In B-DNA, there are two grooves, viz. major and minor grooves that are not equal in size to each other as a consequence of the geometry of the base pairs and the double helical structure of the two chains (Figure 1.6).

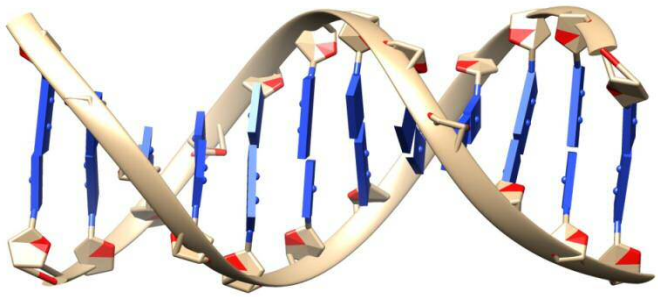

Figure 1.6 Major and minor grooves of DNA (NDB ID: BD0003)

As its name implies, the major groove is wider (12 Å) than the minor groove (6Å).[19, 20] These grooves provide sites for DNA binders such as small molecules and proteins to interact with double stranded DNA because the edges of the bases in the major and minor grooves are exposed at the surface of DNA.[21]

The major and minor grooves can be distinguished in several ways such as through patterns of available hydrogen bond donors and acceptors, electrostatic potential, steric factors (Figure 1.7).

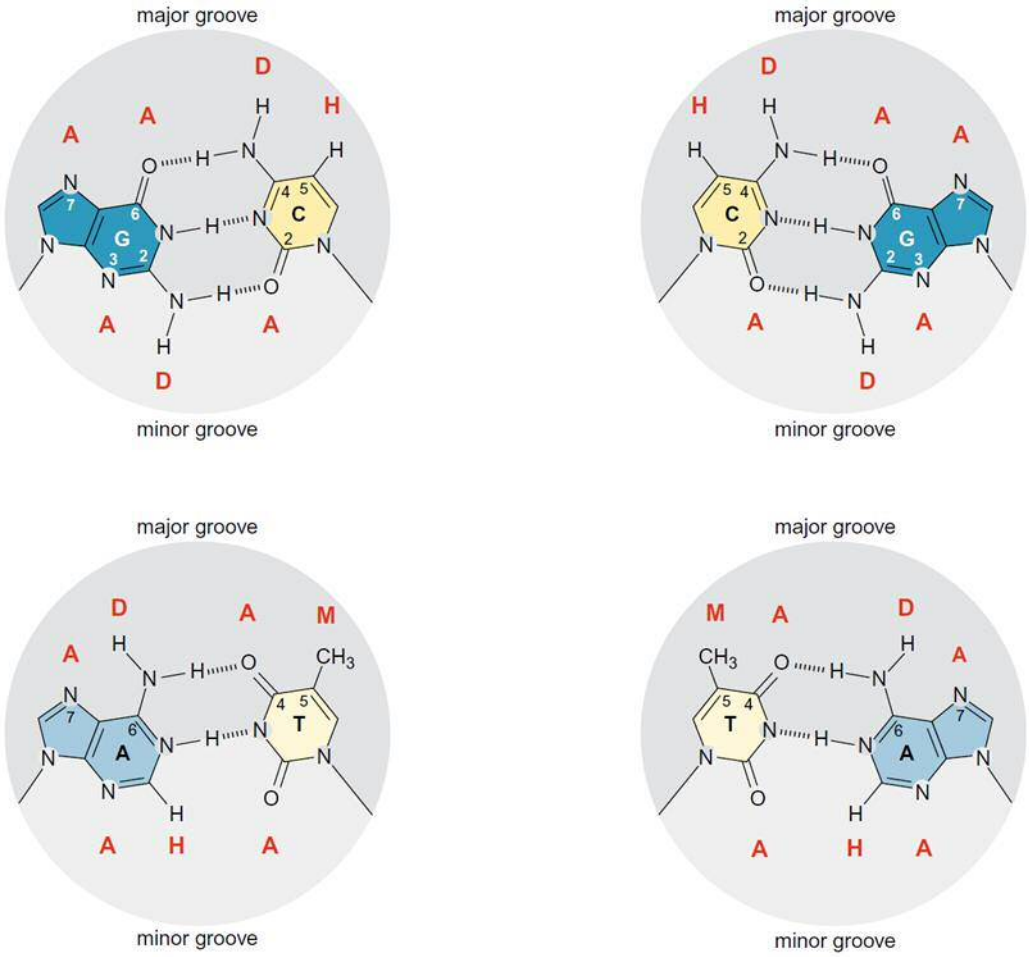

Figure 1.7 H-bond donor and acceptor sites for the base pairs in the minor and major groove of DNA. The letters in red identify hydrogen bond acceptors (**A**), hydrogen bond donors (**D**), nonpolar hydrogens (**H**), and methyl groups (**M**).[15]

In the major groove, the edge of a G●C base pair displays the following chemical groups in the following order in the major groove: **AAD**, whereas the edge of C●G base pair in the major groove displays the reverse pattern **DAA**. On the other hand, the edges of A●T and T●A base pairs show the same hydrogen bonding patterns (**ADA**). However, the presence of the methyl group on the thymine make these bases lose their symmetry (**ADAM**) and (**MADA**) and can be distinguished.

In contrast, in the minor groove, the hydrogen bonding patterns produce no difference between C●G and G●C base pairs or between A●T and T●A because the hydrogen bonding patterns for each base pair are symmetrical; i.e. for C●G and G●C base pairs are (**ADA**) pattern and for A●T and T●A are (**AA**) pattern.

1.6 Small molecules binding to DNA

As a result of the geometry of the base pairs of DNA and the double helical structure of the two complementary stands, DNA can interact with small molecules and proteins in several different ways. Irreversible binding typically involves non-specific covalent bonding to the sugar or phosphate parts of the DNA backbone. Irreversible binding can have an influence on transcription processes, which normally ends with cell death or alters gene expression.[22] Small molecules that bind to DNA in this way can bind to sites of duplex DNA either in the same strand (intrastrand) or crosslink from different strands i.e. complementary strands.[23]

In addition, drugs can attach to other sites on the DNA; for instance, the well-known anticancer drug cisplatin can form intrastrand bonds with the basic sites of the DNA helix, the drug binds to the nitrogen atom of either guanine or adenine base (Figure 1.8)

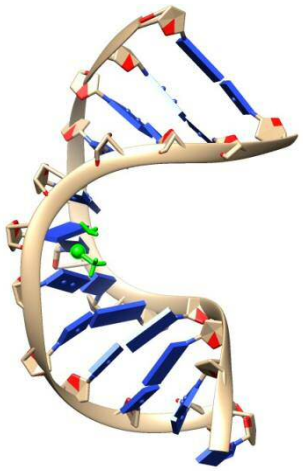

Figure 1.8 Cisplatin interactions with DNA (NDB ID: 1A84)

A wide range of chemical species can also bind reversibly to DNA, including water, metal complexes, proteins, and small molecules.[18] Reversible binding can occur in several modes such as electrostatic interactions, groove binding or intercalation between the base pairs (Figure 1.9) and a brief description for each mode is provided next.

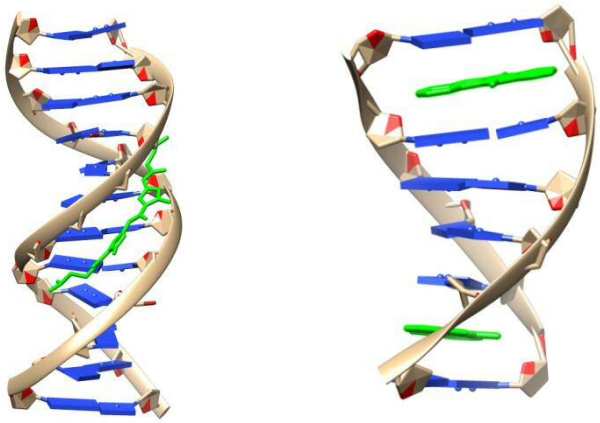

Figure 1.9 Examples of different reversible interactions between molecules and DNA, (left) minor groove binding (NDB ID: GDLB05), (right) intercalation (NDB ID: DD0070).

1.6.1 Electrostatic interactions

DNA molecules carry high negative charges under physiological conditions, due to the presence of the negatively charged phosphate groups that run along the exterior surface of the double helix structure of DNA.[24] Thus, cationic molecules are able to interact with DNA by electrostatic interactions. This mode of interaction is influenced by size of ligand, the charge on the ligand and hydrophobicity of ligand.[25-27] The stability of the DNA conformation usually increases upon this interaction. Cation sizes can range from small ions for example Na^+ or Mg^{2+} to larger cationic polyamines such as spermidine and spermine. The binding of these cations with DNA leads to neutralization of the phosphate backbone's charge,[28] therefore the binding of small molecules with DNA is influenced by the ionic strength of the medium.

1.6.2 Intercalations and Intercalators

The concept of intercalation was first introduced in 1961 by Lerman and was modified in 1966 by Pritchard. In this mode of binding, flat polycyclic aromatic ring molecules such as acridine dyes can intercalate between two base pairs of the DNA double helix. The main binding forces are provided by π-π stacking interactions and Van der Waals interactions between the aromatic DNA binder and the base pairs of DNA.[29, 30] Intercalation is usually enthalpically driven, leading to significant changes in geometry and length of the DNA helix.[25] There are many well-known intercalators

such as, proflavine, acridine orange, N,N-dimethyl proflavine, 9-aminoacridine and ethidium bromide (Figure 1.10).

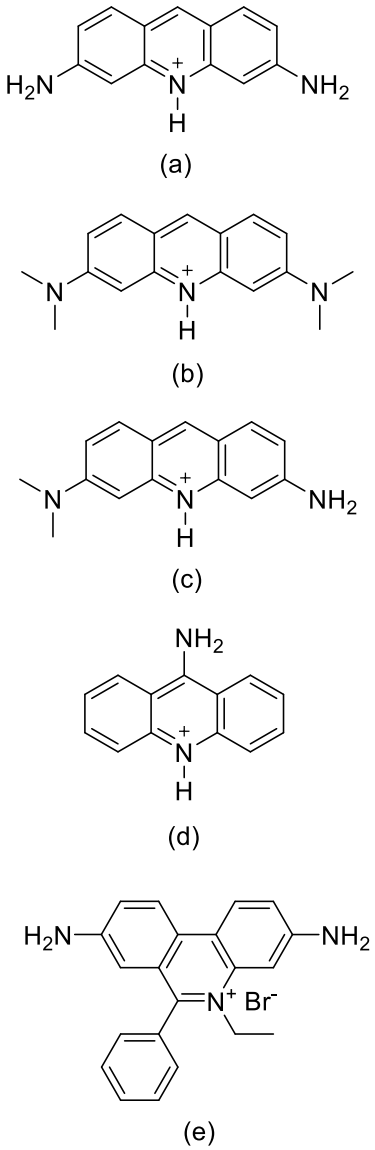

Figure 1.10 Chemical formulae of intercalators, (a) proflavine, (b) acridine orange, (c) N,N-dimethyl proflavine, (d) 9-aminoacridine and (e) ethidium bromide.

In B-form DNA, the vertical separation of two consecutive base pairs is normally about 3.4 Å, this distance must be expanded noticeably to accommodate the considerably large aromatic ring molecule. The expansion of DNA helix can vary over a wide range (1.8-4.5 Å per intercalation), depending on the ligand and type of nucleotide involved.

Most intercalators have a preference for a specific binding site. Some prefer to intercalate between a 5′-purine–pyrimidine-3′ base step rather than between a 5′-pyrimidine–purine-3′ base step (or vice versa), while, others have preference for certain base-pair sequences (Figure 1.11).[31]

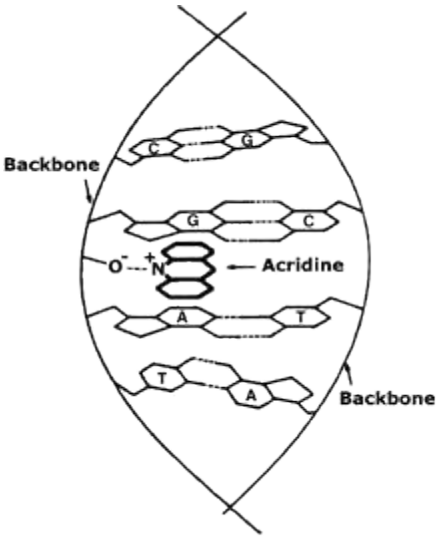

Figure 1.11 Structure of an acridine–DNA complex.[31]

According to the "neighbor exclusion principle",[26] DNA binders cannot occupy two successive base steps because during intercalation the conformation of neighboring binding sites also changes, leading to block the accommodation of a second intercalator between base pairs adjacent to a bound intercalator. Binding site sizes for intercalators are therefore typically larger than one base pair. Furthermore, those intercalators that carry positive charges have additional electrostatic interactions with the anionic sugar-phosphate backbone, causing the duplex DNA to become more stable.

1.6.3 Groove binding (Major and Minor)

The double-helix structure of DNA exhibits the major and minor grooves as a consequence of the geometry of base pair formation and the double helical structure of the two complementary strands.[15] These grooves are different in many patterns such as patterns of available hydrogen bond donors and acceptors, electrostatic potential, steric factors and sizes. Therefore, binding of DNA binders in these grooves can become selective.

Larger biomolecules, such as proteins, usually bind to duplex DNA in the major groove, allowing sequence-specific recognition.[27] On the other hand, smaller molecules tend to bind with duplex DNA in the minor groove because the environment is more convenient in the minor groove for the smaller molecules since the minor groove provides more sites for interactions. Key interactions include hydrophobic interactions of small molecules with the hydrophobic interior walls of the minor groove. Typically, the minor groove is preferred by molecules with a hydrophobic framework linked by bonds with torsional freedom in order to enable these molecules to twist and adopt the curvature of the minor groove of DNA.

The majority of minor groove binders binds selectively to A●T rather than to G●C rich sequences because the minor groove becomes narrower in the presence of A●T sequences and therefore facilitates the formation of Van der Waals interactions with the walls of the groove. Lower affinity for G●C rich sequences is also due to the existence of the NH_2 group of guanine, which prevents the penetration of molecules into minor groove. Additionally, negative electrostatic potentials in A●T minor grooves are greater than in G●C minor grooves.[32-34]

Classic minor groove binders, such as netropsin and distamycin, are long, flexible, and crescent-shaped molecules. Netropsin and distamycin possess two and three N-methylpyrrole rings, respectively, which are linked through peptide linkage to the positively charged amidinium ($C(NH_2)(NH_2)^+$) group at the terminal position(s).[31] This class of minor groove binders served as inspiration for the so-called hairpin polyamides later developed by Dervan's group, who particularly focused on development of modular sequence-selective minor groove binders.[35, 36]

The driving forces for selective binding of netropsin and distamycin to A-T rich regions of B-DNA (Figure 1.12) are the result of displacement of water molecules that hydrate the minor groove of DNA and formation of hydrogen bonds between the NH groups on netropsin and the nitrogen in adenine and oxygen of thymine on each adjacent base pair, together with electrostatic and Van der Waals interactions.[37]

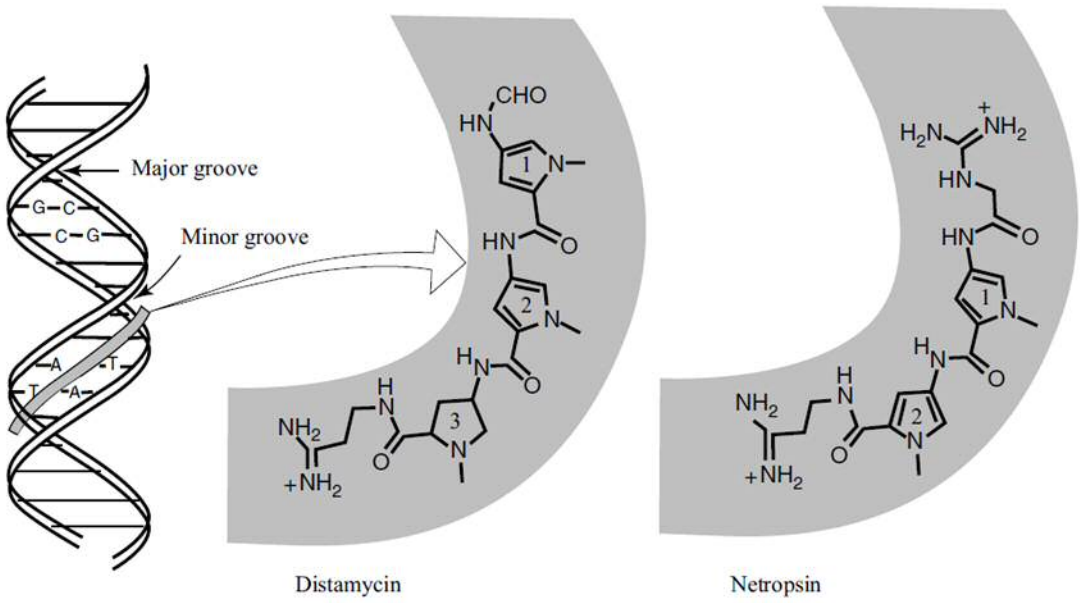

Figure 1.12 Structures of distamycin and netropsin.[31]

Binding of netropsin to DNA usually occurs in a 1:1 ratio along four consecutive A•T base pairs, whereas distamycin is able to bind with DNA in the minor groove in two different modes, viz. a 1:1 and 2:1 ratio along five base pairs (Figure 1.13).[38, 39]

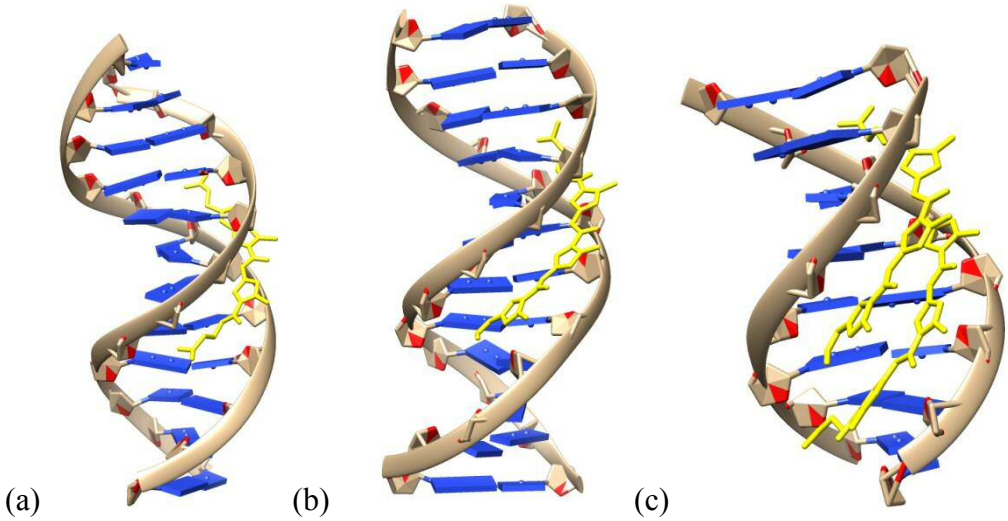

Figure 1.13 The groove binding modes of netropsin and distamycin with duplex DNA: 1:1 binding of netropsin to the 5'-CGCAATTGCG-3' sequence (NDB ID: GDLB05) (a), 1:1 binding of distamycin to the 5'-CGCAAATTTGCG-3' sequence (NDB ID: GDL003) (b) and side-by-side binding of distamycin to the 5'-GTATATAC-3' sequence (NDB ID: GDH060) (c).

Another familiar minor groove binder is Hoechst 33258, which has shape resemblances with netropsin and distamycin (i.e. they have crescent shape). Hoechst

33258 possesses a π-conjugated oligoheteroaromatic framework. However, the presence of the single bonds that link the aromatic rings allows enough rotational flexibility to fit into the minor groove (Figure 1.14).[40]

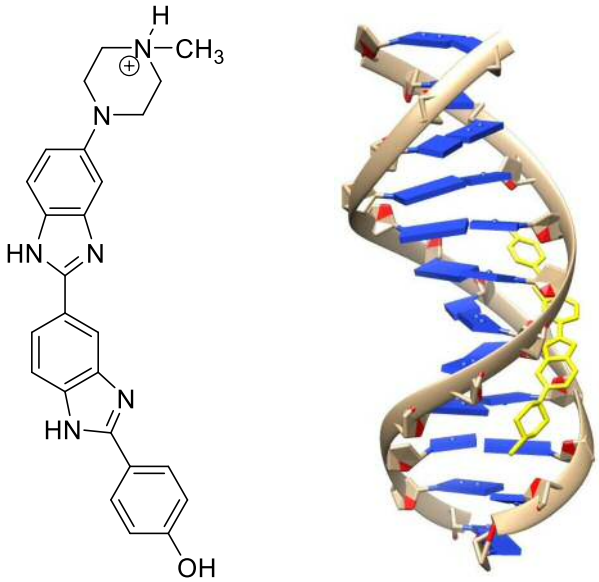

Figure 1.14 Structure of H33258 (left), the minor groove binding of H33258 to d(CGCAAATTTGCG)2 (NDB ID: GDL028) (right).

Binding studies of H33258 with duplex DNA show that this ligand binds to A●T-rich sequence of DNA in the minor groove with a binding site size between 4 and 5 base pairs. In addition, H33258 shows low affinity for G●C-rich sequence of DNA.[41]

Other minor groove binders include compounds such as chromomycin A3 and mithramycin, which are antitumor antibiotics extracted from Streptomyces grisius and Streptomyces plicatus. In contrast to A●T-rich groove-binding molecules such as distamycin and netropsin discussed before, chromomycin A3 and mithramycin bind to the G●C-rich region of the duplex DNA sequences in the minor groove with a stoichiometry of 2:1 (ligand/duplex) molar ratio in the presence of a divalent metal ion such as Mg^{+2} (Figure 1.15).[31]

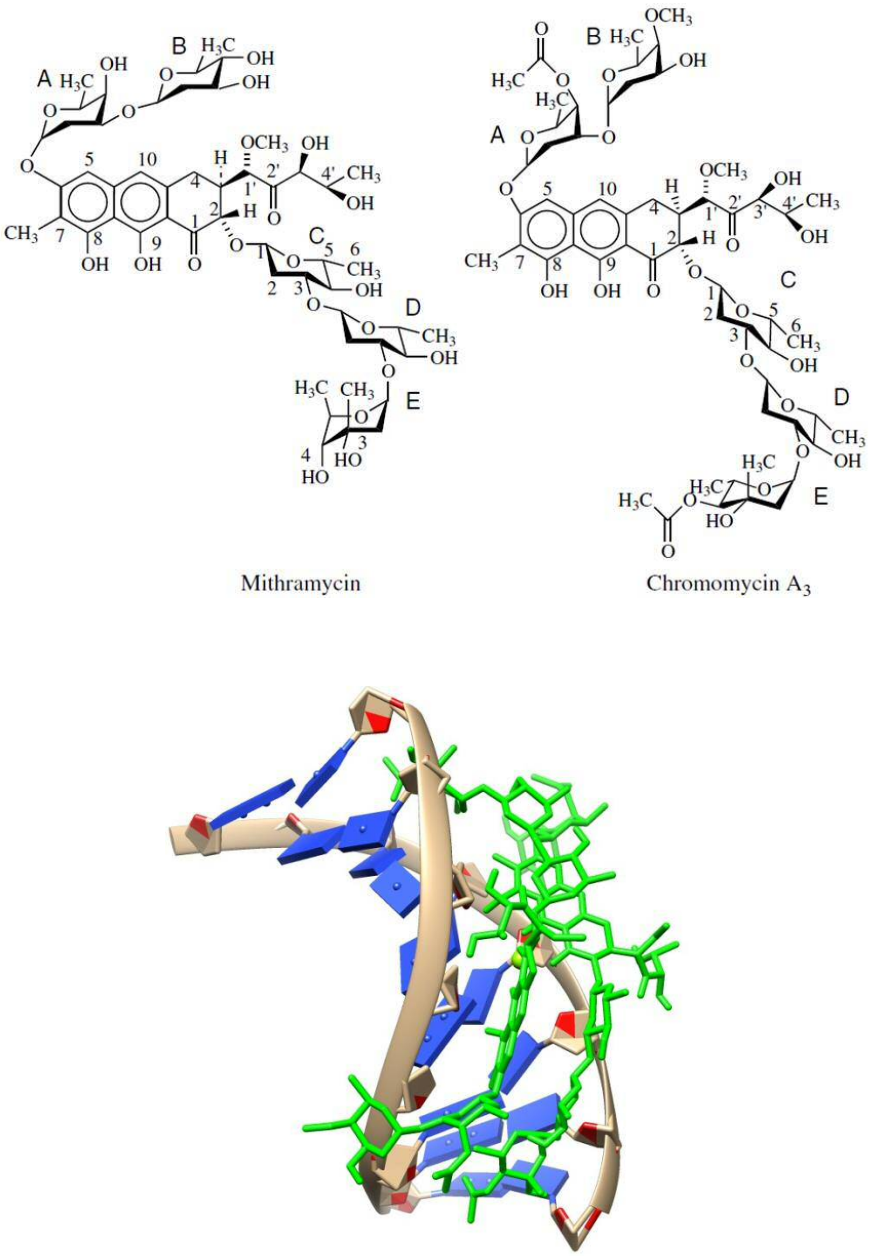

Figure 1.15 Structures of mithramycin and chromomycin A3,[31] and side-by-side binding of chromomycin A3 to d(AAGGCCTT)$_2$ (NDB ID: 1D83).

A very interesting class of minor groove binders is formed by Dervan's hairpin polyamides (DHP), which are synthetic minor groove binders inspired by natural sequence-selective ligands netropsin and distamycin. DHPs provide modular and programmable sequence recognition of duplex DNA.[36, 42] However, the sequence recognition of DHPs for double-stranded DNA is limited for 5 base pairs because the polyamide curvature no longer matches the curvature of the minor groove of DNA.[43]

Therefore, new developed structures of polyamides were prepared by Dervan's group. The developed polyamides linked turn to turn or turn to tail which recognise extended DNA sequence without losing selectivity along 10 base pairs (Figure 1.16).[44, 45]

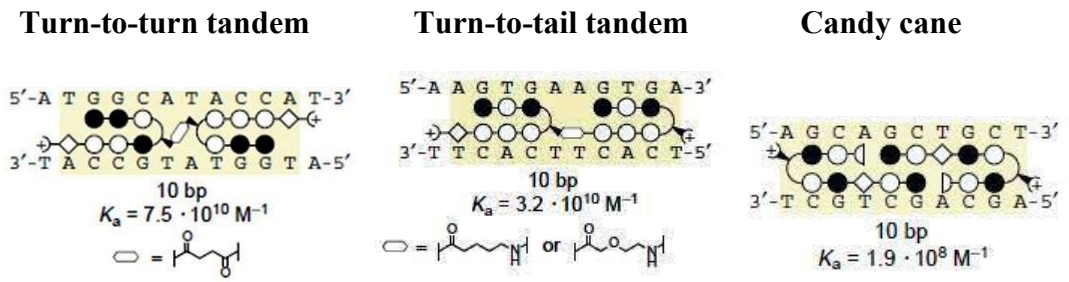

Figure 1.16 Schematic representations of polyamide for binding extended DNA sequences.[36]

Another interesting class of DNA minor groove binders is provided by CC-1065 and its derivatives (Adozelesin, bizelesin and carzelesin) (Scheme 1.5).[86, 87] These compounds specifically bind to AT-rich regions of the DNA minor groove, leading to alkylation of DNA.

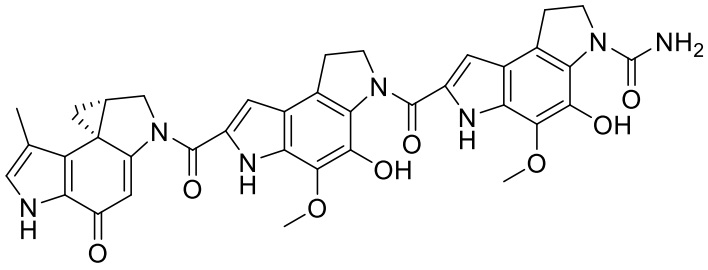

CC-1065

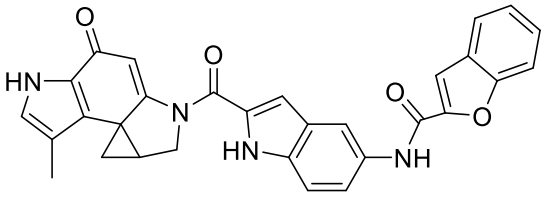

Adozelesin

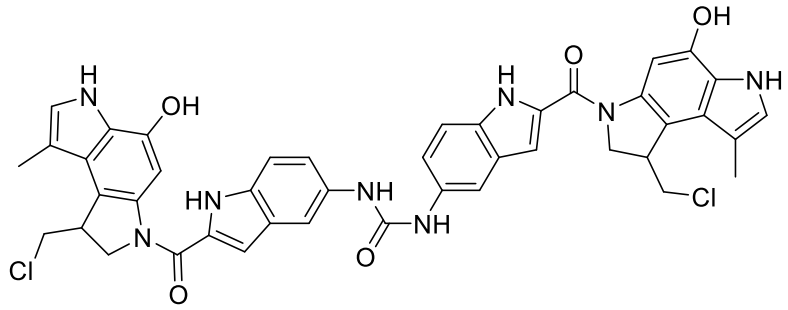

Bizelesin

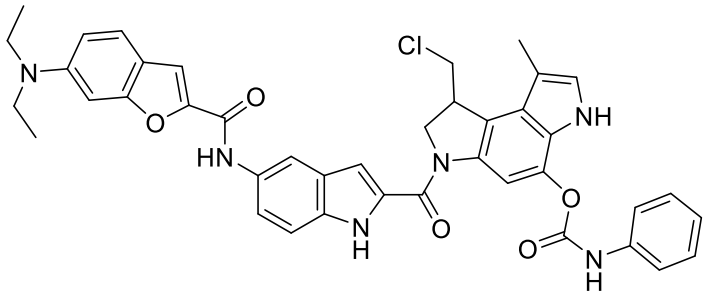

Carzelesin

Scheme 1.5 Chemical structures of CC-1065 and its derivatives.

Duocarmycin derivatives (Scheme 1.6) are also considered a potent class of antitumor agents. They bind to duplex DNA through the minor groove binding and lead to alkylation of DNA at the N3 position of adenine.[88]

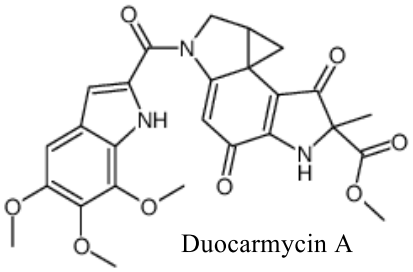

Duocarmycin A

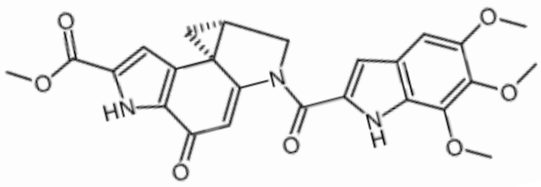

Duocarmycin SA

Scheme 1.6 Some structures of duocarmycin derivatives.

1.7 π-Conjugated polymers and oligomers

Fundamentally, polymers are macromolecules consisting of a high but finite number of repeated monomer units which are linked by covalent bonds, whereas oligomers consist of a low numbers of repeated monomer units. With respect to repeating unit types, polymers could be homo-polymers (consisting of one type of monomer) or co-polymers (composed of two or more different monomers).[46] Conjugated polymers have characteristic of π−delocalisation along the main chain, leading to their use as organic semiconductors (Scheme 1.7).[47, 48] In addition, π-conjugated polymers typically possess rigid structures and interchain forces cause them to be insoluble in many organic solvents and aqueous medium. Therefore, cationic or anionic charged side chains are typically placed onto the polymer backbone to increase their solubility.

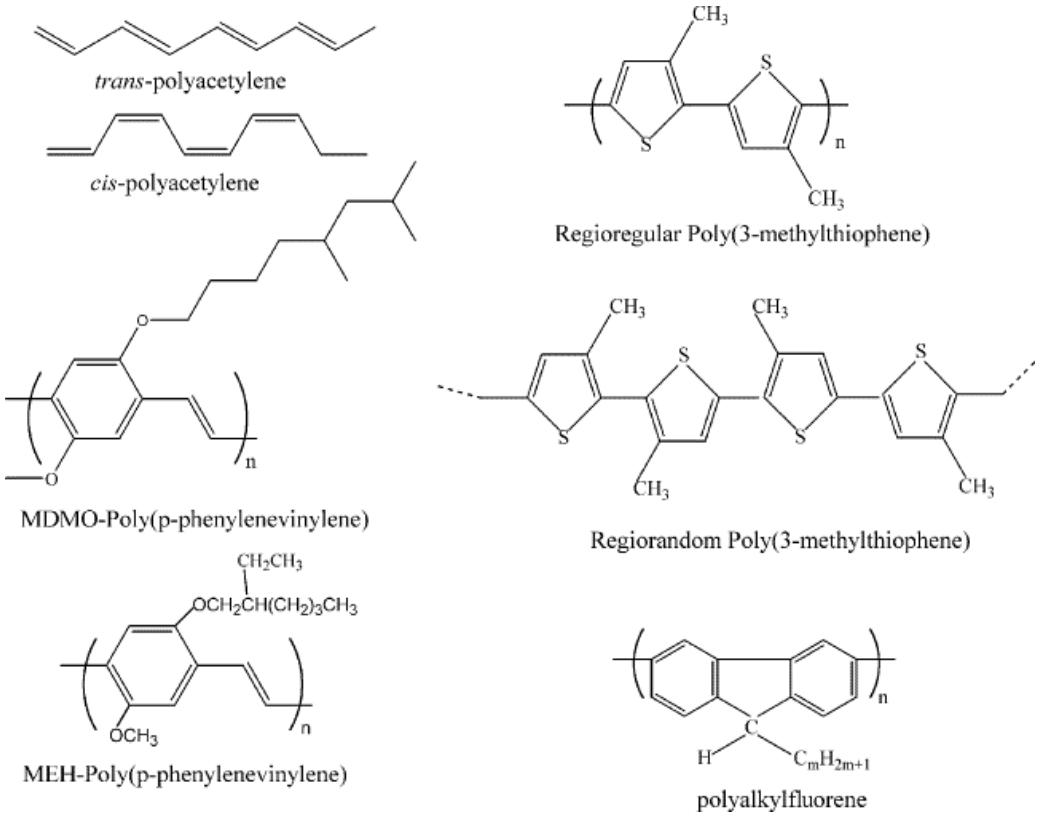

Scheme 1.7 Chemical structures of some semiconducting polymers.[47]

There are many π-conjugated oligomeric systems which bind to DNA. In general, these π-conjugated DNA binders are either composed of several heteroaromatic rings linked to each other, or have extended frameworks involving alkene units for further conjugation. The presence of cationic functional groups in some conjugated oligomers has been shown to increase the driving forces for these compounds to bind with DNA

via electrostatic interactions with the negatively charged phosphate ester backbone of DNA.[49] In addition, optical and electrical properties of the conjugated polymers change upon interaction with bio-macromolecules such as DNA. Therefore, these optoelectronically active bio-macromolecules binders are promising components for biosensors.[50, 51]

1.8 Optical detection of DNA

The detection and quantification of small amounts of DNA in biological samples is of significant interest. Leclerc and co-workers first introduced the use of cationic polythiophenes to study DNA-hybridisation.[50] Some structures which were used in the detection of DNA are shown in Scheme 1.8.

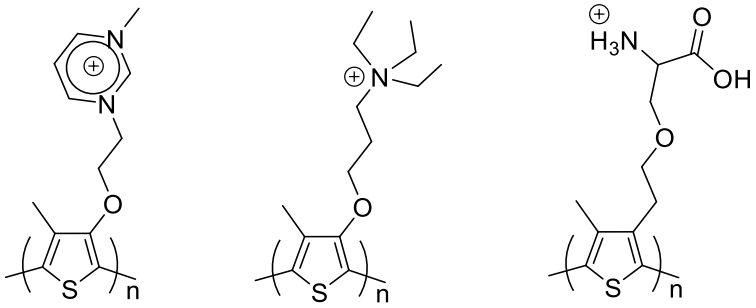

Scheme 1.8

The exploitation of cationic polythiophenes in the optical detection of DNA can be illustrated as follows (Figure 1.18). The free cationic polythiophene is yellow in an aqueous solution with a maximum absorption around 400 nm due to forming a random-coil conformation which leads to a decrease in the effective conjugation length. Upon addition of a single-stranded DNA (ssDNA), the colour of the solution becomes red and the UV-visible spectrum shows a maximum absorption around 527 nm (Figure 1.17), owing to the formation of a double-stranded structure (duplex) between the polythiophene and single-stranded DNA probe (Figure 1.18), leading to planarising the polythiophene backbone and an increase in the effective conjugation length (i.e. causes to produce a strong red-shift). When the complementary strand of DNA is added to the mixture of polythiophene and ssDNA, the solution becomes yellow again with a maximum absorption around 420 nm. This change in lambda maximum is presumably caused by the formation of a new complex triplex structure. As described before, the cationic polythiophene shows different λ_{max} in the duplex and

triplex forms. This difference in λ_{max} is attributed to the presence of different conformations of polythiophene. Additionally, a fluorometric detection of DNA hybridization is also accomplishable as the fluorescence of polythiophene is quenched in the planar and aggregated form i.e. in the complex with single stranded DNA.[51]

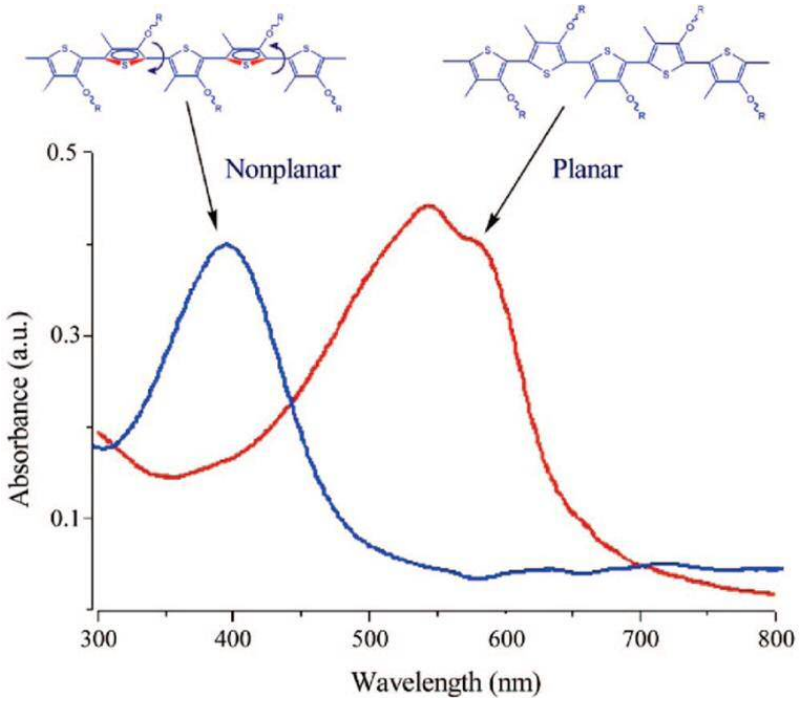

Figure 1.17 Conformations and corresponding UV-visible absorption spectra of polythiophene.[50]

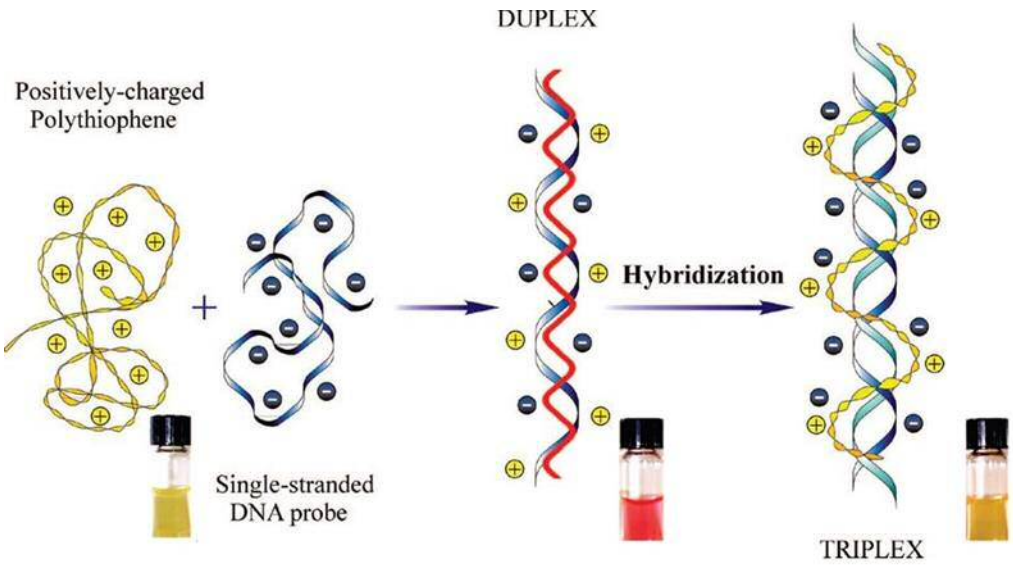

Figure 1.18 Optical detection of DNA. Reproduced from reference 50.

1.9 Electrochemical detection of DNA

Electrochemical techniques are considered one of the most attractive methods to study oligonucleotides since these techniques offer low instrumentation costs, high sensitivity, ease of miniaturization and direct electronic readout.[52-56] Garnier and co-workers first reported electrochemically detection of DNA hybridization, where they designed a biosensor using an electroactive polypyrrole functionalized with an oligonucleotide probe.[57] When a grafted oligonucleotide hybridizes with its complementary oligonucleotide target in solution, this causes a significant modification in the electrochemical response of polypyrrole, leading to a sensitive electrical reading of the recognition process. The modifications in electronic properties of polypyrrole were attributed to changes in the polymer conformation as a result of binding of the polymer-oligonucleotide probe to the target oligonucleotide strand.

Based on the method proposed by Garnier and co-workers, a variety of functionalized polythiophenes have been used to electrochemically detect DNA hybridization.[58] For instance, Lee *et al.* introduced a terthiophene-carrying a carboxyl group which can be electropolymerized on a glass carbon electrode (Scheme 1.9).[59]

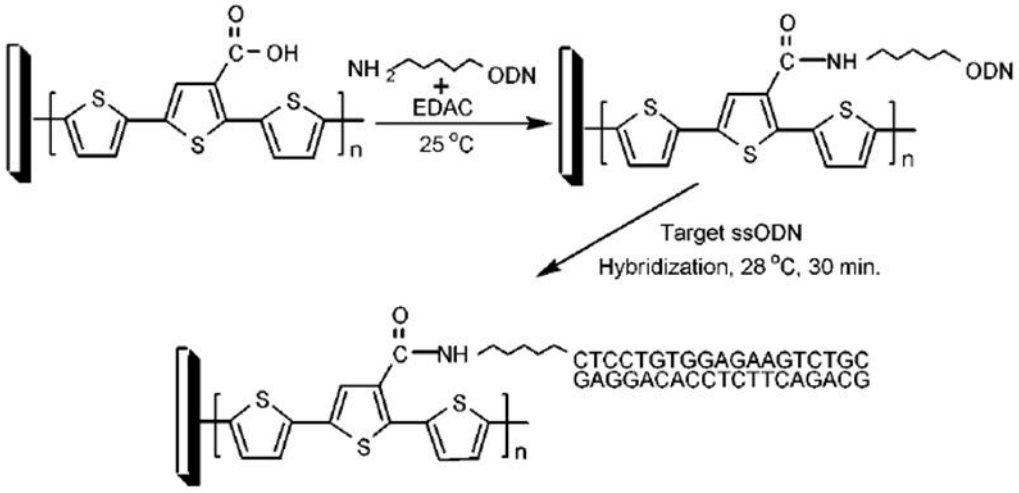

Scheme 1.9

In this study, the hybridization of the target oligonucleotide with immobilized polythiophene-oligonucleotide probe leads to a decrease in impedance values since the double-stranded DNA has higher impedance than single-stranded DNA. Thus, the

hybridization process can be easily confirmed based on the changes in the impedance values before and after hybridization.

In addition, Lee *et al.* carried out experiments to determine the response of the polythiophene-oligonucleotide probe to mismatched target oligonucleotides, such as one-base mismatch and two-base mismatch. The results showed very limited difference in impedance between before and after hybridization, indicating that polythiophene-oligonucleotide probe constructed in this study specifically recognizes matched and mismatched oligonucleotide sequences.[59]

Recently, several advances in electrochemical detection of DNA have been achieved, including detection of hybridization of single-stranded DNA on surfaces using voltammetry or electrochemical impedance spectroscopy.[60-63]

Zongbing and co-workers proposed a method for enhancing electrochemical detection of double-stranded DNA by using a hybridization chain reaction (HCR) and positively charged gold nanoparticles.[64] They constructed a sensor where the capture probe was immobilized on a gold electrode surface (Figure 1.19). A sandwich complex was formed between capture probe and detection probe upon addition of dsDNA. Then two alternating ferrocene-modified DNA hairpins (H1 and H2) in turn were opened by the detection probe, initiating HCR to form double-helix. Meanwhile, the positively charged gold nanoparticles were electrostatically absorbed onto the negatively charged backbone of the double-helix to magnify the electrochemical signal.

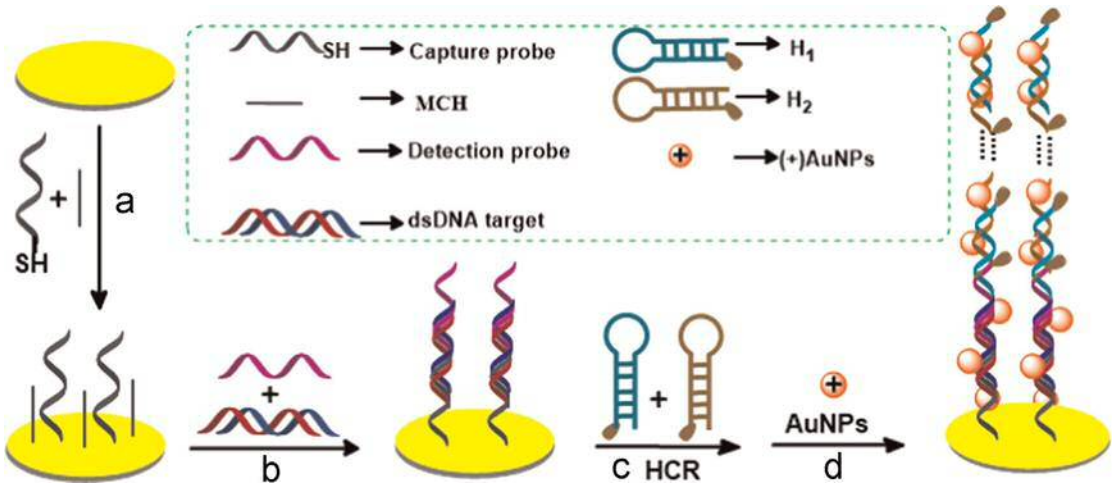

Figure 1.19 Scheme of the proposed method for dsDNA recognition.[64]

Another example of enhancing electrochemical detection of DNA is using a novel complex $[Co(GA)_2(aqphen)]Cl$ as a signal enhancer that was introduced by our group.[65]

In addition, there are other examples where peptide nucleic acids (PANs) are used as probes in DNA biosensing instead of conventional single-stranded DNA.[66-70] Peptide nucleic acids are DNA mimics in which the sugar-phosphate backbone is replaced by 2-aminoethyl-glycine linkages and the nucleotide bases are attached to the PNA backbone by a methylene bridge and a carbonyl group. There are several advantages of using PNAs as probes in biosensing, such as elimination of repulsion forces between two hybridized strands since the PNA backbone is neutral. Furthermore, PNA can bind to complementary strands with a higher affinity and selectivity than DNA does.

Zhang and co-workers[68] introduced a novel DNA biosensor based on electrochemical reduced graphene oxide (EGRO) and peptide nucleic acid PNA-DNA hybridization. The working principle of this biosensor is as follows; firstly, the graphene oxide is reduced onto the glassy carbon electrode (GCE, Figure 1.20) and then a PNA probe is immobilized onto the graphene surface using a linker (1-pyrenebutanoic acid succinimidyl ester, PASE). Thus, different PNA probes can be used for hybridization of different target DNA sequences. Methylene blue is used as an indicator for monitoring the hybridization event using deferential pulse voltammetry because it shows different reduction signals upon interactions with PNA and dsDNA.

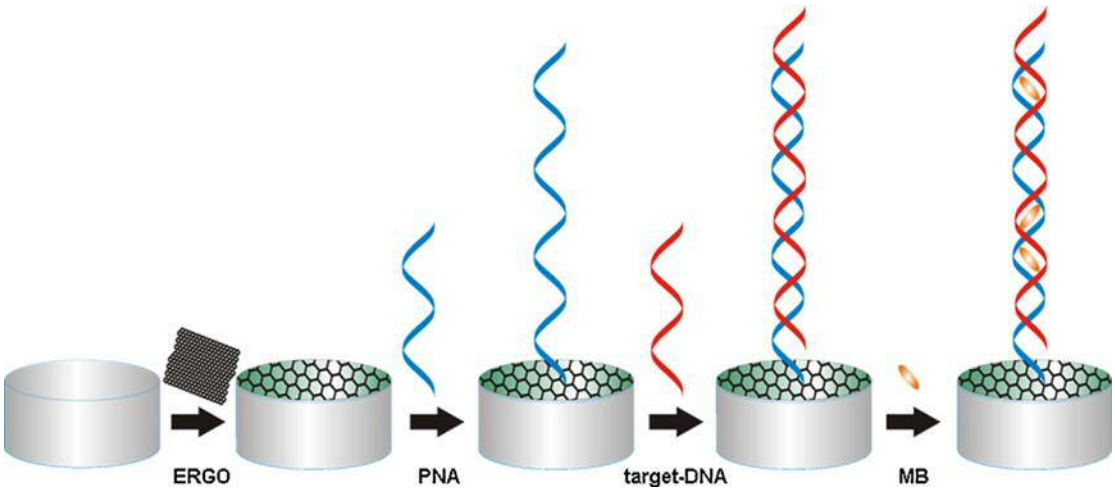

Figure 1.20 Schematic illustration of the electrochemical DNA biosensor.[68]

1.10 Techniques used for quantification of affinity of small molecules for DNA

DNA-small molecules interactions can be studied through a variety of techniques, including UV-visible and circular dichroism (CD) spectroscopy, isothermal titration calorimetry (ITC), viscometry. These techniques will be briefly described below.

1.10.1 UV-visible spectroscopy

UV-visible spectroscopy is a technique that measures the interaction of electromagnetic radiation with matter. This technique is usually applied to those molecules which are able to absorb radiation energy in the UV-visible range. The absorbed energy is used to excite electrons from the electronic ground state to an excited state. Most organic molecules with highly conjugated systems, and many biological macromolecules such as proteins and nucleic acids, can be analysed using UV-visible spectroscopy.[71]

Typically, there is a linear relation between the amount of radiation that is absorbed by a compound and its concentration with the linear correlation valid at a defined wavelength, solvent type and optical path length. This linear correlation is known as the Lambert-Beer law. Absorption spectroscopy is therefore considered a good method to study ligand-DNA interactions because data can be deconvoluted to yield concentrations of free and bound species. As a result of interactions of molecules with DNA alteration in structural conformations of ligands and local medium effects occur and these effects can lead to changes in spectroscopic response. The change may correspond to an increase (hyperchromicity) or decrease (hypochromicity) in molar absorptivity of ligands or possibly a shift of the wavelength of maximum absorption to higher wavelength (red shift) or lower wavelength (blue shift).

When several spectra are plotted in one graph we may see a point that is called isosbestic point, where two species have the same molar absorptivity, suggesting the presence of only two species viz. free and bound ligands in the equilibrium.[72,73]

The changes in the ligand absorption properties can be exploited to quantify the interaction of ligands with DNA. When a titration curve is extracted from recorded UV-visible data, this curve can be analysed using a binding model. A frequently used model is the multiple independent binding sites (MIS) model. This model can be fitted to the data and give binding parameters (binding constant *K* and binding site size *N*).

The MIS model is derived starting from the complexation equilibrium (equation 1.1) and the concentrations of free ligand, free DNA and bound ligand (complex) are related through K_{bind} (equation 1.2). Each binding site consists of a specific number of base pairs (N), which is occupied by a single ligand molecule, thus the concentration of binding sites can be defined as the concentration of DNA base pairs divided by N (equation 1.3).

K_{bind} is defined based on the equilibrium between the free ligand, free DNA and the complex (1.2). Since the concentration of free ligand $[L]_f$ and free binding site $[bs]_f$ with complex concentration $[C]$ are related through the total ligand concentration $[L]_t$ and total binding site concentration $[bs]_t$ (1.4), (1.5) respectively, it is possible to establish an overall equation describing the equilibrium (1.6). Rearrangement of equation (1.6) leads to a quadratic representation of the complex concentration (1.7).

$$L_f + bs_f \longleftrightarrow L_b \tag{1.1}$$

$$K_{bind} = [L]_b / [L]_f . [bs]_f, [L]_b = [C] \tag{1.2}$$

$$[bs] = [DNA] / N \tag{1.3}$$

$$[L]_t = [L]_f + [C] \quad \longleftrightarrow \quad [L]_f = [L]_t - [C] \tag{1.4}$$

$$[bs]_t = [bs]_f + [C] \quad \longleftrightarrow \quad [bs]_f = [bs]_t - [C] \tag{1.5}$$

$$[C] = K_{bind}.([bs]_t - [C]).([L]_t - [C])$$

$$[C] = K_{bind}\,[bs]_t.[L]_t - K_{bind}.[C].[bs]_t - K_{bind}.[C].[L]_t - K_{bind}.[C]^2 \tag{1.6}$$

$$K_{bind}\,[C]^2 - (1 + K_{bind}.[bs]_t + K_{bind}.[L]_t).[C] + K_{bind}.[bs]_t.[L]_t = 0 \tag{1.7}$$

The classic equation (1.8) can be used to solve the quadratic equation (1.7), thus the concentration of complex $[C]$ can be expressed as a function of total ligand and binding site concentrations (1.9).

(1.8)

By adding the Beer-lambert Law ( ), modified for background absorbance, into Equation 1.9, the observed absorbance is given by Equation 1.10. This equation can be fit to a plot of absorption against total DNA concentration to obtain the optimal approximations for binding constant and binding site size.

$$signal_{obsd} = background + signal_{free,\,m}.[L]_t + \Delta_{binding}\, signal_m \quad \text{—} \quad \text{—} \quad \text{—}$$

Equation 1.10

The terms in equation 1.10 are defined as follows;

$signal_{obsd}$ is the observed absorbance; background is the buffer absorbance; $signal_{free,m}$ is the product of the cuvette pathlength and molar extinction coefficient; $\Delta_{binding}$ $signal_m$ is the product of the cuvette path length and the change in extinction coefficient upon binding; K is the binding constant; [DNA] is the DNA concentration in terms of base pairs; $[L]_{tot}$ is the total ligand concentration; N is the binding site size in base pairs.

For weak binders, the fraction of the bound binding sites in the presence of ligand can be estimated using the so-called c-value as demonstrated below.

$K_b.[L]_f = [C] / [bs]_f$ for $[C] << [bs]_f$

$[bs]_f$ $[bs]_t$ and $[L]_f$ $[L]_t$

Therefore, $K_b.[L]_f$ $[C] / [bs]_t$

Define the c-value as = $K_b.[L]_f$ ⟷ c-value = $K_b.[L]_t$

Thus, c-value $[C] / [bs]_t$ ⟷ c-value $[bs]_b / [bs]_t$

c-value ratio of bound binding sites to the total binding sites.

If c-value = 0.05, indicating only 5% of binding sites occupied, confirming negligible binding.

1.10.2 Circular Dichroism Spectroscopy (CDS) and Induced Circular Dichroism (ICD)

Circular dichroism spectroscopy is a technique that measures the difference in the absorption of left handed circularly polarised light (L CPL) and right handed circularly polarised light (R CPL) by chiral chromophores or by chromophores in a chiral environment. CD spectroscopy is in widespread use to study chiral molecules and biological macromolecules such as proteins and DNA.[74]

CD spectroscopy is usually carried out in the UV-visible wavelength region. Molecules that contain chiral chromophores will absorb one form of circularly polarised light to a higher extent than the other form. Thus the difference between the intensity of R-CPL and L-CPL being transmitted through the sample would be non-zero and a CD signal will appear at the corresponding wavelength (Figure 1.21).[75]

CD spectroscopy can be exploited to determine binding parameters of small molecules binding to DNA. Duplex DNA usually shows a negative CD band around 250 nm, which is attributed to a right handed helical form of DNA and a positive band around 275 nm resulting from base stacking in B-DNA structures (Figure 1.8). Upon binding of small molecules with DNA, a change in ellipticity of DNA bands can occur. A plot of changes in DNA ellipticity against added ligand can be analysed using binding models, such as multiple independent binding sites (MIS) model to obtain binding parameters.

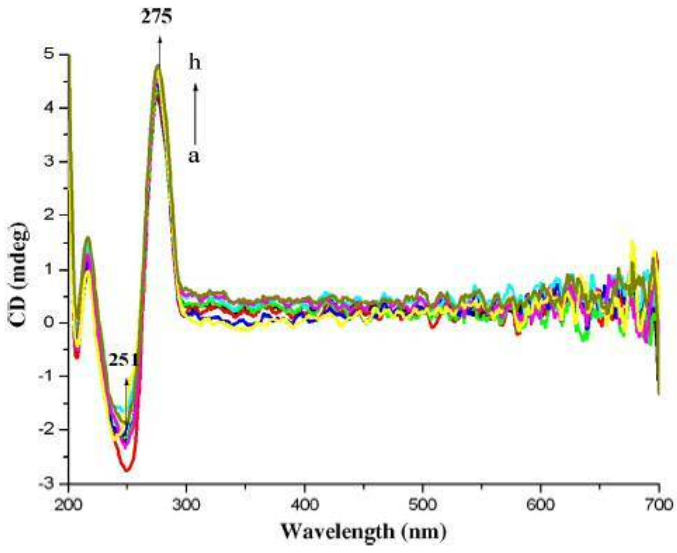

Figure 1.21 Circular dichroism spectra of d-$(CTCGAG)_2$ interacting with mitoxantrone.

Molecular interactions between chiral and achiral compounds can lead to induced circular dichroism (ICD) of the achiral counterpart (Figure 1.22). The induced CD spectra that are obtained give information about configuration of the chiral component and the direction of the molecules relative to each other in the complex.

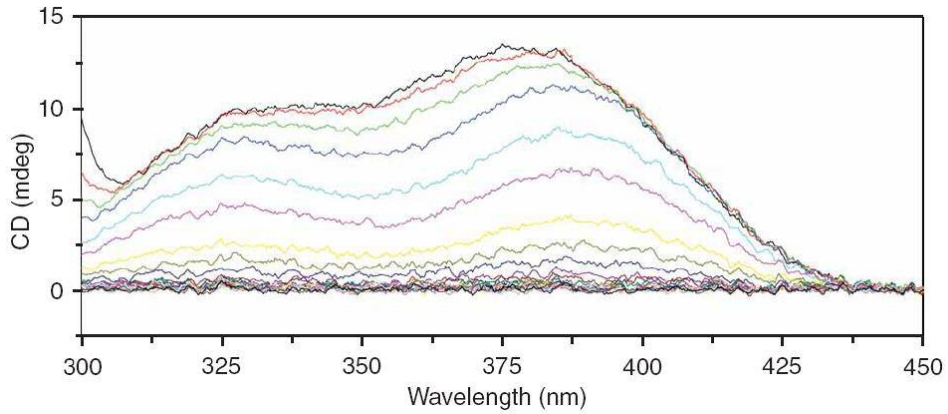

Figure 1.22 Induced circular dichroism (ICD) spectra for beneril interacting with CTDNA.[76]

Induced CD spectra for DNA binders can be interpreted empirically in terms of the binding mode,[76] because for molecules interacting with DNA, the interaction between the transition dipole moments of the ligand and the DNA bases substantially affects the ICD signal of the binder.[77] Minor groove binders usually produce a transition moment that is orientated along the groove of B-form DNA and is at an angle of 45° with the DNA bases, leading to a strong positive ICD signal. On the other hand, the ICD signal for an intercalator is significantly dependent on the displacement experienced with respect to the double helix and the nature of the base-pairs on either side of the site of intercalation. For example, for those intercalators which possess transition moments oriented along the main axis of the DNA, such as ethidium bromide, a negative ICD signal is observed.

1.10.3 Isothermal Titration Calorimetry (ITC)

Isothermal titration calorimetry is a technique that directly measures the heat generated or absorbed as a result of molecular interactions. Modern and sensitive ITC has gained wide acceptance in drug discovery in general and in DNA binding studies in particular.[78, 79] ITC is considered a unique technique because it allows simultaneous determination of all binding parameters (Binding constant (*K*), stoichiometry (*N*), ΔH and ΔS) in a single experiment.

An isothermal titration calorimeter (Figure 1.23) consists of two cells, viz. a reference and a sample cell. A constant heat flow is applied to the reference cell and the sample cell is heated in such a way that both cells stay at the same temperature.[80] When ligand from the syringe is added to the macromolecule in the sample cell there are two possible scenarios. If the interaction is exothermic the temperature in the sample cell increases upon addition of the ligand to the macromolecule and this leads to the feedback power to the sample cell being decreased. In case of an endothermic interaction the sample cell cools down and the feedback power to the sample cell would be increased.

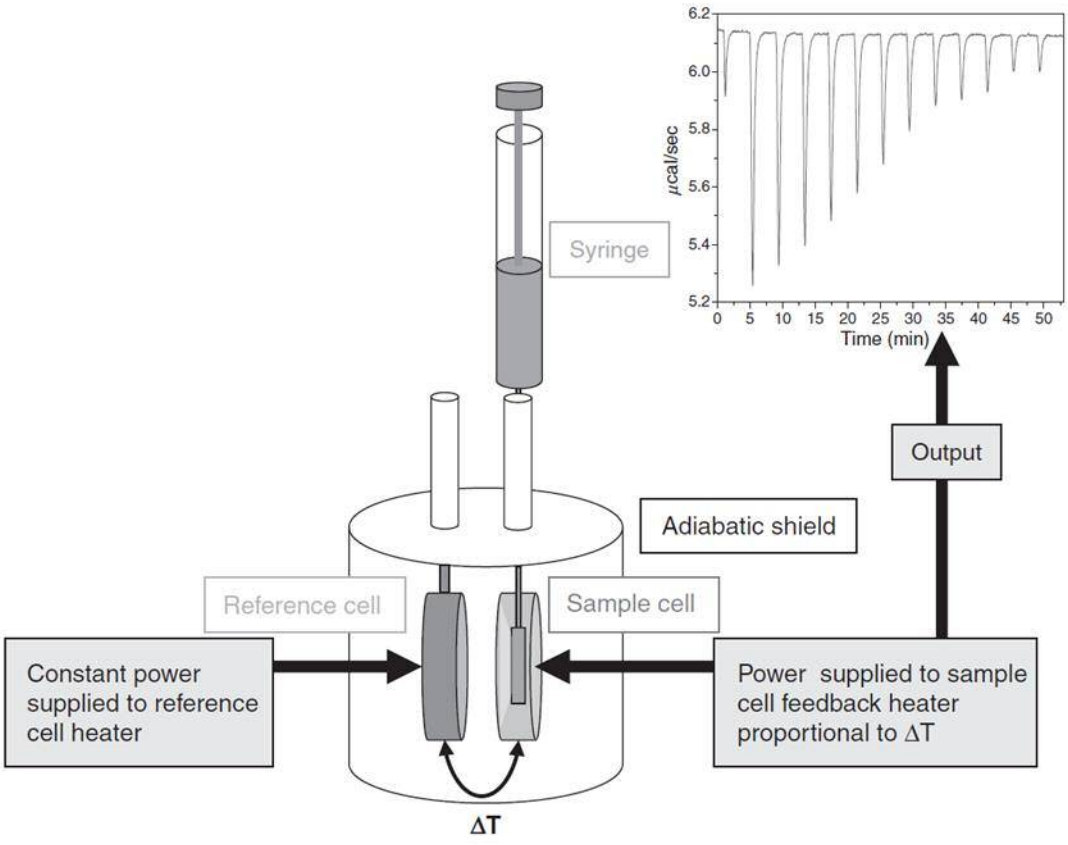

Figure 1.23 Schematic representation of the ITC instrument.[80]

In a typical experiment, the raw data are plotted as power (heat flow per unit time) needed to maintain the sample cell at the same temperature as the reference cell against time. Integration of the raw data and dividing by the amount of material injected then gives the molar heat effects. These heat effects are then analysed in terms of a binding model.

Isothermal Titration Calorimetry data analysis using IC-ITC

In many ITC experiments high concentrations of ligand are required in order to obtain detectable heat effects. However, this high ligand concentration can result in self-aggregation of ligand and leads to measurable heat effects for deaggregation upon dilution of the ligand into the cell. Therefore, self-aggregation of ligand should be taken into account during the data analysis, in conjunction with the consideration of DNA binding processes. When considering ligand self-aggregation in combination with binding processes, the mass balance equations become complex and cannot be solved analytically. Therefore, we use custom data analysis software, IC-ITC, which has been developed in-house.[78, 79] Our developed IC-ITC software enables us to analyse numerically calorimetric data for combined self-aggregation and DNA binding in order to determine thermodynamic parameters for the various equilibria involved (Scheme 1.10). This analysis involves equilibrium concentrations determined numerically using the Newton-Raphson algorithm and simulated annealing for optimization of thermodynamic parameters.[81, 82]

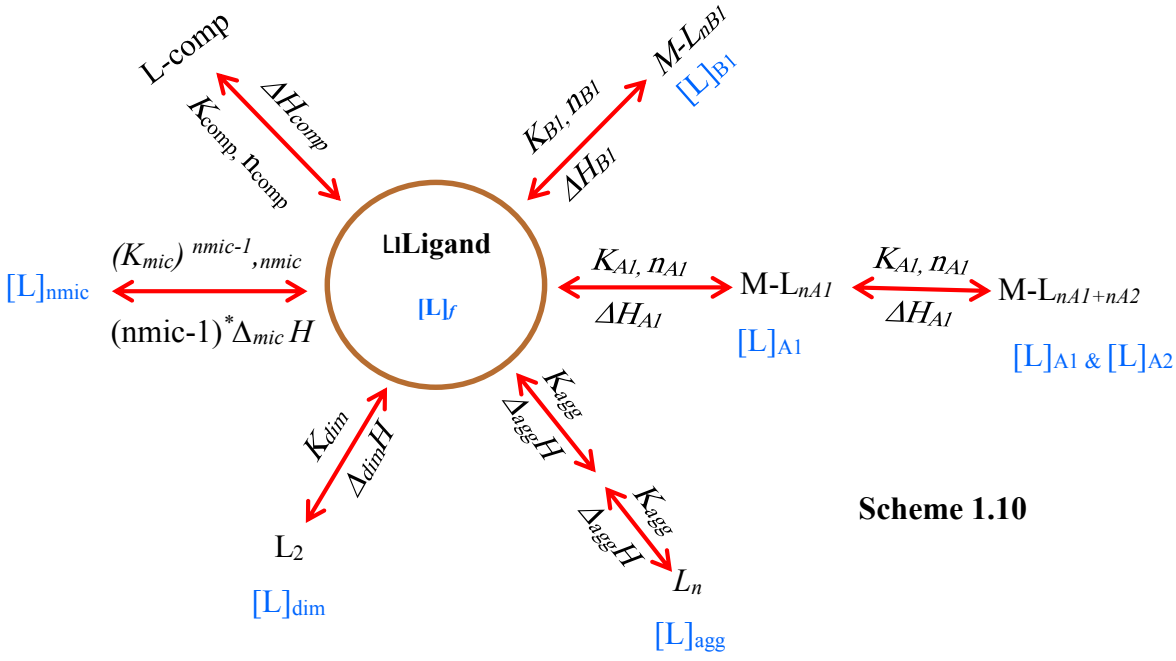

Scheme 1.10

The first important step that IC-ITC performs is calculating all relevant total concentrations (e.g. biomolecule, ligand) in the sample cell after each injection and subsequently solving the mass balance equation (Equation 4.2).

$-[L]_t + \qquad = 0$ Equation 4.2

In equation 4.2, $[L]_t$ is the total ligand concentration, and $[L]_x$ represents the concentrations of ligand in all different states X, for example, free, bound to DNA, aggregated, etc. The formal relation between the concentrations of ligand taken up in the complexes and aggregated forms, $[L]_x$, the free ligand concentration $[L]_f$, total macromolecule concentrations $[M]_t$ and interaction parameters $\mathbf{a}_x$ for the complexation events (i.e. equilibrium constants and stoichiometries) are illustrated in Equation 4.5.

$[L]_x = f([L]_t, [M]_t, \mathbf{a}_x)$ Equation 4.5

During data analysis, IC-ITC determines the optimal parameter values $\mathbf{a}_x$, as identified by the lowest sum over square deviations. In addition, IC-ITC calculates the error margins and covariances for different variables.

1.10.4 Viscosimetry

Viscosimetry is a useful technique for the study of the interaction mode of a binder with DNA in aqueous solution.[83, 84] Intercalation of a species between the base pairs of DNA causes the separation of these bases, leading to an overall increase in the length of the DNA helix and therefore an increased viscosity of the DNA solution. In contrast, a minor groove binder results in negligible perturbation of the DNA length, the net result of which is a negligible change or no change in the viscosity of the DNA solution.

The relative viscosity (η) of the DNA solution can be determined using a glass capillary viscometer, and is calculated through equation 1.5.

Where t is the observed flow time of the DNA solution in the viscometer and t_0 is the flow time of the buffer. As stated by Cohen and Eisenberg,[85] the change in the viscosity of the free and bound DNA (L / L_0) is given by calculating equation 1.6.

The terms in Equation 1.6 are defined as follows;

L is the contour length of rod-like macromolecules; p is the axial ratio of the rods; r is ratio of bound complex to DNA; η is the intrinsic viscosity of the DNA solution at different binding ratios, r.

The subscripts zero indicate the absence of the binder. The relative viscosity $(\eta/\eta_0)^{1/3}$ is plotted against the binding ratio r, and an increase or no increase in the viscosity of DNA is observed, depending on the modes of interaction (i.e. groove binding or intercalation).

1.10.5 Competition dialysis

Another powerful quantitative tool for finding structure-selective compounds that bind with specific nucleic acid structures is competition dialysis.[89] The competition dialysis experiment is based on the basic thermodynamic principle of equilibrium dialysis. This experiment is usually carried out by dialysis of an array of nucleic acid structures against a ligand solution. The array containing the nucleic acid structures is placed above ligand solution and separated through a semi-permeable membrane that is characterized by pore sizes which permit ligands to go through but disallow large macromolecules (Figure 1.24).[90]

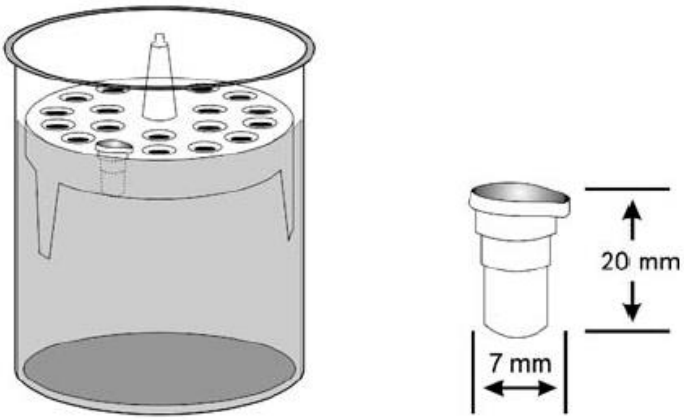

Figure 1.24 Schematic of the competition dialysis experiment.[90]

At equilibrium, the amount of free ligand in both of the dialysis parts (i.e. a chamber that contains ligand and a chamber that contains nucleic acid) must be same. Any increase in total ligand at the nucleic acid side, is the result of the affinity between nucleic acid and ligand, and the increase therefore corresponds to bound ligand with nucleic acid. Thus, equilibrium dialysis can be manipulated to determine binding affinities of small molecules for nucleic acids such as duplex DNA.

1.10.6 Melting temperature (T_m)

Melting temperature of nucleic acids can be exploited to study interaction of small-molecules to nucleic acids, particularly DNA and RNA. A plot of recorded UV absorption of DNA as a function of temperature gives a so-called melting curve.[91] The midpoint of that melting curve is defined as a melting temperature (T_m), where absorbance increases most strongly with increasing temperature. Mainly, the melting temperature (T_m) is affected by nature of base composition of DNA, length of DNA strands, salt concentration and type of counter-ion in the solution. Interaction of small molecules to duplex DNA also affects the melting temperature (T_m). Binding of small molecules as intercalators to duplex DNA can increase stability of DNA, leading to increase melting temperature (T_m) considerably around 5-8 °C, whereas, non-intercalative binding results in smaller or negligible change in melting temperature (T_m).[92]

1.11 Project Aims

Compounds binding to DNA have interested many scientists and researchers since the importance of DNA has been revealed. Binding of a compound with selectivity for a specific DNA sequence is of significant interest in medical and pharmaceutical respects. Compounds that are able to bind with a specific DNA sequence can be used as anti-cancer agents, blocking interaction of mutated sequences with proteins. Alternatively, if DNA binding is accompanied by changes in physical properties of the DNA binders (such as absorbance spectra, redox properties), such binders can be used as components of genosensors. In addition, binding of ligands with nucleic acids can be manipulated for the assembly of functional multicomponent structures containing active components.

The main aim of this project is to advance optoelectronically active DNA-binding compounds that show sequence selectivity for use as sensitisers in sensors for detection of genetic biomarkers. The sensitisers bind to DNA and their spectroscopic and electronic properties may change upon interaction with DNA, thus allowing different applications including in biosensors. Of particular interest are sensitisers that can be used in multimodal genosensors such as the design we have recently published.[65]

In our project we have introduced three different sets of DNA binders. The first group is composed of 1,8-naphthalimide derivatives which are oligoheteroaromatic compounds having a flat π-conjugated framework attached to different side-groups. Based on their structure, we anticipate the compounds of this group to bind to duplex DNA mostly through intercalation and this binding may change spectroscopic and electronic properties of these DNA binders. The second group of DNA binders is a family of dendrimeric compounds. These compounds consist of a highly fluorescent flat moiety that is attached to small poly(amido amine) side-groups to increase solubility in aqueous medium. According to their structure, we also expect the compounds of dendrimeric family bind to duplex DNA via intercalation and they may change their optical and electronic behaviours upon binding. The third group of our DNA binders consists of a variety of compounds that have diverse structural frameworks.

1.12 References

1) Lippert, B., *Cisplatin: chemistry and biochemistry of a leading anticancer drug*, John Wiley & Sons, 1999.

2) Najari, A.; Ho, H. A.; Gravel, J. F.; Nobert, P.; Boudreau, D.; Leclerc, M., *Anal. Chem.* 2006, 78 (22), 7896-7899.

3) Gottesfeld, J. M.; Neely, L.; Trauger, J. W.; Baird, E. E.; Dervan, P. B., *Nature* 1997, 387 (6629), 202-205.

4) Voet, D. and Voet, J. G., *Biochemistry*, 2nd ed., John Wiley & Sons, New York, 1995.

5) McMurry, J., *Organic Chemistry*, 3rd ed., Brooks/Cole, 1992.

6) Mainwaring, W.I.P.; Parish, J.H.; Pickering, J. D. and Mann N.H., *Nucleic acid biochemistry and molecular biology*, Blackwell Scientific, Oxford, 1982.

7) Sriram, M.; Vandermarel, G. A.; Roelen, H.; Vanboom, J. H.; Wang, A. H. J., *Embo Journal* 1992, 11 (1), 225-232.

8) Lowe, C. R., *Trends in Biotechnology* 1984, 2(3), 59–65.

9) Sun, Z.; Liao, T.; Zhang, Y.; Shu, J.; Zhang, H. and Zhang, G. J., *Biosensors and Bioelectronics* 2015, 86, 194-201.

10) Zhang, F.T.; Cai, L.Y.; Zhou, Y. L. and Zhang, X. X., *TrAC Trends in Analytical Chemistry* 2016, 85, 17-32.

11) Chao, J.; Zhu, D.; Zhang, Y.; Wang, L. and Fan, C., *Biosensors and Bioelectronics* 2016, 76, 68-79.

12) Justino, C. I.; Freitas, A. C.; Pereira, R.; Duarte, A. C. and Santos, T. A. R., *TrAC Trends in Analytical Chemistry* 2015, 68, 2-17.

13) Drummond, T.G.; Hill, M.G. and Barton, J.K., *Nature biotechnology* 2003, 21(10), 1192-1199.

14) Marazuela, M.; Moreno-Bondi, M., *Anal. Bioanal. Chem.* 2002, 372- 664.

15) [Anonymous], The Structures of DNA and RNA, p1-33, 2002. Available from: http://biology.kenyon.edu/courses/biol63/watson_06.pdf.

16) Watson, J. D. and Crick, F. H., *Nature* 1953,171, 737-738.

17) Yakovchuk, P.; Protozanova, E.; Frank-Kamenetskii, M. D., *Nucleic Acids Research* 2006, 34 (2), 564-574.

18) Blackburn, G. M.; Gait M. J.; Loakes, D.; Williams, D. M., *Nucleic Acids in Chemistry and Biology 3rd Edition Introduction and Overview*, Royal Soc Chemistry: 2006.

19) Jeremy, M.; Berg, J. L. T.; Lubert Stryer, *Biochemistry*, WH Freeman and Company: New York, 2006.

20) Wing R.; Drew, H.; Takano, T.; Broka, C.; Tanaka, S.; Itakura, K.; Dickerson, R. E., *Nature* 1980, 287 (5784), 755-758.

21) Alberts, B.; Johnson, A.; Walter, P.; Lewis, J.; Raff, M. and Roberts, K., *Molecular biology of the cell*. References edition, 5th ed. Edn., Garland Science, New York, N.Y.; Abingdon, 2008.

22) Kastan, M.B. and Bartek, J., *Nature*, 2004, 432, 316-323.

23) Roat-Malone, R.M.; Wiley, J.; Sons, I., *Bioinorganic Chemistry*, 2002.

24) Stryer, L., *Biochemistry*, 4th ed., W.H. Freeman, 1999.

25) Chaires, J. B.; Dattagupta, N.; Crothers, D. M., *Biochemistry* 1982, 21 (17), 39333940.

26) Neto, B. A. D.; Lapis, A. A. M., *Molecules* 2009, 14 (5), 1725-1746.

27) Zimmer, C.; Wahnert U., *Progress in Biophysics & Molecular Biology* 1986, 47 (1), 31-112.

28) Shui, X. Q.; Sines C. C.; McFail-Isom, L.; Van Derveer, D.; Williams, L. D., *Biochemistry* 1998, 37 (48), 16877-16887.

29) Boresch, S.; Karplus M., *Journal of Molecular Biology* 1995, 254 (5), 801-807.

30) Strekowski, L.; Wilson, B., *Mutation Research-Fundamental and Molecular Mechanisms of Mutagenesis* 2007, 623 (1-2), 3-13.

31) Nakamoto, K.; Tsuboi, M.; Strahan, G. D., *Drug-DNA interactions: structures and spectra*; John Wiley & Sons, Inc., Hoboken, New Jersey; 2008.

32) Goodsell, D.S.; Kopka, M. L. and Dickerson, R. E., *Biochemistry,* 1995, 34, 4983-4993.

33) Wartell, R. M.; Larson, J. E. and Wells, R.D., *The Journal of Biological Chemistry,* 1974, 249, 6719-6731.

34) Pullmanand, A.; Pullman, B., *Quarterly Reviews of Biophysics,* 1981, 14, 289-380.

35) Dickinson, L. A.; Burnett, R.; Melander C.; Edelson, B. S.; Arora, P. S.; Dervan, P. B.; Gottesfeld, J. M., *Chemistry & Biology* 2004, 11 (11), 1583-1594.

36) Dervan, P. B.; Edelson, B. S., *Current Opinion in Structural Biology* 2003, 13 (3), 284-299. 38.

37) Kopka, M. L.; Yoon, C.; Goodsell, D.; Pjura, P.; Dickerson, R. E., *Proceedings of the National Academy of Sciences of the United States of America* 1985, 82 (5), 13761380.

38) Pelton, J. G.; Wemmer, D. E., *Proc. Natl. Acad. Sci. U.S.A.* 1989, 86 (15), 5723-5727.

39) Lah, J.; Carl, N.; Drobnak, I.; Sumiga, B.; Vesnaver, G., *Acta Chim. Slov*. 2006, 53(3), 284-291.

40) Harshman, K. D.; Dervan, P. B., *Nucleic Acids Research* 1985, 13 (13), 48254835.

41) Moon, J. H.; Kim, S. K.; Sehlstedt, U.; Rodger, A.; Norden, B., *Biopolymers* 1996, 38 (5), 593-606.

42) Dervan, P. B., *Bioorg. Med. Chem.* 2001, 9 (9), 2215-2235.

43) Kelly, J. J.; Baird, E. E.; Dervan, P. B., *Proc. Natl. Acad. Sci. U.S.A.* 1996, 93 (14), 6981-6985.

44) Herman, D. M.; Baird, E. E.; Dervan, P. B., *Chem.-Eur. J.* 1999, 5 (3), 975-983.

45) Weyermann, P.; Dervan, *P. B., J. Am. Chem. Soc.* 2002, 124 (24), 6872-6878.

46) Painter, P. C. C., Michael M., *Fundamentals of Polymer Science: an introductory text.* Technomic Pub. Co.: Lancaster, 1997.

47) Jaiswal, M.; Menon, R., *Polym. Int.* 2006, 55, 1371-1384.

48) Murphy, A. R.; Frechet, *J. M. J., Chem. Rev.* 2007, 107, 1066-1096.

49) Wilson, W. D.; Tanious, F. A.; Ding, D. Y.; Kumar, A.; Boykin, D. W.; Colson, P.; Houssier, C.; Bailly, C., *Journal of the American Chemical Society* 1998, 120 (40), 10310-10321.

50) Ho, H. A.; Najari, A.; Leclerc, M., *Accounts Chem. Res.* 2008, 41 (2), 168-178.

51) Leclerc, M. *Optical and Electrochemical Transducers Based on Functionalized Conjugated Polymers. Adv. Mater.* 1999, 11, 1491–1498.

52) Bakker, E.; Telting-Diaz, M., *Anal. Chem.* 2002, 74 (12), 2781-2800

53) Alligrant, T.M.; Nettleton, E.G. and Crooks, R.M., *Lab on a Chip* 2013, 13(3), 349-354.

54) Cai, Z.; Song, Y.; Wu, Y.; Zhu, Z.; Yang, C.J. and Chen, X., *Biosensors and Bioelectronics* 2013, 41, 783-788.

55) Jing, X.; Cao, X.; Wang, L.; Lan, T.; Li, Y. and Xie, G., *Biosensors and Bioelectronics* 2014, 58, 40-47.

56) Balintová, J.; Špaček, J.; Pohl, R.; Brázdová, M.; Havran, L.; Fojta, M. and Hocek, M., *Chemical Science* 2015, 6(1), 575-587.

57) Korri-Youssoufi, H.; Garnier, F.; Srivastava, P.; Godillot, P.; Yassar, A., *J. Am. Chem. Soc.* 1997, 119, 7388–7389.

58) Li, G. T.; Kossmehl, G.; Welzel, H. P.; Engelmann, G.; Hunnius, W. D.; Plieth, W.; Zhu, H. S., *Macromol. Chem. Phys.* 1998, 199 (4), 525-533.

59) Lee, T. Y.; Shim, Y. B., *Anal. Chem.* 2001, 73 (22), 5629-5632.

60) Ronkainen, N. J.; Halsall, H. B.; Heineman, W. R., *Chem. Soc. Rev.* 2010, 39 (5), 1747-1763.

61) Keighley, S. D.; Li, P.; Estrela, P.; Mighorato, P., *Biosens. Bioelectron.* 2008, 23 (8), 1291-1297.

62) Peng, H.; Zhang, L. J.; Soeller, C.; Travas-Sejdic, J., *Biomaterials* 2009, 30 (11), 2132-2148.

63) Keighley, S. D.; Estrela, P.; Li, P.; Mighorato, P., *Biosens. Bioelectron.* 2008, 24 (4), 906-911.

64) Li, Z.; Miao, X.; Xing, K.; Zhu, A. and Ling, L., *Biosens. Bioelectron.* 2015, 74, 687-690.

65) Regan, E. M.; Hallett, A. J.; Wong, L. C.; Saeed, I. Q.; Jones, E. E.; Buurma, N. J.; Pope, S.; Estrela, P., *Electrochimica Acta* 2014, 128, 10-15.

66) Nielsen, P. E., *Current Opinion in Biotechnology* 2001, 12(1), 16-20.

67) Cao, M.; Deng, L. and Xu, H., *Colloids and Surfaces A: Physicochemical and Engineering Aspects* 2015, 470, 46-51.

68) Du, D.; Guo, S.; Tang, L.; Ning, Y.; Yao, Q. and Zhang, G. J., *Sensors and Actuators B: Chemical* 2013, 186, 563-570.

69) Liu, X.; Qu, X.; Fan, H.; Ai, S. and Han, R., *Electrochimica Acta* 2010, 55(22), 6491-6495.

70) Choi, Y.; Metcalf, G.; Sleiman, M.H.; Vair-Turnbull, D. and Ladame, S. *Bioorganic & medicinal chemistry* 2014, 22(16), 4395-4398.

71) S. L. Upstone, *Encyclopedia of Analytical Chemistry*, R.A. Meyers (Ed.) John Wiley & Sons Ltd, Chichester, 2000, 1699–1714.

72) Moore, J. W. and Pearson, R. G., *Kinetics and Mechanism*, John Wiley & Sons. Inc., New York, USA, 1981.

73) Pavia, D. L.; Lampman, G. M. and Kriz, G. S., *Ultraviolet Spectroscopy. Introduction to Spectroscopy.* Harcourt College Publishers, Edition 3, 2001, 353-358.

74) Corrêa, D. H. A. and C. H. I. Ramos, *African Journal of Biochemistry Research*, 2009, 3, 164-173.

75) SH. M. Kelly and N. C. Price, *Current Protein and Peptide Science*, 2000, 1, 349-384.

76) N.C. Garbett, P.A. Ragazzon, and J.B. Chaires, *Nature protocols*, 2007, 2, 3166-3172.

77) Eriksson, M.; Norden, B., *Drug-Nucleic Acid Interactions* 2001, 340, 68-98.

78) Buurma, N. J.; Haq, I., *Methods*, 2007, 42, 2, 162-172.

79) Burrma, N. J.; Haq, I., *J. Mol. Biol.*, 2008, 381, 3, 607-621.

80) Freyer, M. W.; Lewis, E.A., *Biophysical Tools for Biologists, Volume One: In Vitro Techniques*, 4, 2008, 79-113.

81) Press, W. H.; Flannery, B. P.; Teukolsky, S. A.; Vetterling, W. T., *Numerical Recipes in Pascal* 2004, 270.

82) Kirkpatrick, S.; Gelatt, C. D.; Vecchi, M. P., *Science* 1983, 220 (4598), 671-680.

83) Satyanarayana, S.; Dabrowiak, J. C.; Chaires, J. B., *Biochemistry* 1993, 32 (10), 2573-2584.

84) Suh, D.; Chaires, J. B., *Bioorg. Med. Chem.* 1995, 3 (6), 723-728.

85) Cohen, G.; Eisenber.H, *Biopolymers* 1969, 8 (1), 45-55.

86) Hidalgo, M.; Izbicka, E.; Cerna, C.; Gomez, L.; Rowinsky, E.K.; Weitman, S.D. and Von Hoff, D.D., *Anti-cancer drugs* 1999, 10 (3), 295-302.

87) Cai, X.; Gray, P.J. and Von Hoff, D.D., *Cancer treatment reviews* 2009, 35 (5), 437-450.

88) Boger, D.L., *Pure and applied chemistry* 1994, 66 (4), 837-844.

89) Jaumot, J. and Gargallo, R., *Current pharmaceutical design* 2012, 18 (14), 1900-1916.

90) Waring, M.J.; Chaires, J.B. and Armitage, B.A., *DNA binders and related subjects* 2005, (Vol. 253). Springer Science & Business Media.

91) Blackburn, G.M., *Nucleic acids in chemistry and biology* 2006. Royal Society of Chemistry.

92) Bi, S.; Zhao, T.; Wang, Y.; Zhou, H.; Pang, B. and Gu, T., *Spectrochimica Acta Part A: Molecular and Biomolecular Spectroscopy* 2015, *150*, 921-927.

93) Schöning, M.J. and Poghossian, A., *Analyst* 2002, 127 (9), 1137-1151.

94) Pejcic, B. and De Marco, R., *Electrochimica Acta* 2006, 51 (28), 6217-6229.

95) Daniels, J.S. and Pourmand, N., *Electroanalysis* 2007, 19 (12), 1239-1257.

96) Park, J.Y. and Park, S.M., *Sensors* 2009, 9 (12), 9513-9532.

97) Brand, U.; Brandes, L.; Koch, V.; Kullik, T.; Reinhardt, B.; Rüther, F.; Scheper, T.; Schügerl, K.; Wang, S.; Wu, X. and Ferretti, R., *Applied microbiology and biotechnology* 1991, 36 (2), 167-172.

98) Maddalena, F.; Kuiper, M.J.; Poolman, B.; Brouwer, F.; Hummelen, J.C.; de Leeuw, D.M.; De Boer, B. and Blom, P.W., *Journal of Applied Physics* 2010, 108 (12), 124501.

99) Zhang, J.; Song, S.; Wang, L.; Pan, D. and Fan, C., *Nature protocols* 2007, 2 (11), 2888-2895.

100) Wei, F.; Lillehoj, P.B. and Ho, C.M., *Pediatric research* 2010, 67 (5), 458-468.

101) Perumal, V. and Hashim, U., *Journal of Applied Biomedicine* 2014, 12 (1), 1-15.

102) Daly, C.J. and McGrath, J.C., *Pharmacology & therapeutics* 2003, 100 (2), 101-118.

103) Ramanathan, A.; Pape, L. and Schwartz, D.C., *Analytical biochemistry* 2005, 337 (1), 1-11.

Chapter 2

DNA BINDING STUDIES FOR 1,8-NAPHTHALIMIDE DERIVATIVES

Abstract

In this chapter we describe the results of studies of the interactions of a group of 1,8-naphthalimide derivatives with double- stranded DNA using variety of techniques viz. spectroscopy, calorimetry, viscosity and molecular docking studies. Most ligands bind to duplex DNA moderately strongly through different binding modes varying from minor-groove binding to intercalation to side-by-side binding in the minor groove. Sequence selectivity of this group of compounds for specific sequences $(dAdT)_{12}$●$(dAdT)_{12}$ *and* $(dGdC)_{12}$●$(dGdC)_{12}$ *was also studied via UV-visible spectroscopy, showing that the 1,8-naphthalimide derivatives have a higher affinity for* $(dAdT)_{12}$●$(dAdT)_{12}$ *than for* $(dGdC)_{12}$●$(dGdC)_{12}$.

2.1 Introduction

DNA-binding can be studied using a variety of techniques, including UV-visible spectroscopy, isothermal titration calorimetry (ITC), circular dichroism spectroscopy and viscosimetry. A full description and discussion of these techniques is provided in Chapter 1 but a short review of these methods is provided below.

2.1.1 UV-Visible Spectroscopy (UV-Vis)

UV-visible spectroscopy is a technique that measures the interaction of electromagnetic radiation with matter. This technique is usually applied to those molecules which are able to absorb radiation energy in the UV-visible range. The absorbed energy is used to excite electrons from the electronic ground state to an excited state. Most organic molecules with highly conjugated systems, and many biological macromolecules such as proteins and nucleic acids, can be analysed using UV-visible spectroscopy.[10]

Absorption spectroscopy is therefore considered a good method to study ligand-DNA interactions because data can be deconvoluted to yield concentrations of free and bound species. As a result of interactions of molecules with DNA alteration in structural conformations of ligands and local medium effects occur and these effects can lead to changes in spectroscopic response. The change may correspond to an increase (hyperchromicity) or decrease (hypochromicity) in molar absorptivity of ligands or possibly a shift of the wavelength of maximum absorption to higher wavelength (red shift) or lower wavelength (blue shift).

2.1.2 Circular Dichroism Spectroscopy (CDS)

Circular dichroism spectroscopy is a technique that measures the difference in the absorption of left handed circularly polarised light (L CPL) and right handed circularly polarised light (R CPL) by chiral chromophores or by chromophores in a chiral environment. CD spectroscopy is in widespread use to study chiral molecules and biological macromolecules such as proteins and DNA.[8]

CD spectroscopy is usually carried out in the UV-visible wavelength region. Molecules that contain chiral chromophores will absorb one form of circularly polarised light to a higher extent than the other form. Thus the difference between the

intensity of R-CPL and L-CPL being transmitted through the sample would be non-zero and a CD signal will appear at the corresponding wavelength.[5]

Molecular interactions between chiral and achiral compounds can lead to induced circular dichroism (ICD) of the achiral counterpart. The induced CD spectra that are obtained give information about configuration of the chiral component and the direction of the molecules relative to each other in the complex. Induced CD spectra for DNA binders can be interpreted empirically in terms of the binding mode.[1]

2.1.3 Isothermal Titration Calorimetry (ITC)

Isothermal titration calorimetry is a technique that directly measures the heat generated or absorbed as a result of molecular interactions. Modern and sensitive ITC has gained wide acceptance in drug discovery in general, and in DNA binding studies in particular.[2,3] ITC is considered a unique technique because it allows simultaneous determination of all binding parameters (K, N, ΔH and ΔS) in a single experiment.

An isothermal titration calorimeter consists of two cells, viz. a reference and a sample cell. A constant heat flow is applied to both cells and the cells should stay at the same temperature. When ligand from the syringe is added to the macromolecule in the sample cell there are two possible scenarios. If the interaction is exothermic the temperature in the sample cell increases upon addition of the ligand to the macromolecule and this leads to the feedback power to the sample cell being decreased. In case of an endothermic interaction the sample cell cools down and the feedback power to the sample cell would be increased.

In a typical experiment, the raw data are plotted as power (heat flow per unit time) needed to maintain the sample cell at the same temperature as the reference cell against time. Integration of the raw data and dividing by the amount of material injected then gives the molar heat effects. These heat effects are then analysed in terms of a binding model.

2.1.4 Viscosimetry

Viscosimetry is a useful technique for the study of the mode of interaction of a binder with DNA in aqueous solution.[7] Intercalation of a species between the base pairs of DNA causes the separation of these bases, leading to an overall increase in the length of the DNA helix and therefore an increased viscosity of the DNA solution. In contrast, binding of a minor groove binder results in negligible perturbation of the DNA length, the net result of which is a negligible change or no change in the viscosity of the DNA solution.

2.1.5 Aims

Our objectives in this chapter are to quantify thermodynamics of binding for a group of 1,8-naphthalimide derivatives (Scheme 2.1) to duplex DNA, and establish the mode of interactions, using several techniques viz, UV-visible spectroscopy, isothermal titration calorimetry, circular dichroism spectroscopy, viscometry and molecular docking study.

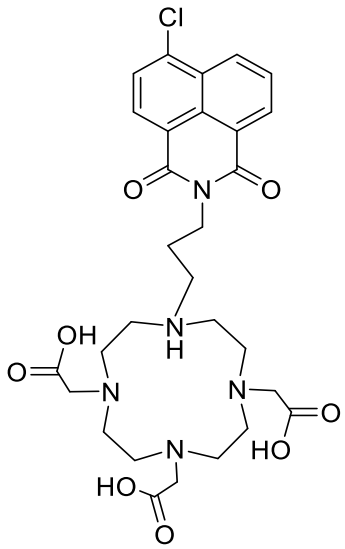

2.1

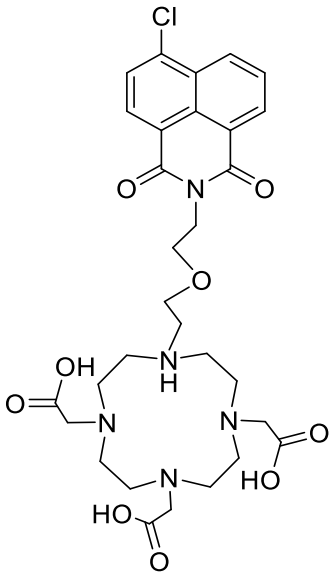

2.2

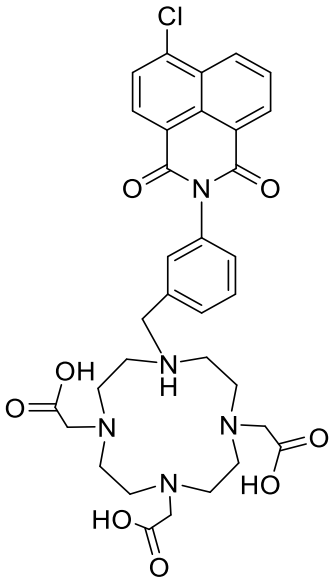

2.3

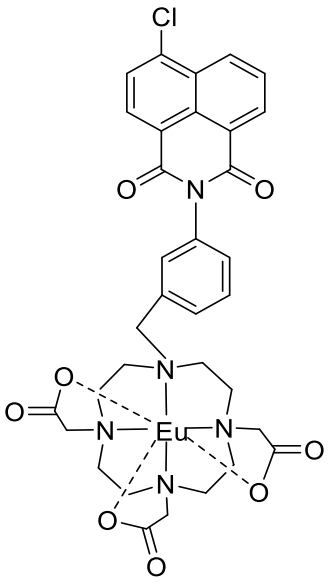

2.4

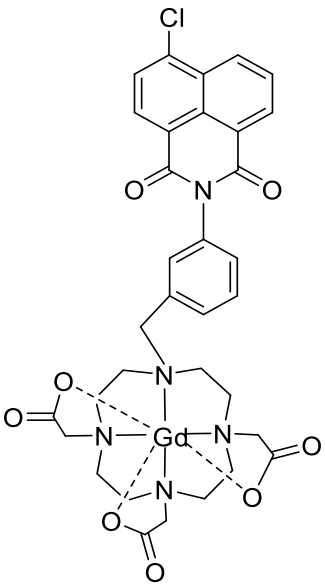

2.5

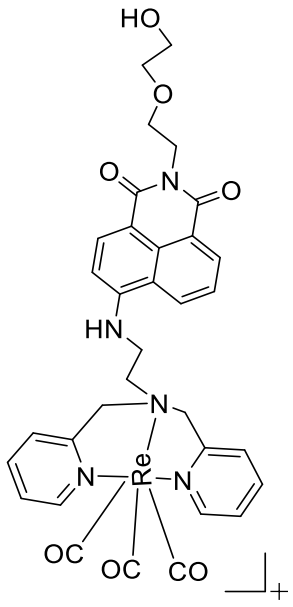

2.6

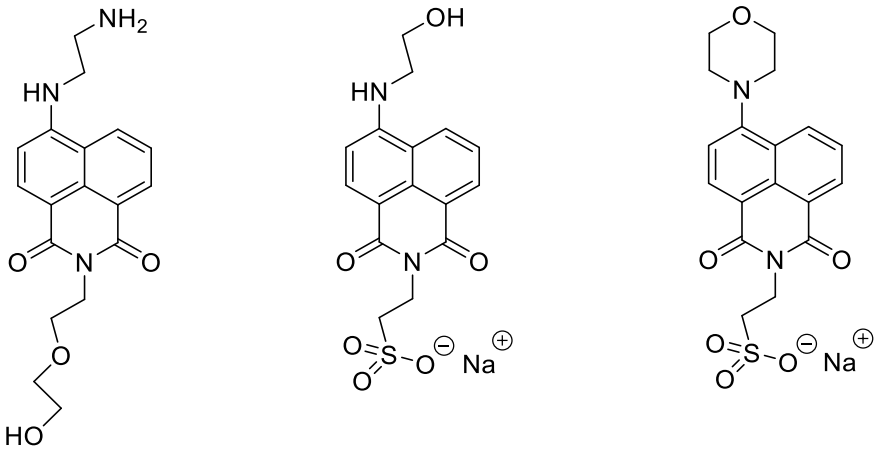

2.7 **2.8** **2.9**

Scheme 2.1

All compounds in Scheme 2.1 were provided by our collaborator (Simon Pope group). These compounds consist of flat aromatic frameworks (1,8-naphthalimide) with a variety of side-groups attached. According to their structure, we expect that the compounds of this family bind to duplex DNA via intercalation and their optical and electronic behaviours may change upon binding. For all compounds **2.1**-**2.9**, their structural frameworks are fluorescent, which allows use in fluorimetry-based assays. Compounds **2.1**-**2.3** carry significant negative charges, which may make these compounds of interest for use as sensitisers in electrochemical impedance spectroscopy (EIS) genosensors upon binding with DNA. Compound **2.4** is redoxactive and could be used in coulometry. Like **2.1**-**2.3** compounds **2.8** and **2.9** carry negative charges, which make these compounds potentially interesting as signal enhancer in genosensors based on EIS.

2.2 Results and Discussion

The results of the interaction studies for compounds **2.1-2.9** with DNA will be shown and discussed for each individual compound.

2.2.1 UV-visible spectroscopy

2.2.1.a UV-visible spectroscopy studies of 2.1 binding to DNA

The binding of **2.1** to DNA was studied using UV-visible spectroscopy; the changes in absorption of **2.1** upon addition of FSDNA were measured in buffer (25 mM MOPS, pH 7.0, 50 mM NaCl) at 25 °C (Figure 2.1).

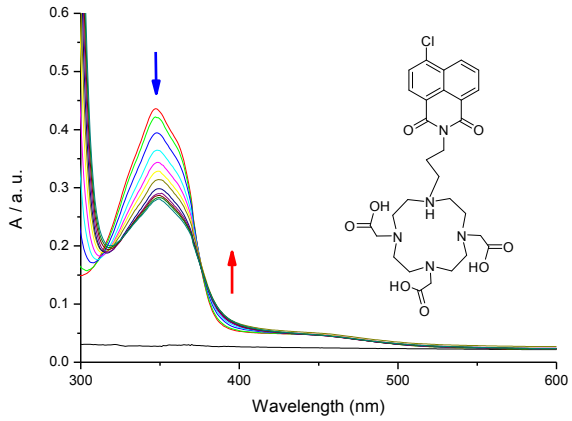

Figure 2.1 UV-visible spectra for 0.066 mM **2.1** upon addition of 0 – 3.33 mM FSDNA in buffer (25 mM MOPS, pH 7.0, 50 mM NaCl) at 25 °C.

Figure 2.1 shows a hypochromic shift in absorbance (at the λ_{max} of 347 nm) and a hyperchromic shift (at 390 nm) of **2.1** upon addition of FSDNA. This change in UV-visible absorption may occur as a result of geometrical distortion of **2.1** when it interacts with DNA, but it may also be a local medium effect.

To quantify the affinity of **2.1** for FSDNA, the absorbances at 347 and 390 nm were plotted as a function of concentration of FSDNA (Figure 2.2, for data in tabular format see appendix, Tables A15.1 & A15.2).

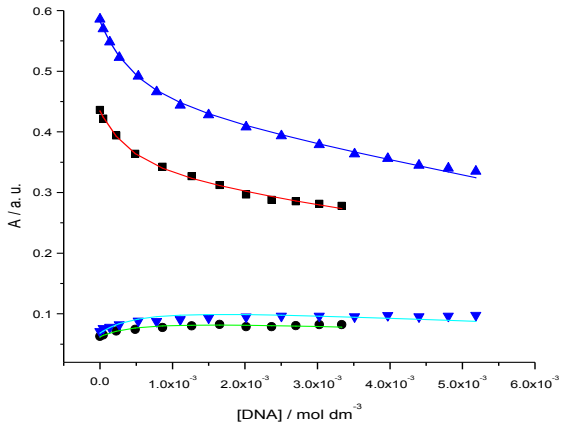

Figure 2.2 Absorbance at 347 nm (■) and at 390 nm (●) of a solution of 0.066 mM **2.1** as a function of DNA concentration, absorbance at 347 nm (▲) and at 390 nm (▼) of a solution of 0.093 mM **2.1** as a function of DNA concentration, in buffer (25 mM MOPS, pH 7.0, 50 mM NaCl) at 25 °C. The solid lines represent a global fit of a multiple independent sites model to the data.

The titration curves in Figure 2.2 were analysed globally in terms of a multiple independent binding sites model, which also takes ligand dilution into account, giving an equilibrium constant ($K_{binding}$) of (5.21 ± 5.76) $\times 10^3$ M^{-1} and a binding site size of (2.01 ± 1.80) base pairs. The large error margins suggest significant parameter covariance. We therefore re-analysed the data for a binding site size n restricted to 3 base pairs (for these types of DNA binders the average binding site size n is around 3 base pairs). The fit gave an equilibrium constant ($K_{binding}$) of (8.58 ± 0.85) $\times 10^3$ M^{-1}.

2.2.1.b UV-visible spectroscopy studies of 2.2 binding to DNA

The binding of **2.2** to DNA was similarly studied using UV-visible spectroscopy; the changes in absorption of **2.2** upon addition of FSDNA were measured in buffer (25 mM MOPS, pH 7.0, 50 mM NaCl) at 25 °C (Figure 2.3).

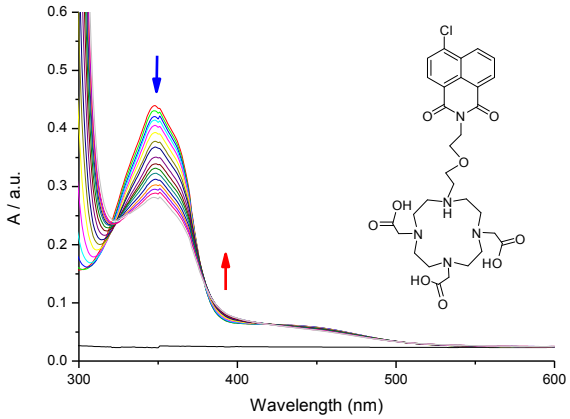

Figure 2.3 UV-visible spectra for 0.068 mM **2.2** upon addition of 0 – 2.9 mM FSDNA in buffer (25 mM MOPS, pH 7.0, 50 mM NaCl) at 25 °C.

Figure 2.3 shows a hypochromic shift in absorbance (at the λ_{max} of 347 nm) and a hyperchromic shift (at 390 nm) of **2.2** upon addition of FSDNA. This change in UV-visible absorption may occur as a result of geometrical distortion of **2.2** when it interacts with DNA, but it may also be a local medium effect.

To quantify the affinity of **2.2** for FSDNA, the absorbances at 347 and 390 nm for three titrations were plotted as a function of concentration of FSDNA (Figure 2.4, for data in tabular format see appendix, Tables A15.3, A15.4 & A15.5).

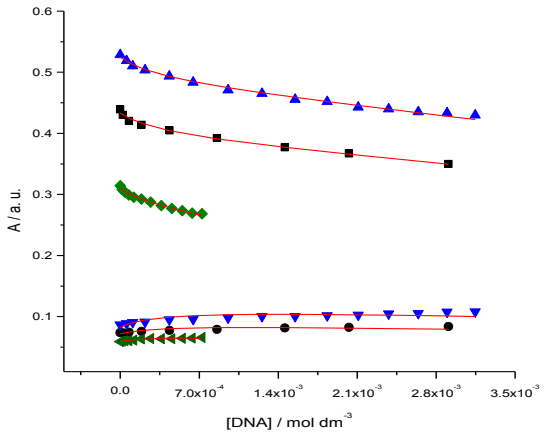

Figure 2.4 Absorbance at 347 nm (■) and at 390 nm (●) of a solution of 0.068 mM **2.2** as a function of DNA concentration, absorbance at 347 nm (▲) and at 390 nm (▼) of a solution of 0.082 mM **2.2** as a function of DNA concentration, absorbance at 347 nm (♦) and at 390 nm (◄) of a solution of 0.046 mM **2.2** as a function of DNA

concentration, in buffer (25 mM MOPS, pH 7.0, 50 mM NaCl) at 25 °C. The solid lines represent a global fit of a multiple independent sites model to the data.

The titration curves in Figure 2.4 were analysed globally in terms of a multiple independent binding sites model, which also takes ligand dilution into account. This fit produces an equilibrium constant ($K_{binding}$) of (0.016 ± 2.28) $\times 10^4$ M^{-1} and a binding site size of (0.061 ± 8.16) base pairs. The obtained binding parameters from data analysis were not reasonable therefore the data were reanalyzed with the stoichiometry restricted to binding sites of 3.0 base pairs, giving a binding constant ($K_{binding}$) of (10.94 ± 2.82) $\times 10^3$ M^{-1}.

2.2.1.c UV-visible spectroscopy studies of 2.3 binding to DNA

The binding of **2.3** to DNA was studied using UV-visible spectroscopy; the changes in absorption of **2.3** upon addition of FSDNA were measured in buffer (25 mM MOPS, pH 7.0, 50 mM NaCl) at 25 °C (Figure 2.5).

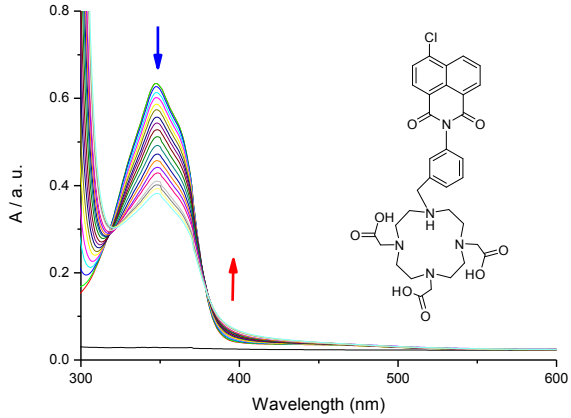

Figure 2.5 UV-visible spectra for 0.052 mM **2.3** upon addition of 0 – 8.6 mM DNA in buffer (25 mM MOPS, pH 7.0, 50 mM NaCl) at 25 °C.

Figure 2.5 shows a hypochromic shift in absorbance (at the λ_{max} of 347 nm) and a hyperchromic shift (at 390 nm) of **2.3** upon addition of DNA. This change in UV-visible absorption may occur as a result of geometrical distortion of **2.3** when it interacts with DNA, but it may also be a local medium effect.

To quantify the affinity of **2.3** for FSDNA, the absorbances at 347 and 390 nm for two titrations were plotted as a function of concentration of FSDNA (Figure 2.6, for data in tabular format see appendix, Tables A15.6 & A15.7).

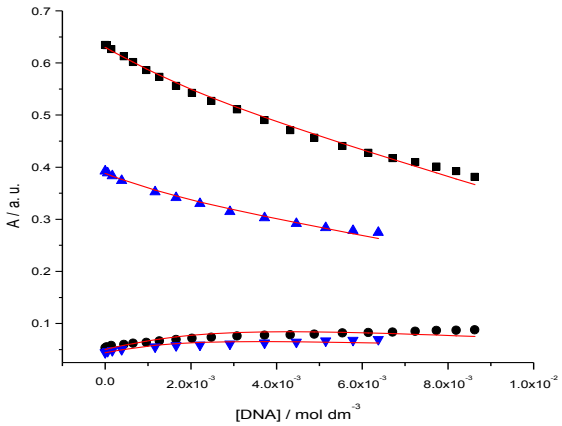

Figure 2.6 Absorbance at 347 nm (■) and at 390 nm (●) of a solution of 0.052 mM **2.3** as a function of DNA concentration, absorbance at 347 nm (▲) and at 390 nm (▼) of a solution of 0.031 mM **2.3** as a function of DNA concentration, in buffer (25 mM MOPS, pH 7.0, 50 mM NaCl) at 25 °C. The solid lines represent a global fit of a multiple independent sites model to the data.

The titration curves in Figure 2.6 were analysed globally by fitting of a multiple independent binding sites model, which also takes ligand dilution into account, to the data. The fit indicates an equilibrium constant ($K_{binding}$) of (4.20 ± 6.62) $\times 10^4$ M^{-1} and a binding site size of (41.68 ± 27.37) base pairs. The obtained value of binding site size was unreasonable therefore the data of the titration curves were reanalysed, giving an equilibrium constant ($K_{binding}$) of (1.20 ± 0.35) $\times 10^3$ M^{-1} for a binding site size restricted to 3 base pairs.

2.2.1.d UV-visible spectroscopy studies of 2.4 binding to DNA

The binding of **2.4** to DNA was studied using UV-visible spectroscopy; the changes in absorption of **2.4** upon addition of DNA were recorded in buffer (25 mM MOPS, pH 7.0, 50 mM NaCl) at 25 °C (Figure 2.7).

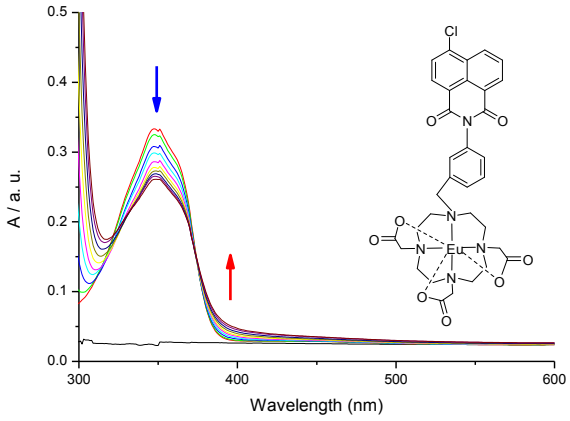

Figure 2.7 UV-visible spectra for 0.032 mM **2.4** upon addition of 0 – 2.84 mM DNA in buffer (25 mM MOPS, pH 7.0, 50 mM NaCl) at 25 °C.

Figure 2.7 shows a hypochromic shift in absorbance (at the λ_{max} of 347 nm) and a hyperchromic shift (at 390 nm) of **2.4** upon addition of DNA. This change in UV-visible absorption may occur as a result of geometrical distortion of **2.4** when it interacts with DNA, but it may also be a result of a local medium effect.

To quantify the affinity of **2.4** for FSDNA, the absorbances at 347 and 390 nm for two titrations were plotted as a function of concentration of FSDNA (Figure 2.8, for data in tabular format see appendix, Tables A15.8 & A15.9).

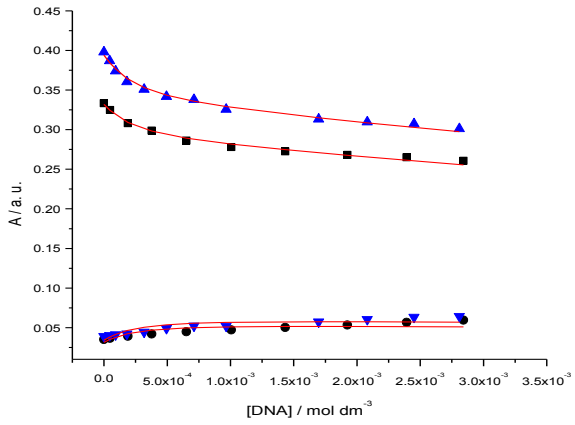

Figure 2.8 Absorbance at 347 nm (■) and at 390 nm (●) of a solution of 0.027 mM **2.4** as a function of DNA concentration, absorbance at 347 nm (▲) and at 390 nm (▼) of a solution of 0.034 mM **2.4** as a function of DNA concentration, in buffer (25 mM

MOPS, pH 7.0, 50 mM NaCl) at 25 °C. The solid lines represent a global fit to a multiple independent sites model.

The titration curves in Figure 2.8 were analysed globally in terms of a multiple independent binding sites models, which also takes ligand dilution into account, giving an equilibrium constant ($K_{binding}$) of (1.65 ± 26.2) $\times 10^3$ M^{-1} and a binding site size of (0.37 ± 5.69) base pairs. The obtained value of the stoichiometry was small therefore the data of the titration curves were reanalysed, with the binding site size restricted to 3 base pairs, giving an equilibrium constant ($K_{binding}$) of (1.7 ± 0.4) $\times 10^4$ M^{-1}.

2.2.1.e UV-visible spectroscopy studies of 2.5 binding to DNA

The binding of **2.5** to FSDNA was studied using UV-visible spectroscopy; the changes in absorption of **2.5** upon addition of FSDNA were measured in buffer (25 mM MOPS, pH 7.0, 50 mM NaCl) at 25 °C (Figure 2.9).

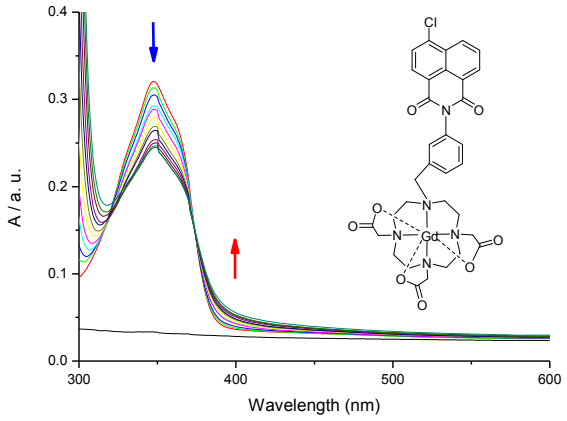

Figure 2.9 UV-visible spectra for 0.027 mM **2.5** upon addition of 0 – 2.64 mM DNA in buffer (25 mM MOPS, pH 7.0, 50 mM NaCl) at 25 °C.

Figure 2.9 shows a hypochromic shift in absorbance (at the λ_{max} of 347 nm) and a hyperchromic shift (at 390 nm) of **2.5** upon addition of DNA. This change in UV-visible absorption may occur as a result of geometrical distortion of **2.5** when it interacts with DNA, but it may also be a local medium effect.

To quantify the affinity of **2.5** for FSDNA, the absorbances at 347 and 390 nm for two titrations were plotted as a function of concentration of FSDNA (Figure 2.10, for data in tabular format see appendix, Tables A15.10 & A15.11).

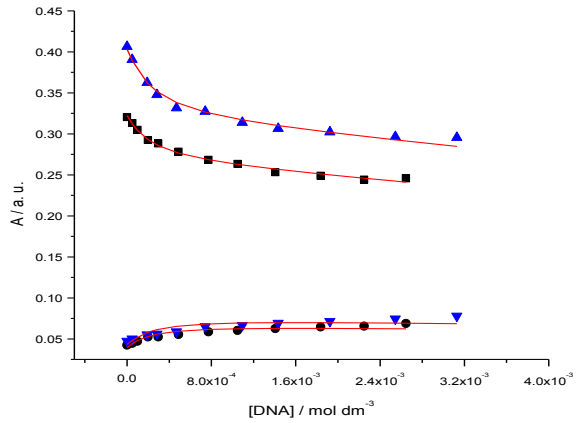

Figure 2.10 Absorbance at 347 nm (■) and at 390 nm (●) of a solution of 0.027 mM **2.5** as a function of DNA concentration, absorbance at 347 nm (▲) and at 390 nm (▼) of a solution of 0.034 mM **2.5** as a function of DNA concentration, in buffer (25 mM MOPS, pH 7.0, 50 mM NaCl) at 25 °C. The solid lines represent a global fit of a multiple independent sites model to the data.

The titration curves in Figure 2.10 were analysed globally in terms of a multiple independent binding sites models, which also takes ligand dilution into account, giving an equilibrium constant ($K_{binding}$) of (2.42 ± 3.53) $\times 10^4$ M^{-1} and a binding site size of (3.97 ± 4.15) base pairs. The large error margins suggest significant parameter covariance. We therefore re-analysed the data for a binding site size n restricted to 3 base pairs (for these types of DNA binders the average binding site size n is around 3 base pairs). The resulting fit gave an equilibrium constant ($K_{binding}$) of (1.67 ± 0.28) $\times 10^4$ M^{-1}.

2.2.1.f UV-visible spectroscopy studies of 2.6 binding to DNA

The binding of **2.6** to DNA was studied using UV-visible spectroscopy; the changes in absorption of **2.6** upon addition of DNA were measured in buffer (25 mM MOPS, pH 7.0, 50 mM NaCl) at 25 °C (Figure 2.11).

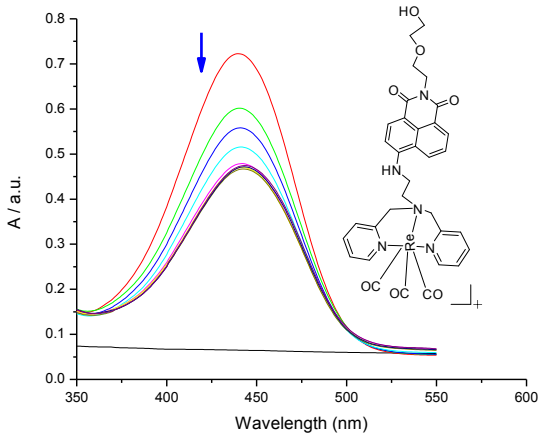

Figure 2.11 UV-visible spectra for 0.039 mM **2.6** upon addition of 0 – 0.172 mM DNA in buffer (25 mM MOPS, pH 7.0, 50 mM NaCl) at 25 °C.

Figure 2.11 shows a hypochromic shift in absorbance (at the λ_{max} of 440 nm) of **2.6** upon addition of DNA. This change in UV-visible absorption may occur as a result of geometrical distortion of **2.6** when it interacts with DNA, but it may also be a local medium effect.

To quantify the affinity of **2.6** for FSDNA, the absorbances at 440 nm for two titrations were plotted as a function of concentration of FSDNA (Figure 2.12, for data in tabular format see appendix, Tables A15.12 & A15.13).

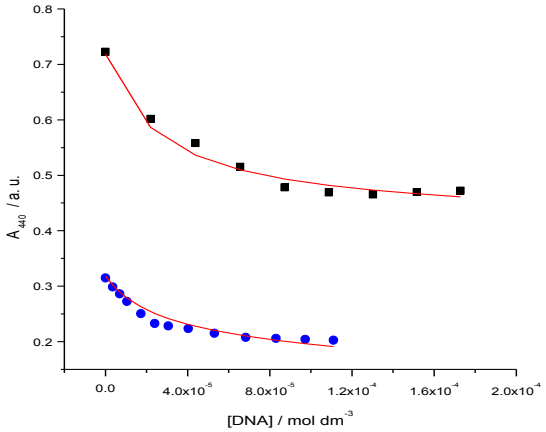

Figure 2.12 Absorbance at 440 nm of solutions of 0.039 mM **2.6** (■) and 0.017 mM **2.6** (●), as a function of DNA concentration, in buffer (25 mM MOPS, pH 7.0, 50 mM NaCl) at 25 °C. The solid lines represent a global fit of a multiple independent sites model to the data.

The titration curves in Figure 2.12 were analysed by fitting a multiple independent binding sites models, which also takes ligand dilution into account, to the data, giving an equilibrium constant ($K_{binding}$) of (0.03 ± 3) M^{-1} and a binding site size (0.08 ± 8) $\times 10^{-5}$ base pairs. The obtained values of the stoichiometry and binding constant were too small and unreasonable. Therefore the data were reanalysed, with a binding site size restricted to 3 base pairs, giving an equilibrium constant ($K_{binding}$) of (1.15 ± 3.08) $\times 10^{6}$ M^{-1} (Figure 2.13).

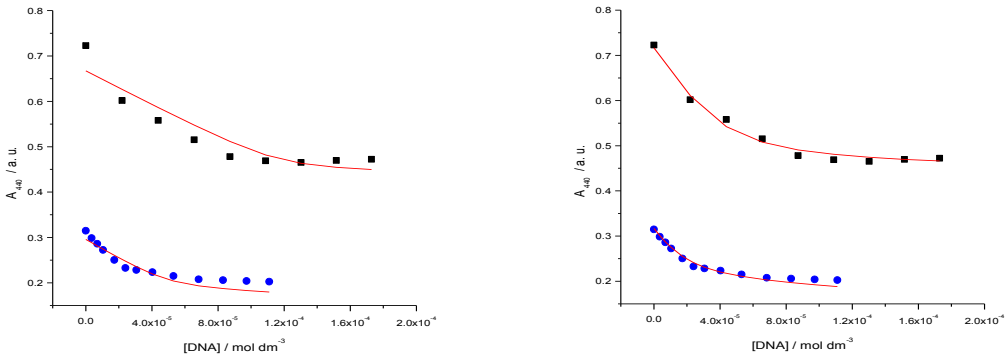

(a) (b)

Figure 2.13 Absorbance at 440 nm of a solution of 0.039 mM **2.6** (■) and 0.017 mM **2.6** (●), as a function of DNA concentration, in buffer (25 mM MOPS, pH 7.0, 50

mM NaCl) at 25 °C. The solid lines represent a global fit of a multiple independent sites model to the data, binding site size restricted to 3 base pairs (a), restricted to 1 base pair (b).

The solid lines in Figure 2.13-(a) do not reproduce the titration data well. Therefore the data were reanalysed at 1.0 base pair per binding site, giving an equilibrium constant ($K_{binding}$) of $(11.36 \pm 2.70) \times 10^4\ M^{-1}$.

2.2.1.g UV-visible spectroscopy studies of 2.7 binding to DNA

The binding of **2.7** to DNA was studied using UV-visible spectroscopy; the changes in absorption of **2.7** upon addition of DNA were measured in buffer (25 mM MOPS, pH 7.0, 50 mM NaCl) at 25 °C (Figure 2.14).

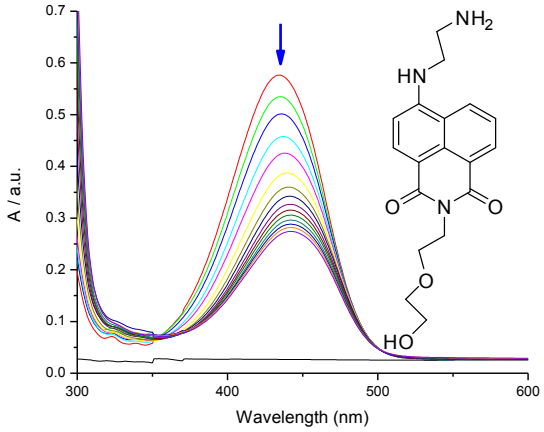

Figure 2.14 UV-visible spectra for 0.05 mM **2.7** upon addition of 0 – 2.42 mM DNA in buffer (25 mM MOPS, pH 7.0, 50 mM NaCl) at 25 °C.

Figure 2.14 shows a hypochromic shift in absorbance (at the λ_{max} of 434 nm) of **2.7** upon addition of DNA. This change in UV-visible absorption may occur as a result of geometrical distortion of **2.7** when it interacts with DNA, but it may also be a local medium effect.

To quantify the affinity of **2.7** for FSDNA, the absorbances at 434 nm for two titrations were plotted as a function of concentration of FSDNA (Figure 2.15, for data in tabular format see appendix, Tables A15.14 & A15.15).

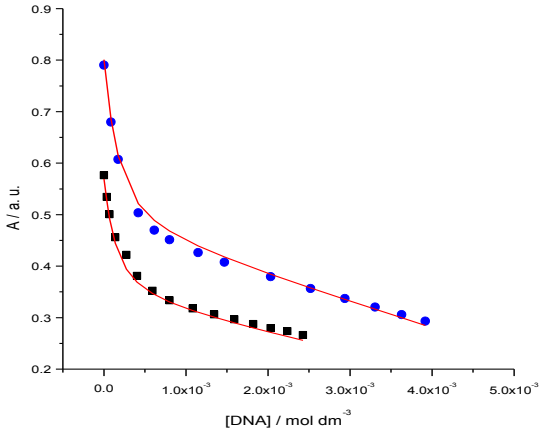

Figure 2.15 Absorbance at 434 nm of solutions of 0.05 mM **2.7** (■) and 0.07 mM **2.7** (●) as a function of DNA concentration, in buffer (25 mM MOPS, pH 7.0, 50 mM NaCl) at 25 °C. The solid lines represent a global fit of a multiple independent sites model to the data.

The titration curves in Figure 2.15 were analysed globally in terms of a multiple independent binding sites models, which also takes ligand dilution into account, giving an equilibrium constant ($K_{binding}$) of (1.93 ± 1.32) $\times 10^4$ M^{-1} and a binding site size of (1.81 ± 0.79) base pairs.

2.2.1.h UV-visible spectroscopy studies of 2.8 binding to DNA

The binding of **2.8** to DNA was studied using UV-visible spectroscopy; the changes in absorption of **2.8** upon addition of DNA were measured in buffer (25 mM MOPS, pH 7.0, 50 mM NaCl) at 25 °C (Figure 2.16).

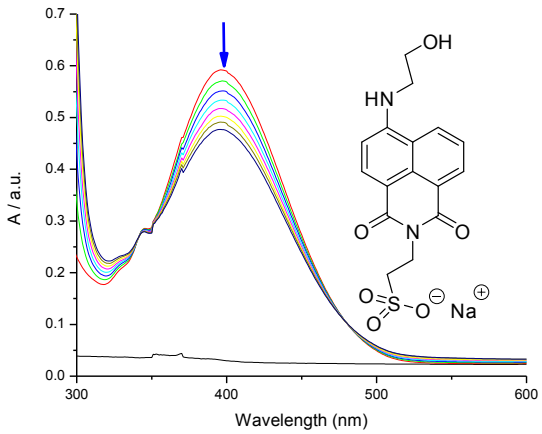

Figure 2.16 UV-visible spectra for 0.056 mM **2.8** upon addition of 0 – 1.84 mM DNA in buffer (25 mM MOPS, pH 7.0, 50 mM NaCl) at 25 °C.

Figure 2.16 shows a small hypochromic shift in absorbance (at the λ_{max} of 400 nm) of **2.8** upon addition of DNA. This change in UV-visible absorption may occur as a result of geometrical distortion of **2.8** when it interacts with DNA, but it may also be a local medium effect or simply dilution.

To quantify the affinity of **2.8** for FSDNA, the absorbances at 400 nm were plotted as a function of concentration of FSDNA (Figure 2.17, for data in tabular format see appendix, Tables A15.16).

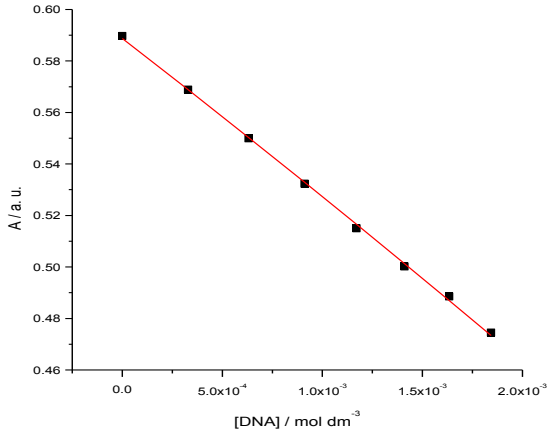

Figure 2.17 Absorbance at 400 nm of a solution of 0.056 mM **2.8** as a function of DNA concentration (■), in buffer (25 mM MOPS, pH 7.0, 50 mM NaCl) at 25 °C. The solid line represents a best fit of a multiple independent sites model to the data.

The fits to the data in Figure 2.17 show a straight line, suggesting negligible binding and only dilution causing a change in the absorbance of the sample. The titration data of Figure 2.17 were analysed globally in terms of a multiple independent binding sites model, which also takes ligand dilution into account, giving an equilibrium constant ($K_{binding}$) of (0.53 ± 489) M^{-1} for a binding site size restricted to 3 base pairs. Because equilibrium constants cannot be negative, we express the error margin as a confidence interval so that the equilibrium constant is 0.53 [0 – 489] M^{-1}. The highest reasonable value of equilibrium constant is therefore 489 M^{-1}, corresponding to a c-value of 0.027. This value indicates negligible binding for the concentrations used in this experiment.

2.2.1.i UV-visible spectroscopy studies of 2.9 binding to DNA

The binding of **2.9** to DNA was studied using UV-visible spectroscopy; the changes in absorption of **2.9** upon addition of DNA were measured in buffer (25 mM MOPS, pH 7.0, 50 mM NaCl) at 25 °C (Figure 2.18).

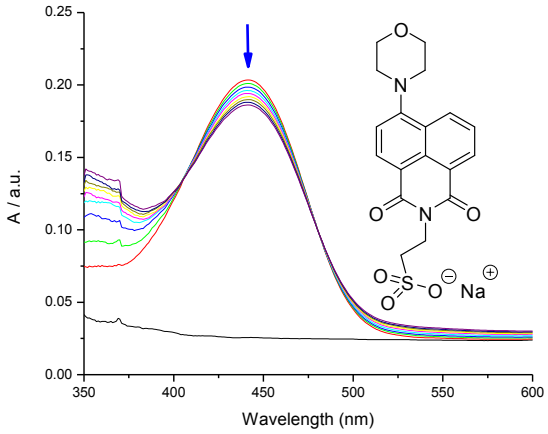

Figure 2.18 UV-visible spectra for 0.017 mM **2.9** upon addition of 0 – 1.17 mM DNA in buffer (25 mM MOPS, pH 7.0, 50 mM NaCl) at 25 °C.

Figure 2.18 shows a small hypochromic shift in absorbance (at the λ_{max} of 445 nm) of **2.9** upon addition of DNA. This change in UV-visible absorption may occur as a result of geometrical distortion of **2.9** when it interacts with DNA, but it may also be a local medium effect or simply dilution. In addition, the change in absorbance in the range of 350 – 390 nm is due to poor performance of the UV-visible machine in this region.

To quantify the affinity of **2.9** for FSDNA, the absorbances at 445 nm were plotted as a function of concentration of FSDNA (Figure 2.19, for data in tabular format see appendix, Tables A15.17).

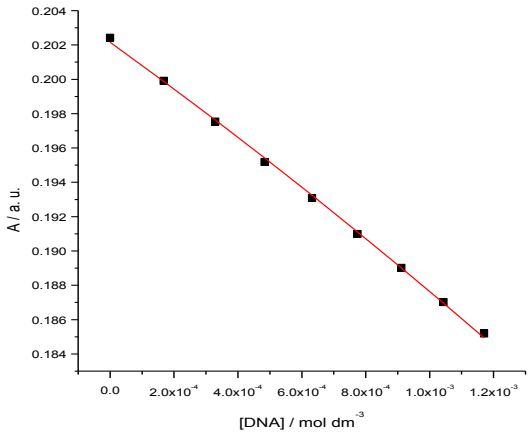

Figure 2.19 Absorbance at 445 nm of a solution of 0.017 mM **2.9** as a function of DNA concentration (■), in buffer (25 mM MOPS, pH 7.0, 50 mM NaCl) at 25 °C. The solid line represents a best fit of a multiple independent sites model to the data.

Figure 2.19 shows a straight line fit to the data, suggesting only dilution of the ligand is occurring. The titration data of Figure 2.19 were analysed in terms of a multiple independent binding sites model, which also takes ligand dilution into account to the data, giving an equilibrium constant ($K_{binding}$) of (0.33 ± 140) M^{-1} for a binding site size restricted to 3 base pairs. Because equilibrium constants cannot be negative, we express the error margin as a confidence interval so that the equilibrium constant is 0.33 [0 – 140] M^{-1}. The highest reasonable value of the equilibrium constant is therefore 140 M^{-1}, corresponding to a c-value of 0.002. This value indicates negligible binding for the concentrations used in this experiment.

Summary

The UV-visible titrations for 1,8-naphthalimide derivatives with duplex DNA show that ligands **2.1-2.7** bind to FS-DNA. The affinities of these compounds for FS-DNA are summarised in Table 2.1.

Table 2.1 Binding affinities and binding site sizes for binding of 2.1-2.9 to FS-DNA in buffer (25 mM MOPS, pH 7.0, 50 mM NaCl) at 25 °C.

Ligand	Binding constant K / M^{-1}	Binding site size n / bp

2.1	$(8.58 \pm 0.85) \times 10^3$	3*
2.2	$(10.94 \pm 2.82) \times 10^3$	3*
2.3	$(1.20 \pm 0.35) \times 10^3$	3*
2.4	$(1.71 \pm 0.398) \times 10^4$	3*
2.5	$(1.67 \pm 0.28) \times 10^4$	3*
2.6	$(11.3 \pm 2.7) \times 10^4$	1*
2.7	$(1.93 \pm 1.32) \times 10^4$	1.81 ± 0.79
2.8	No binding	
2.9	No binding	

* restricted.

Table 2.1 shows that the highest affinity is for the rhenium complex **2.6** with a binding constant of ~ 10^5 M^{-1}. We may attribute this high affinity to the presence of more aromatic rings which leads to an increase in hydrophobic interactions between ligand and DNA. The weakest binders are **2.1**-**2.3** with a binding constant ~ 10^3. These low affinities of **2.1**-**2.3** to duplex FS-DNA may be attributed to presence a negatively charged group (COO^-) on the ligand, leading to an increase of repulsion force between ligand and DNA.

Compounds **2.4**, **2.5** and **2.7** have moderate affinity (~ 10^4 M^{-1}) for DNA. The differences in affinity between ligand **2.3** and its metal complexes **2.4** and **2.5** are clearly observed. A lower negative charge density on the metal complex compared to the ligand may cause an increase of affinity of metal complex to DNA. However compounds **2.8** and **2.9** do not show any affinity for duplex FS-DNA. We may attribute this to the negative charge of the sulphonate group on the ligand, leading to an increase in repulsion force between ligand and DNA. The binding site size for some ligands is restricted to 3.0 base pairs in order to obtain a good fit to the titration curve.

2.2.2 *Isothermal titration calorimetry (ITC)*

To investigate further the binding of 1,8-naphthalimide derivatives with DNA, we used isothermal titration calorimetry (ITC). In order to obtain thermodynamic parameters for binding of these compounds with DNA, the titration data were analysed using our IC ITC software.

2.2.2.a Dilution of 2.1

In order to evaluate self-aggregation of **2.1** in MOPS buffer, the dilution of a 2.23 mM solution of **2.1** in MOPS buffer (25 mM MOPS, 50 mM NaCl, pH 7.0) was studied using isothermal titration calorimetry. The differential heat flow and derived integrated heat effects for this dilution were recorded at 25 °C (Figure 2.20).

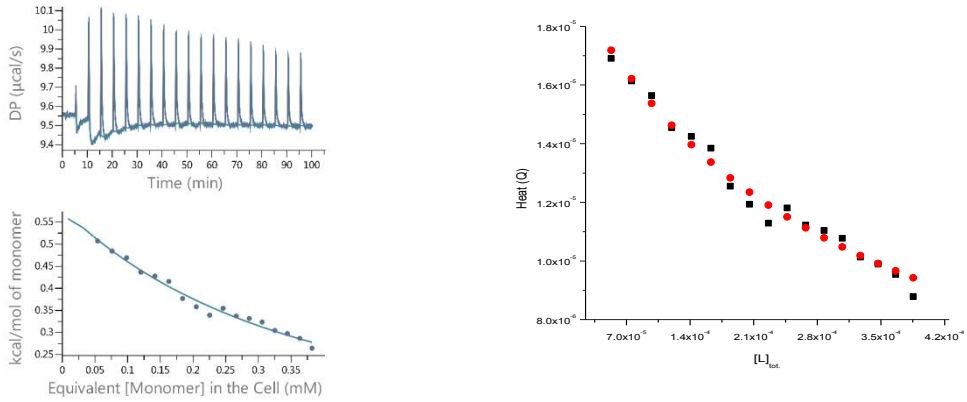

(a) (b)

Figure 2.20 Enthalpogram for dilution of a 2.23 mM solution of **2.1** (a), fit for the integrated heat effects for the same experiment (b) in buffer (25 mM MOPS, 50 mM NaCl, pH 7.0), at 25 °C, experimental heat (■), calculated heat (●).

Figure 2.20 shows heats of dilution of 2.23 mM **2.1** in MOPS buffer. Our IC ITC software was used to analyse the data, giving self-aggregation parameters as summarised in Table 2.2.

Table 2.2 Thermodynamic parameters for self aggregation of 2.1 in MOPS buffer, pH 7.0, at 25 °C.

K aggregation/ x 10^3 M^{-1}	ΔH aggregation/ kcal mol^{-1}
1.06 (0.51 – 2.95)	-0.837 (-0.83 – -129)

Table 2.2 shows self aggregation parameters for **2.1** in MOPS buffer. The results of dilution analysis show that **2.1** self aggregates to a significant extent and that an appreciable amount of heat of deaggregation is involved in the dilution process.

2.2.2.b ITC studies of 2.1 binding to DNA

To further explore the binding of **2.1** with DNA, the binding of **2.1** to DNA was studied using isothermal titration calorimetry. The differential heat flow and derived integrated heat effects for titrations of solutions of **2.1** (all 2.23 mM) into fish sperm DNA solutions (0.2, 0.3 & 0.4) mM were measured in buffer (25 mM MOPS, 50 mM NaCl, pH 7.0), at 25 °C (Figure 2.21).

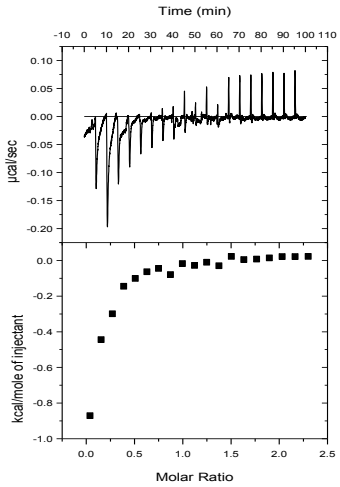

(a)

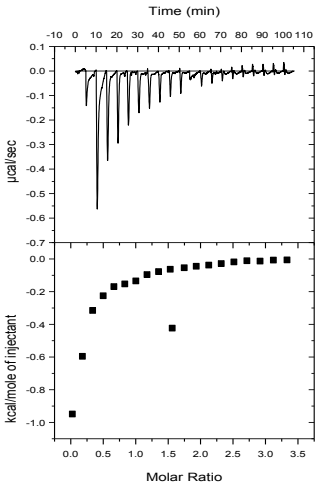

(b)

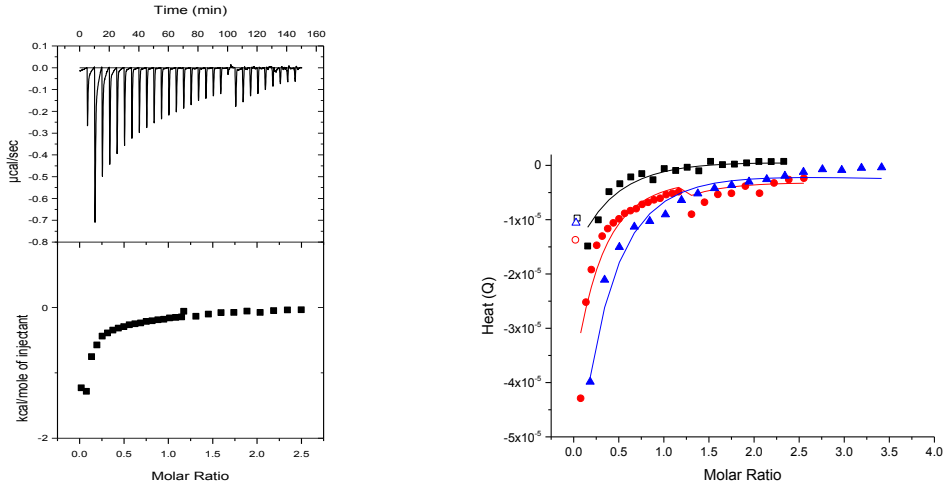

(c) (d)

Figure 2.21 Titration of a 2.23 mM solution of **2.1** into a 0.2 mM solution of DNA (a), titration of a 2.23 mM solution of **2.1** into a 0.3 mM solution of DNA (b), titration of a 2.23 mM solution of **2.1** into a 0.4 mM solution of DNA (c), global fit for integrated heat effects of titrations (a) and (b) and (c) in terms of a binding model involving one type of binding site, aggregation included (d), in buffer (25 mM MOPS, 50 mM NaCl, pH 7), at 25 °C.

Figure 2.21 shows enthalpograms for the interaction of **2.1** with DNA, which suggest weakly exothermic interactions. In order to quantify the binding parameters of **2.1** binding to DNA we used our IC ITC software to analyse the titration data globally. The results of global data analysis showed a big binding site size (see appendix, Table A1.1). Therefore, the data were reanalyzed with the stoichiometry within error margin (see appendix, Figure A1.3), restricted to 3.0 base pairs. The resulting binding parameters are summarised in Table 2.3.

Table 2.3 Thermodynamic parameters for binding of 2.1 to FSDNA in 25 mM MOPS, 50 mM NaCl, pH 7.0, at 25 °C

	K_{A1} ($10^3 M^{-1}$)	$1/n_{A1}$ (bp)	ΔH_{A1} (kcal mol^{-1})	$-T\Delta S_{A1}$ (kcal mol^{-1})	$\{\Sigma dev^2/dof\}^{1/2}$ (µcal)
2.1	3.16 (0.46 – 9.43)	3*	-4.75 (-4.75 – -485)	-0.018	2.31

* restricted.

2.2.2.c Dilution of 2.2

In order to explore self aggregation of **2.2** in MOPS buffer, the dilution of **2.2** in MOPS buffer was studied using isothermal titration calorimetry. The differential heat flow and derived integrated heat effects for dilution of a series of solutions of **2.2** (1.25 & 2.51) mM into buffer (25 mM MOPS, 50 mM NaCl, pH 7.0), at 25 °C were measured (Figure 2.22).

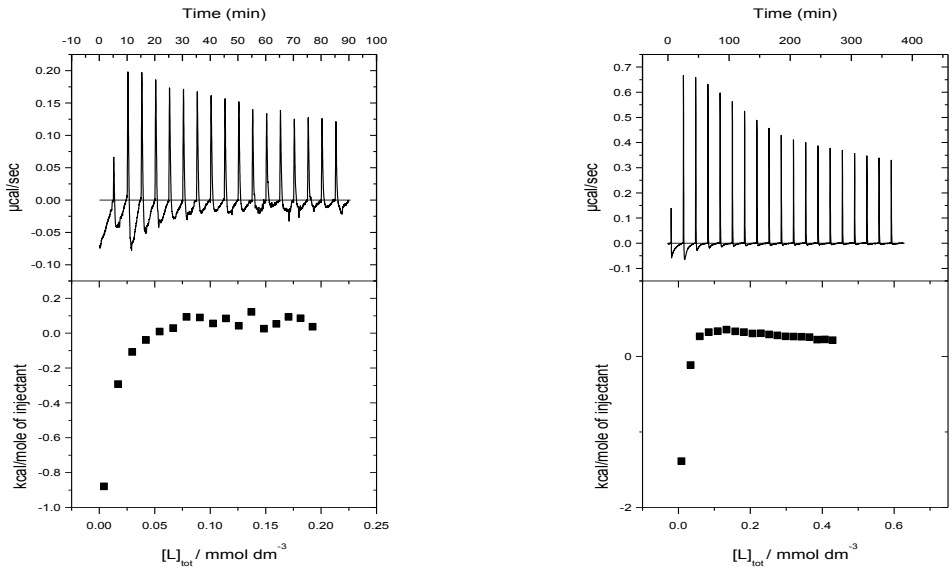

(a) (b)

Figure 2.22 Enthalpograms for dilution of a 1.25 mM solution of **2.2** (a), dilution of a 2.51 mM solution of **2.2** (b), into buffer (25 mM MOPS, 50 mM NaCl, pH 7.0) at 25 °C.

Figure 2.22 shows heats of dilution of 1.25 & 2.51 mM **2.2** in MOPS buffer. Because of the complexity of the heat effects of dilution and non-reproducibility of dilution enthalpograms we were unable to analyse the data of dilutions.

2.2.2.d ITC studies of 2.2 binding to DNA

To investigate further the binding of **2.2** with DNA, the binding of **2.2** to DNA was studied using isothermal titration calorimetry. The differential heat flow and derived integrated heat effects for titrations of solutions of **2.2** (all 2.51 mM) into fish sperm DNA solutions (0.2 & 0.5) mM were measured in buffer (25 mM MOPS, 50 mM NaCl, pH 7.0), at 25 °C (Figure 2.23).

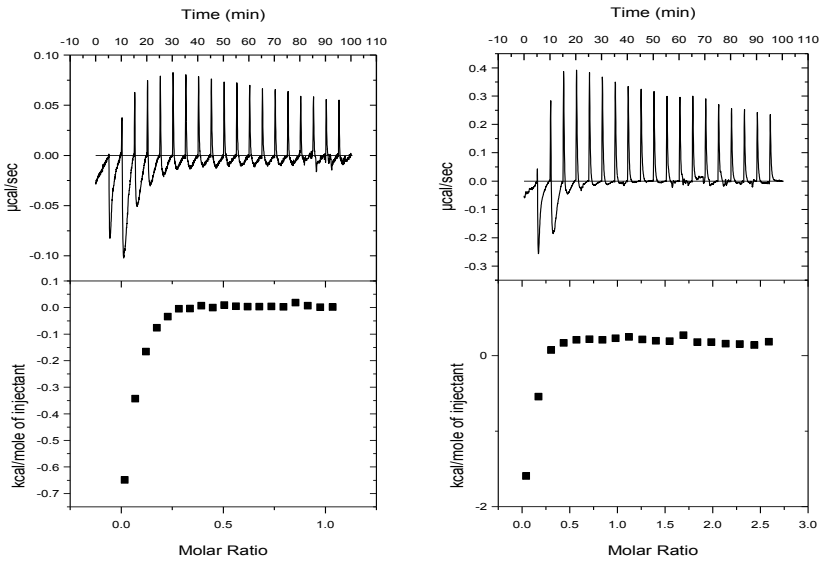

(a) (b)

Figure 2.23 Titration of a 2.51 mM solution of **2.2** into a 0.5 mM solution of DNA (a), titration of a 2.51 mM solution of **2.2** into a 0.2 mM solution of DNA (b), in buffer (25 mM MOPS, 50 mM NaCl, pH 7.0), at 25 °C.

The enthalpograms for the interaction of **2.2** with DNA in Figure 2.23 suggest negligible binding of **2.2** with DNA or weakly exothermic interactions.

2.2.2.e Dilution of 2.6

To determine the heats of dilution for **2.6** in MOPS buffer, the dilution of **2.6** to MOPS buffer was studied using isothermal titration calorimetry. The differential heat flow and derived integrated heat effects for dilution of a solution of 0.184 mM **2.6** into buffer (25 mM MOPS, 50 mM NaCl, pH 7.0), at 25 °C were measured (Figure 2.24).

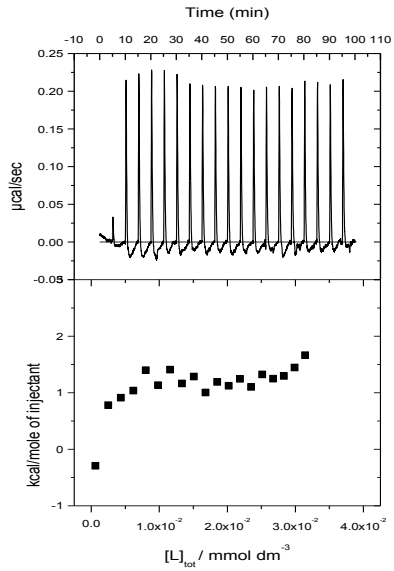

Figure 2.24 Enthalpogram for dilution of a 0.184 mM solution of **2.6** in buffer (25 mM MOPS, 50 mM NaCl, pH 7.0), at 25 °C.

The enthalpogram in the figure 2.24 shows small heat effects resulting from dilution which suggests that self-aggregation is negligible at the concentration used.

2.2.2.f ITC studies of 2.6 binding to DNA

To further explore the binding of **2.6** with DNA, the binding of **2.6** to DNA was studied using isothermal titration calorimetry. The differential heat flow and derived integrated heat effects for titrations of solutions of **2.6** (all 0.184 mM) into fish sperm DNA solutions (both 0.1 mM) were measured in buffer (25 mM MOPS, 50 mM NaCl, pH 7.0), at 25 °C (Figure 2.25).

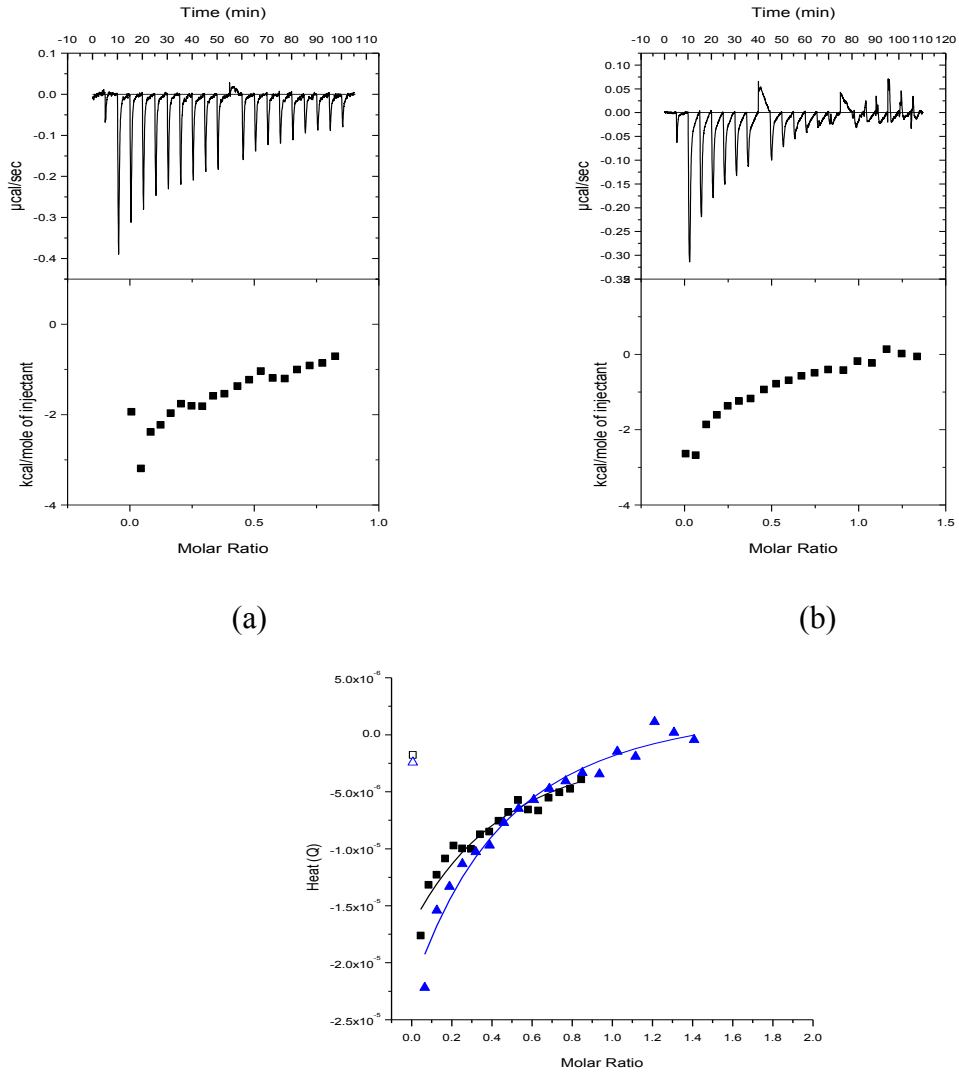

Figure 2.25 Titration of a 0.184 mM solution of **2.6** into a 0.1 mM solution of DNA (a), repeat titration of a 0.184 mM solution of **2.6** into a 0.1 mM solution of DNA (b), global fit for integrated heat effects of titrations (a) and (b) in terms of a binding model involving one type of binding site, aggregation not included (c), in 25 mM MOPS, 50 mM NaCl, pH 7.0, at 25 °C.

Figure 2.25 shows two enthalpograms (a) and (b) for the interactions of **2.6** with DNA. Both titrations were carried out at the same DNA concentration and conditions. The titrations (a) and (b) show exothermic interactions, suggesting one binding event. In order to determine binding parameters for the interaction of **2.6** with DNA, the titrations data were analysed globally using IC ITC software. The results of global data analysis for

titrations (a) and (b) showed a big binding site size (see appendix, Table A6.1). Therefore the data were reanalyzed with the stoichiometry restricted to 3.0 base pairs. The resulting binding parameters are summarised in Table 2.4.

Table 2.4 Thermodynamic parameters for binding of 2.6 to FSDNA in 25 mM MOPS, 50 mM NaCl, pH 7.0, at 25 °C.

	K_{A1} (10^3 M^{-1})	$1/n_{A1}$ (bp)	ΔH_{A1} (kcal mol^{-1})	$-T\Delta S_{A1}$ (kcal mol^{-1})	$\{\Sigma dev^2/dof\}^{½}$ (μcal)
2.6	12.5 (11.2 – 122)	3.0*	-9.94 (-7.9 – -267)	4.35	1.02

* restricted.

The thermodynamic parameters in Table 2.4 obtained from data analysis where the binding site size was not restricted were not reasonable values. When the stoichiometry was restricted to 3.0 all thermodynamic parameters values become reasonable. The negative value of enthalpy change for interaction of **2.6** with FSDNA suggests that intercalation is a likely mode of binding. It should be pointed out that ligand self-aggregation was not taken in to account in the data analysis because the heat effects of aggregation were small and constant.

2.2.2.g Dilution of 2.7

To quantify aggregation of **2.7** in MOPS buffer, the dilution of a solution of 1.53 mM **2.7** in MOPS buffer (25 mM MOPS, 50 mM NaCl, pH 7.0) was studied using isothermal titration calorimetry. The differential heat flow and derived integrated heat effects for this dilution were recorded at 25 °C (Figure 2.26).

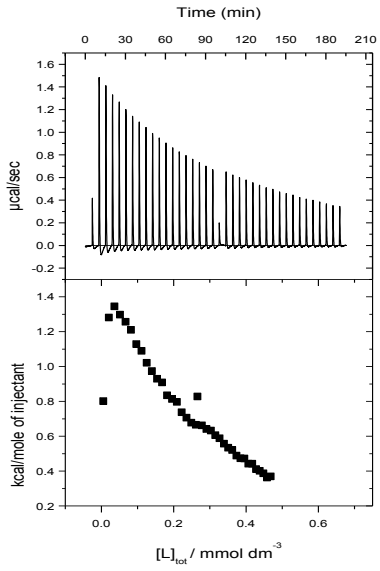

(a)

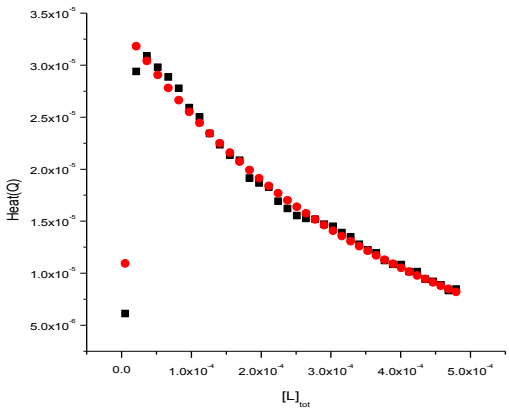

(b)

Figure 2.26 Heat effects for dilution of a 1.53 mM solution of **2.7** into a 25m M MOPS, 50 mM NaCl, pH 7.0, at 25 °C (a) and, fit for the integrated heat effects for the same experiment (b), experimental heat (■), calculated heat (●).

Figure 2.26 shows non-constant heat effects for diluting **2.7** into MOPS buffer, indicating ligand self-aggregation. The data were analysed using IC ITC software, giving diluting parameters as summarised in Table 2.5.

Table 2.5 Thermodynamic parameters for diluting 2.7 into MOPS buffer, pH 7.0, at 25 °C.

K aggregation/ M^{-1}	ΔH aggregation/ kcal mol^{-1}
453 (87 – 1050)	-4.68 (-4.68 – -22.2)

Table 2.5 shows aggregation parameters for **2.7** in MOPS buffer. The results of dilution analysis show that a considerable amount of heat of aggregation is involved in the dilution process but that self aggregation is not too strong.

2.2.2.h ITC studies of 2.7 binding to DNA

The binding of **2.7** to DNA was studied using isothermal titration calorimetry. The differential heat flow and derived integrated heat effects for titrations of solutions of **2.7** (all 1.53 mM) into fish sperm DNA solutions (both 0.2 mM) were measured in buffer (25 mM MOPS, 50 mM NaCl, pH 7.0), at 25 °C (Figure 2.27).

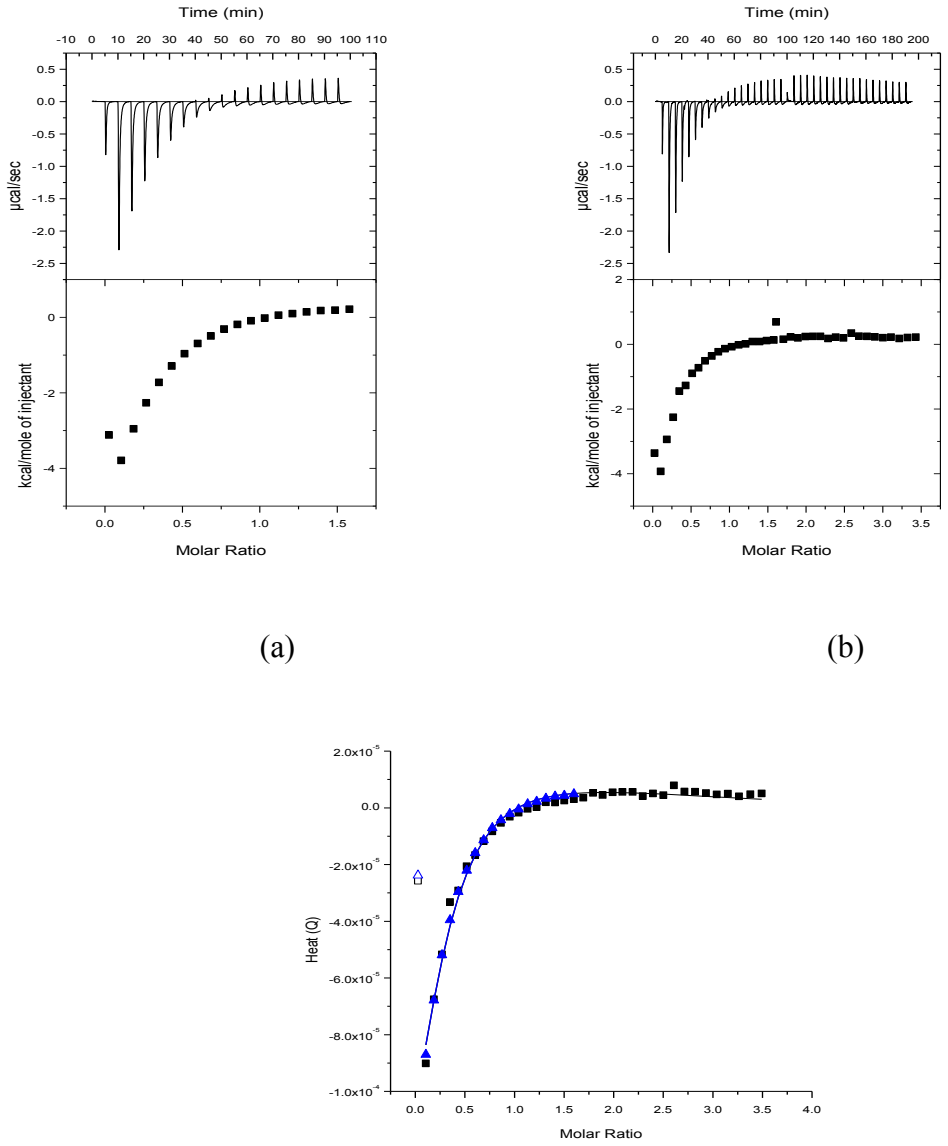

Figure 2.27 Titration of a 1.53 mM solution of **2.7** into a 0.2 mM solution of DNA (a), repeat titration of a 1.53 mM solution of **2.7** into a 0.2 mM solution of DNA (b), global fit for integrated heat effects of titrations (a) and (b) in terms of a binding model involving

one type of binding site with aggregation included(c), in 25 mM MOPS, 50 mM NaCl, pH 7.0, at 25 °C.

The enthalpograms for interactions of **2.7** with DNA (Figure 2.27) suggest one binding event. In order to quantify the binding parameters of **2.7** interacting with DNA, the data were analysed using IC ITC software. The obtained binding site size from the global fit (see appendix, Table A7.1) was considered unreasonably big. Therefore the data were reanalysed with a stoichiometry within error margin (see appendix, Figure A7.2), restricted to 4 base pairs. All thermodynamic parameters were determined and are summarised in Table 2.6.

Table 2.6 Thermodynamic parameters for binding of 2.7 to FSDNA in MOPS buffer, pH 7.0, at 25 °C.

	K_{A1} ($10^3 M^{-1}$)	$1/n_{A1}$ (bp)	ΔH_{A1} (kcal mol^{-1})	$-T\Delta S_{A1}$ (kcal mol^{-1})	$\{\Sigma dev^2/dof\}^{½}$ (µcal)
2.7	11.8 (8.69 – 15.9)	4*	-15.7 (-13.1 – -19.1)	10.15	1.13

* restricted.

The binding constant and binding site size in the table 2.6 show a good agreement with UV-visible results. The exothermic interaction suggests **2.7** binds to FSDNA via intercalation.

Summary

The interactions of **2.1-2.2** and **2.6-2.7** with DNA were further investigated by isothermal titration calorimetry. The thermodynamic parameters for these compounds interacting with DNA and for their dilution in MOPS buffer were determined and are summarised in Tables 2.7 and 2.8.

Table 2.7 Thermodynamic parameters for self aggregations of 2.1-2.2 and 2.6-2.7 in MOPS buffer, pH 7.0, at 25 °C.

Ligand	*K* aggregation/ x 10^3 M^{-1}	Δ*H* aggregation/ kcal mol^{-1}
2.1	1.06 (0.51 – 2.95)	-0.837 (-0.83 – -129)
2.2	n.d.	n.d.
2.6	n.d.	n.d.
2.7	0.453 (0.08 – 1.0)	-4.68 (-4.68 – -22.2)

n.d. not determined.

Table 2.8 Thermodynamic parameters for binding of 2.1-2.2 and 2.6-2.7 to FSDNA in 25 mM MOPS, pH 7.0, 50 mM NaCl at 25 °C.

Ligand	K_{A1} (M^{-1})	$1/n_{A1}$ (bp)	ΔH_{A1} (kcal mol^{-1})	$-T\Delta S_{A1}$ (kcal mol^{-1})	$\{\Sigma dev^2/dof\}^{½}$ (µcal)
2.1	(3.16×10^3)	3.0*	-4.75	-0.018	2.31
2.2	No binding	-	-	-	-
2.6	(12.5×10^3)	3.0*	-9.94	4.35	1.02
2.7	(11.8×10^3)	4.0*	-15.7	10.15	1.13

* restricted.

Compound **2.1** shows an exothermic interaction with fish sperm DNA, this interaction can be clearly seen from its heat effects. The enthalpograms for the interaction of **2.2** with DNA suggest negligible binding of **2.2** with DNA or very weakly exothermic interactions. Compound **2.6** interacts with fish sperm DNA and exothermic interaction can be observed. The titration data of **2.6** interacting with FS-DNA were analysed using IC-ITC software where the heat of dilution was neglected, giving a binding constant of 12.5×10^3 M^{-1} for a binding site size restricted to 3.0 base pairs. Compound **2.7** also binds to FS-DNA and shows an exothermic interaction. The

enthalpograms of **2.7** were analysed and the heat of aggregation was also taken into account, giving a binding constant of 11.8×10^3 M^{-1} for a binding size of 4.0 base pairs. The binding site sizes for all titrations were restricted to a number with in the margin of error in order to obtain reasonable binding parameters. Furthermore, the binding constants of these compounds obtained from ITC titrations are smaller compared to the binding constants obtained from UV-visible titrations.

2.2.3 *Induced circular dichroism (ICD)*

2.2.3.a Induced circular dichroism for 2.1 interacting with FSDNA

The binding mode of interaction of **2.1** with FSDNA was studied using circular dichroism spectroscopy. Circular dichroism spectra for **2.1** were recorded at different FSDNA concentrations (0 mM – 1.58 mM) in buffer (25 mM MOPS, pH 7.0 and 50 mM NaCl) at 25 °C (Figure 2.28).

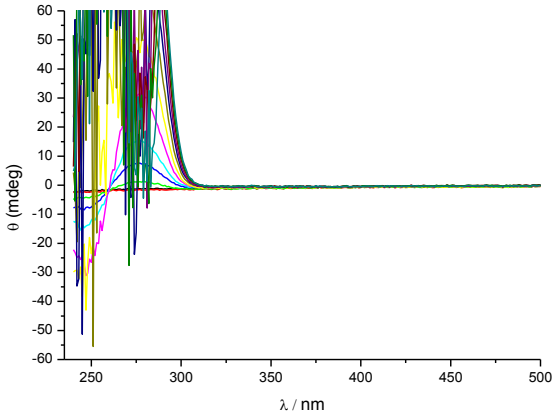

Figure 2.28 Circular dichroism spectra for 0.065 mM of **2.1** in the presence of different concentrations of FSDNA (0 mM – 1.58 mM) in buffer (25 mM MOPS, 50 mM NaCl, pH 7.0) at 25 °C.

Figure 2.28 does not show any significant induced circular dichroism around the wavelength of interest 347 nm where compound **2.1** absorbs.

2.2.3.b Induced circular dichroism for 2.2 interacting with FSDNA

The binding mode of interaction of **2.2** with FSDNA was also studied using circular dichroism spectroscopy. Circular dichroism spectra for **2.2** were recorded at different FSDNA concentrations (0 mM – 1.83 mM) in buffer (25 mM MOPS, pH 7.0 and 50 mM NaCl) at 25 °C (Figure 2.29).

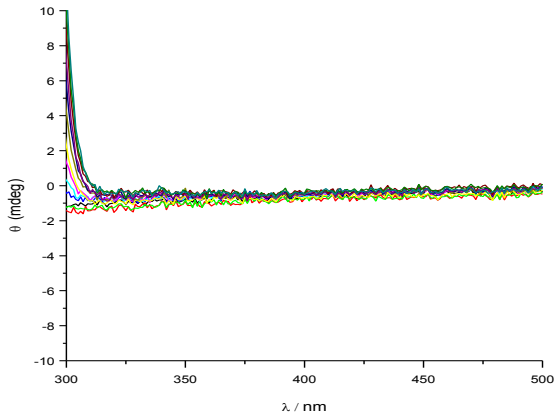

Figure 2.29 Circular dichroism spectra for 0.065 mM of **2.2** in the presence of FSDNA (0 mM – 1.83 mM) in buffer (25 mM MOPS, 50 mM NaCl, pH 7.0) at 25 °C.

The spectra in the figure 2.29 do not show any significant induced circular dichroism around the wavelength of interest 347 nm.

2.2.3.c Induced circular dichroism for 2.3 interacting with FSDNA

The binding mode of interaction of **2.3** with FSDNA was studied using circular dichroism spectroscopy. Circular dichroism spectra for **2.3** were recorded at different FSDNA concentrations (0 mM – 1.8 mM) in buffer (25 mM MOPS, pH 7.0 and 50 mM NaCl) at 25 °C (Figure 2.30).

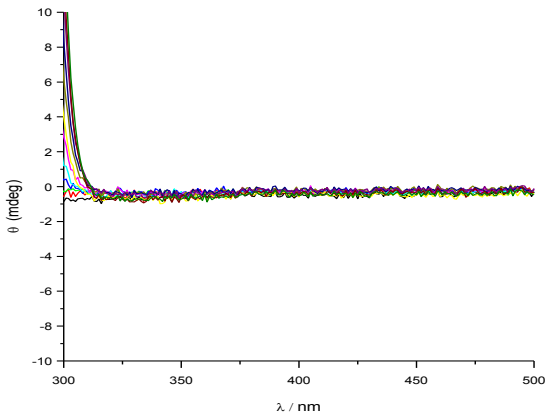

Figure 2.30 Circular dichroism spectra for 0.046 mM of **2.3** in the presence of FSDNA (0 mM – 1.8 mM) in buffer (25 mM MOPS, 50 mM NaCl, pH 7.0) at 25 °C.

The circular dichroism spectra in Figure 2.30 again do not show any significant induced signal around the wavelength of interest 347 nm.

2.2.3.d Induced circular dichroism for 2.4 interacting with FSDNA

The binding mode of interaction of **2.4** with FSDNA was studied using circular dichroism spectroscopy. Circular dichroism spectra for a solution of **2.4** were recorded at different FSDNA concentrations (0 mM – 1.27 mM) in buffer (25 mM MOPS, pH 7.0 and 50 mM NaCl) at 25 °C (Figure 2.31).

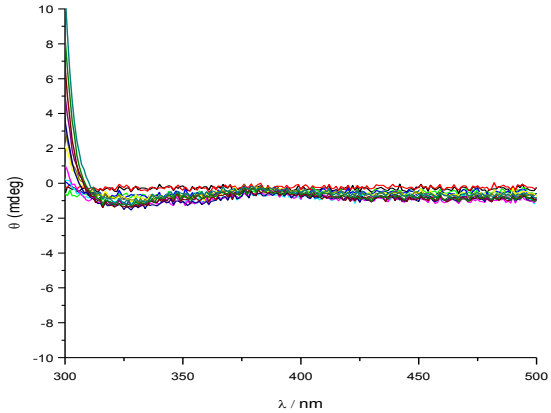

Figure 2.31 Circular dichroism spectra for 0.029 mM **2.4** in the presence of different concentrations of FSDNA (0 mM – 1.27 mM) in buffer (25 mM MOPS, 50 mM NaCl, pH 7.0) at 25 °C.

As before, circular dichroism spectra in Figure 2.31 do not show any significant induced signal around the wavelength of interest 347 nm.

2.2.3.e Induced circular dichroism for 2.5 interacting with FSDNA

The binding mode of interaction of **2.5** with FSDNA was studied using circular dichroism spectroscopy. Circular dichroism spectra for **2.5** were measured at different FSDNA concentrations (0 mM – 1.24 mM) in buffer (25 mM MOPS, pH 7.0 and 50 mM NaCl) at 25 °C (Figure 2.32).

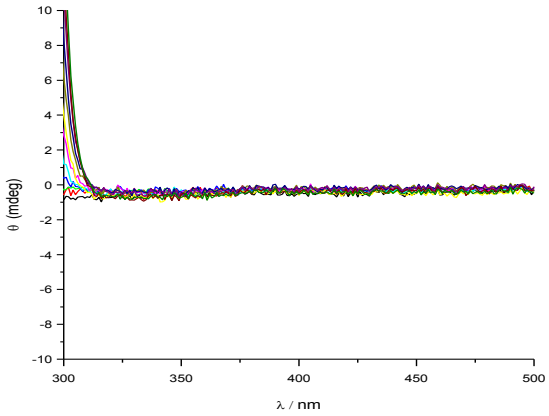

Figure 2.32 Circular dichroism spectra for a solution of 0.031 mM of **2.5** in the presence of different concentrations of FSDNA (0 mM – 1.24 mM) in buffer (25 mM MOPS, 50 mM NaCl, pH 7.0) at 25 °C.

The circular dichroism spectra in the figure 2.32 do not show any significant induced signal around the wavelength of interest 347 nm.

2.2.3.f Induced circular dichroism for 2.6 interacting with FSDNA

The binding mode of interaction of **2.6** with FSDNA was studied using circular dichroism spectroscopy. Circular dichroism spectra for **2.6** were measured at different FSDNA concentrations (0 mM – 0.46 mM) in buffer (25 mM MOPS, pH 7.0 and 50 mM NaCl) at 25 °C (Figure 2.33).

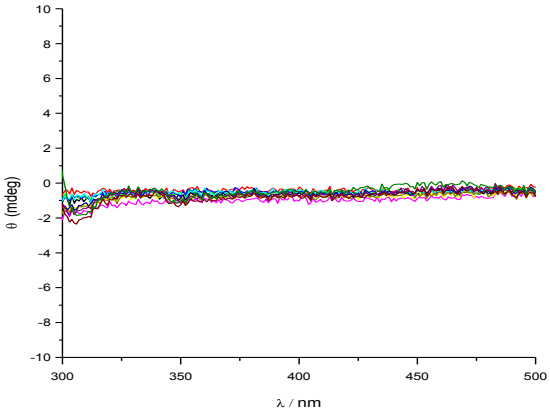

Figure 2.33 Circular dichroism spectra for 0.012 mM of **2.6** in the presence of FSDNA (0 mM – 0.46 mM) in buffer (25 mM MOPS, 50 mM NaCl, pH 7.0) at 25 °C.

The circular dichroism spectra in the figure 2.33 do not show significant induced signal around the wavelength of interest 440 nm.

2.2.3.g Induced circular dichroism for 2.7 interacting with FSDNA

The binding mode of interaction of **2.7** with FSDNA was studied using circular dichroism spectroscopy. Circular dichroism spectra for **2.7** were recorded at FSDNA concentrations between 0 and 1.85 mM in buffer (25 mM MOPS, pH 7.0 and 50 mM NaCl) at 25 °C (Figure 2.34).

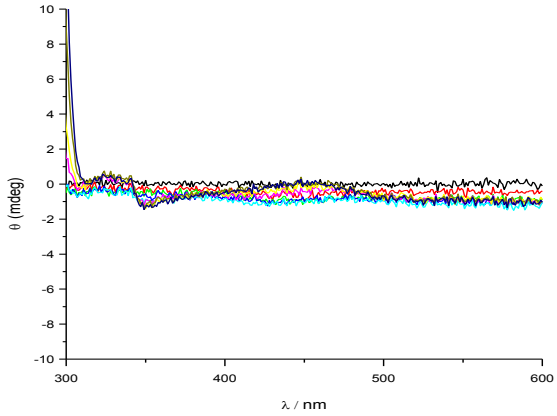

Figure 2.34 Circular dichroism spectra for 0.051 mM of **2.7** in the presence of 0 – 1.85 mM FSDNA in buffer (25 mM MOPS, 50 mM NaCl, pH 7.0) at 25 °C.

The circular dichroism spectra in Figure 2.34 do not show induced ellipticity around the wavelength of interest 434 nm.

Summary

All compounds in this group do not show any significant induced circular dichroism signal upon titration with DNA, therefore no important observation was found to be used as an evidence to determine the mode of interactions of this group with DNA.

2.2.4 Viscosity

2.2.4.a Binding of 2.1 and 2.2 to calf thymus DNA (CT-DNA)

The mode of binding of **2.1** and **2.2** to double-stranded DNA was further studied using viscometry. In order to find out whether **2.1** and **2.2** are groove binders or intercalators, the relative viscosity of DNA upon addition of **2.1** and **2.2** was compared with viscosities of equivalent DNA solutions that contained known DNA binders which are either an intercalator (ethidium bromide) or a minor groove binder (H33258).[7] The relative viscosities of CT-DNA solutions were measured upon addition of **2.1** and **2.2** in buffer (25 mM MOPS, pH 7.0 and 50 mM NaCl) at 25 °C (Figure 2.35).

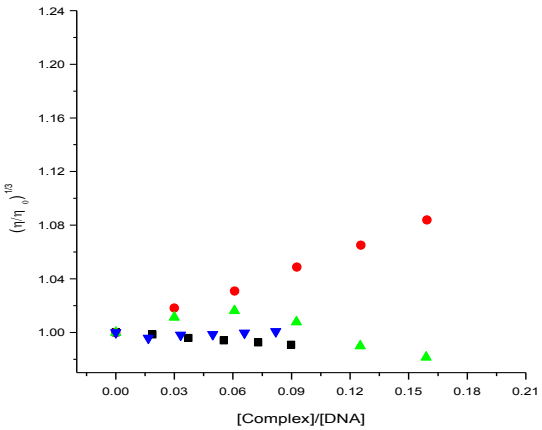

Figure 2.35 Relative viscosity of a 0.5 mM CT-DNA solution upon addition of **2.1** (■), **2.2** (▼), H33258 (▲) and ethidium bromide (●) at 25 °C in 25 mM MOPS pH 7.0, 50 mM NaCl.

Figure 2.35 shows a small decrease in relative viscosity upon the first addition of **2.1** and **2.2** and then increases slightly; suggesting groove binding is the dominant binding mode for both **2.1** and **2.2**.

2.2.4.b Binding of 2.4 and 2.5 to calf thymus DNA

The modes of binding of **2.4** and **2.5** to double-stranded DNA were similarly studied using viscometry. In order to find out whether these two compounds are groove binders or intercalators, the relative viscosity of DNA upon addition **2.4** and **2.5** were compared with viscosities of equivalent DNA solutions that contained known DNA binders which act either as an intercalator (ethidium bromide) or a minor groove binder (H33258). The

relative viscosities of CT-DNA solutions were measured upon addition of **2.4** and **2.5** in buffer (25 mM MOPS, pH 7.0 and 50 mM NaCl) at 25 °C (Figure 2.36).

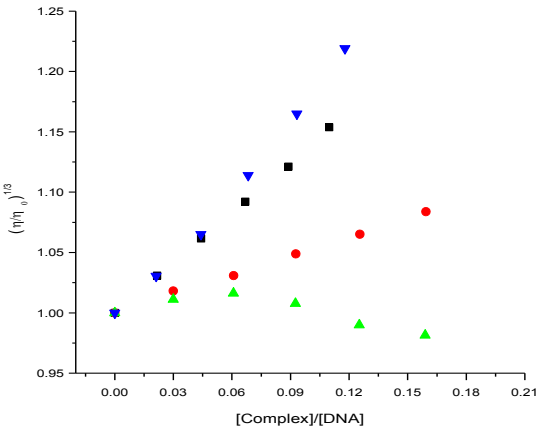

Figure 2.36 Relative viscosity of a 0.5 mM CT-DNA solution upon addition of **2.4** (▼), **2.5** (■), H33258 (▲) and ethidium bromide (●) at 25 °C in 25 mM MOPS, pH 7.0, 50 mM NaCl.

Figure 2.36 shows that the relative viscosity of CT-DNA solution significantly increased upon addition of **2.4** or **2.5**, with an even bigger increase in viscosity than the increase observed upon addition of ethidium bromide. This observation indicates both compounds **2.4** and **2.5** bind with CT-DNA via intercalation.

2.2.4.c Binding of 2.6 to calf thymus DNA

The mode of binding of **2.6** to double-stranded DNA was studied using viscometry. In order to find out whether **2.6** is a groove binder or an intercalator, the relative viscosity of DNA upon addition **2.6** was compared with the viscosities of equivalent DNA solutions that contained known DNA binders which act either as an intercalator (ethidium bromide) or a minor groove binder (H33258). The relative viscosities of CT-DNA solutions were measured upon addition of **2.6** in buffer (25 mM MOPS, pH 7.0 and 50 mM NaCl) at 25 °C (Figure 2.37).

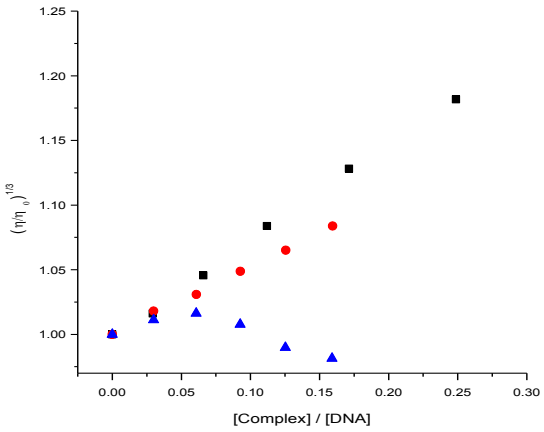

Figure 2.37 Relative viscosity of a 0.5 mM CT-DNA solution upon addition of **2.6** (■), H33258 (▲) and ethidium bromide (●) at 25 °C in 25 mM MOPS pH 7.0, 50 mM NaCl.

Figure 2.37 shows that the relative viscosity of CT-DNA solution increased upon addition of **2.6** and this increase is bigger than the increase observed upon addition of ethidium bromide, indicating that **2.6** interacts with CT-DNA via intercalation, like complexes **2.4** and **2.5**.

2.2.4.d Binding of 2.7 to calf thymus DNA

The mode of binding of **2.7** to double-stranded DNA was also studied using viscometry. In order to find out whether **2.7** is a groove binder or an intercalator, the relative viscosity of DNA upon addition **2.7** was compared with viscosities of equivalent DNA solutions that contained known DNA binders which act either as an intercalator (ethidium bromide) or a minor groove binder (H33258). The relative viscosities of CT-DNA solutions were measured upon addition of **2.7** in buffer (25 mM MOPS, pH 7.0 and 50 mM NaCl) at 25 °C (Figure 2.38).

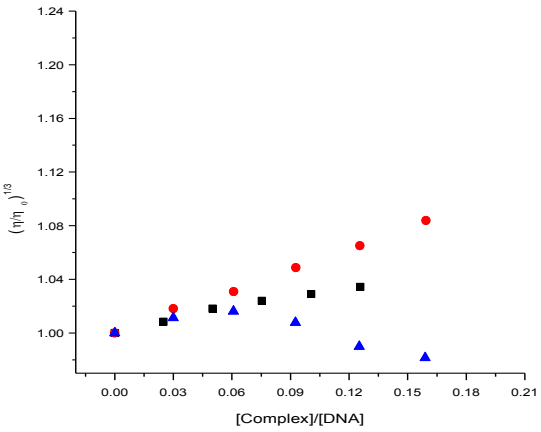

Figure 2.38 Relative viscosity of a 0.5 mM CT-DNA solution upon addition of **2.7** (■), H33258 (▲) and ethidium bromide (●) at 25 °C in 25 mM MOPS, pH 7.0, 50 mM NaCl.

Figure 2.38 shows that the relative viscosity of CT-DNA solution increased upon addition of **2.7** although less than ethidium bromide. This increase in viscosity suggests that **2.7** interacts with CT-DNA through intercalation; however the minor groove binding of **2.7** with DNA is not excluded since the increase in viscosity of **2.7** solution is relatively smaller than the increase in viscosity upon addition of ethidium bromide.

Summary

To further study the mode of the binding for **2.1-2.2** and **2.4-2.7** with duplex DNA, viscometry was used. The relative viscosity of CT-DNA solution significantly increased upon addition of **2.4-2.6**, suggesting intercalation is a mode of binding for the interactions of **2.4-2.6** with CT-DNA. Also, adding of **2.7** to CT-DNA solution caused to increase the relative viscosity of CT-DNA; however this increase in viscosity is relatively smaller than the increase in viscosity upon addition of known binder ethidium bromide, which suggests that intercalation and groove binding are both possible modes.

On the other hand, the small decrease in viscosity in the first addition of **2.1** and **2.2** into CT-DNA solution and then increase slightly, suggesting groove binding is the dominant binding mode.

2.2.5 Molecular docking studies

2.2.5.a Docking studies of 2.1 and 2.2 binding to DNA

The binding mode for interactions of **2.1** and **2.2** with duplex DNA was further studied through molecular docking using Auto Dock Vina.[6] Our previously developed[9] open-d(ATCGAGACGTCTCGAT)$_2$ was used as a biomacromolecular target.

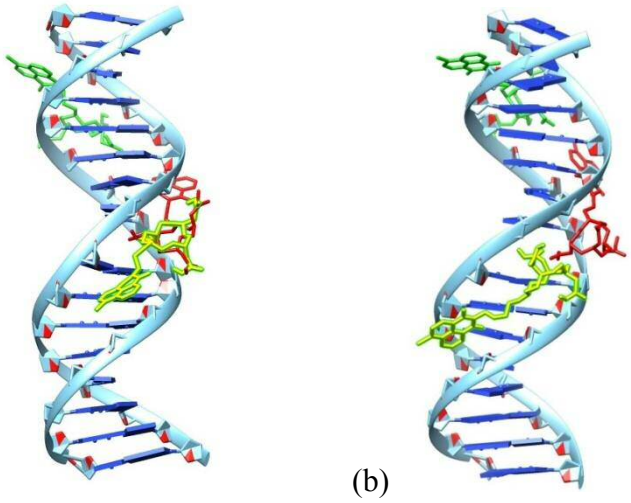

(a) (b)

Figure 2.39 Top 3 docked poses for **2.1** (a), **2.2** (b) interacting with open-d(ATCGAGACGTCTCGAT)$_2$.

The results of the molecular docking study show that minor groove binding is a favourable binding mode for **2.1** and **2.2**. From orientation of these compounds along the double-stranded DNA structure we observed that non-planarity of the hydrophilic parts of **2.1** and **2.2** hinder the intercalation of the hydrophobic parts between the base pairs. The complex structure in Figure 2.39 is in a reasonable agreement with the results of the binding mode study using viscometry (Section 2.2.4).

2.2.5.b Docking studies of 2.3- 2.5 binding to DNA

The binding modes for interactions of **2.3-2.5** with duplex DNA were similarly studied through a molecular docking study.

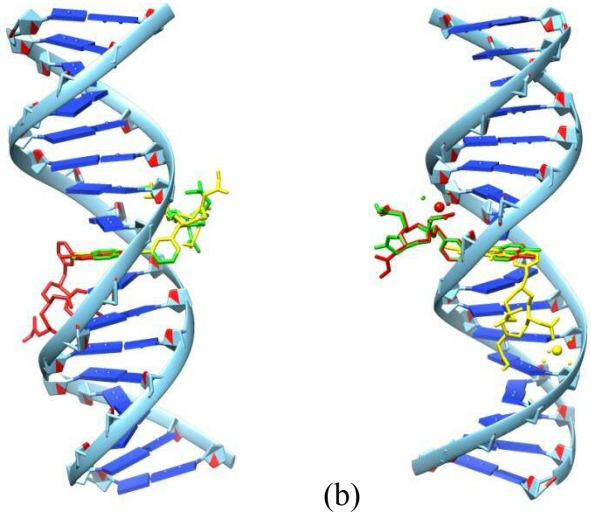

(a) (b)

Figure 2.40 Top 3 docked poses for **2.3** (a), **2.4** and **2.5** (b) interacting with open-d(ATCGAGACGTCTCGAT)$_2$.

The results of molecular docking study show that intercalation is a favourable binding mode for **2.3-2.5**. Docking shows that for these compounds, the hydrophobic parts can penetrate between the base pairs. The complex structure in Figure 2.40 is in agreement with the result of the binding mode study using viscometry.

2.2.5.c Docking studies of 2.6 and 2.7 binding to DNA

Finally, the binding modes for interactions of **2.6** and **2.7** with duplex DNA were also studied through the analogous molecular docking study.

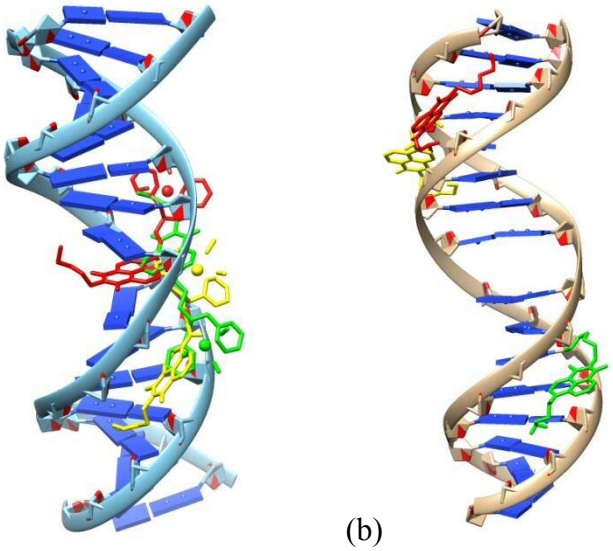

(a) (b)

Figure 2.41 Top 3 docked poses for **2.6** (a) and **2.7** (b) interacting with open-d(ATCGAGACGTCTCGAT)$_2$.

The results of the molecular docking study show that minor groove binding and intercalation are both possible binding modes for **2.6**. The complex structures (a) in Figure 2.41 are in agreement with the results of the binding mode study of viscometry. On the other hand, according to the results of docking study compound **2.7** is a groove binder; however, this finding cannot be conclusive since the binding mode study by viscometry shows that intercalation and minor groove binding are both potential binding modes for **2.7**.

2.2.6 Sequence selectivity

The affinities for FS-DNA as reported in section 2.2.1 represent averaged affinities for the heterogeneous sequence of FS-DNA. In order to study the selectivity of a group of 1,8-naphthalimide derivatives for selected specific sequences of DNA, viz. $(dAdT)_{12}$●$(dAdT)_{12}$ and $(dGdC)_{12}$●$(dGdC)_{12}$, additional UV-visible spectroscopy titrations were carried out.

2.2.6.a Binding of 2.1 to $(dAdT)_{12}$●$(dAdT)_{12}$

The binding of **2.1** to $(dAdT)_{12}$●$(dAdT)_{12}$ was studied using UV-visible spectroscopy; the changes in absorption of **2.1** upon addition of $(dAdT)_{12}$●$(dAdT)_{12}$ were measured in buffer (25 mM MOPS, pH 7.0 and 50 mM NaCl) at 25 °C (Figure 2.42).

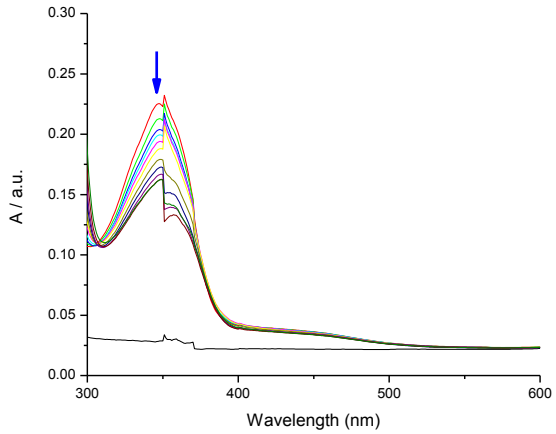

Figure 2.42 UV-visible spectra for 0.032 mM **2.1** upon addition of 0 – 0.64 mM $(dAdT)_{12}$●$(dAdT)_{12}$ in 25 mM MOPS, pH 7.0, 50 mM NaCl, at 25 °C.

Figure 2.42 shows a hypochromic shift in absorbance (at the λ_{max} of 347 nm) and hyperchromic shift (at 390 nm) of **2.1** upon addition of $(dAdT)_{12}$●$(dAdT)_{12}$, this change in UV-visible absorption may occur as a result of geometrical distortion of **2.1** when it interacts with DNA, but it may also be a local medium effect.

To quantify the affinity of **2.1** for $(dAdT)_{12}$●$(dAdT)_{12}$, the absorbances at 347 were plotted as a function of concentration of $(dAdT)_{12}$●$(dAdT)_{12}$ (Figure 2.43). This choice of wavelength avoids the data at $\lambda > 350$ nm that appears to be affected by a poorly performing visible light source.

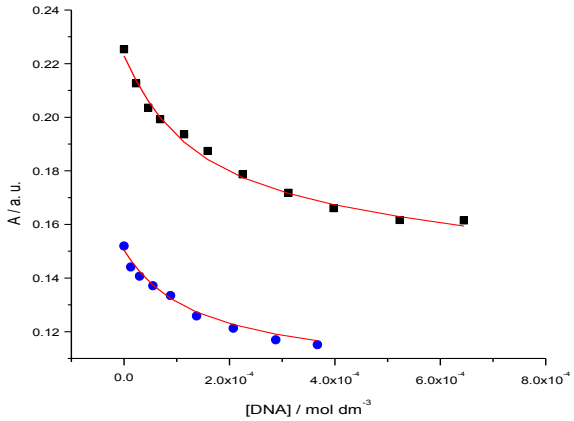

Figure 2.43 Absorbance at 347 nm of a solution of 0.032 mM **2.1** (■) and of a solution of 0.020 mM **2.1** (●), as a function of $(dAdT)_{12}$●$(dAdT)_{12}$ concentration, in 25 mM MOPS, pH 7.0, 50 mM NaCl, at 25 °C. The solid lines represent a global fit of a multiple independent sites model to the data.

The titration curves of Figure 2.43 were analysed globally by fitting a version of the multiple independent binding sites models, which also takes ligand dilution into account, to the data. This fit gives an equilibrium constant ($K_{binding}$) of (18.35 ± 20.6) $\times 10^3$ M^{-1} and a binding site size of (1.7 ± 1.4) base pairs. The large error margins suggest significant parameter covariance. We therefore re-analysed the data for a binding site size n restricted to 3 base pairs (for these types of DNA binders the average binding site size n is around 3 base pairs). The fit gave an equilibrium constant ($K_{binding}$) of (4.10 ± 0.80) $\times 10^4$ M^{-1}.

2.2.6.b Binding of 2.1 to $(dGdC)_{12}$●$(dGdC)_{12}$

The binding of **2.1** to $(dGdC)_{12}$●$(dGdC)_{12}$ was studied using UV-visible spectroscopy; the changes in absorption of **2.1** upon addition of $(dGdC)_{12}$●$(dGdC)_{12}$ were measured in buffer (25 mM MOPS, pH 7.0 and 50 mM NaCl) at 25 °C (Figure 2.44).

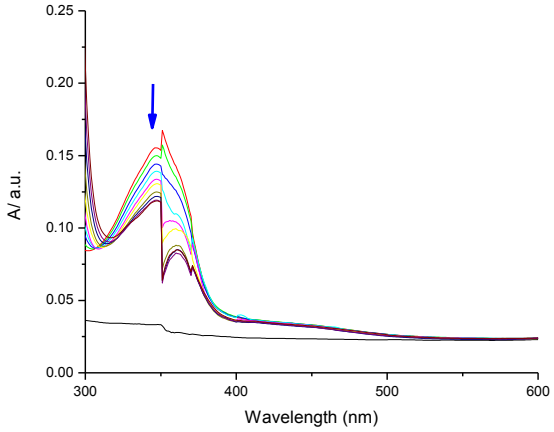

Figure 2.44 UV-visible spectra for 0.020 mM **2.1** upon addition of 0 – 0.26 mM $(dGdC)_{12}$●$(dGdC)_{12}$ in 25 mM MOPS, pH 7.0, 50 mM NaCl, at 25 °C.

Figure 2.44 shows a hypochromic shift in absorbance (at the λ_{max} of 347 nm) and hyperchromic shift (at 390 nm) of **2.1** upon addition of $(dGdC)_{12}$●$(dGdC)_{12}$. This change in UV-visible absorption may occur as a result of geometrical distortion of **2.1** when it interacts with $(dGdC)_{12}$●$(dGdC)_{12}$, but it may also be a local medium effect.

To quantify the affinity of **2.1** for $(dGdC)_{12}$●$(dGdC)_{12}$, the absorbances at 347 were plotted as a function of concentration of $(dGdC)_{12}$●$(dGdC)_{12}$ (Figure 2.45).

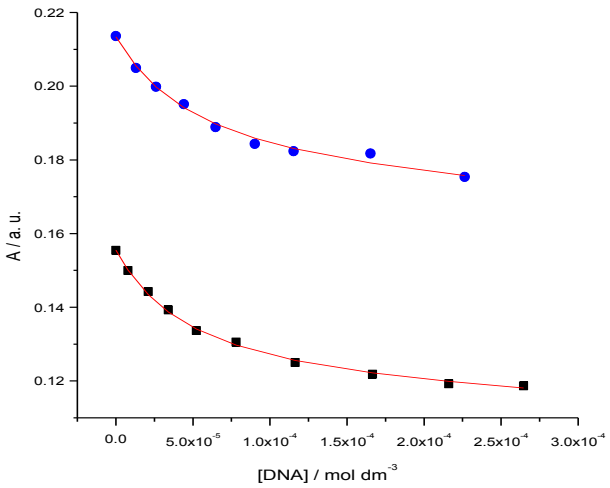

Figure 2.45 Absorbance at 347 nm of a solution of 0.020 mM **2.1** (■) and of a solution of 0.029 mM **2.1** (●), as a function of $(dGdC)_{12}$●$(dGdC)_{12}$ concentration in 25 mM MOPS, pH 7.0, 50 mM NaCl, at 25 °C. The solid lines represent a global fit in term of a multiple independent sites model.

The titration curves of Figure 2.45 were analysed globally in terms of a multiple independent binding sites models, which also takes ligand dilution into account. The analysis gave an equilibrium constant ($K_{binding}$) of $(1.05 \pm 1.7) \times 10^4\ M^{-1}$ and a binding site size of (0.45 ± 0.62) base pairs. The obtained binding site size was small therefore the data were reanalysed at stoichiometry (n) restricted to 2.0 base pairs, giving a binding constant of $(9.64 \pm 1.81) \times 10^4\ M^{-1}$.

The sequence selectivity study of compounds **2.2** and **2.4-2.7** for selected specific sequences of DNA, $(dAdT)_{12}$●$(dAdT)_{12}$ and $(dGdC)_{12}$●$(dGdC)_{12}$ were similarly carried out using UV-visible spectroscopy (see appendix, A14). The binding parameters for these compounds interacting with specific sequences of DNA were determined and are summarised in Table 2.9.

Table 2.9 Binding parameters from UV-visible spectroscopy for 2.1-2.2 and 2.4-2.7 binding to $(dAdT)_{12}$●$(dAdT)_{12}$ and $(dGdC)_{12}$●$(dGdC)_{12}$, in 25 mM MOPS, pH 7.0, 50 mM NaCl, at 25 °C.

	$(dAdT)_{12}$●$(dAdT)_{12}$		$(dGdC)_{12}$●$(dGdC)_{12}$	
Compound	*Binding constant* K / M^{-1}	*Binding site size* n / *bp*	*Binding constant* K / M^{-1}	*Binding site size* n / *bp*
2.1	$(4.10 \pm 0.80) \times 10^4$	3.0*	$(9.64 \pm 1.81) \times 10^4$	2.0*
2.2	$(92.49 \pm 19.97) \times 10^3$	1.0*	$(25.45 \pm 5.85) \times 10^3$	1.0*
2.4	$(14.41 \pm 3.12) \times 10^3$	3.0*	$(8.05 \pm 2.03) \times 10^3$	3.0*
2.5	$(25.61 \pm 13.02) \times 10^3$	3.42 ± 1.07	$(9.30 \pm 2.70) \times 10^3$	3.0*
2.6	$74 \times 10^4 [0 - 76 \times 10^4]$	1.0*	$(13.67 \pm 1.93) \times 10^4$	3.0*
2.7	$(10.28 \pm 2.56) \times 10^4$	2.53 ± 0.28	$(18.18 \pm 3.07) \times 10^4$	4.23 ± 0.17

* restricted.

Table 2.9 shows that all compounds studied for sequence selectivity show different affinities toward specific sequences of DNA, $(dAdT)_{12}$●$(dAdT)_{12}$ and $(dGdC)_{12}$●$(dGdC)_{12}$. All compounds **2.1-2.2** and **2.4-2.7** bind to $(dAdT)_{12}$●$(dAdT)_{12}$ with binding affinities between 10^4 to $10^5\ M^{-1}$. The binding site size for ligands **2.1-**

2.2 and **2.4-2.7** is between 1 to 3 base pairs. Also, all compounds bind to $(dGdC)_{12}$●$(dGdC)_{12}$ with binding affinities between 10^4 to 10^5 M^{-1}. The binding site size for compounds **2.1-2.2** and **2.4-2.7** interacting with $(dGdC)_{12}$●$(dGdC)_{12}$ is between 1 to 4 base pairs. In general, most compounds of this family have preferences for the $(dAdT)_{12}$●$(dAdT)_{12}$ sequence over $(dGdC)_{12}$●$(dGdC)_{12}$.

2.3 Conclusion

Most compounds of the group of 1,8-naphthalimide derivatives bind to double-stranded DNA moderately and the binding is accompanied by change in optoelectronic properties of the compound with a hypochromic shift in absorbance at maximum absorption and a hypochromic shift mostly observed. The binding constants for **2.1**-**2.7** are in the range of 10^3 to 10^5 M^{-1} with the binding site size between 1.0 to 3.0 base pairs. The binding site size of 1.0 base pair for some bindings seems to be small, suggesting a side by side interaction is a mode of binding. The affinity of the metal complexes (Eu, Gd) of ligand **2.3** are greater than the ligand **2.3** itself, this might be due to the net negative charges of metal complex is smaller than the ligand, leading to decrease in repulsion force between negative charges of DNA and the metal complex. Both compounds **2.8** and **2.9** do not show any affinity for duplex DNA. The reason for not interacting with duplex DNA may be the presence of a sulphonate group, which places negative charges on the compounds, leading to increased repulsion between duplex DNA and ligands.

Isothermal titration calorimetry shows one binding event for **2.1** and **2.6-2.7** binding to FS-DNA. Although, the result of UV-visible spectroscopy of **2.2** interacting with DNA shows that compound **2.2** has affinity toward FS-DNA; the enthalpograms for the interaction of **2.2** with DNA from ITC suggest negligible binding of **2.2** with DNA or very weakly exothermic interactions.

We used induced circular dichroism spectroscopy (ICD) as a first technique to study and investigate the mode of binding between **2.1**-**2.7** and duplex DNA, unfortunately none of compounds **2.1**-**2.7** showed any significant ICD signal to provide support for either binding mode.

The binding mode was further studied using viscometry. The small decrease in relative viscosity of calf thymus DNA solution followed by a small increase upon addition of **2.1**, indicating the minor groove is the dominant binding site. On the other hand, the relative viscosities of CT-DNA solutions significantly increased upon addition of **2.4-2.6**, suggesting intercalation is a mode of interaction. The relative viscosity of CT-DNA solution also increased upon addition of ligand **2.7**, however, this increase is relatively smaller compared to the known intercalator ethidium

bromide, and therefore two modes of interactions are suggested viz. intercalation as a dominant mode and a minor groove.

Molecular docking studies were also used to support the results of viscometry. The results of molecular docking study for **2.1** showed that this ligand interacts with duplex DNA in the minor groove which is also suggested by viscometry. On the other hand, the docking results of **2.4** and **2.5** confirm that intercalation is a mode of binding, in agreement with viscometry results. We attribute this difference in the binding mode to a presence of a benzene ring in between hydrophobic and hydrophilic parts of **2.4** and **2.5** which helps the hydrophobic parts of these molecules to intercalate easily between base pairs. The docking studies for **2.6** and **2.7** suggest that intercalation is a dominant mode of binding for **2.6**, and **2.7** interacting with duplex DNA through groove binding, although the intercalation is not excluded as a second mode of interaction for **2.7**. This observation is also supported by viscometry.

Compounds **2.1-2.2** and **2.4-2.7** bind to a specific DNA sequence $(dAdT)_{12}\bullet(dAdT)_{12}$ with binding affinities between 10^4 to 10^5 M^{-1}. The binding site size for ligands **2.1-2.2** and **2.4-2.7** is between 1 to 3 base pairs. Also, all the compounds bind to $(dGdC)_{12}\bullet(dGdC)_{12}$ with binding affinities between 10^4 to 10^5 M^{-1}. The binding site size for compounds **2.1-2.2** and **2.4-2.7** interacting with $(dGdC)_{12}\bullet(dGdC)_{12}$ is between 1 to 4 base pairs. In general, both compounds **2.1** and **2.7** show greater affinities for $(dGdC)_{12}\bullet(dGdC)_{12}$ over $(dAdT)_{12}\bullet(dAdT)_{12}$. In contrast, compounds **2.2** and **2.4**–**2.6** have more affinty toward $(dAdT)_{12}\bullet(dAdT)_{12}$.

The driving forces for the compounds of this family binding to DNA could be provided by hydrophobic interactions between the conjugated aromatic frameworks of binders and hydrophobic parts of the base pairs, in addition to electrostatic interaction between cationic charge on (NH_3^+) and the negative charges on the DNA.

2.4 Materials and Methods

2.4.1 DNA preparation

All compounds studied in this chapter were provided by our collaborators. All experiments were carried out in buffer (25 mM MOPS, 50 mM NaCl, pH 7.0, at 25 °C). The pH of the buffer was determined using a Hanna Instruments pH 210 pH meter equipped with a VWR 662-1759 glass electrode. The buffer components were purchased from Acros and Sigma-Aldrich. Fish sperm DNA and Calf thymus DNA were also purchased from Acros and Sigma-Aldrich. The stock solution of calf thymus DNA was prepared by sonicating a solution of CT-DNA for about 30 minutes whereas the stock solution of fish sperm DNA was prepared by sonicating a solution of FS-DNA for about 10 minutes. The sonicator was used in DNA preparation in order to quicken the solvation of DNA in buffer. Fish sperm DNA needs less sonicating because FS-DNA dissolves more quickly in MOPS buffer.

The DNA solution was dialysed against 2.0 litre of buffer using a 3.5 kDa MWCO dialysis membrane for 24 hours. The concentration of DNA was determined by UV-visible spectroscopy using an extension coefficient of 12800 M^{-1} cm^{-1} at 260 nm.[4]

2.4.2 Spectroscopic studies

UV-visible spectra were measured using a Jasco V-630Bio spectrophotometer equipped with a peltier temperature controller at 25 °C. Circular dichroism spectra were recorded on a Chirascan CD Spectrophotometer. Stock solutions of **2.1-2.9** in buffer were freshly prepared and volumes of these stock solutions were added into 2000-2500 µl of buffer as required in a 1.0 cm path length cuvette. All UV-visible titrations were carried out by adding aliquots of the DNA stock solution into 1 cm path length cuvette which contains ligand solution, measuring the absorption in the range of 200-600 after each addition. The absorption in the range of 0.1-0.6 a.u. was measured in a cuvette to avoid self-aggregation and precipitation of the ligand. The absorptions at selected wavelength were plotted against DNA concentrations and a multiple independent binding sites model (see section 1.10.1 in Chapter 1) was used to analyse the UV-visible spectra by Origin 9.0. The baseline absorbance in a titration, and hence in the data analysis, corresponds to the absorbance of a cuvette containing

buffer only because the spectrophotometer was calibrated without cuvettes in the sample or reference position ("air versus air"). For CD titrations the same steps were followed except the ICD signals were used instead of absorptions in UV-visible titrations.

2.4.3 Isothermal titration calorimetry

All ITC experiments were carried out using a Microcal VP ITC microcalorimeter. The ligand solutions were prepared in buffer (25 mM MOPS, 50 mM NaCl, pH 7.0) and concentrations were determined using UV-visible spectroscopy based on extinction coefficients. All calorimetric binding experiments were carried out at 25 °C. The sample cell and syringe were always cleaned with ethanol followed by distilled water before starting any experiment. The sample cell was filled with FS-DNA solution (approximately 1.9 ml). The syringe was filled with ligand solution (approximately 300 µl) with a concentration usually12-fold higher than DNA solution (exact ratios depends on individual experiments). The ligand solution was added in 1 injection of 5 µl for the first addition and 19 injections of 15 µl each to the sample cell, injecting every 300 second automatically. During the titration the solutions in the sample cell was mixed with a stirring speed of 307 rpm. The heat effects per injection (dh) were calculated using Origin (Microcal, Inc). The integrated heat effects were analysed using IC ITC.[2]

2.4.4 Viscometry

All viscosimetry experiments were carried out in buffer (25 mM MOPS, 50 mM NaCl, pH 7.0). A Cannon-Flenske routine viscometer was placed in a temperature-controlled circulated water bath at 25 °C. The viscometer was filled with fixed amount of Calf thymus DNA (3.0 ml of 0.5 mM) and adding ligand solutions with concentrations calculated from the ratio of ligand/ DNA (0.03, 0.06, 0.09, 0.12 and 0.15). The flow time was measured three times for each ligand addition and the results were averaged. The relative viscosity was calculated and plotted as a function of the ratio $[ligand]_{bound}/[DNA]$ where $[ligand]_{bound}$ was calculated using binding parameters from UV-visible spectroscopy.

2.4.5 Docking studies

Molecular docking studies were performed using Auto Dock Vina.[6] The ligand structures were generated using chemdraw and then optimised using Avogadro, using force fields MMFF94 for ligands and GAFF for metal complexes. The rotable bonds in the ligand were assigned using Auto Dock Tools 1.5.6 and the output files were saved in PDBQT format. Our previously developed[9] open-d(ATCGAGACGTCTCGAT)$_2$ was used as a biomacromolecular target. An exhaustiveness of 200 and number modes of 10 were selected. The results of Auto Dock Vina were rendered using Chimera 1.10.2.

References

1- Garbett, N. C.; Ragazzon, P. A.; Chaires, J. B., Nat. Protoc 2007, 2 (12), 3166-3172.

2- Buurma, N. J.; Haq, I., J. Mol. Biol. 2008, 381 (3), 607-621.

3- Buurma, N. J.; Haq, I., Methods 2007, 42 (2), 162-172.

4- Ren, J. S.; Chaires, J. B., Biochemistry 1999, 38 (49), 16067-16075.

5- SH. M. Kelly and N. C. Price, Current Protein and Peptide Science, 2000, **1**, 349-384.

6- O. Trott, A. J. Olson, AutoDock Vina: improving the speed and accuracy of docking with a new scoring function, efficient optimization and multithreading, Journal of Computational Chemistry 31 (2010) 455-461.

7- Satyanarayana, S.; Dabrowiak, J. C.; Chaires, J. B., Biochemistry 1993, 32 (10), 2573-2584.

8- D. H. A. Corrêa and C. H. I. Ramos, African Journal of Biochemistry Research, 2009, 3, 164-173.

9- Jones, J. E.; Amoroso, A. J.; Dorin, I. M., Parigi, G.; Ward, B.D.; Buurma, N.J. and Pope, S.J., Chemical Communications 2011, 47 (12), 3374-3376.

10- Upstone, S. L., Encyclopedia of Analytical Chemistry, R.A. Meyers (Ed.) John Wiley & Sons Ltd, Chichester, 2000, 1699–1714.

Chapter 3

DNA BINDING STUDIES OF A FAMILY OF DENDRIMERIC COMPOUNDS

Abstract

We studied the interactions of a family of dendrimeric compounds and the corresponding fluorescent core with double- stranded DNA using a variety of techniques viz. spectroscopy, calorimetry, viscosity and molecular docking studies. The cationic ligands bind to duplex DNA strongly through different binding modes predominately intercalation and side-by-side binding in the minor groove. An anionic compound was found to interact weakly with duplex DNA. The sequence selectivity of this group for $(dAdT)_{12}$●$(dAdT)_{12}$ *and* $(dGdC)_{12}$●$(dGdC)_{12}$ *was also studied via UV-visible spectroscopy. A preference for the* $(dAdT)_{12}$●$(dAdT)_{12}$ *sequence over* $(dGdC)_{12}$●$(dGdC)_{12}$ *was observed.*

3.1 Introduction

Our objectives in this chapter are to quantify the thermodynamics of binding for a family of dendrimeric compounds and the corresponding fluorescent core to duplex DNA, and the mode of interactions. We aim to achieve these objectives by using several techniques viz. UV-visible and circular dichroism spectroscopy, isothermal titration calorimetry, and viscosity. The structures investigated are summarised in Scheme 3.1.

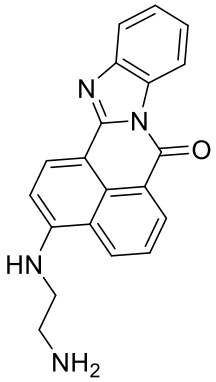

3.1

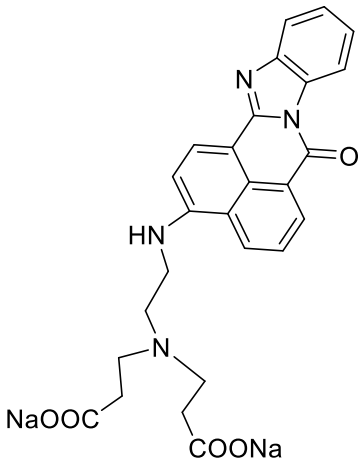

3.2

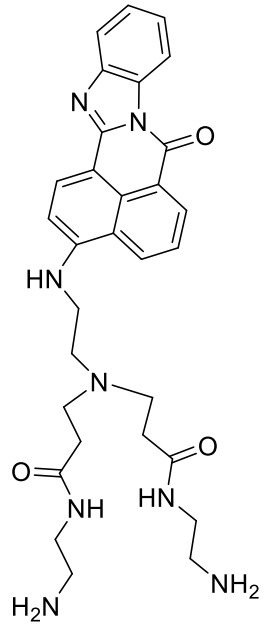

3.3

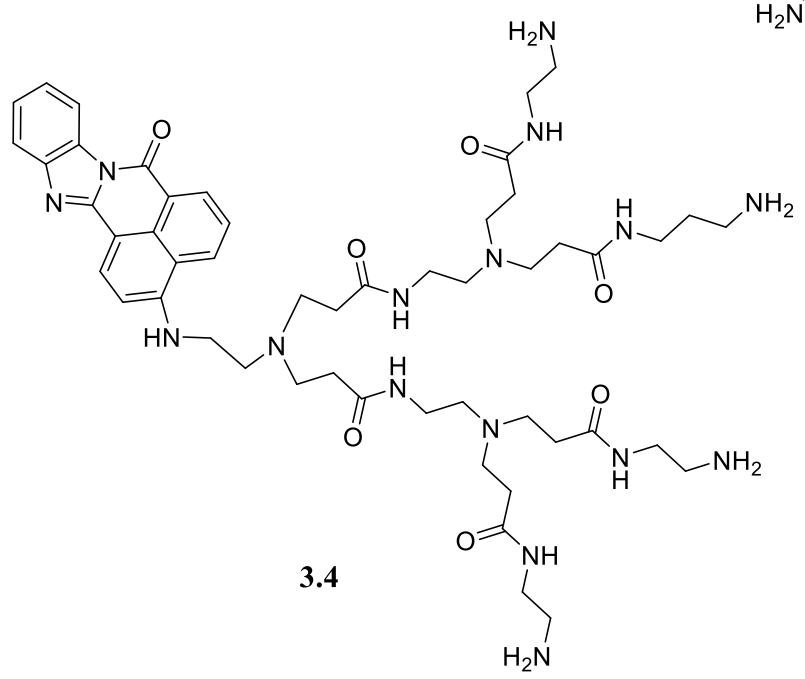

3.4

Scheme 3.1

All compounds in Scheme 3.1 were provided by our collaborator (Alla M.M. El-Betany).[9] These compounds consist of a highly fluorescent flat core (*7H*-benz[*de*]benzimidazo[*2,1-a*]isoquinoline-*7*-one) which is attached to different small poly(amidoamine) side-groups to increase solubility in aqueous medium. According to their structure, we expect the compounds of dendrimeric family bind to duplex DNA via intercalation and their optical and electronic behaviours may change upon binding.

These compounds are highly fluorescent and they could therefore be used as components in genosensors based on fluorimetric detection. Additionally, we expect these compounds to bind with duplex DNA as intercalators, enabling these compounds to be used as signal enhancers in electrochemical impedance spectroscopy (EIS) based biosensors. Furthermore, anionic compound **3.2** carries significant negative charges and, provided it binds to DNA, could therefore be an excellent element for use as sensitiser in EIS-based biosensors where surface charge on the electrode palys an important role.

3.2 Results and Discussion

The results of the interaction studies for compounds **3.1-3.4** with DNA will be shown and discussed for each individual compound.

3.2.1 UV-visible spectroscopy

The binding of **3.1**, **3.3** and **3.4** to duplex DNA were studied through UV-visible spectroscopy. The binding study of **3.2** by UV-visible was not carried out because this compound had already been studied by our collaborator and showed low affinity to duplex DNA.

3.2.1.a Binding of 3.1 to DNA

The binding of **3.1** to DNA was studied using UV-visible spectroscopy; the changes in absorption of **3.1** upon addition of FSDNA were measured in buffer (25 mM MOPS, pH 7.0 and 50 mM NaCl) at 25 °C (Figure 3.1).

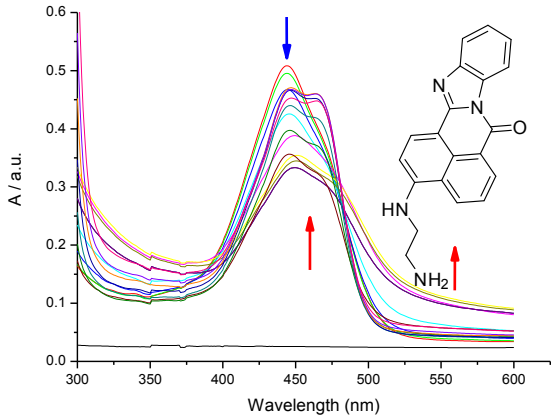

Figure 3.1 UV-visible spectra for 0.03 mM **3.1** upon addition of 0 – 1.72 mM FS-DNA in buffer (25 mM MOPS, pH 7.0, 50 mM NaCl) at 25 °C.

Figure 3.1 shows a hypochromic shift in absorbance (at the λ_{max} of 444 nm) followed by hyperchromic shift (at the λ_{max} of 444 nm) of **3.1** upon addition of FSDNA. In addition, a peak at 475 nm grows considerably. This change in UV-visible absorption may occur as a result of geometrical distortion of **3.1** when it interacts with DNA, but it may also be a local medium effect. On the other hand, absorbance in the range of 550-600 nm increases upon the first additions of DNA but subsequently decreases again. This observation suggests precipitation and subsequent dissolution of a DNA-ligand complex. Precipitation was also observed by naked-eye.

To quantify the affinity of **3.1** for FSDNA, the absorbances at 444 nm were plotted as a function of concentration of FSDNA (Figure 3.2, for data in tabular format see appendix, Table A16.1).

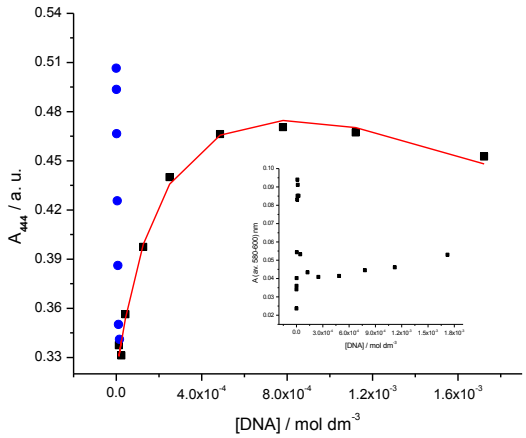

Figure 3.2 Absorbance at 444 nm of a solution of 0.03 mM **3.1** as a function of DNA concentration of 0 – 0.015 mM (●) and of 0.023 – 1.7 mM (■), average absorbance of 580-600 nm as a function of DNA concentration (inset), in buffer (25 mM MOPS, pH 7.0, 50 mM NaCl) at 25 °C. The solid line represents a fit of a multiple independent sites model to the data in the 0.023 – 1.7 mM range.

Figure 3.2 shows two binding events. In the first binding event a rapid decrease in absorbance was observed. We attribute this rapid decrease in absorption to strong binding of **3.1** to the sugar-phosphate backbone of DNA at low DNA/ligand ratios, leading to charge neutralization of **3.1**-DNA complexes and eventually precipitation. The titration data in Figure 3.2 (with the first event not included) were analysed in terms of a multiple independent binding sites models, which also takes ligand dilution into account, giving an apparent equilibrium constant ($K_{binding}$) of (0.002 ± 0.126) M^{-1} and a binding site size of (0.05 ± 3.3) $\times 10^{-5}$ base pairs. The obtained binding parameters were unreasonably small with an ill-defined stoichiometry. Therefore the data were reanalyzed with the stoichiometry restricted to 3.0 base pairs, giving an apparent binding constant of (1.36 ± 0.15) $\times 10^{4}$ M^{-1}.

3.2.1.b Binding of 3.3 to DNA

The binding of **3.3** to DNA was studied using UV-visible spectroscopy; the changes in absorption of **3.3** upon addition of FSDNA were measured in buffer (25 mM MOPS, pH 7.0 and 50 mM NaCl) at 25 °C (Figure 3.3).

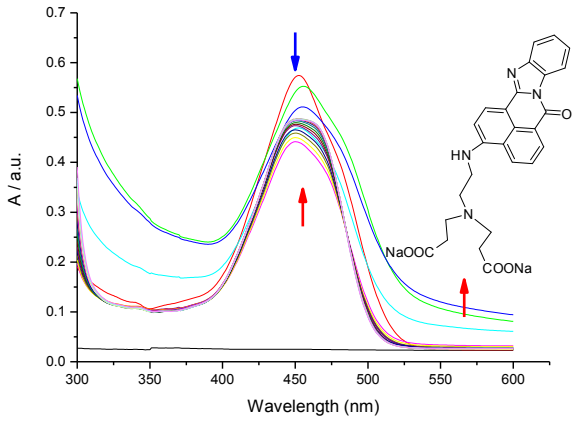

Figure 3.3 UV-visible spectra for 0.029 mM **3.3** upon addition of 0 – 0.69 mM FSDNA in buffer (25 mM MOPS, pH 7.0, 50 mM NaCl) at 25 °C.

Figure 3.3 shows a hypochromic shift in absorbance (at the λ_{max} of 452 nm) followed by hyperchromic shift (at the λ_{max} of 452 nm) of **3.3** upon addition of FSDNA.This change in UV-visible absorption may occur as a result of geometrical distortion of **3.3** when it interacts with DNA, but it may also be a local medium effect. In addition, this compound shows an increase in absorbance in the range of 550 – 600 nm upon the first additions of DNA. This observation suggests precipitation and subsequent dissolution of a DNA-ligand complex. Precipitation was also observed by naked-eye.

To quantify the affinity of **3.3** for FSDNA, the absorbances at 452 nm were plotted as a function of concentration of FSDNA (Figure 3.4, for data in tabular format see appendix, Table A16.2).

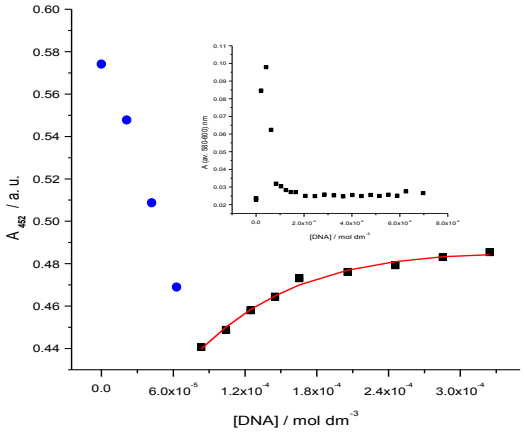

Figure 3.4 Absorbance at 452 nm of a solution of 0.029 mM **3.3** as a function of DNA concentration of 0 – 0.062 mM (●) and of 0.083 – 0.69 mM (■), average absorbance of 580-600 nm as a function of DNA concentration (inset), in buffer (25 mM MOPS, pH 7.0, 50 mM NaCl) at 25 °C. The solid line represents a fit of a multiple independent sites model to the data in the 0.083 – 0.69 mM range.

Figure 3.4 also shows two binding events. In the first binding event a steep decrease in absorbance was observed. We attribute this steep decrease in absorption to strong binding of **3.3** to the sugar-phosphate backbone of DNA at low DNA/ligand ratios, leading to charge neutralization of **3.3**-DNA complexes and eventually precipitation. The titration data in Figure 3.4 (with the first event not included) were analysed in

terms of a multiple independent binding sites model, which also takes ligand dilution into account, to the data. The fit gave an apparent equilibrium constant ($K_{binding}$) of (9.83 ± 17.7) $\times 10^4$ M^{-1} and a binding site size of (3.85 ± 3.67) base pairs. The large error margins suggest significant parameter covariance. We therefore re-analysed the data for a binding site size n restricted to 3 base pairs (for these types of DNA binders the average binding site size n is around 3 base pairs). The fit gave an equilibrium constant ($K_{binding}$) of (6.43 ± 1.61) $\times 10^4$ M^{-1}.

3.2.1.c Binding of 3.4 to DNA

The binding of **3.4** to DNA was studied using UV-visible spectroscopy; the changes in absorption of **3.4** upon addition of FSDNA were measured in buffer (25 mM MOPS pH, 7.0 and 50 mM NaCl) at 25 °C (Figure 3.5).

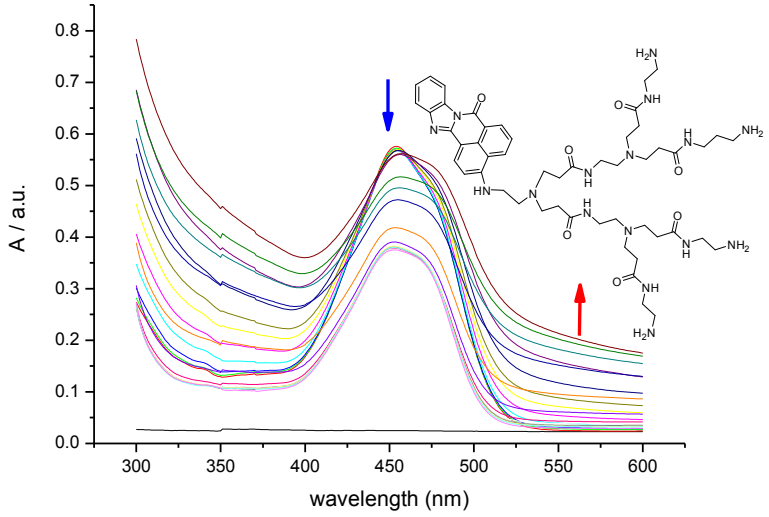

Figure 3.5 UV-visible spectra for 0.04 mM **3.4** upon addition of 0 – 0.18 mM FSDNA in buffer (25 mM MOPS, pH 7.0, 50 mM NaCl) at 25 °C.

Figure 3.5 shows a hypochromic shift in absorbance (at the λ_{max} of 454 nm) of **3.4** upon addition of FSDNA. This change in UV-visible absorption may occur as a result of geometrical distortion of **3.4** when it interacts with DNA, but it may also be a local medium effect. In addition, this compound shows a significant increase in absorbance in the range of 550 – 600 nm upon the first additions of DNA, indicative of precipitation followed by dissolution of a DNA-ligand complex. Precipitation was also clearly observed by naked-eye during the titration.

To quantify the affinity of **3.4** for FSDNA, the absorbances at 454 nm were plotted as a function of concentration of FSDNA (Figure 3.6, for data in tabular format see appendix, Table A16.3).

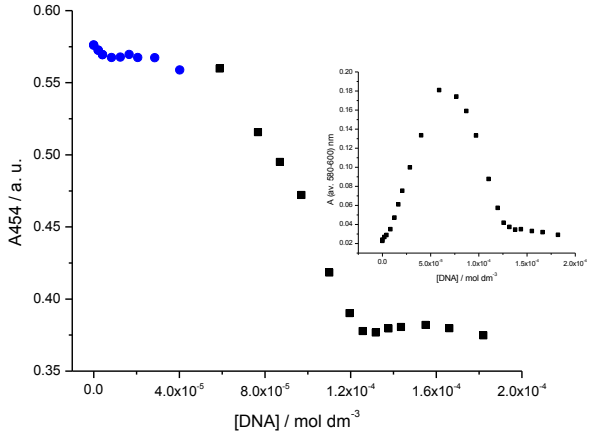

Figure 3.6 Absorbance at 454 nm of a solution of 0.04 mM **3.4** as a function of DNA concentration of 0 – 0.04 mM (●) and of 0.058 – 0.18 mM (■), average absorbance of 580-600 nm as a function of DNA concentration (inset), in buffer (25 mM MOPS, pH 7.0, 50 mM NaCl) at 25 °C. The solid line represents a fit of a multiple independent sites model to the data in the 0.058 – 0.18 mM range.

Figure 3.6 shows changes in absorbance of **3.4** upon addition of DNA. We may attribute these changes in absorption to strong binding of **3.4** to DNA, leading to precipitation of ligand-DNA complexes. However, when we tried to analyse the data in terms of a multiple independent binding sites model, we were unable to analyse the titration curve satisfactorily due to the complexity of the data. Therefore, we tried to analyse titration data in another way. We believe that the increase in absorbance at 530 nm is solely due to scattering and that the increase as a result of scattering at the λ_{max} of 454 nm is almost the same. Thus, we subtracted the absorbances at 530 nm from the absorbances at 454 nm in order to remove the amount of absorbance resulting from scattering.

To quantify the affinity of **3.4** for FSDNA, the absorbances at 454 nm – 530 nm were plotted as a function of concentration of FSDNA (Figure 3.7, for data in tabular format see appendix, Table A16.4).

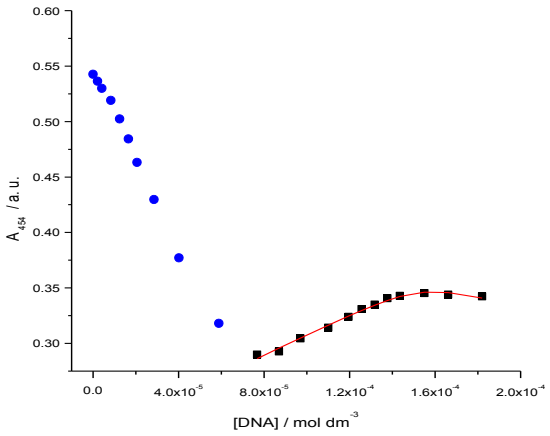

Figure 3.7 Absorbance at 454 nm – 530 nm of a solution of 0.04 mM **3.4** as a function of DNA concentration of 0 – 0.058 mM (●) and of 0.076 – 0.18 mM (■), in buffer (25 mM MOPS, pH 7.0, 50 mM NaCl) at 25 °C. The solid line represents a fit of a multiple independent sites model to the data in the 0.076 – 0.18 mM range.

Figure 3.7 shows two binding events. In the first binding event a sharp decrease in absorbance was observed. We attribute this sharp decrease in absorption to strong binding of **3.4** to the sugar-phosphate backbone of DNA at low DNA/ligand ratios, leading to charge neutralization of **3.4**-DNA complexes and eventually precipitation. The titration data in Figure 3.7 (with the first event not included) were analysed in terms of a multiple independent binding sites models, which also takes ligand dilution into account, giving an apparent equilibrium constant ($K_{binding}$) of (5.07± 4.41) $\times 10^6$ M^{-1} and a binding site size of (4.69 ± 0.09) base pairs.

Summary

The results of UV-visible titrations for compounds of **3.1** and **3.3-3.4** with duplex DNA show that these ligands **3.1** and **3.3-3.4** bind to FSDNA. The apparent affinities of these compounds to FS-DNA are summarised in Table 3.1.

Table 3.1 Apparent binding affinities and binding site sizes for binding of 3.1 and 3.3-3.4 to FSDNA, in buffer (25 mM MOPS, pH 7.0, 50 mM NaCl) at 25 °C.

Ligand	Binding constant K / M^{-1}	Binding site size n / bp
3.1	$(1.30 \pm 0.21) \times 10^4$	3*
3.3	$(6.43 \pm 1.61) \times 10^4$	3*
3.4	$(5.07 \pm 4.41) \times 10^6$	4.69 ± 0.09

* restricted.

Table 3.1 shows that all ligands bind to duplex DNA with different affinities. Ligand **3.4** binds more strongly with DNA compares to **3.3** and **3.1**. We may attribute these differences in affinities to structural variation of these ligands. Compound **3.4** has bigger poly(amideamido) PAMAM side-group compared to **3.1** and **3.3**, therefore, compound **3.4** possesses more sites of interactions and can bind more strongly with DNA. All ligands **3.1**, **3.3-3.4** bind to fish sperm DNA in two separate events. The first event occurs at low DNA/ligand ratio where the ligand binds to both the highest affinity binding sites but also to the sugar-phosphate backbone of DNA, leading to precipitation of charge-neutralised ligand-DNA complexes. At high DNA/ligand ratio the second event occurs where ligand binds to main binding sites viz. minor groove or intercalation of DNA. The binding site sizes of **3.1** and **3.3** were restricted to 3.0 base pairs in order to obtain reasonable binding parameters. Compound **3.4** also shows affinity to FSDNA and causes a hypochromic shift in absorbance at maximum absorption 454 nm. However, this interaction cannot be analysed directly due to forming a lot of precipitation of ligand-DNA complexes which makes the titration curve difficult to analyse by our present model. Therefore, we decided to analyse the titration data of compound **3.4** in another way, as we discussed before (Section 3.2.1.c).

3.2.2 Isothermal titration calorimetry (ITC)

To investigate further the binding of compounds **3.1-3.3** with duplex DNA, we used isothermal titration calorimetry (ITC). In order to obtain thermodynamic parameters for binding of compounds **3.1-3.3** with DNA, the titrations data were analysed using our IC ITC software. We started these investigations by studying the interactions of the anionic compound **3.2** with DNA.

3.2.2.a dilution of anionic 3.2

In order to determine the heats of dilution for **3.2** in MOPS buffer, the dilutions of a series of solutions of 3.12, 2.34 and 2.34 mM of **3.2** in MOPS buffer (25 mM MOPS, 50 mM NaCl, pH 7.0) were studied using isothermal titration calorimetry. The differential heat flow and derived integrated heat effects for these dilutions were recorded at 25 °C (Figure 3.8).

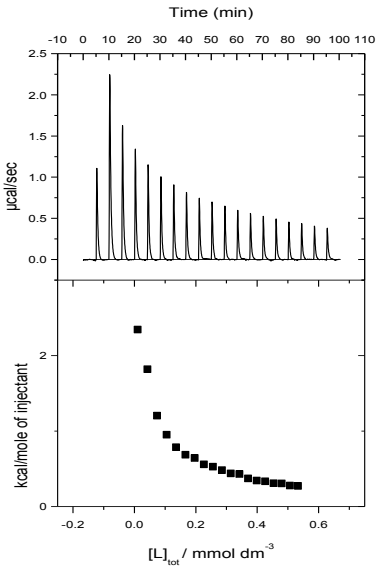
Time (min)
µcal/sec
kcal/mole of injectant
[L]tot / mmol dm-3

(a)

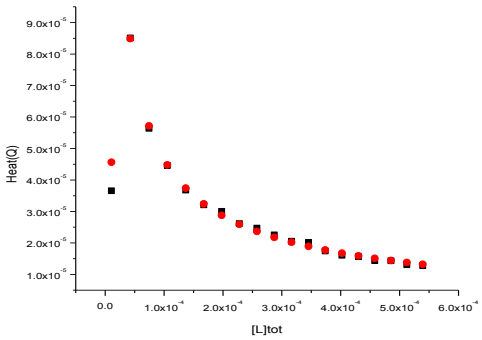
Heat(Q)
[L]tot

(d)

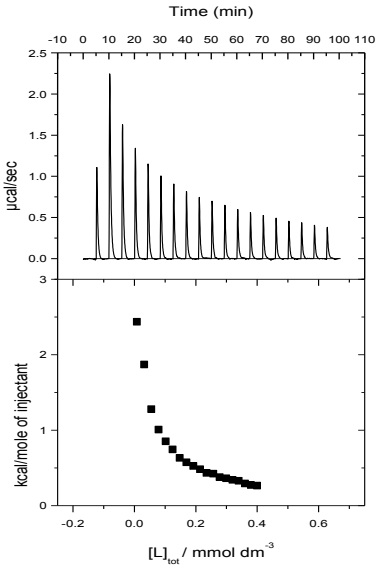
Time (min)
µcal/sec
kcal/mole of injectant
[L]tot / mmol dm-3

(b)

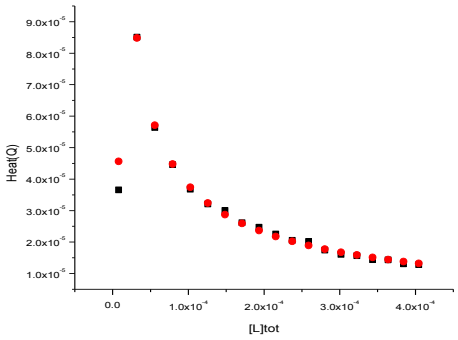
Heat(Q)
[L]tot

(e)

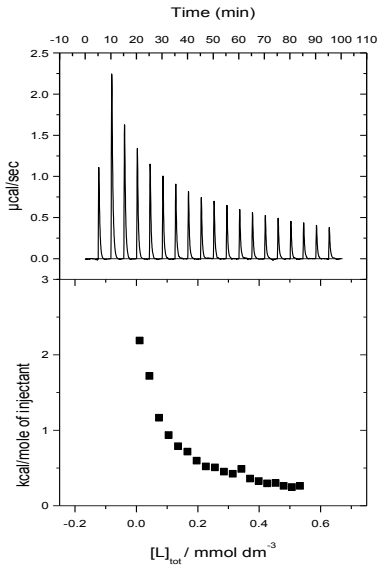

(c)

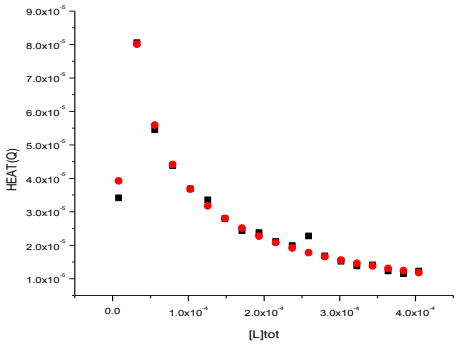

(f)

Figure 3.8 Enthalpograms for dilution of a 3.12 mM solution of **3.2** (a), of a 2.34 mM solution of **3.2** (b), and of a 2.34 mM solution of **3.2** (c), into a 25 mM MOPS, 50 mM NaCl, pH 7.0, at 25 °C, fit in terms of dilution (d), (e) and (f), experimental heat (■), calculated heat (●).

Figure 3.8 shows the heats of dilution of 3.12, 2.34 and 2.34 mM of **3.2** in MOPS buffer. Our IC ITC software was used to analyse the data, giving self-aggregation parameters as summarised in Table 3.2.

Table 3.2 Thermodynamic parameters for self-aggregation of 3.2 in a 25 mM MOPS, 50 mM NaCl, pH 7.0, at 25 °C

Experiment	*K*agg /10^4 M^{-1}	Δ*H*agg / kcal mol^{-1}
(a)	2.39 ± (1.47-7.61)	-3.95 ±(-6.03- -3.29)
(b)	3.19 ± (2.07- 7.14)	-5.27 ± (-6.99- -4.53)
(c)	1.93 ± (1.28- 3.64)	-4.4 3± (-5.30- -3.97)
Average	2.50	-4.55

The obtained dilution parameters in Table 3.2 show that a significant amount of heat is absorbed as a result of diluting **3.2** into MOPS buffer. The results of all three

experiments also show good reproducibility which can be seen clearly from the margin of errors of their dilution parameters (Figure 3.10).

3.2.2.b ITC studies of anionic 3.2 binding to DNA

To explore the interaction of anionic **3.2** with DNA, the binding of **3.2** to DNA was studied using isothermal titration calorimetry. The differential heat flow and derived integrated heat effects for titration of a 3.12 mM solution of **3.2** into a 0.5 mM FSDNA solution were measured in 25 mM MOPS, 50 mM NaCl, pH 7.0, at 25 °C (Figure 3.9).

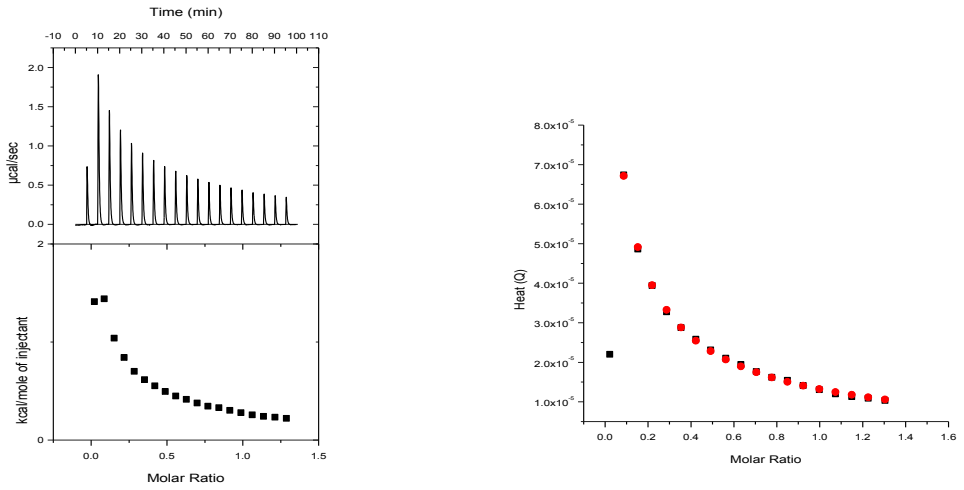

(a) (b)

Figure 3.9 Titration of a 3.12 mM solution of **3.2** into a 0.5 mM solution of FSDNA (a-top), integrated heat effects of titrations (a-bottom), fit in terms dilution (b), experimental heat (■), calculated heat (●), in 25 mM MOPS, 50 mM NaCl, pH 7, at 25 °C.

The enthalpogram for interaction of **3.2** with DNA in Figure 3.9 does not show big differences compared to the enthalpogram for dilution of **3.2** in MOPS buffer. We attribute this to a weak to negligible interaction between **3.2** and DNA, leading to small additional heat effects. Therefore, in order to find whether the binding is fully absent or only weak, we decided to analyse the titration data in terms of a model accounting only for dilution. The resulting thermodynamic parameters are summarized in Table 3.3.

Table 3.3 Thermodynamic parameters for interaction of 3.2 to FSDNA in 25 mM

MOPS, 50 mM NaCl, pH 7.0, at 25 °C, analysed in terms of a self-aggregation model only.

K aggregation/ x10^3 M^{-1}	ΔH aggregation/ kcal mol^{-1}
9.18 (7.57 – 11.4)	-2.55 (-2.46 – -2.67)

The dilution parameters obtained from analyzing the titration data in terms of self aggregation only (Table 3.3) can be compared with the parameters obtained from previous dilution experiments of **3.2**. The comparison shows that analyzing the titration data of **3.2** in the presence of DNA in the sample cell in terms of diluting model involving self-aggregation only yields parameters (K_{agg} and ΔH_{agg}) which are not in the ranges of the margin of error of (K_{agg} and ΔH_{agg}) obtained from the dilution experiments (Figure 3.10). Therefore, we decided to reanalyse the titration data in terms of self-aggregation in combination with binding (Figure 3.11).

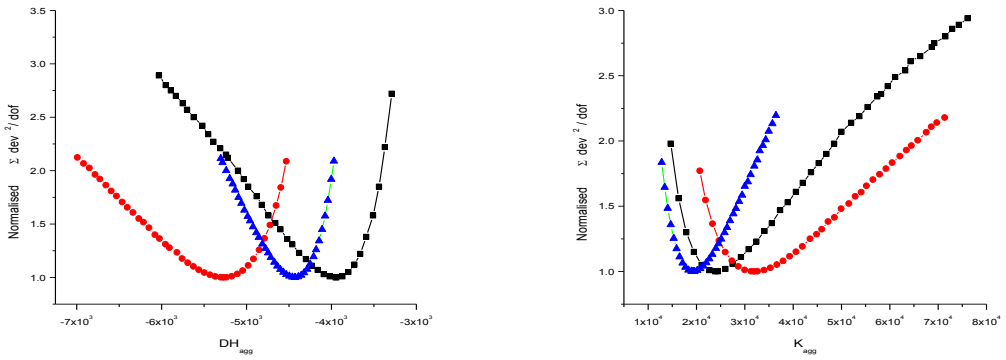

(a) (b)

Figure 3.10 Normalised Σdev^2/dof for dilution parameters of dilutions of 3.12 mM solution of **3.2** (■), of 2.34 mM solution of **3.2** (●), and of 2.34 mM solution of **3.2** (▲), into 25 mM MOPS, 50 mM NaCl, pH 7, at 25 °C.

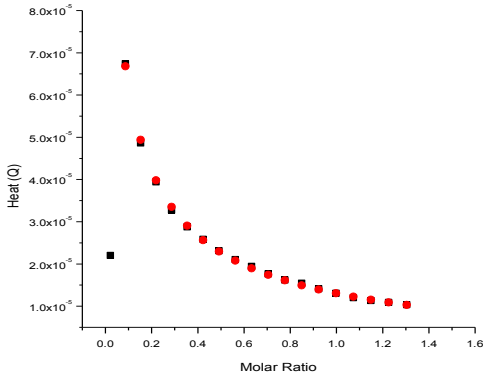

Figure 3.11 Fit for integrated heat effects of a titration of a 3.12 mM solution of **3.2** into a 0.5 mM solution of DNA in 25 mM MOPS, 50 mM NaCl, pH 7, at 25 °C, in terms of a binding model involving one type of binding site, aggregation included, experimental heat (■), calculated heat (●).

The titration data were reanalysed by our IC ITC software. Ligand aggregation was included with the values of K_{agg} and ΔH_{agg} restricted to numbers which were obtained from the dilution experiments. All binding parameters were determined are summarized in Table 3.4.

Table 3.4 Thermodynamic parameters for binding of 3.2 to FSDNA in 25 mM MOPS, 50 mM NaCl, pH 7.0, at 25 °C.

	K_{A1} (M^{-1})	$1/n_{A1}$ (bp)	ΔH_{A1} (kcal mol^{-1})	$-T\Delta S_{A1}$ (kcal mol^{-1})	$\{\Sigma dev^2/dof\}^{½}$ (µcal)
3.2	$8.62^{n.d.}$	0.73 (0.08 – 9)	-357 (-18.3 – -492)	355.7	0.42

n.d. the margin of error not determined.

The obtained binding constant in Table 3.4 is small and the enthalpy of interaction is too big. Therefore the data were reanalyzed where $1/n_{A1}$ was restricted to 3 base pairs (Figure 3.12)

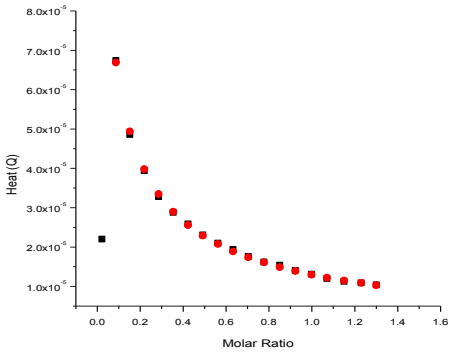

Figure 3.12 Fit for integrated heat effects of a titration of a 3.12 mM solution of **3.2** into a 0.5 mM solution of DNA in 25 mM MOPS, 50 mM NaCl, pH 7, at 25 °C, in terms of a binding model involving one type of binding site, aggregation included, experimental heat (■), calculated heat (●).

The titration data were reanalysed using IC ITC software. As before, the ligand aggregation was included and the values of K_{agg} and ΔH_{agg} were restricted to numbers which were obtained from dilution experiments. All resulting binding parameters are summarized in Table 3.5.

Table 3.5 Thermodynamic parameters for binding of 3.2 to FSDNA in 25 mM MOPS, 50 mM NaCl, pH 7.0, at 25 °C.

	K_{A1} (M^{-1})	$1/n_{A1}$ (bp)	ΔH_{A1} (kcal mol^{-1})	$-T\Delta S_{A1}$ (kcal mol^{-1})	$\{\Sigma dev^2/dof\}^{½}$ (µcal)
3.2	$25.2^{n.d.}$	3*	-500 (-500 – -19.3)	498	0.40

* restricted; n.d. the margin of error not determined.

The obtained enthalpy of interaction in Table 3.5 is still too big and unreasonable. Therefore the data were reanalyzed where ΔH_{A1} is restricted to -10 kcal. mol^{-1} (Figure 1.5). The reason for restricting ΔH_{A1} to this value is that the average enthalpy of binding for this group of binders is around -10 kcal. mol^{-1} (vide infra).

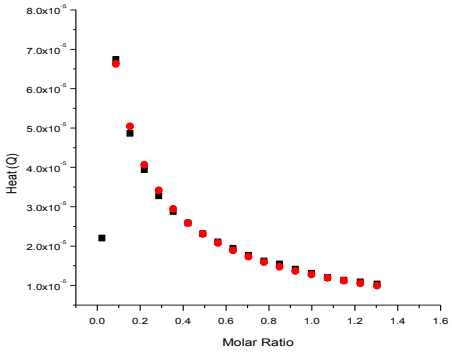

Figure 3.13 Fit for integrated heat effects of a titration of a 3.12 mM solution of **3.2** into a 0.5 mM solution of DNA in 25 mM MOPS, 50 mM NaCl, pH 7, at 25 °C, in terms of a binding model involving one type of binding site, aggregation included, experimental heat (■), calculated heat (●).

The titration data were reanalysed using IC ITC software. As before, ligand aggregation was also included and the values of K_{agg} and ΔH_{agg} were restricted to numbers which were obtained from dilution experiments. Binding parameters were determined as summarized in Table 3.6.

Table 3.6 Thermodynamic parameters for binding of 3.2 to FSDNA in 25 mM MOPS, 50 mM NaCl, pH 7.0, at 25 °C.

	K_{A1} (M^{-1})	$1/n_{A1}$ ($x10^{-3}$ bp)	ΔH_{A1} (kcal mol^{-1})	$-T\Delta S_{A1}$ (kcal mol^{-1})	$\{\Sigma dev^2/dof\}^{½}$ (µcal)
3.2	$1.61^{n.d.}$	2.6 (1.4 – 30)	-10*	9.7	0.81

* restricted; n.d. the margin of error not determined.

The obtained binding site size in Table 3.6 is unreasonably small. Therefore, we decided to reanalyze the data one more time with a stoichiometry restricted to 3 base pairs (Figure 3.14). As before, the ligand aggregation was also included and the values of K_{agg} and ΔH_{agg} were restricted to the numbers which were obtained from dilution experiments. The resulting binding parameters are summarized in Table 3.7.

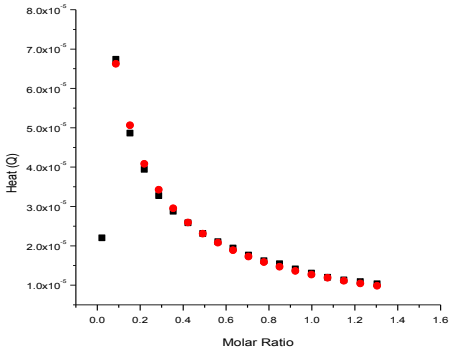

Figure 3.14 Fit for integrated heat effects of a titration of a 3.12 mM solution of **3.2** into a 0.5 mM solution of DNA in 25 mM MOPS, 50 mM NaCl, pH 7, at 25 °C, in terms of a binding model involving one type of binding site, aggregation included, experimental heat (■), calculated heat (●).

Table 3.7 Thermodynamic parameters for binding of 3.2 to FSDNA in 25 mM MOPS, 50 mM NaCl, pH 7.0, at 25 °C.

	K_{A1} (M^{-1})	$1/n_{A1}$ (bp)	ΔH_{A1} (kcal mol^{-1})	$-T\Delta S_{A1}$ (kcal mol^{-1})	$\{\Sigma dev^2/dof\}^{1/2}$ (µcal)
3.2	$1930^{n.d.}$	3*	-10*	5.52	0.86

* restricted; n.d. the margin of error not determined.

The obtained binding constant in Table 3.7 suggests that compound **3.2** has low affinity to duplex DNA, but does indeed bind to duplex DNA despite its negative charge.

3.2.2.c dilution of 3.1

In order to determine the heats of dilution for **3.1** in MOPS buffer, the dilutions of a series of solutions of **3.1** in MOPS buffer (25 mM MOPS, 50 mM NaCl, pH 7.0) were studied using isothermal titration calorimetry. The dilution experiments were repeated five times but the results were non-reproducible. We attribute this surprising non-reproducibility of the dilution experiments to self-aggregation of the ligand in unknown aggregate types in the sample cell. Therefore we were unable to determine the dilution parameters for compound **3.1**.

3.2.2.d ITC studies of 3.1 binding to DNA

To investigate further the binding of **3.1** with DNA, the binding of **3.1** to DNA was studied using isothermal titration calorimetry. The differential heat flow and derived integrated heat effects for titrations of solutions of **3.1** (1.06 & 1.29) mM into fish sperm DNA solutions (both 0.12 mM) were measured in 25 mM MOPS, 50 mM NaCl, pH 7.0, at 25 °C (Figure 3.15).

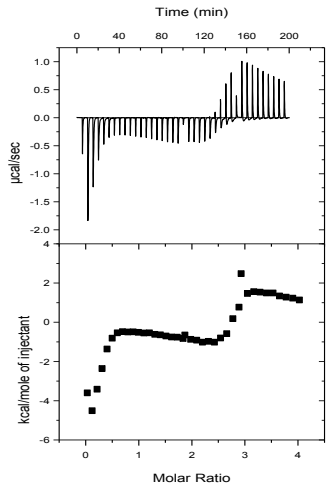

(a)

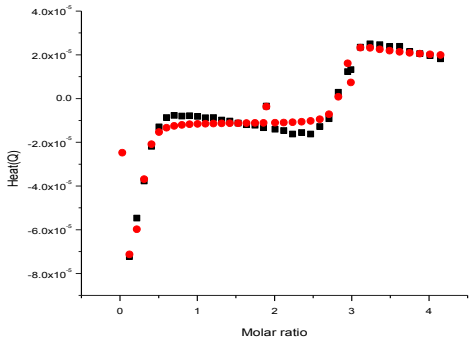

(c)

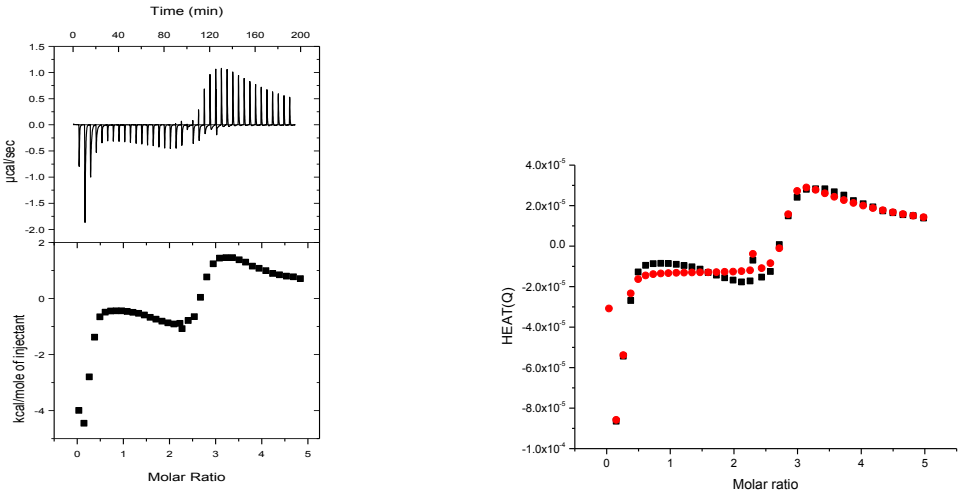

(b) (d)

Figure 3.15 Titration of a 1.06 mM solution of **3.1** into a 0.12 mM solution of FSDNA (a), of a 1.29 mM solution of **3.1** into a 0.12 mM solution of FSDNA (b), fit for integrated heat effects of titrations (a) and (b) in terms of a binding model involving two types of binding site, aggregation included (c) and (d), in 25 mM MOPS, 50 mM NaCl, pH 7, at 25 °C, experimental heat (■), calculated heat (●).

The enthalpograms for binding of **3.1** to FSDNA suggest more than one binding event, which was also observed by UV-visible titration. The first event occurs at high DNA/ligand ratio where ligand binds to the main binding sites of DNA viz. minor groove or intercalation. At low DNA/ligand ratio the second event occurs where the ligand binds to the sugar-phosphate backbone of DNA which leads to forming a precipitate of ligand-DNA complexes.[2, 3] According to Figure 3.11 the interaction between **3.1** and DNA is exothermic. The titration data were analysed using our ITC data analysis IC ITC software. Ligand aggregation was included and the values of K_{agg} and ΔH_{agg} were non-restricted because these parameters could not be obtained from the independent dilution experiments (vide supra). The resulting thermodynamic parameters are summarized in Table 3.8.

Table 3.8 Thermodynamic parameters for binding of 3.1 to FSDNA in 25 mM MOPS, 50 mM NaCl, pH 7.0, at 25 °C.

Binding parameters	Experiment (a)	Experiment (b)
K_{A1} (10^9 M^{-1})	1.24 (0.1 - 1.24)	0.91 (0.12 - 0.91)
$1/n_{A1}$ (bp)	4 (2.27 - 17)	4.76 (3.4 - 10)
ΔH_{A1} (kcal mol^{-1})	-7.15 (-15 - -0.83)	-7.08 (-22.4 - -4.84)
$-T\Delta S_{A1}$ (kcal mol^{-1})	-5.24	-5.2
K_{B1} (10^6 M^{-1})	6.92[n.d.]	3.78[n.d.]
$1/n_{B1}$ (bp)	0.38 (0.15 - 0.4)	0.4 (0.41 - 0.36)
ΔH_{B1} (kcal mol^{-1})	-2.93 (-5.9 - 1.52)	-2.75 (-3.73 - -1.7)
$-T\Delta S_{B1}$ (kcal mol^{-1})	-6.39	-6.21
$\{\Sigma dev^2/dof\}^{1/2}$ (µcal)	3.46	3.43

n.d. not determined.

Table 3.8 shows that **3.1** binds to FS-DNA in two separate events, the first event occurs at low ligand/DNA ratio with an affinity of ~ $10^9 M^{-1}$and a binding site size of ~ 4 base pairs. At high ligand/DNA ratio the second event happens with an affinity of ~ 10^6 M^{-1} and a binding site size of ~ 0.4 base pair. The results of data analysis for both titrations in Table 3.8 show good reproducibility of the experimental data. The negative molar enthalpy change and favorable standard molar entropy change for the first binding event suggest that **3.1** binds to FS-DNA as a groove binder, however it is difficult to decide based on ITC result to confirm the mode of binding of **3.1** with DNA because the ratio $\Delta H/\Delta G$ of **3.1** is close to the range for typical intercalators (0.83 - 1.97).[5]

3.2.2.e Dilution of 3.3

In order to determine whether compound **3.3** aggregates in MOPS buffer, the dilution of 0.99 mM solution of **3.3** in MOPS buffer (25 mM MOPS, 50 mM NaCl, pH 7.0) was studied using isothermal titration calorimetry. The differential heat flow and derived integrated heat effects for this dilution were recorded at 25 °C (Figures 3.16)

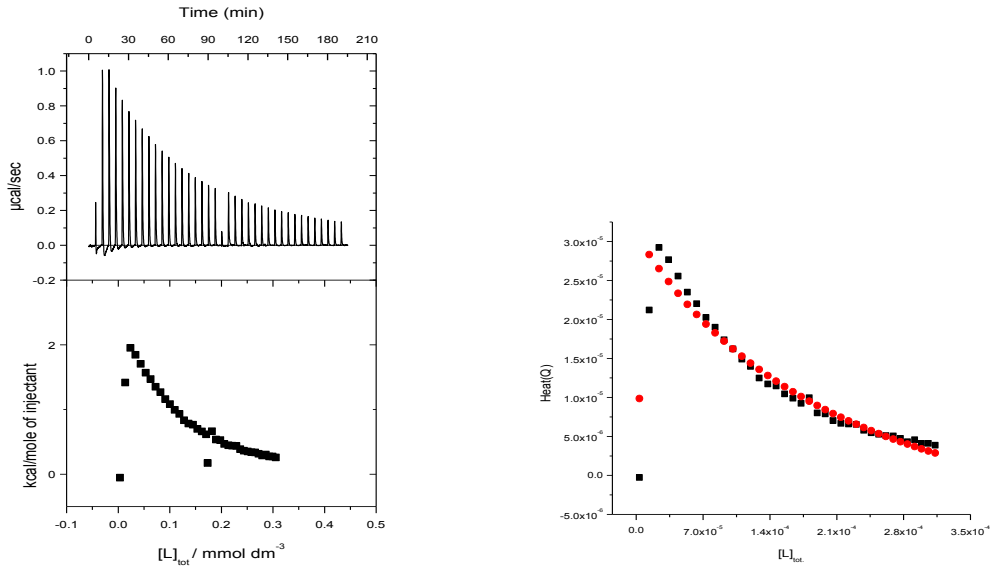

(a) (b)

Figure 3.16 Enthalpogram for dilution of a 0.99 mM solution of **3.3** (a), into a 25 mM MOPS, 50 mM NaCl, pH 7.0, at 25 °C, fit for integrated heat effects of the dilution (b), experimental heat (■), calculated heat (●).

Figure 3.16 shows non-constant heats of dilution of 0.99 mM of **3.3** in MOPS buffer, indicating self aggregation. Our IC ITC software was used to analyse the data. The obtained self aggregation parameters were determined and are summarised in Table 3.9.

Table 3.9 Thermodynamic parameters for diluting of 3.3 into a 25 mM MOPS, 50 mM NaCl, pH 7.0, at 25 °C

K aggregation/ M^{-1}	ΔH aggregation/ kcal mol^{-1}
$1100^{n.d.}$	$-5.87^{n.d.}$

n.d. the margin of error not determined.

The obtained dilution parameters for diluting of **3.3** into MOPS in Table 3.9 suggest that a considerable amount of heat is absorbed in the sample cell as a result of ligand disaggregation.

3.2.2.f ITC studies of 3.3 binding to DNA

In order to further explore the binding of **3.3** with DNA, the interactions of **3.3** with DNA were studied using isothermal titration calorimetry. The differential heat flow and derived integrated heat effects for titrations of solutions (both 0.99 mM) of **3.3** into fish sperm DNA solutions (0.20 & 0.25) mM were measured in 25 mM MOPS, 50 mM NaCl, pH 7.0, at 25 °C (Figure 3.17, a & b).

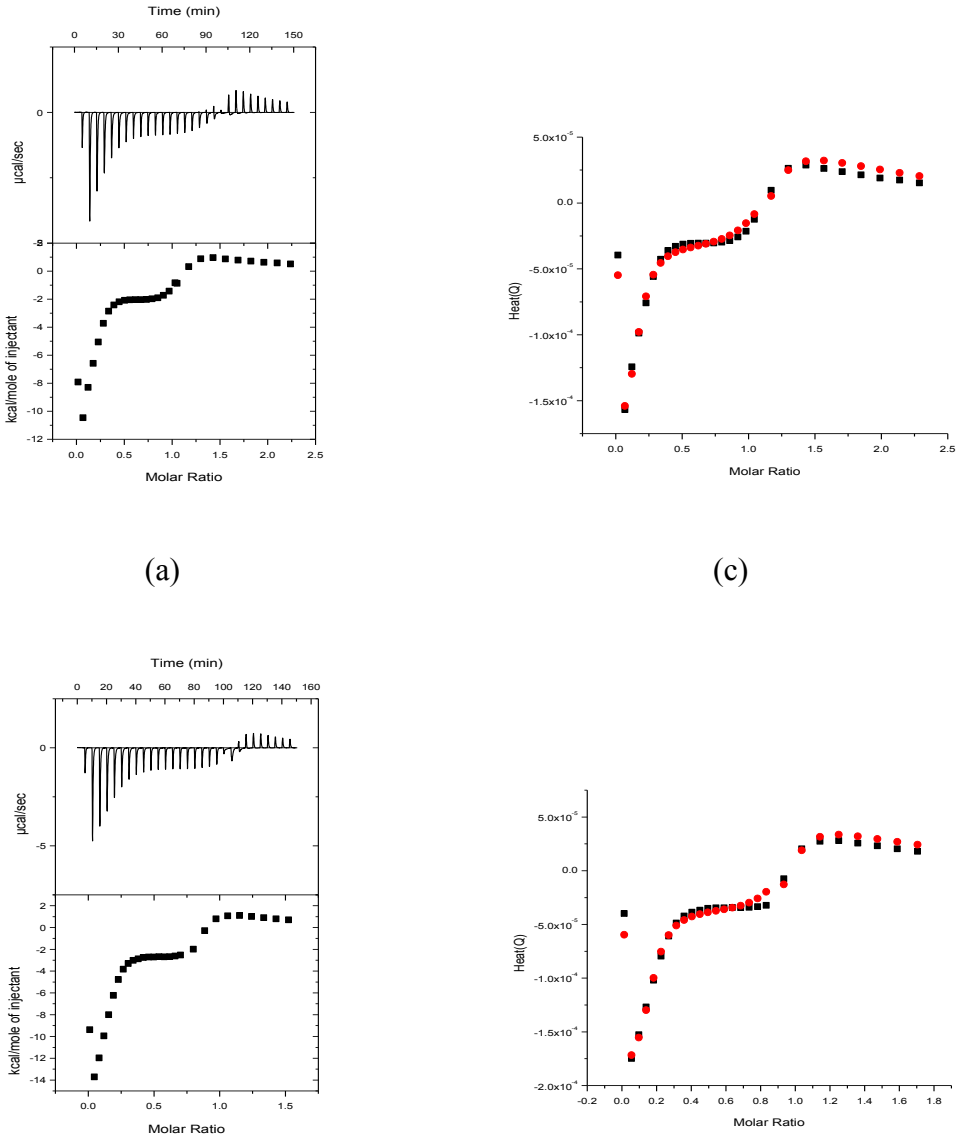

Figure 3.17 Titration of a 0.99 mM solution of **3.3** into a 0.20 mM solution of FSDNA (a), and of a 0.99 mM solution of **3.3** into a 0.25 mM solution of FSDNA (b), fit for integrated heat effects of titrations (a) and (b) in terms of a binding model

involving two types of binding site, aggregation included (c) and (d), in 25 mM MOPS, 50 mM NaCl, pH 7, at 25 °C, experimental heat (■), calculated heat (●).

The enthalpograms for binding of **3.3** to FSDNA again suggest more than one binding event, as was the case for **3.1**, which also confirms the results from the UV-visible titrations. The first event occurs at high DNA/ligand ratio where ligand binds to main binding sites of DNA viz. minor groove or intercalation. At low DNA/ligand ratio the second event occurs where the ligand binds to the sugar-phosphate backbone of DNA, leading to formation of a precipitate of ligand-DNA complexes.[2, 3] According to Figure 3.17 the interaction between **3.3** and DNA is exothermic. The titration data were analysed using our IC ITC software. All thermodynamic parameters are summarized in Table 3.10.

Table 3.10 Thermodynamic parameters for binding of 3.3 to FSDNA in 25 mM MOPS, 50 mM NaCl, pH 7.0, at 25 °C.

Binding parameters	Experiment (a)	Experiment (b)
K_{A1} (10^7 M^{-1})	1.55 (0.56 - 9.0)	2.22 (1.6 - 4.1)
$1/n_{A1}$ (bp)	6.6 (5.2 - 25)	6.6 (5.5 - 11.1)
ΔH_{A1} (kcal mol^{-1})	-14.6 (-48.8 - -11.6)	-15.3 (-33.7 - -15.3)
$-T\Delta S_{A1}$ (kcal mol^{-1})	4.8	5.3
K_{B1} (10^5 M^{-1})	4.10 (1.8 - 16.2)	5.67 (5.1 - 31)
$1/n_{B1}$ (bp)	1.1 (0.93 - 1.2)	1.35 (1.2 - 1.47)
ΔH_{B1} (kcal mol^{-1})	-4.2 (-4.95 - -3.3)	-4.45 (-3.6 - -5.2)
$-T\Delta S_{B1}$ (kcal mol^{-1})	-3.5	-3.4
$\{\Sigma dev^2/dof\}^{½}$ (µcal)	4.83	5.5

Table 3.10 shows that compound **3.3** binds to FSDNA in two different events. The first event occurs at low ligand/DNA ratio with an affinity of ~ $10^7 M^{-1}$and a binding site size of ~ 6 base pairs. At high ligand/DNA ratio the second event happens with an affinity of ~ 10^5 M^{-1} and a binding site size of ~ 1.0 base pair. The results of data analysis for both titrations in Table 3.10 show good reproducibility of the experimental data. The negative values of enthalpy and entropy change in the first binding event suggest that **3.3** binds to FSDNA between base pairs as an intercalator.[5]

Summary

The interactions of **3.1-3.3** with DNA were investigated by isothermal titration calorimetry. The thermodynamic parameters for these compounds interacting with FSDNA were determined and are summarised in Table 3.11.

Table 3.11 Thermodynamic parameters for binding of 3.1-3.3 to FSDNA in 25 mM MOPS, 50 mM NaCl, pH 7.0, at 25 °C.

3.1	Binding parameters	Experiment (a)	Experiment (b)
	K_{A1} (10^9 M^{-1})	1.24 (0.1 - 1.24)	0.91 (0.12 - 0.91)
	$1/n_{A1}$ (bp)	4 (2.27 - 17)	4.76 (3.4 - 10)
	ΔH_{A1} (kcal mol^{-1})	-7.15 (-15 - -0.83)	-7.08 (-22.4 - -4.84)
	$-T\Delta S_{A1}$ (kcal mol^{-1})	-5.24	-5.2
	K_{B1} (10^6 M^{-1})	6.92[n.d.]	3.7[n.d.]
	$1/n_{B1}$ (bp)	0.38 (0.15 - 0.4)	0.4 (0.41 - 0.36)
	ΔH_{B1} (kcal mol^{-1})	-2.93 (-5.9 - 1.52)	-2.75 (-3.73 - -1.7)
	$-T\Delta S_{B1}$ (kcal mol^{-1})	-6.39	-6.21
	$\{\Sigma dev^2/dof\}^{½}$ (µcal)	3.46	3.43
3.3			
	K_{A1} (10^7 M^{-1})	1.55 (0.56 - 9.0)	2.22 (1.6 - 4.1)
	$1/n_{A1}$ (bp)	6.6 (5.2 - 25)	6.6 (5.5 - 11.1)
	ΔH_{A1} (kcal mol^{-1})	-14.6 (-48.8 - -11.6)	-15.3(-33.7 - -15.3)
	$-T\Delta S_{A1}$ (kcal mol^{-1})	4.8	5.29
	K_{B1} (10^5 M^{-1})	4.10 (1.8 - 16.2)	5.67 (5.1 - 31)
	$1/n_{B1}$ (bp)	1.1 (0.93 - 1.2)	1.35 (1.2 - 1.47)
	ΔH_{B1} (kcal mol^{-1})	-4.2 (-4.95 - -3.3)	-4.45 (-3.6 - -5.2)
	$-T\Delta S_{B1}$ (kcal mol^{-1})	-3.49	-3.39
	$\{\Sigma dev^2/dof\}^{½}$ (µcal)	4.83	5.5
3.2			
	K_{A1} (10^3 M^{-1})	1.93[n.d.]	
	$1/n_{A1}$ (bp)	3*	
	ΔH_{A1} (kcal mol^{-1})	-10*	
	$-T\Delta S_{A1}$ (kcal mol^{-1})	5.52	

$\{\Sigma dev^2/dof\}^{1/2}$ (μcal)	0.86

* restricted; n.d. the margin of error not determined.

Both compound **3.1** and **3.3** show strong exothermic interactions with FSDNA in two separate events. The titration data of **3.1** and **3.3** interacting with FS-DNA were analysed using our IC-ITC software where the effects of aggregation were included, giving thermodynamic binding parameters (see Table 3.11). The results of data analysis for both ligands in Table 3.11 show good reproducibility of experimental data. The negative values of enthalpy and entropy change in the first binding event suggest that **3.3** binds to FSDNA via intercalation. In addition, the obtained binding constant in Table 3.7 suggests that compound **3.2** has low, but non-zero affinity to duplex DNA.

3.2.3 Induced circular dichroism (ICD)

3.2.3.a Induced circular dichroism for 3.1 interacting with FSDNA

The binding mode of interaction of **3.1** with FSDNA was further studied using circular dichroism spectroscopy. Circular dichroism spectra for **3.1** were recorded at different FSDNA concentrations (0 mM – 0.11 mM) in buffer (25 mM MOPS, pH 7.0 and 50 mM NaCl) at 25 °C (Figure 3.18).

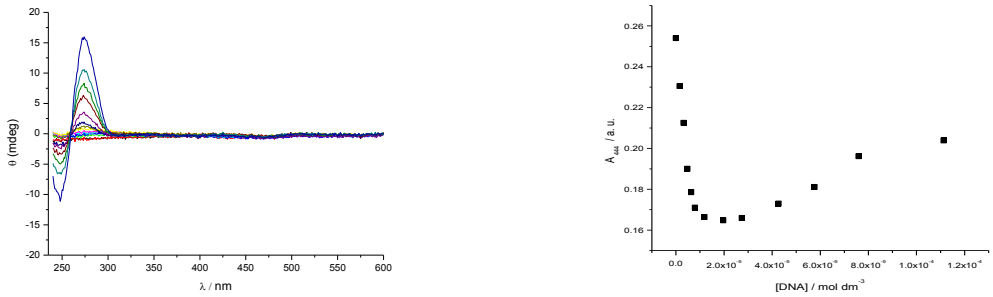

(a) (b)

Figure 3.18 Circular dichroism spectra for 0.015 mM of **3.1** in the presence of different concentrations of FSDNA (0 mM – 0.11 mM) (a), recorded UV-visible spectra for the same titration (b), in buffer (25 mM MOPS, 50 mM NaCl, pH 7.0) at 25 °C.

Figure 3.18 does not show any significant induced circular dichroism around the wavelength of interest 347 nm where compound **3.1** absorbs.

3.2.3.b Induced circular dichroism for 3.3 interacting with FSDNA

The binding mode of interaction of **3.3** with FSDNA was further studied using circular dichroism spectroscopy. Circular dichroism spectra for **3.3** were recorded at different FSDNA concentrations (0 mM – 0.11 mM) in buffer (25 mM MOPS, pH 7.0 and 50 mM NaCl) at 25 °C (Figure 3.19).

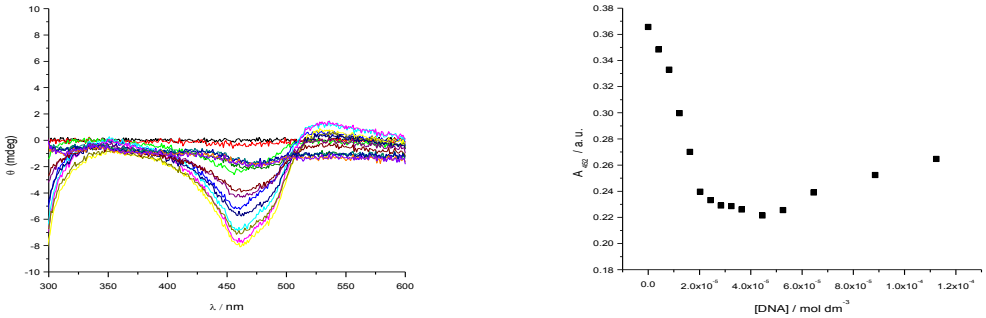

(a) (b)

Figure 3.19 Circular dichroism spectra for 0.02 mM of **3.3** in the presence of different concentrations of FSDNA (0 mM – 0.11 mM) (a), recorded UV-visible spectra for the same titration (b), in buffer (25 mM MOPS, 50 mM NaCl, pH 7.0) at 25 °C.

Figure 3.19 shows a significant induced circular dichroism spectrum around the wavelength of interest 452 nm where compound **3.3** absorbs. To quantify the affinity of **3.3** for FSDNA, the ellipticities at 452 nm were plotted as a function of concentration of FSDNA (Figure 3.20).

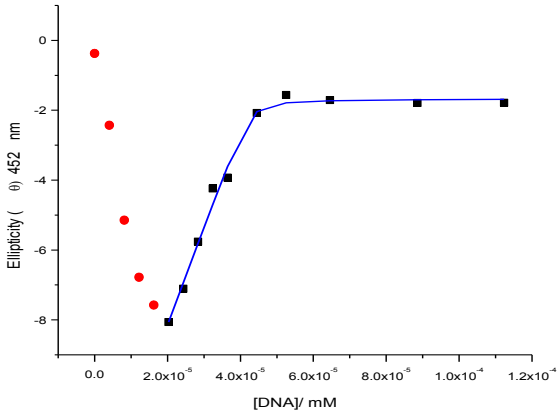

Figure 3.20 Ellipticity at 452 nm plotted against FSDNA concentrations for 0.02 mM of **3.3**, in buffer (25 mM MOPS, 50 mM NaCl, pH 7.0) at 25 °C. The solid line represents the best fit to a multiple independent sites model.

The titration curve in Figure 3.20 was analysed by fitting a multiple independent binding sites model, which also takes ligand dilution into account, to the data. The fit gives an equilibrium constant ($K_{binding}$) of (2.10 ± 3.3) $\times 10^7$ M^{-1} and a binding site size of (1.97 ± 0.07) base pairs. A negative ICD signal suggests that **3.3** intercalates between the base pairs.[1]

Summary

The titration of **3.1** against FSDNA did not show any noticeable ICD signal therefore no evidence was found to determine the mode of binding. In contrast, the titration of **3.3** against FSDNA showed a significant negative ICD signal which suggests that **3.3** binds with FSDNA through intercalation. The titration data of **3.3** with FSDNA were analysed in terms of a multiple independent binding sites model, giving an apparent equilibrium constant ($K_{binding}$) of (2.10 ± 3.3) $\times 10^7$ M^{-1} and an apparent binding site size of (1.97 ± 0.07) base pairs. The large error margins suggest significant parameter covariance. We therefore re-analysed the data for a binding site size n restricted to 2 base pairs (the reason for not restricting n to 3 base pairs is that for n = 3 the fit doesnot reproduce the experimental data well). The fit gave an equilibrium constant ($K_{binding}$) of (2.8 ± 3.8) $\times 10^7$ M^{-1}. Because equilibrium constants cannot be negative, we express the error margin as a confidence interval so that the equilibrium constant is 2.8 $\times 10^7$ [0 – 6.6$\times 10^7$] M^{-1}.

3.2.4 Viscosity

3.2.4.a Binding of 3.1 and 3.3 to calf thymus DNA (CT-DNA)

In order to find out whether compound **3.1** and **3.3** are groove binders or intercalators, the relative viscosity of CT-DNA upon addition of **3.1** or **3.3** was compared with viscosities of equivalent CT-DNA solutions that contained known DNA binders which are either an intercalator (ethidium bromide) or a minor groove binder (H33258).[7] The relative viscosities of CT-DNA solutions were measured upon addition of **3.1** and **3.3** in buffer (25 mM MOPS, pH 7.0 and 50 mM NaCl) at 25 °C (Figure 3.21).

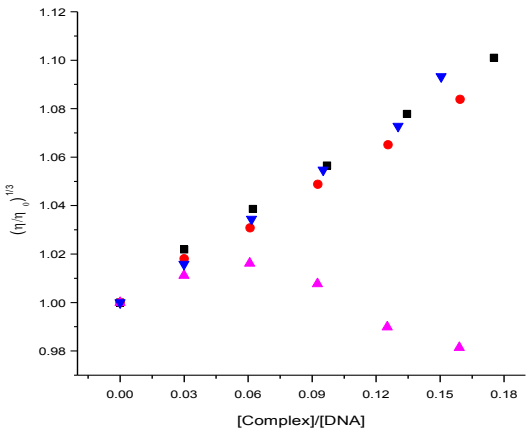

Figure 3.21 Relative viscosity of a 0.5 mM CT-DNA solution upon addition of **3.1** (■), **3.3** (▼), H33258 (▲) and ethidium bromide (●) at 25 °C in 25 mM MOPS, pH 7.0, 50 mM NaCl.

Figure 3.21 shows a significant increase in relative viscosity of CT-DNA solution upon the addition of **3.1** and **3.3**. The increase in viscosity is similar to the increase observed upon addition of ethidium bromide, suggesting intercalation as the binding mode.

Summary

The addition of **3.1** and **3.3** to CT-DNA solution cause a significant increase in relative viscosity of CT-DNA solution, similar to the increase in the viscosity of CT-DNA solution that is observed upon addition of known intercalator ethidium bromide which suggests that both compound **3.1** and **3.3** bind to CT-DNA via intercalation.

3.2.5 Molecular docking studies

3.2.5.a Docking studies of 3.1 and 3.3 binding to DNA

The binding mode for interaction of **3.1** and **3.3** with ds-DNA was further studied through a molecular docking study using Auto Dock Vina.[6] Our previously developed[8] open-d(ATCGAGACGTCTCGAT)$_2$ was used as the biomacromolecular target.

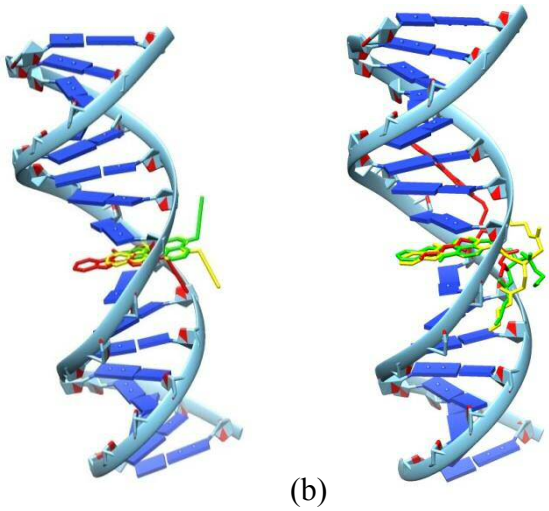

(a) (b)

Figure 3.22 Top 3 docked poses for **3.1** (a) and **3.3** (b) interacting with open-d(ATCGAGACGTCTCGAT)$_2$.

The results of the molecular docking study (Table 3.12) show that intercalation is a favourable binding mode for **3.1** and **3.3** where the planar hydrophobic parts of molecule intercalate between base pairs. The complex structures in Figure 3.22 are in agreement with the results of the binding mode study by viscometry.

Table 3.12 Mode and enthalpy of binding for top 3 docked poses of 3.1 and 3.3.

Compound **3.1**	Mode of binding	Energy / kcal. mole^{-1}
Pose 1	intercalated	-9.6
Pose 2	intercalated	-8.9
Pose 3	intercalated	-8.9
Compound **3.3**		
Pose 1	minor groove	-8.8
Pose 2	intercalated	-8.7
Pose 3	intercalated	-8.7

3.2.6 Sequence selectivity

The selectivity of a family of dendrimeric compounds **3.1** and **3.3** for selected specific sequences of DNA, viz. $(dAdT)_{12}$●$(dAdT)_{12}$ and $(dGdC)_{12}$●$(dGdC)_{12}$ was studied using UV-visible spectroscopy.

3.2.6.a Binding of 3.1 to $(dAdT)_{12}$●$(dAdT)_{12}$

The binding of **3.1** to $(dAdT)_{12}$●$(dAdT)_{12}$ was studied using UV-visible spectroscopy; the changes in absorption of **3.1** upon addition of $(dAdT)_{12}$●$(dAdT)_{12}$ were measured in buffer (25 mM MOPS, pH 7.0 and 50 mM NaCl) at 25 °C (Figure 3.23).

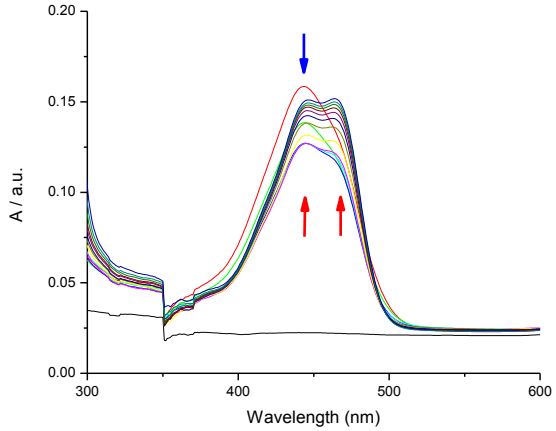

Figure 3.23 UV-visible spectra for 0.008 mM **3.1** upon addition of 0 – 2.2 mM $(dAdT)_{12}$●$(dAdT)_{12}$ in 25 mM MOPS, pH 7.0, 50 mM NaCl, at 25 °C.

Figure 3.23 shows a hypochromic shift in absorbance (at the λ_{max} of 444 nm) followed by hyperchromic shift (at the λ_{max} of 444 nm) of **3.1** upon addition of $(dAdT)_{12}$●$(dAdT)_{12}$. In addition, a peak at 475 nm grows considerably. This change in UV-visible absorption may occur as a result of geometrical distortion of **3.1** when it interacts with DNA, but it may also be a local medium effect. On the other hand, absorbance in the range of 550-600 nm increases slightly at the first additions of DNA, suggesting some precipitation. Precipitation was also observed by naked-eye.

To quantify the affinity of **3.1** for $(dAdT)_{12}$●$(dAdT)_{12}$, the absorbances at 444 nm were plotted as a function of concentration of $(dAdT)_{12}$●$(dAdT)_{12}$ (Figure 3.24).

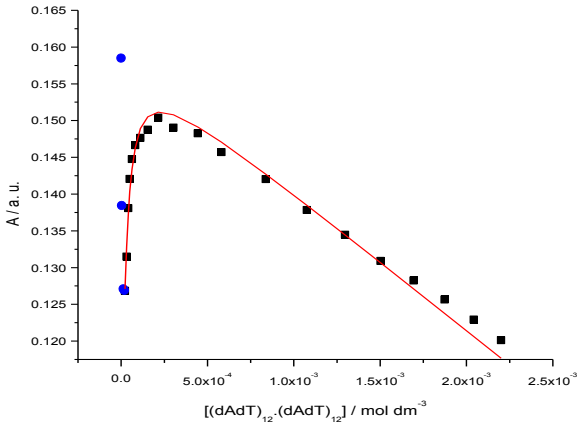

Figure 3.24 Absorbance at 444 nm of a solution of 0.008 mM **3.1** as a function of $(dAdT)_{12}$●$(dAdT)_{12}$ concentration of 0 – 0.018 mM (●) and of 0.022 – 2.2 mM (■), in 25 mM MOPS, pH 7.0, 50 mM NaCl, at 25 °C. The solid line represents a fit of a multiple independent sites model to the data in the range of 0.022 – 2.2 mM.

Figure 3.24 shows two binding events. In the first binding event a sudden decrease in absorbance was observed. We attribute this sudden decrease in absorption to strong binding of **3.1** to the sugar-phosphate backbone of DNA at low DNA/ligand ratio, leading to charge neutralization of **3.1**-DNA complexes and eventually precipitation. The titration data of Figure 3.20 (with the first event excluded) were analysed in terms of a multiple independent binding sites models, which also takes ligand dilution into account, giving an apparent equilibrium constant ($K_{binding}$) of (0.15 ± 49) M^{-1} and a binding site size of (2.1 ± 0.06) $\times 10^{-6}$ base pairs. The obtained binding parameters were unreasonably small with an ill-defined stoichiometry therefore the data were reanalyzed at fixed stoichiometry n=3. The fit gave an apparent binding constant of (17.35 ± 3.3) $\times 10^{4}$ M^{-1}.

3.2.6.b Binding of 3.1 to $(dGdC)_{12}$●$(dGdC)_{12}$

The binding of **3.1** to $(dGdC)_{12}$●$(dGdC)_{12}$ was studied using UV-visible spectroscopy; the changes in absorption of **3.1** upon addition of $(dGdC)_{12}$●$(dGdC)_{12}$ were measured in buffer (25 mM MOPS, pH 7.0 and 50 mM NaCl) at 25 °C (Figure 3.25).

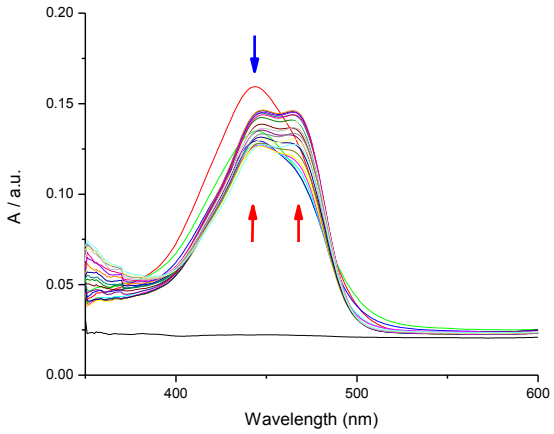

Figure 3.25 UV-visible spectra for 0.0085 mM **3.1** upon addition of 0 – 2.26 mM $(dGdC)_{12}$●$(dGdC)_{12}$ in 25 mM MOPS, pH 7.0, 50 mM NaCl, at 25°C.

Figure 3.25 shows a hypochromic shift in absorbance (at the λ_{max} of 444 nm) followed by hyperchromic shift (at the λ_{max} of 444 nm) of **3.1** upon addition of $(dGdC)_{12}$●$(dGdC)_{12}$. In addition, a peak at 475 nm grows considerably. This change in UV-visible absorption may occur as a result of geometrical distortion of **3.1** when it interacts with DNA, but it may also be a local medium effect. On the other hand, absorbance in the range of 550-600 nm increases at the first additions of DNA, again suggesting some precipitation. Precipitation was also observed by naked-eye.

To quantify the affinity of **3.1** for $(dGdC)_{12}$●$(dGdC)_{12}$, the absorbances at 444 nm were plotted as a function of concentration of $(dGdC)_{12}$●$(dGdC)_{12}$ (Figure 3.26).

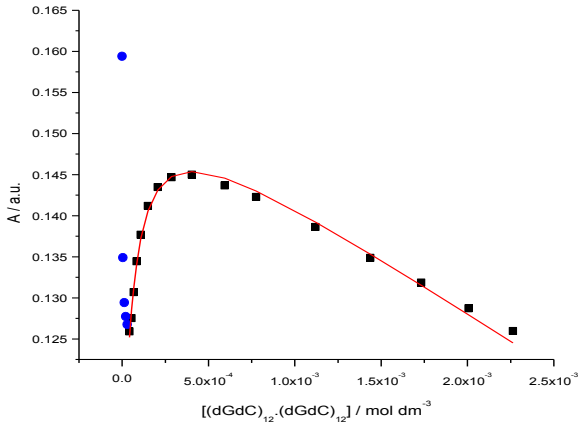

Figure 3.26 Absorbance at 444 nm of a solution of 0.0085 mM **3.1** as a function of $(dGdC)_{12}$●$(dGdC)_{12}$ concentration of 0 – 0.029 mM (●) and of 0.041 – 2.26 mM (■), in 25 mM MOPS, pH 7.0, 50 mM NaCl, at 25 °C. The solid line represents a fit of a multiple independent sites model to the data in the range of 0.041 – 2.2 mM.

Figure 3.26 shows two binding events. For the first binding event a sudden decrease in absorbance was observed. We attribute this sudden decrease in absorption to strong non-specific binding of **3.1** to the sugar-phosphate backbone of $(dGdC)_{12}$●$(dGdC)_{12}$ at low DNA/ligand ratio, leading to charge neutralization of **3.1**-DNA complexes and eventually precipitation. The titration data of Figure 3.26 (with the first event not included) were analysed by fitting a multiple independent binding sites model, which also takes ligand dilution into account, to the data, giving an apparent equilibrium constant ($K_{binding}$) of (5.7 ± 0.7) $\times 10^4$ M^{-1} for a binding site size restricted to 3.0 base pairs.

3.2.6.c Binding of 3.3 to $(dAdT)_{12}$●$(dAdT)_{12}$

The binding of **3.3** to $(dAdT)_{12}$●$(dAdT)_{12}$ was studied using UV-visible spectroscopy; the changes in absorption of **3.3** upon addition of $(dAdT)_{12}$●$(dAdT)_{12}$ were measured in buffer (25 mM MOPS, pH 7.0 and 50 mM NaCl) at 25 °C (Figure 3.27).

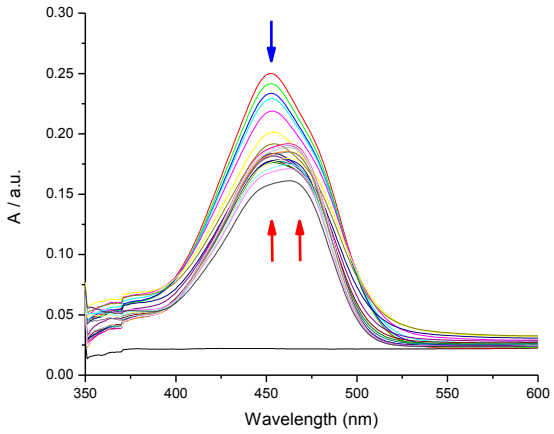

Figure 3.27 UV-visible spectra for 0.011 mM **3.3** upon addition of 0 – 1.8 mM $(dAdT)_{12}$●$(dAdT)_{12}$ in 25 mM MOPS, pH 7.0, 50 mM NaCl, at 25°C.

Figure 3.27 shows a hypochromic shift in absorbance (at the λ_{max} of 452 nm) followed by hyperchromic shift (at the λ_{max} of 452 nm) of **3.3** upon addition of $(dAdT)_{12}$●$(dAdT)_{12}$. In addition, peak at 475 nm grows considerably. This change in UV-visible absorption may occur as a result of geometrical distortion of **3.3** when it interacts with DNA, but it may also be a local medium effect. As before, the absorbance in the range of 550-600 nm increases at the first additions of DNA, suggesting some precipitation. Precipitation was also observed by naked-eye.

To quantify the affinity of **3.3** for $(dAdT)_{12}$●$(dAdT)_{12}$, the absorbances at 452 nm were plotted as a function of concentration of $(dAdT)_{12}$●$(dAdT)_{12}$ (Figure 3.28).

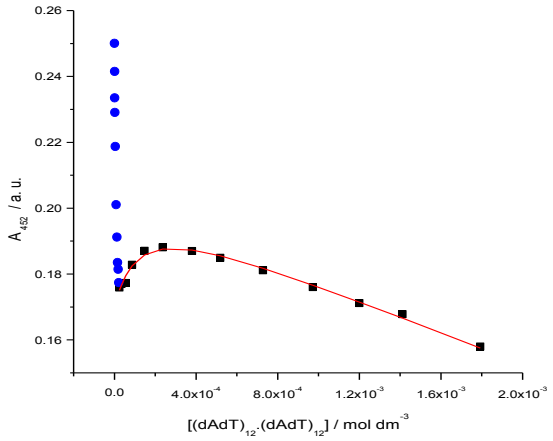

Figure 3.28 Absorbance at 452 nm of a solution of 0.011 mM **3.3** as a function of $(dAdT)_{12}$●$(dAdT)_{12}$ concentration of 0 – 0.021 mM (●) and of 0.024 – 1.8 mM (■), in 25 mM MOPS, pH 7.0, 50 mM NaCl, at 25 °C. The solid line represents a fit in terms of a multiple independent sites model to the data in the range of 0.024 – 1.8 mM.

Figure 3.28 shows two binding events. In the first binding event a sudden decrease in absorbance was observed. We attribute this sudden decrease in absorption to strong binding of **3.3** to the sugar-phosphate backbone of $(dAdT)_{12}$●$(dAdT)_{12}$ at low DNA/ligand ratio, leading to charge neutralization of **3.3**-DNA complexes and eventually precipitation. The titration data of Figure 3.28 (with the first event not included) were analysed in terms of a multiple independent binding sites model, which also takes ligand dilution into account, to the data. The fit gave an apparent equilibrium constant ($K_{binding}$) of (30.9 ± 5.57) $\times 10^3$ $M^{-1}$for a binding site size restricted to 3.0 base pairs.

3.2.6.d Binding of 3.3 to $(dGdC)_{12}$●$(dGdC)_{12}$

The binding of **3.3** to $(dGdC)_{12}$●$(dGdC)_{12}$ was studied using UV-visible spectroscopy; the changes in absorption of **3.3** upon addition of $(dGdC)_{12}$●$(dGdC)_{12}$ were measured in buffer (25 mM MOPS, pH 7.0 and 50 mM NaCl) at 25 °C (Figure 3.29).

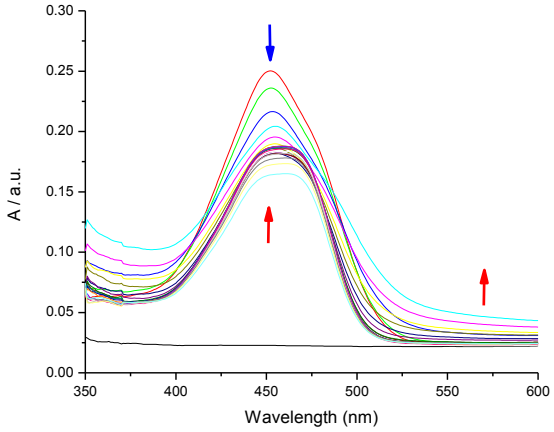

Figure 3.29 UV-visible spectra for 0.011 mM **3.3** upon addition of 0 – 2.2 mM $(dGdC)_{12}$●$(dGdC)_{12}$ in 25 mM MOPS, pH 7.0, 50 mM NaCl, at 25°C.

Figure 3.29 shows a hypochromic shift in absorbance (at the λ_{max} of 452 nm) followed by hyperchromic shift (at the λ_{max} of 452 nm) of **3.3** upon addition of $(dGdC)_{12}$●$(dGdC)_{12}$. This change in UV-visible absorption may occur as a result of geometrical distortion of **3.3** when it interacts with DNA, but it may also be a local medium effect. The absorbance in the range of 550-600 nm increases at the first additions of DNA, as before, suggesting some precipitation. Precipitation was also visible by naked-eye.

To quantify the affinity of **3.3** for $(dGdC)_{12}$●$(dGdC)_{12}$, the absorbances at 452 nm were plotted as a function of concentration of $(dGdC)_{12}$●$(dGdC)_{12}$ (Figure 3.30).

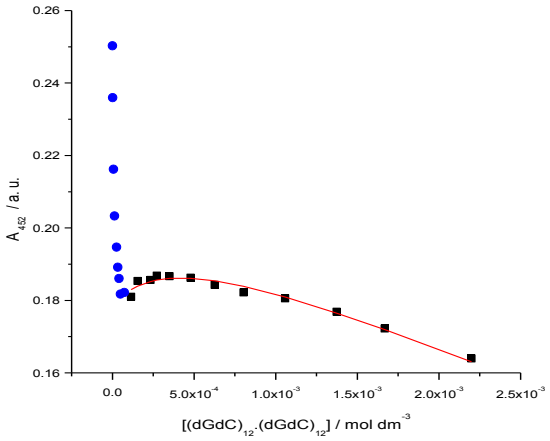

Figure 3.30 Absorbance at 452 nm of a solution of 0.011 mM **3.3** as a function of $(dGdC)_{12}$●$(dGdC)_{12}$ concentration of 0 – 0.07 mM (●) and of 0.11 – 2.2 mM (■), in 25 mM MOPS, pH 7.0, 50 mM NaCl, at 25 °C. The solid line represents a fit in terms of a multiple independent sites model to the data in the range of 0.11 – 2.2 mM.

Figure 3.30 shows two binding events. For the first binding event a rapid decrease in absorbance was observed. We attribute this sudden decrease in absorption to strong binding of **3.3** to the sugar-phosphate backbone of $(dGdC)_{12}$●$(dGdC)_{12}$ at low DNA/ligand ratio, leading to charge neutralization of **3.3**-DNA complexes and eventually precipitation. The titration data of Figure 3.30 (with the first event excluded) were analysed in terms of a multiple independent binding sites model, which also takes ligand dilution into account, giving an apparent equilibrium constant ($K_{binding}$) of $(7.19 \pm 2.64) \times 10^3\ M^{-1}$ for a binding site size restricted to 3.0 base pairs.

Summary

The results of UV-visible titrations for compounds of **3.1** and **3.3** with specific sequences of DNA, $(dAdT)_{12}\bullet(dAdT)_{12}$ and $(dGdC)_{12}\bullet(dGdC)_{12}$ show that these ligands **3.1** and **3.3** have different affinities toward $(dAdT)_{12}\bullet(dAdT)_{12}$ and $(dGdC)_{12}\bullet(dGdC)_{12}$. The obtained affinities of these compounds are summarised in Table 3.13.

Table 3.13 Apparent binding constants K_{bind} and binding site sizes *n* from UV-visible spectroscopy for 3.1 and 3.3 binding to $(dAdT)_{12}\bullet(dAdT)_{12}$, $(dGdC)_{12}\bullet(dGdC)_{12}$, and FS-DNA in 25 mM MOPS, pH 7.0, 50 mM NaCl, at 25 °C.

Compound	*$(dAdT)_{12}\bullet(dAdT)_{12}$*		*$(dGdC)_{12}\bullet(dGdC)_{12}$*		*FS-DNA*	
	K_{bind} / $\times 10^4$ M^{-1}	*n / bp*	*K_{bind} / $\times 10^4$ M^{-1}*	*n / bp*	*K_{bind} / $\times 10^4$ M^{-1}*	*n / bp*
3.1	17.35 ± 3.3	3*	5.7 ± 0.7	3*	1.30 ± 0.21	3*
3.3	2.95 ± 0.54	3*	0.65 ± 0.23	3*	6.43 ± 1.61	3*

* restricted.

Compounds **3.1** and **3.3** bind to specific sequences of DNA, viz. $(dAdT)_{12}\bullet(dAdT)_{12}$ and $(dGdC)_{12}\bullet(dGdC)_{12}$ with different affinities. Compound **3.1** binds to $(dAdT)_{12}\bullet(dAdT)_{12}$ with a binding constant of $(17.35 \pm 3.3) \times 10^4$ M^{-1} for a binding site size restricted to 3.0 base pairs, whereas **3.1** has a weaker affinity to $(dGdC)_{12}\bullet(dGdC)_{12}$ with a binding constant of $(5.7 \pm 0.7) \times 10^4$ M^{-1} for a binding site size restricted to 3.0 base pairs. Similarly, compound **3.3** shows a bigger affinity to $(dAdT)_{12}\bullet(dAdT)_{12}$ with a binding constant of $(29.57 \pm 5.4) \times 10^3$ M^{-1} for a binding site size restricted to 3.0 base pairs, whereas, compound **3.3** binds more weakly to $(dGdC)_{12}\bullet(dGdC)_{12}$ with a binding constant of $(6.5 \pm 2.3) \times 10^3$ M^{-1} for a binding site size restricted to 3.0 base pairs. In addition, the binding parameters that were determined here are apparent binding constants and binding site sizes since the ligands have non-specific binding to the sugar-phosphate backbone of DNA. The binding site size was restricted to 3.0 base pairs for most titrations in order to obtain reasonable binding parameters.

3.3 Conclusions

All compounds of the dendrimeric family bind to duplex DNA to a different extent and binding is typically accompanied by change in optoelectronic properties of the compound with consecutive hypochromic and hyperchromic shifts in absorbances at maximum absorption. The binding constants for **3.1** and **3.3** are in the range of (10^4 to 10^5) M^{-1} with the binding site size restricted to 3.0 base pairs. **3.1** and **3.3** bind strongly to duplex FSDNA in two separate binding events. In the UV-visible titration the first event occurs at high ligand/DNA ratio, leading to a sudden decrease in the maximum absorption. We attribute this change in absorption to strong binding of **3.1** and **3.3** to both high affinity binding sites and to the sugar-phosphate backbone of duplex FSDNA, leading to charge neutralization of ligand-DNA complexes and eventually precipitation. The second event occurs at low ligand/DNA ratio where ligand binds to main binding sites of DNA viz. minor groove or intercalation. Compound **3.2** binds more weakly with FSDNA compared to **3.1** and **3.3**. We attribute this difference to the presence of a negatively charged caboxylate group (COO^-) in **3.2** which leads to increase net charges on the ligand and results in a repulsive force between the negative charges of the DNA backbone and the ligand. The interaction between **3.4** and duplex FSDNA leads to significant precipitation and changes in UV-visible absorption that makes a titration curve difficult to analyse. Therefore, we decided to analyse the titration data of compound **3.4** in another way, as we described in Section 3.2.1.c.

Isothermal titration calorimetry also suggests two binding events for **3.1** and **3.3** to FSDNA, confirming results from UV-visible titrations. The negative enthalpy and entropy change of the first binding event for **3.3** suggests that this ligand intercalates between base pairs. In addition, the results of ITC show that compound **3.2** has low affinity to duplex DNA.

Circular dichroism spectroscopy was used to study the mode of binding. Only **3.3** showed a significant negative ICD signal upon the addition of FSDNA, suggesting intercalation as a binding mode. The binding mode was further studied using viscometry. The relative viscosity of CTDNA solution increased rapidly upon the addition of **3.1** and **3.3**. This rapid increase in the viscosity is similar to the change in relative viscosity of CTDNA upon the addition of known intercalator ethidium

bromide, again suggesting intercalation as a binding mode. To further support the results of binding mode studies by ICD and viscometry, a molecular docking study was carried out. The results of molecular docking study for **3.1** and **3.3** showed that both ligands interact with duplex DNA via intercalation. Finally, the sequence selectivity of **3.1** and **3.3** were explored using UV-visible spectroscopy and the results showed that these compounds have higher affinity for $(dAdT)_{12}\bullet(dAdT)_{12}$ than for $(dGdC)_{12}\bullet(dGdC)_{12}$.

The driving forces for the compounds of dendrimeric family binding to DNA could be provided by hydrophobic interactions between the conjugated aromatic frameworks and hydrophobic parts of the base pairs, in addition to electrostatic interaction between cationic charge on NH_3^+ and the negative charges on the DNA.

3.4 Materials and Methods

3.4.1 DNA preparation

All compounds studied in this chapter were provided by our collaborators. All experiments were carried out in buffer (25 mM MOPS, 50 mM NaCl, pH 7.0, at 25 °C). The pH of the buffer was determined using a Hanna Instruments pH 210 pH meter equipped with a VWR 662-1759 glass electrode. The buffer components were purchased from Acros or Sigma-Aldrich. Fish sperm DNA and Calf thymus DNA were also purchased from Acros or Sigma-Aldrich. The stock solution of calf thymus DNA was prepared by sonicating a solution of CT-DNA for about 30 minutes whereas the stock solution of fish sperm DNA was prepared by sonicating a solution of FS-DNA for about 10 minutes. The sonicator was used in DNA preparation in order to quicken the solvation of DNA in buffer. Fish sperm DNA needs less sonicating because FS-DNA dissolves more quickly in MOPS buffer.

The DNA solution was dialysed against 2.0 litres of buffer using a 3.5 kDa MWCO dialysis membrane for 24 hours. The concentration of DNA was determined using UV-visible spectroscopy using an extinction coefficient of 12800 M^{-1} cm^{-1} at 260 nm.[4]

3.4.2 Spectroscopic studies

UV-visible spectra were recorded using a Jasco V-630 Bio spectrophotometer equipped with a peltier temperature controller at 25 °C. Circular dichroism spectra were recorded on a Chirascan CD spectrophotometer. Stock solutions of **3.1**-**3.4** in buffer were freshly prepared and volumes of these stock solutions were added into 2000-2500 µl of buffer as required in a 1.0 cm path length cuvette. All UV-visible titrations were carried out by adding aliquots of the DNA stock solution into a 1 cm path length cuvette which contains ligand solution, measuring the absorption in the range of 200-600 after each addition. The absorption in the range of 0.1-0.6 a.u. was measured in a cuvette to avoid self-aggregation and precipitation of the ligand. The absorptions at selected wavelength were plotted against DNA concentrations and a multiple independent binding sites model (see section 1.10.1 in Chapter 1) was used to analyse the UV-visible spectra by Origin 9.0. The baseline absorbance in a titration, and hence in the data analysis, corresponds to the absorbance of a cuvette containing buffer only because the spectrophotometer was calibrated without cuvettes in the sample or reference position ("air versus air"). For CD titrations the same steps were followed except the ICD signals were used instead of absorptions in UV-visible titrations.

3.4.3 Isothermal titration calorimetry

All ITC experiments were carried out using a Microcal VP ITC microcalorimeter. The ligand solutions were prepared in buffer (25 mM MOPS, 50 mM NaCl, pH 7.0) and concentrations were determined using UV-visible spectroscopy based on extinction coefficients. All calorimetric binding experiments were carried out at 25 °C. The sample cell and syringe were always cleaned with ethanol followed by distilled water before starting any experiment. The sample cell was filled with FS-DNA solution (approximately 1.9 ml). The syringe was filled with ligand solution (approximately 300 µl) with a concentration usually 12-fold higher than DNA solution (exact ratios depend on individual experiments). The ligand solution was added in 1 injection of 5 µl for the first addition and 19 injections of 15 µl each to the sample cell, injecting every 300 second automatically. During the titration the solutions in the contents of the sample cell were mixed with a stirring speed of 307 rpm. The heat effects per

injection (dh) were calculated using Origin (Microcal, Inc). The integrated heat effects were analysed using IC ITC.[2]

3.4.4 Viscometry

All viscosimetry experiments were carried out in buffer (25 mM MOPS, 50 mM NaCl, pH 7.0). A Cannon-Flenske routine viscometer was placed in a temperature-controlled circulated water bath at 25 °C. The viscometer was filled with fixed volume of a Calf thymus DNA solution (3.0 ml of 0.5 mM) and adding ligand solutions with concentrations calculated from the ratio of ligand/ DNA (0.03, 0.06, 0.09, 0.12 and 0.15). The flow time was measured three times for each ligand addition and the results were averaged. The relative viscosity was calculated and plotted as a function of the ratio $[ligand]_{bound}/[DNA]$ where $[ligand]_{bound}$ was calculated using binding parameters from UV-visible spectroscopy.

2.4.5 Docking studies

Molecular docking studies were performed using Auto Dock Vina.[6] The ligand structures were generated using chemdraw and then optimised using Avogadro, using force fields MMFF94 for ligands and GAFF for metal complexes. The rotable bonds in the ligand were assigned using Auto Dock Tools 1.5.6 and the output files were saved in PDBQT format. Our previously developed[9] open-$d(ATCGAGACGTCTCGAT)_2$ was used as a biomacromolecular target. An exhaustiveness of 200 and number modes of 10 were selected. The results of Auto Dock Vina were rendered using Chimera 1.10.2.

References

1- Garbett, N. C.; Ragazzon, P. A.; Chaires, J. B., Nat. Protoc 2007, 2 (12), 3166-3172.

2- Buurma, N. J.; Haq, I., J. Mol. Biol. 2008, 381 (3), 607-621.

3-Buurma, N. J.; Haq, I., Methods 2007, 42 (2), 162-172.

4- Ren, J. S.; Chaires, J. B., Biochemistry 1999, 38 (49), 16067-16075.

5- Chaires, J. B., Arch. Biochem. Biophys. 2006, 453 (1), 26-31.

6- O. Trott, A. J. Olson, AutoDock Vina: improving the speed and accuracy of docking with a new scoring function, efficient optimization and multithreading, Journal of Computational Chemistry 31 (2010) 455-461.

7- Satyanarayana, S.; Dabrowiak, J. C.; Chaires, J. B., Biochemistry 1993, 32 (10), 2573-2584.

8- Jones, J. E.; Amoroso, A. J.; Dorin, I. M., Parigi, G.; Ward, B.D.; Buurma, N.J. and Pope, S.J., Chemical Communications 2011, 47 (12), 3374-3376.

9- El-Betany, A. M.; Vachova, L.; Bezzu, C.G.; Pope, S. J. and McKeown, N. B., Tetrahedron 2013, 69 (39), 8439-8445.

Chapter 4

DNA BINDING STUDIES FOR MISCELLANEOUS COMPOUNDS

Abstract

*In this chapter we describe the results of studies of the interactions of miscellaneous compounds with double-stranded DNA using a variety of techniques viz. spectroscopy, calorimetry, viscosity and molecular docking studies. Most ligands bind to duplex DNA moderately strongly with a range of affinities from 10^4 to 10^5 M^{-1}. Binding modes vary from minor-groove binding to intercalation to side-by-side binding in the minor groove. Compound **4.1** binds to duplex DNA via intercalation whereas compound **4.2** binds to duplex DNA and the dominant binding site for **4.2** is in the minor groove. Compound **4.3** also shows affinity to duplex DNA. Sequence selectivity of **4.2** for specific sequences $(dAdT)_{12}$●$(dAdT)_{12}$ and $(dGdC)_{12}$●$(dGdC)_{12}$ was also explored via UV-visible spectroscopy, showing that $(dAdT)_{12}$●$(dAdT)_{12}$ was selected over $(dGdC)_{12}$●$(dGdC)_{12}$.The results presented in part A of this Chapter have been published.*[7]

Part A

4.1 Introduction

Our aims in the first part of Chapter 4 are to quantify the thermodynamics of binding for compound **4.1** (Scheme 4.1) to duplex DNA, using UV-visible spectroscopy. Binding modes will be explored through a molecular docking study.

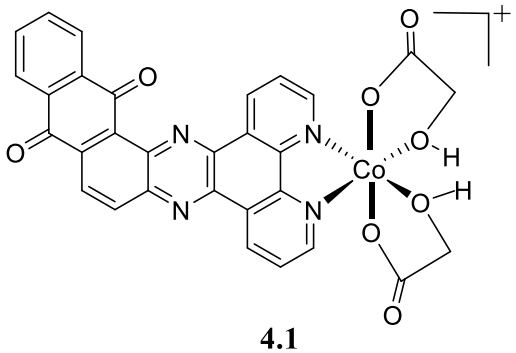

4.1

Scheme 4.1

Compound **4.1** in Scheme 4.1 was provided by our collaborator. Compound **4.1** is somewhat water-soluble, redox active, absorbs light with a λ_{max} at 394 nm and has a flat aromatic framework. Based on its structure, we anticipate compound **4.1** binds to double-stranded DNA through intercalation. This compound could be used as a signal enhancer in EIS-based biosensors upon binding with duplex DNA. In addition, compound **4.1** is redox active and could therefore be useful in biosensors based on-coulometry.

4.2 Results and discussion

The results of the interaction studies for compound **4.1** with DNA will be presented and discussed for each individual technique.

UV-visible spectroscopy

4.2.1 UV-visible spectroscopy studies of 4.1 binding to DNA

Binding of **4.1** to duplex DNA was studied using UV-visible spectroscopy; the changes in absorption of **4.1** upon addition of FSDNA were recorded in deionised water at 25 °C (Figure 4.1). These experiments were carried out in deionised water because of poor solubility of compound **4.1** in MOPS buffer.

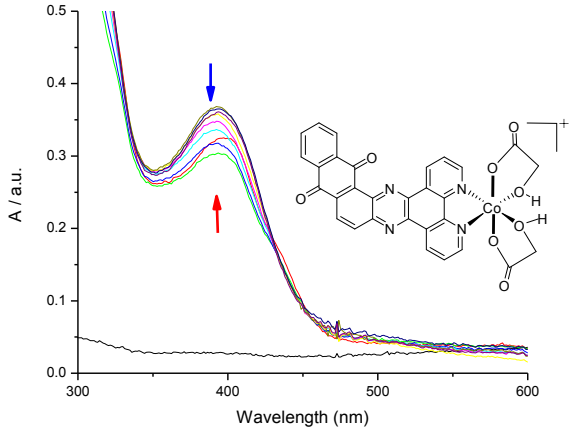

Figure 4.1 UV-visible spectra for 0.041 mM **4.1** upon addition of 0 – 0.25 mM FSDNA in deionised water at 25 °C.

Figure 4.1 shows a hypochromic shift in absorbance followed by a hyperchromic shift (at the λ_{max} of 394 nm) of **4.1** upon addition of FSDNA. This change in UV-visible absorption may occur as a result of geometrical distortion of **4.1** when it interacts with DNA, but in light of the rigidity of **4.1**, it is likely to be a local medium effect.

To quantify the affinity of **4.1** for FSDNA, the absorbances at 394 nm for two titrations were plotted as a function of concentration of FSDNA (Figure 4.2, for data in tabular format see appendix, Tables A17.1 & A17.2).

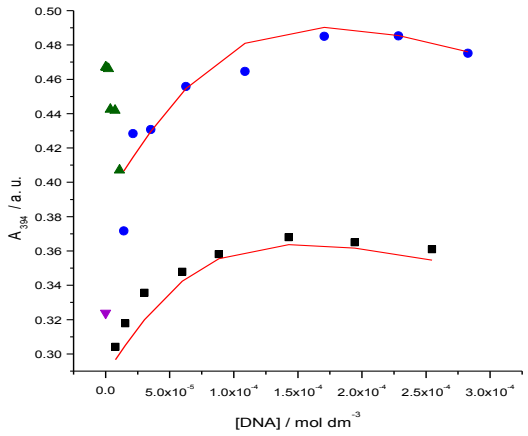

Figure 4.2 Absorbance at 394 nm of solutions of 0.041 mM **4.1** as a function of DNA concentration (0 – 0.007 mM (▼) and of 0.007 – 0.25 mM (■)), and of 0.084 mM **4.1** as a function of DNA concentration (0 – 0.01 mM (▲) and of 0.014 – 0.28 mM (●)), in deionised water at 25 °C. The solid lines represent a global fit of a multiple independent sites model to the second part of both data sets.

Figure 4.2 shows two binding events. In the "first" binding event a rapid decrease in absorbance was observed. We attribute this rapid decrease in absorption to strong non-selective binding of **4.1** to the sugar-phosphate backbone of DNA at low DNA/ligand ratios, leading to charge neutralization of **4.1**-DNA complexes and eventually precipitation. In the "second" phase of titration a hypechromic shifit in absorbance was observed as a result of binding of **4.1** to its preferred binding sites of DNA. The titration data of Figure 4.2 (with the first event not included) were analysed in terms of a multiple independent binding sites models, which also takes ligand dilution into account, giving an apparent equilibrium constant ($K_{binding}$) of (5.54 ± 10.9) $\times 10^4$ M^{-1} and a binding site size of (1.34 ± 0.83) base pairs. The large error margins suggest significant parameter covariance. We therefore re-analysed the data for a binding site size n restricted to 1 base pair (when n is restricted to a value higher than one it gives large error margins). The fit gave an equilibrium constant ($K_{binding}$) of (3.0 ± 1.87) $\times 10^4$ M^{-1}.

Molecular docking studies

4.2.2 Docking study of 4.1 binding to DNA

The binding mode for interaction of **4.1** with duplex DNA was studied through molecular docking using Auto Dock Vina.[4] Open-d(ATCGAGACGTCTCGAT)$_2$, a duplex structure, with a pre-formed intercalation gap, was used as a biomacromolecular target.[6]

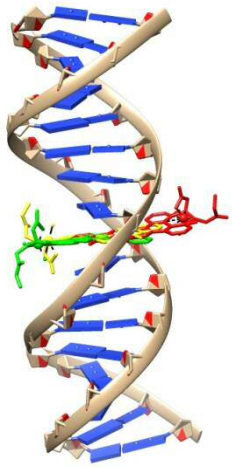

Figure 4.3 Top 3 docked poses for **4.1** interacting with open-d(ATCGAGACGTCTCGAT)$_2$.

The result of the molecular docking study (Table 4.1) shows that intercalation is a favourable binding mode for **4.1** binding with DNA as anticipated based on its structure.[7]

Table 4.1 Mode and enthalpy of binding for top 3 docked poses of 4.1.

Compound **4.1**	Mode of binding	Energy / kcal. mole^{-1}
Pose 1	intercalated	-10.3
Pose 2	intercalated	-10.3
Pose 3	intercalated	-10.3

Summary

The UV-visible titrations for compound **4.1** with duplex DNA show that ligand **4.1** binds to FS-DNA. The binding parameters for this compound interacting with FS-DNA are summarised in Table 4.2.

Table 4.2 Binding constant and binding site size for binding of 4.1 to FS-DNA, in deionised water, at 25 °C.

Ligand	Binding constant $K / \times 10^4$ M^{-1}	Binding site size n / bp
4.1	3.0 ± 1.87	1*

*restricted.

Compound **4.1** has a moderate affinity ~ 10^4 M^{-1} to FS-DNA with a small binding site size. The low apparent affinity reflects competition between specific and non-specific binding sites, rather than full binding of the ligand to its preferred binding sites. We attribute this small binding site size to binding of the ligand with DNA backbone in the minor groove in "side-by-side" fashion at low DNA concentration, leading to precipitation of ligand-DNA complex at the beginning of titration. The result of the molecular docking study suggests that intercalation is a favourable binding mode for **4.1** binding with duplex DNA.

4.3 Conclusion

Compound **4.1** binds to duplex DNA and binding is accompanied by a change in the optoelectronic properties of the compound. Compound **4.1** shows two binding events, at low DNA/ligand ratio the ligands bind in the preferred binding sites and to DNA backbone, leading to precipitation of ligand-DNA complexes. At high DNA/ligand ratio, ligands bind to main binding sites (minor groove or intercalation). The binding constant is in the range of 10^4 M^{-1} with a binding site size restricted to 1 base pair. The binding site size 1 for **4.1** is small which suggests a side by side interaction is also present as a mode of binding.

A docking study was exploited to investigate the mode of binding for **4.1** using Auto Dock Vina. The results of the molecular docking study show that intercalation is a favourable binding mode for **4.1** binding with DNA as expected based on its structure.

Part B

4.4 Introduction

Our aims in the second part of Chapter 4 are to quantify the thermodynamics of binding for compound **4.2** (Scheme 4.2) to duplex DNA, using several techniques viz. UV-visible spectroscopy, isothermal titration calorimetry and circular dichroism spectroscopy. Binding modes will be explored through viscometry and a molecular docking study.

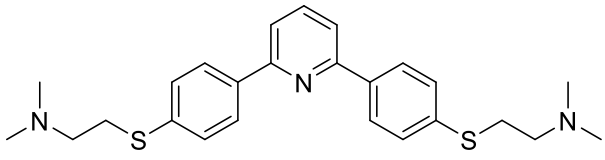

4.2

Scheme 4.2

Compound **4.2** in Scheme 4.2 was provided by our collaborator (Richard Wheelhouse).[8] Compound **4.2** is water-soluble, absorbs light with a λ_{max} at 320 and has a hydrophobic framework linked by bonds with torsional freedom which potentially enables this molecule to bind with DNA, forming a curved shape along the minor groove of duplex DNA. Compound **4.2** is known to bind to DNA●RNA hybrid duplexes, offering further flexibility in targeting nucleic acid biomarkers such as mRNA.

4.5 Results and discussion

The results of the interaction studies for compound **4.2** with DNA will be presented and discussed for each individual technique.

UV-visible spectroscopy

4.5.1 UV-visible spectroscopy studies of 4.2 binding to DNA

The binding of **4.2** to DNA was studied using UV-visible spectroscopy; the changes in absorption of **4.2** upon addition of FSDNA were recorded in buffer (25 mM MOPS, pH 7.0, 50 mM NaCl) at 25 °C (Figure 4.3).

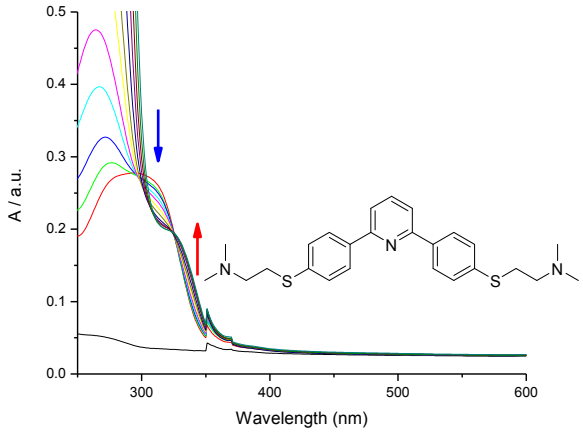

Figure 4.3 UV-visible spectra for 0.010 mM **4.2** upon addition of 0 – 0.44 mM DNA in buffer (25 mM MOPS, pH 7.0, 50 mM NaCl) at 25 °C.

Figure 4.3 shows a hypochromic shift in absorbance (at the λ_{max} of 320 nm) and a hyperchromic shift (at 338 nm) of **4.2** upon addition of DNA. This change in UV-visible absorption may occur because of geometrical distortion of **4.2** when it interacts with DNA, but it may also be a local medium effect. For this relatively flexible molecule, we propose that geometrical distortion is likey the dominant effect.

To quantify the affinity of **4.2** for FSDNA, the absorbances at 320 and 338 nm for two titrations were plotted as a function of concentration of FSDNA (Figure 4.4, for data in tabular format see appendix, Tables A17.3 & A17.4).

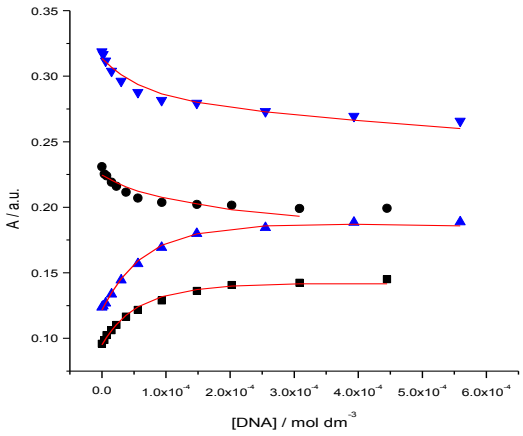

Figure 4.4 Absorbance at 320 nm (●) and at 338 nm (■) of a solution of 0.010 mM **4.2** as a function of DNA concentration, absorbance at 320 nm (▼) and at 338 nm (▲) of a solution of 0.014 mM **4.2** as a function of DNA concentration, in buffer (25 mM MOPS, pH 7.0, 50 mM NaCl), at 25 °C. The solid lines represent a global fit of a multiple independent sites model to the data.

The titration curves in Figure 4.4 were analysed globally by fitting a multiple independent binding sites model, which also takes ligand dilution into account, to the data. The fit indicates an equilibrium constant ($K_{binding}$) of (0.86 ± 50.09) $\times 10^2$ M^{-1} and a binding site size of (0.005 ± 0.3) base pair. The obtained values of binding site size and binding constant were unreasonable therefore the data of the titration curves were reanalysed, giving an equilibrium constant ($K_{binding}$) of (7.51 ± 1.22) $\times 10^4$ M^{-1} for a binding site size restricted to 3 base pairs.

Isothermal titration calorimetry (ITC)

4.5.2 Dilution of 4.2

In order to determine whether **4.2** aggregates in MOPS buffer, the dilution of **4.2** into MOPS buffer was studied using isothermal titration calorimetry. The differential heat flow and derived integrated heat effects for dilution of a solution of 0.91 mM of **4.2** into 25 mM MOPS. pH 7.0, 50 mM NaCl at 25 °C were measured (Figure 4.5).

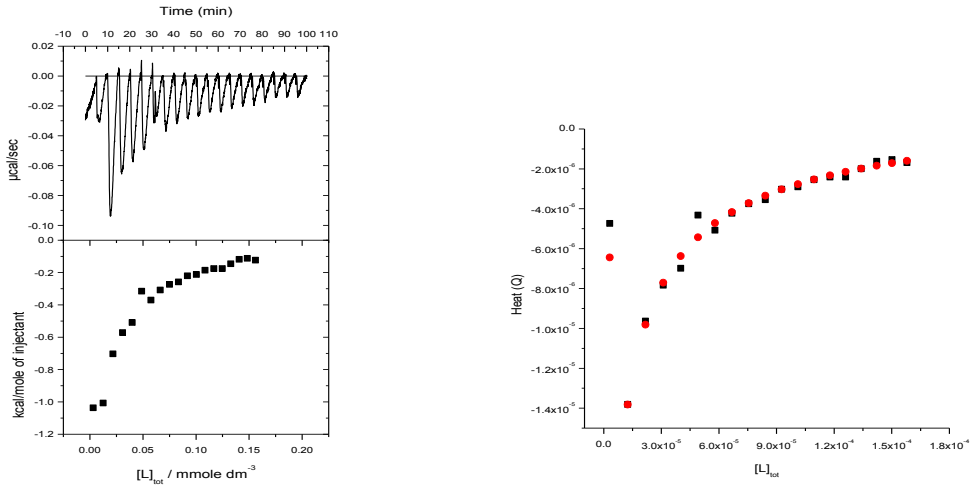

(a) (b)

Figure 4.5 Enthalpograms for dilution of a 0.91 mM solution of **4.2** (a), fit of the isosdesmic self-aggregation model to the integrated heat effects for the same dilution experiment (b), experimental heat (■), calculated heat (●), in buffer (25 mM MOPS, 50 mM NaCl, pH 7.0) at 25 °C.

Figure 4.5 shows the heats of dilution of 0.91 mM **4.2** into MOPS buffer. IC ITC software was used to analyse the titration data. The thermodynamic parameters for dilution of **4.2** in MOPS buffer were determined and are summarised in Table 4.3.

Table 4.3 Thermodynamic parameters for self aggregation of 4.2 in 25 mM MOPS, pH 7.0, 50 mM NaCl, at 25 °C.

K aggregation/ $\times 10^4$ M^{-1}	ΔH aggregation/ kcal mol^{-1}
3.54 (3.54 – 18.1)	1.9 (1.75 – 2.9)

The obtained values for thermodynamic parameters for diluting **4.2** into MOPS buffer in Table 4.3 show that 4.2 self aggregates relatively strongly in aqueous solutions.

4.5.3 ITC studies of 4.2 binding to DNA

The binding of **4.2** to DNA was further studied using isothermal titration calorimetry. The differential heat flow and derived integrated heat effects for titration of a solution of 0.91 mM **4.2** into a 0.2 mM fish sperm DNA solution were measured in buffer (25 mM MOPS, 50 mM NaCl, pH 7.0), at 25 °C (Figure 4.6).

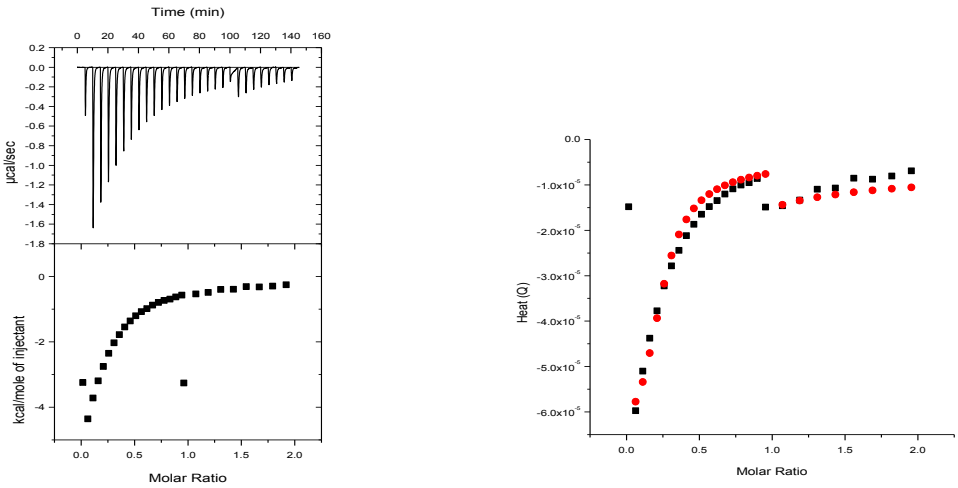

(a) (b)

Figure 4.6 Titration of a 0.91 mM solution of **4.2** into a 0.2 mM solution of DNA (a), fit for integrated heat effects of the titration in terms of a binding model involving one type of binding site which ligand aggregation included (b), experimental heat (■), calculated heat (●), in 25 mM MOPS. pH 7.0, 50 mM NaCl, at 25 °C. The titration was carried out in two consecutive sets of additions.

Figure 4.6 shows the enthalpogram for interaction of **4.2** with DNA, which suggests an exothermic interaction and one type of binding event. In order to find the binding parameters for **4.2** binding to DNA, IC ITC software was used. The aggregation constant and standard molar enthalpy change for aggregation were included and restricted to the values that were obtained from the dilution experiment. All thermodynamic parameters were determined and are summarized in Table 4.4.

Table 4.4 Thermodynamic parameters for binding of 4.2 to FSDNA in 25 mM MOPS. pH 7.0, 50 mM NaCl, at 25 °C.

	K_{A1} (10^4 M^{-1})	$1/n_{A1}$ (bp)	ΔH_{A1} (kcal mol^{-1})	$-T\Delta S_{A1}$ (kcal mol^{-1})	$\{\Sigma dev^2/dof\}^{1/2}$ (µcal)
4.2	10.0 (8.6 – 16.6)	3*	-2.9 (-1.5 – -5.6)	-3.96	2.9

* restricted.

The resulting binding parameters in Table 4.4 are in agreement with the results from UV-visible titrations. The binding site size was restricted to 3 base pairs in order to obtain reasonable binding parameters. The weakly exothermic interaction suggests that **4.2** binds to FSDNA in the minor groove.

Induced circular dichroism (ICD)

4.5.4 Induced circular dichroism for 4.2 interacting with FSDNA

The binding mode of **4.2** interacting with FSDNA was explored using circular dichroism spectroscopy. Circular dichroism spectra for **4.2** were recorded at different FSDNA concentrations (0 mM – 1.3 mM), in buffer (25 mM MOPS, pH 7.0, 50 mM NaCl) at 25 °C (Figure 4.7).

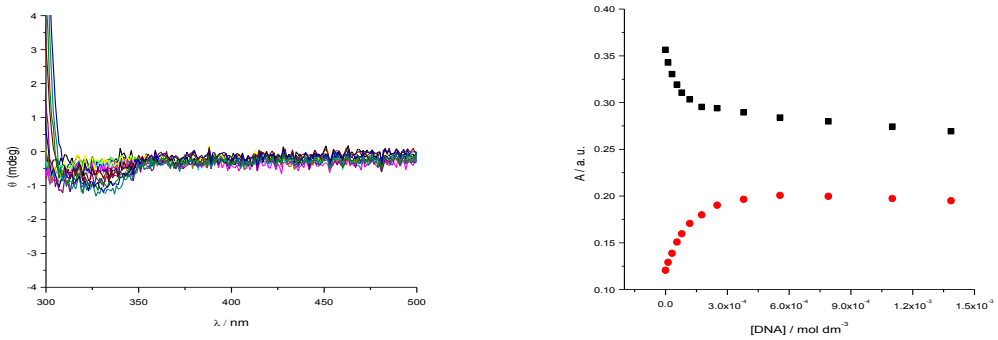

(a) (b)

Figure 4.7 a) Circular dichroism spectra for 0.018 mM of **4.2** in the presence of different concentrations of FSDNA (0 mM – 1.3 mM), and b) recorded UV-visible spectra for the same titration, in buffer (25 mM MOPS, 50 mM NaCl, pH 7.0), at 25 °C.

Figure 4.7 shows a small negative induced circular dichroism signal around the wavelength of interest 320 nm where compound **4.2** absorbs, suggesting intercalation as a mode of binding.[1]

Viscosity

4.5.5 Viscometry study of 4.2 binding to calf thymus DNA (CT-DNA)

The mode of binding of **4.2** to double-stranded DNA was further studied using viscometry. In order to find out whether **4.2** is a groove binder or an intercalator, the relative viscosity of DNA upon addition of **4.2** was compared with viscosities of equivalent DNA solutions that contained known DNA binders which act either as an intercalator (ethidium bromide) or a minor groove binder (H33258).[5] The relative viscosities of CT-DNA solutions were measured upon addition of **4.2** in buffer (25 mM MOPS, pH 7.0, 50 mM NaCl), at 25 °C (Figure 4.8).

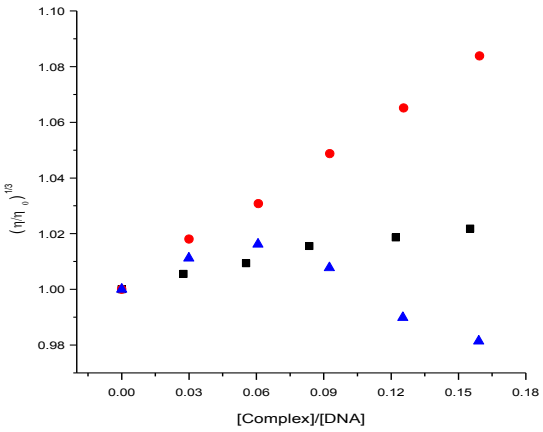

Figure 4.8 Relative viscosity of a 0.91 mM CT-DNA solution upon addition of **4.2** (■), H33258 (▲) and ethidium bromide (●), in buffer (25 mM MOPS, pH7.0, 50 mM NaCl) at 25 °C.

Figure 4.8 shows a small increase in relative viscosity of CTDNA upon the addition of **4.2**. However, the increase is negligible compared with the significant increase observed for ethidium bromide, suggesting minor groove binding as the dominant binding mode.

Molecular docking studies

4.5.6 Docking study of 4.2 binding to DNA

The binding mode for interaction of **4.2** with duplex DNA was also studied through molecular docking using Auto Dock Vina.[4] As before, open-d(ATCGAGACGTCTCGAT)$_2$ was used as a biomacromolecular target.[6]

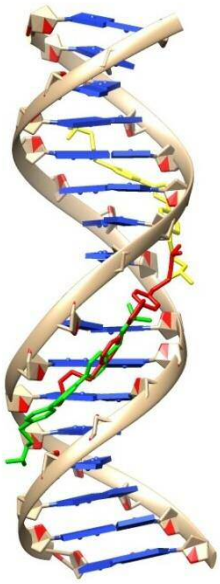

Figure 4.10 Top 3 docked poses for **4.2** interacting with open-d(ATCGAGACGTCTCGAT)$_2$.

The result of the molecular docking study shows that minor groove binding is a favourable binding mode for **4.2**, as expected based on its structure. The complex structure in Figure 6.2 is in a reasonable agreement with the result of the binding mode study by viscometry.

Summary of results from binding experiments with FSDNA

The UV-visible and ITC titrations for compound **4.2** with duplex DNA show that ligand **4.2** binds to FS-DNA. The binding parameters for this compound interacting with FS-DNA are summarised in Table 4.5.

Table 4.5 Thermodynamic parameters for binding of 4.2 to FSDNA, in 25 mM MOPS, pH 7.0, 50 mM NaCl at 25 °C.

	K_{A1} ($10^4 M^{-1}$)	$1/n_{A1}$ (bp)	ΔH_{A1} (kcal mol^{-1})	$-T\Delta S_{A1}$ (kcal mol^{-1})	$\{\Sigma dev^2/dof\}^{½}$ (µcal)
UV-vis.	7.51 ± 1.22	3*	-	-	-
ITC	10.0 (8.6 – 16.6)	3*	-2.88 (-1.5 – -5.6)	-3.96	2.9

* restricted.

Compound **4.2** binds moderately to FS-DNA ~ 10^4 M^{-1} with a binding site size restricted to 3.0 base pairs.

The interaction of **4.2** with DNA was further investigated using isothermal titration calorimetry. The thermodynamic parameters determined for **4.2** interacting with DNA are summarised in Table 4.5.

The enthalpogram for **4.2** interacting with FSDNA indicates only one binding event. The ligand binds to DNA with an affinity of ~10^5 M^{-1} for a binding site size restricted to 3 base pairs. The binding is characterised by a negative enthalpy and a favourable entropy change, which suggests minor groove binding.

The mode of interactions of **4.2** with DNA was investigated using induced circular dichroism spectroscopy. After plotting CD spectra against DNA concentration, a small negative ICD signal was observed around the wavelength of interest 320 nm, suggesting intercalation as a mode of binding. However, this small negative ICD cannot be conclusive to determine the mode of interaction since other binding mode studies such as viscometery and docking study do not confirm this conclusion.

The mode of interaction of **4.2** with CT-DNA was further investigated using viscometry to confirm the conclusion from CD spectroscopy that this binder is an intercalator. In contrast, the result of viscometry of **4.2** binding to CT-DNA shows a small increase in relative viscosity upon the addition of **4.2**. The increase in relative viscosity was found to be negligible compared with the significant increase for

ethidium bromide which suggests minor groove binding as the dominant binding mode.

The mode of binding for **4.2** with duplex DNA was further explored through molecular docking study using Auto Dock Vina. The result of docking study shows that a favourable mode of binding for compound **4.2** is minor groove binding, as expected based on its structure. The result of docking for **4.2** is also in an agreement with the result of binding mode study by viscometry. On balance, we suggest that **4.2** interacts with duplex DNA through minor groove binding.

4.5.7 Sequence selectivity

The selectivity of **4.2** for selected specific sequences of DNA, viz. $(dAdT)_{12}$●$(dAdT)_{12}$ and $(dGdC)_{12}$●$(dGdC)_{12}$ was studied using UV-visible spectroscopy.

The binding of **4.2** to $(dAdT)_{12}$●$(dAdT)_{12}$ was studied using UV-visible spectroscopy; the changes in absorption of **4.2** upon addition of $(dAdT)_{12}$●$(dAdT)_{12}$ were measured in buffer (25 mM MOPS, pH 7.0 and 50 mM NaCl) at 25 °C (Figure 4.11).

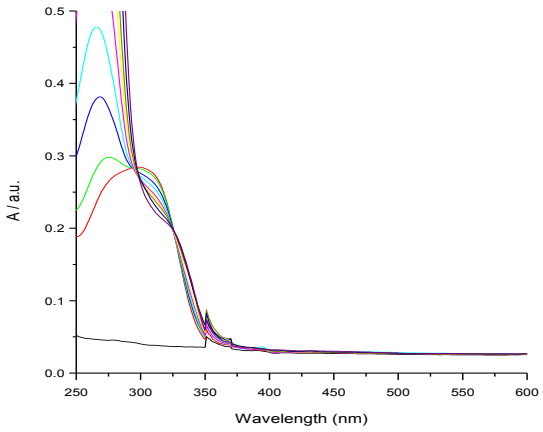

Figure 4.11 UV-visible spectra for 0.009 mM **4.2** upon addition of 0 – 0.12 mM $(dAdT)_{12}$●$(dAdT)_{12}$ in 25 mM MOPS, pH 7.0, 50 mM NaCl, at 25 °C.

Figure 4.11 shows a hypochromic shift in absorbance (at the λ_{max} of 320 nm) and hyperchromic shift (at 338 nm) of **4.2** upon addition of $(dAdT)_{12}$●$(dAdT)_{12}$. As

before, this change in UV-visible absorption is likely the result of geometrical distortion of **4.2** when it interacts with DNA.

To quantify the affinity of **4.2** for $(dAdT)_{12}$●$(dAdT)_{12}$, the absorbances at 320 and 338 nm were plotted as a function of concentration of $(dAdT)_{12}$●$(dAdT)_{12}$ (Figure 4.12).

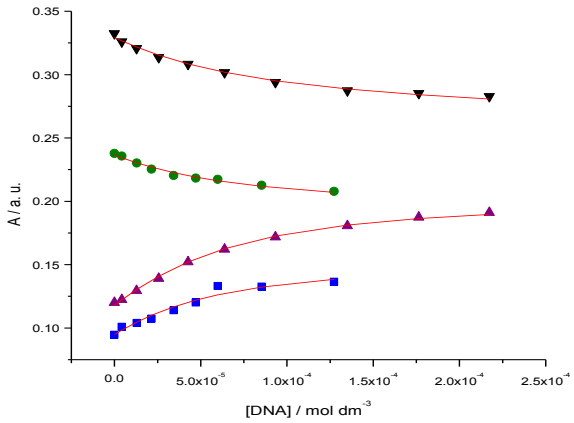

Figure 4.12 Absorbance at 320 nm (●) and at 338 nm (■) of a solution of 0.009 mM **4.2**, absorbance at 320 nm (▼) and at 338 nm (▲) of a solution of 0.013 mM **4.2**, as a function of $(dAdT)_{12}$●$(dAdT)_{12}$ concentration, in buffer (25 mM MOPS, pH 7.0, 50 mM NaCl), at 25 °C. The solid lines represent a global fit of a multiple independent sites model to the data.

The titration curves of Figure 4.12 were analysed globally in terms of a multiple independent binding sites model, which also takes ligand dilution into account, giving an equilibrium constant ($K_{binding}$) of (6.1 ± 0.86) $\times 10^4$ M^{-1} for a binding site size restricted to 3.0 base pairs.

The binding of **4.2** to $(dGdC)_{12}$●$(dGdC)_{12}$ was similarly studied using UV-visible spectroscopy; the changes in absorption of **4.2** upon addition of $(dGdC)_{12}$●$(dGdC)_{12}$ were measured in buffer (25 mM MOPS, pH 7.0, 50 mM NaCl) at 25 °C (Figure 4.13).

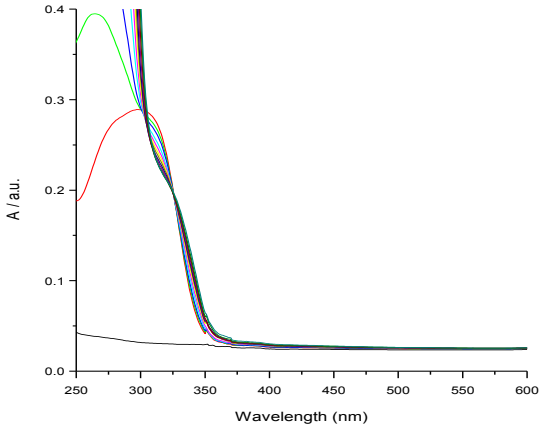

Figure 4.13 UV-visible spectra for 0.009 mM **4.2** upon addition of 0 – 0.36 mM $(dGdC)_{12}$●$(dGdC)_{12}$ in 25 mM MOPS, pH 7.0, 50 mM NaCl, at 25 °C.

Figure 4.13 shows a hypochromic shift in absorbance (at the λ_{max} of 320 nm) and a hyperchromic shift (at 338 nm) of **4.2** upon addition of $(dGdC)_{12}$●$(dGdC)_{12}$. The changes in the absorption spectra are similar to those observed during the titration with $(dAdT)_{12}$●$(dAdT)_{12}$.

To quantify the affinity of **4.2** for $(dGdC)_{12}$●$(dGdC)_{12}$, the absorbances at 320 and 338 nm were plotted as a function of concentration of $(dGdC)_{12}$●$(dGdC)_{12}$ (Figure 4.14).

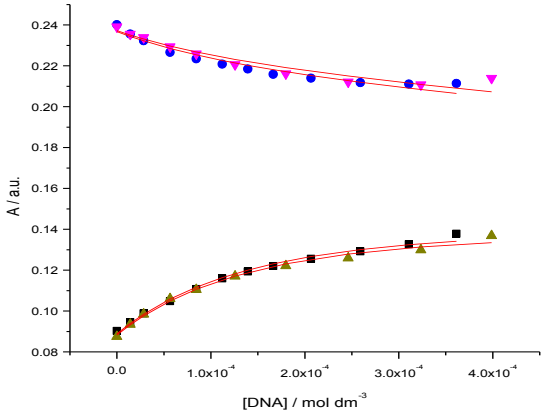

Figure 4.14 Absorbance at 320 nm (●) and at 338 nm (■) of a solution of 0.009 mM **4.2**, absorbance at 320 nm(▼) and at 338 nm (▲) of a solution of 0.009 mM **4.2,** as a function of $(dGdC)_{12}$●$(dGdC)_{12}$ concentration, in buffer (25 mM MOPS, pH 7.0, 50

mM NaCl), at 25 °C. The solid lines represent a global fit of a multiple independent sites model to the data.

The titration curves of Figure 4.14 were also analysed globally in terms of a multiple independent binding sites model, which also takes ligand dilution into account. The fit gave an equilibrium constant ($K_{binding}$) of (1.7 ± 0.3) $\times 10^4$ M^{-1} for a binding site size restricted to 3.0 base pairs.

The results from the titrations are summarised in Table 4.6.

Table 4.6 Binding affinities and binding site sizes for binding of 4.2 to $(dAdT)_{12}\bullet(dAdT)_{12}$ and $(dGdC)_{12}\bullet(dGdC)_{12}$, in buffer (25 mM MOPS, pH 7.0, 50 mM NaCl), at 25 °C.

	$(dAdT)_{12}\bullet(dAdT)_{12}$		$(dGdC)_{12}\bullet(dGdC)_{12}$	
Ligand	***Binding constant*** $K / \times 10^4 M^{-1}$	***Binding site size*** *n / bp*	***Binding constant*** $K / \times 10^4 M^{-1}$	***Binding site size*** *n / bp*
4.2	(6.1 ± 0.86)	3*	(1.7 ± 0.3)	3*

* restricted in order to obtain reasonable binding parameters.

Table 4.6 shows that $(dAdT)_{12}\bullet(dAdT)_{12}$ was mostly selected over $(dGdC)_{12}\bullet(dGdC)_{12}$.

4.6 Conclusion

Compound **4.2** binds to duplex DNA and the binding is accompanied by changes in optoelectronic properties of the compound which a hypochromic shift in absorbance at maximum absorption and a hyperchromic shift were mostly observed. The binding constant is in the range 10^5 M^{-1} with a binding site size restricted to 3.0 base pairs.

Isothermal titration calorimetry indicates one binding event for **4.2** binding to FSDNA with the thermodynamic parameters, viz. negative enthalpy and favourable entropy, suggesting minor groove binding.

Circular dichroism spectroscopy showed that compound **4.2** exhibits a small negative ICD signal, which may be explained by intercalation as the binding mode. The mode of interaction of **4.2** with CT-DNA was further investigated using viscometry to confirm the conclusion from the ICD spectroscopy that this binder is an intercalator.

In contrast to the results from CD spectroscopy, the viscometry experiments for **4.2** binding to CT-DNA show a small increase in relative viscosity upon the addition of **4.2** which nevertheless seems negligible compared with the significant increase in relative viscosity for addition of ethidium bromide. The data thus suggest minor groove as the dominant binding site for **4.2**.

A docking study was exploited to further investigate the mode of binding for **4.2** using Auto Dock Vina. The results of the molecular docking study show that **4.2** binds to duplex DNA via minor groove binding, as expected based on its structure. The selectivity of **4.2** for selected specific sequences of DNA, viz. $(dAdT)_{12}\bullet(dAdT)_{12}$ and $(dGdC)_{12}\bullet(dGdC)_{12}$ was studied using UV-visible spectroscopy. The results show that the affinity of **4.2** is higher for $(dAdT)_{12}\bullet(dAdT)_{12}$ than for $(dGdC)_{12}\bullet(dGdC)_{12}$.

Part C

4.7 Introduction

Our aims in the third part of Chapter 4 are to quantify the thermodynamics of binding for compound **4.3** (Scheme 4.3) to duplex DNA, using UV-visible spectroscopy.

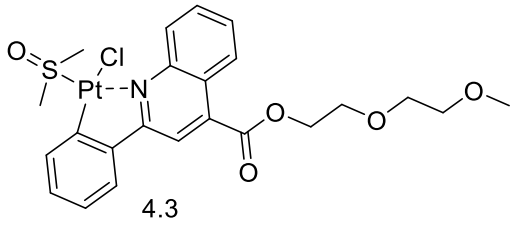

4.3

Scheme 4.3

Compound **4.3** was provided by our collaborator (Simon Pope). Compound **4.3** is a sparingly water-soluble, absorbs light with a λ_{max} at 362 and has a flat aromatic framework attached to a platinum center. Based on its structural properties we expect this compound binds to duplex DNA through intercalation. Compound **4.3** resembles cis-platin, and may therefore interact covalently with DNA, like cis-platin does.

4.8 Results and discussion

The results of the interaction study for compound **4.3** with DNA by UV-visible spectroscopy will be presented and discussed.

4.8.1 UV-visible spectroscopy studies of 4.3 binding to DNA

The binding of **4.3** to DNA was studied using UV-visible spectroscopy; the changes in absorption of **4.3** upon addition of FSDNA were measured in 50 vol-% DMSO-MOPS buffer (25 mM MOPS, pH 7.0, 50 mM NaCl), at 25 °C (Figure 4.15). These experiments were carried out in 50 vol-% DMSO because of the poor solubility of compound **4.3** in the aqueous medium.

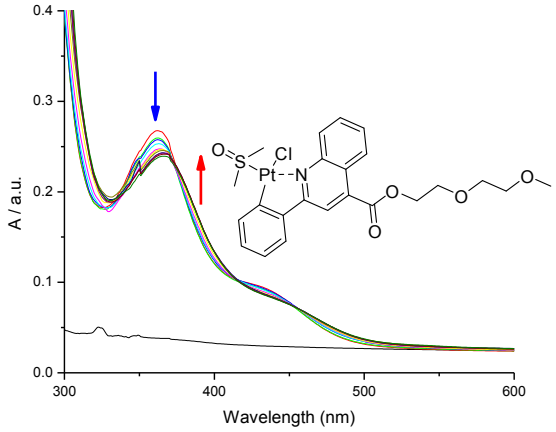

Figure 4.15 UV-visible spectra for 0.020 mM **4.3** upon addition of 0 – 0.9 mM DNA in 50 vol-% DMSO-MOPS buffer (25 mM MOPS, pH 7.0, 50 mM NaCl) at 25 °C.

Figure 4.15 shows a hypochromic shift in absorbance (at the λ_{max} of 362 nm) of **4.3** and three isosbestic points upon addition of DNA. This change in UV-visible absorption may occur as a result of geometrical distortion of **4.3** when it interacts with DNA, but it may also be a local medium effect.

To quantify the affinity of **4.3** for FSDNA, the absorbances at 362 and 390 nm for two titrations were plotted as a function of concentration of FSDNA (Figure 4.16, for data in tabular format see appendix, Tables A17.5 & A17.6)

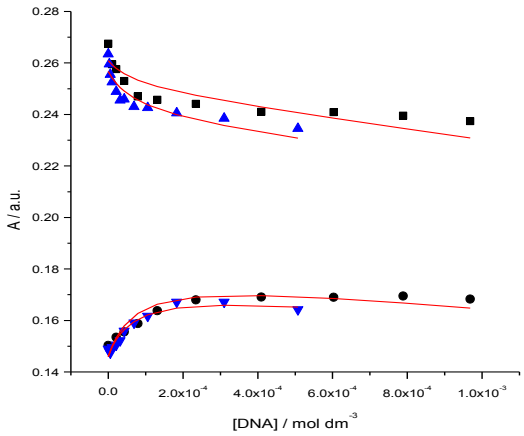

Figure 4.16 Absorbance at 362 nm (■) and at 390 nm (●) of a solution of 0.020 mM **4.3**, absorbance at 362 nm (▲) and at 390 nm (▼) of a solution of 0.020 mM **4.3**, as a

function of FSDNA concentration, in buffer (25 mM MOPS, pH 7.0, 50 mM NaCl), at 25 °C. The solid lines represent a global fit of a multiple independent sites model to the data.

The titration curves of Figure 4.16 were analysed globally by fitting a multiple independent binding sites model, which also takes ligand dilution into account, to the data. The fit gives an equilibrium constant ($K_{binding}$) of (0.47 ± 1064) $\times 10^3$ M^{-1} and a binding site size of (0.03 ± 77) base pair. The obtained binding parameters were small and unreasonable. Therefore the data were reanalysed, giving an equilibrium constant ($K_{binding}$) of (7.4 ± 3.1) $\times 10^4$ M^{-1} for a binding site size restricted to 3 base pairs.

4.9 Conclusion

Compound **4.3** binds to duplex DNA with an affinity of about 10^5 M^{-1} for a binding site size restricted to 3 base pairs and binding is accompanied by change in optoelectronic properties of the compound. The hypochromic shift in absorbance at maximum absorption 362 nm and three isosbestic points for compound **4.3** were observed upon the addition of DNA. The binding site size was restricted to 3 base pairs in order to obtain reasonable binding parameters.

Part D

4.10 Introduction

Our aims in the last part of Chapter 4 are to quantify the thermodynamics of binding for compounds **4.4** and **4.5** (Scheme 4.4) to duplex DNA, using isothermal titration calorimetry.

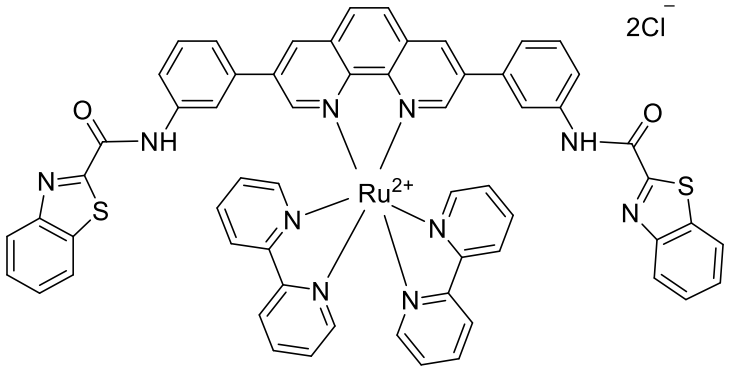

4.4

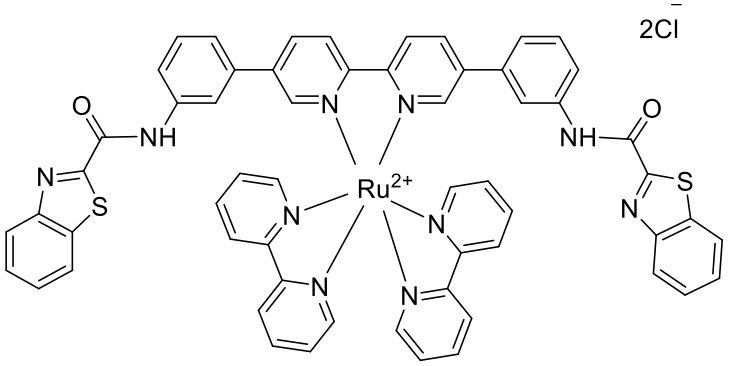

4.5

Scheme 4.4

Compounds **4.4** and **4.5** in Scheme 4.4 were provided by our collaborator (Nicholas C. Fletcher). Both compounds **4.4** and **4.5** are sparingly water-soluble and possess flat aromatic frameworks that are coordinated to a central metal ruthenium (Ru^{2+}). Based on their structural properties we expect that these compounds bind to duplex DNA through intercalation. Binding of similar compounds to DNA was studied by N. Fletcher and co-workers using UV-visible absorption, emission and CD spectroscopy. The results of these studies showed strong affinities of these compounds to DNA.[9]

These compounds are fluorescent and could therefore be used in fluorimetry-based biosensors. Additionally, we anticipate these compounds bind to DNA via intercalation and they could therefore be used as signal enhancers in EIS-based biosensors.

4.11 Results and discussion

The results of the interaction studies for compounds **4.4** and **4.5** with DNA will be presented and discussed for each individual compound.

4.11.1 ITC studies of 4.4 and 4.5 binding to DNA

In order to study the binding of **4.4** and **4.5** with duplex DNA, we used isothermal titration calorimetry (ITC). To analyse the titration data, the heats of dilution for these compounds need to be determined. Therefore, a series of dilution experiments were carried out in different buffers. These dilution experiments also allow the quantification of self-aggregations of these compounds in solution, if any.

4.11.1.a Dilution of 4.4

In order to investigate self-aggregation and quantify the heats of dilution for **4.4** in Tris buffer, the dilution of 0.84 and 0.74 mM solutions of **4.4** in Tris buffer (5 mM Tris + methanol (1:1), pH 7.2) was studied using isothermal titration calorimetry. The differential heat flow and derived integrated molar heat effects for these dilutions were recorded at 25 °C (Figures 4.17). These experiments were carried out in Tris buffer with methanol due to low solubility of **4.4** and **4.5** in MOPS buffer.

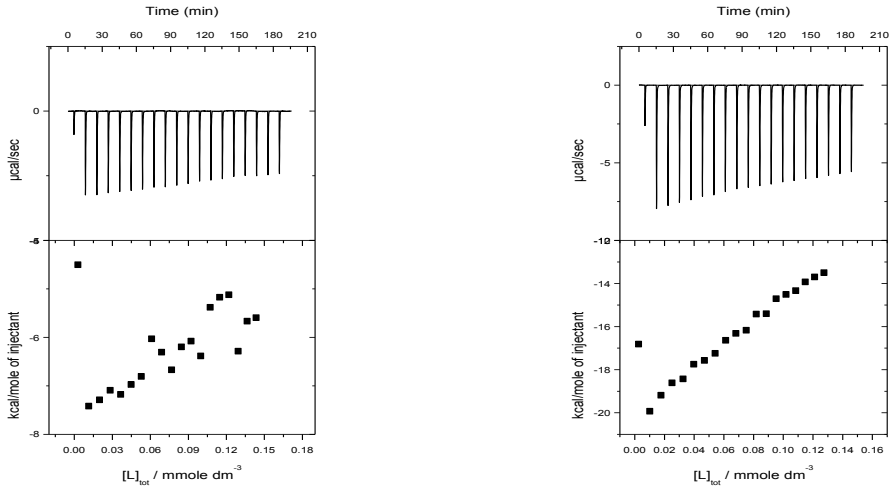

(a) (b)

Figure 4.17 Enthalpograms for dilution of a 0.84 mM solution of **4.4** (a) and of a 0.74 mM solution of **4.4** (b), into 5 mM Tris + methanol (1:1), pH 7.2, at 25 °C.

The enthalpograms for diluting **4.4** in Tris buffer in the figure 4.17 show a lack in reproducibility of experimental data for dilution (a) and (b), therefore we were unable to analyse the dilution data.

4.11.1.b Dilution of 4.5

In order to investigate self-aggregation and quantify the heats of dilution for **4.5** in Tris buffer, the dilution of 1.05 and of 0.8 mM solutions of **4.5** in Tris buffer (5 mM Tris + DMSO (1:1), pH 7.2) were studied using isothermal titration calorimetry. The differential heat flow and derived integrated molar heat effects for these dilutions were recorded at 25 °C (Figures 4.18).

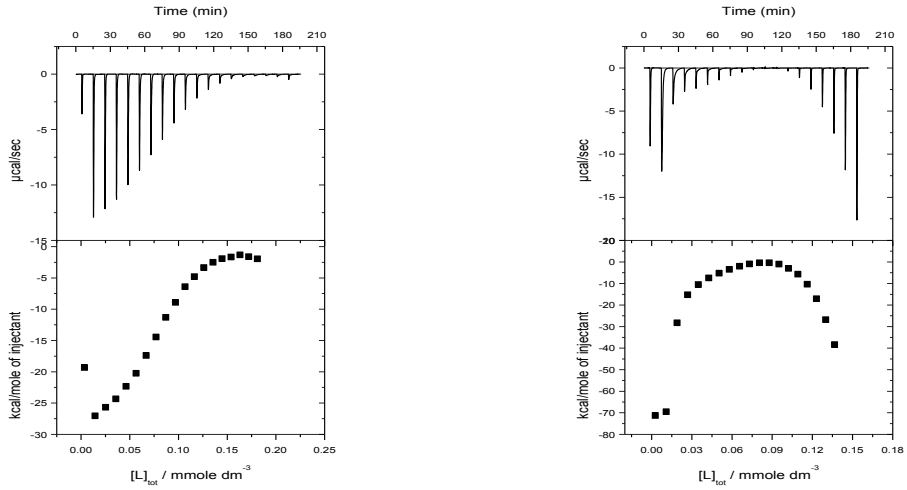

(a) (b)

Figure 4.18 Enthalpograms for dilution of a 1.05 mM solution of **4.5** (a) and of a 0.8 mM solution of **4.5** (b), into 5 mM Tris + DMSO (1:1), pH 7.2, at 25 °C.

The enthalpograms for diluting **4.5** in Tris buffer in Figure 4.18 also show a lack in reproducibility of experimental data for dilution. Therefore we were unable to analyse the dilution data.

4.12 Conclusion

In order to study binding of **4.4** and **4.5** to duplex DNA, we planned to use isothermal titration calorimetry. Unfortunately, the enthalpograms for diluting **4.4** and **4.5** in Tris buffer showed non-reproducibility of the experimental data. Therefore we were unable to analyse the dilution data, quantify the heats of dilution and further investigate binding of **4.4** and **4.5** to DNA.

4.13 Materials and Methods

4.13.1 DNA preparation

All compounds studied in this chapter were provided by our collaborators. The pH of the buffer was determined using a Hanna Instruments pH 210 pH meter equipped with a VWR 662-1759 glass electrode. The buffer components were purchased from Acros or Sigma-Aldrich. Fish sperm DNA and Calf thymus DNA were also purchased from Acros or Sigma-Aldrich. The stock solution of calf thymus DNA was prepared by sonicating a solution of CT-DNA for about 30 minutes whereas the stock solution of fish sperm DNA was prepared by sonicating a solution of FS-DNA for about 10 minutes. The sonicator was used in the DNA preparation in order to quicken the solvation of DNA in buffer. Fish sperm DNA needs less sonicating because FS-DNA dissolves more quickly in MOPS buffer.

The DNA solution was dialysed against 2.0 litres of buffer using a 3.5 kDa MWCO dialysis membrane for 24 hours. The concentration of DNA was determined using UV-visible spectroscopy using an extinction coefficient of 12800 M^{-1} cm^{-1} at 260 nm.[3]

4.13.2 Spectroscopic studies

UV-visible spectra were recorded using a Jasco V-630 Bio spectrophotometer equipped with a peltier temperature controller at 25 °C. Circular dichroism spectra were recorded on a Chirascan CD spectrophotometer. A stock solution of each ligand in buffer was freshly prepared and a volume of this stock solution was added into 2000-2500 µl of buffer, as required, in a 1.0 cm path length cuvette. UV-visible titrations of **4.1** with DNA were carried out in deionised water. Titrations of **4.2** with DNA were carried out in buffer (25 mM MOPS, pH 7.0, 50 mM NaCl). Titrations of **4.3** with DNA were carried out in 50 vol-% DMSO-MOPS buffer (25 mM MOPS, pH 7.0, 50 mM NaCl), at 25 °C. All UV-visible titrations were carried out by adding aliquots of the DNA stock solution into a 1 cm path length cuvette which contains ligand solution, measuring the absorption in the range of 200-600 nm after each addition. The absorption in the range of 0.1-0.6 a.u. was measured in a cuvette to avoid self-aggregation and precipitation of the ligand. The absorptions at selected wavelengths were plotted as a function of DNA concentrations and a multiple

independent binding sites model (see section 1.10.1 in Chapter 1) was used to analyse the UV-visible spectra using Origin 9.0. The baseline absorbance in a titration, and hence in the data analysis, corresponds to the absorbance of a cuvette containing buffer only because the spectrophotometer was calibrated without cuvettes in the sample or reference position ("air versus air"). For CD titrations, the same steps were followed except the ICD signals were used instead of absorptions in UV-visible titrations.

4.13.3 Isothermal titration calorimetry

All ITC experiments were carried out using a Microcal VP ITC microcalorimeter. Compound **4.2** was prepared in 25 mM MOPS, 50 mM NaCl, pH 7.0, compound **4.4** in 5 mM Tris + methanol (1:1), pH 7.2 and compound **4.5** in 5 mM Tris + DMSO (1:1), pH 7.2. All calorimetric binding experiments were carried out at 25 °C. The sample cell and syringe were always cleaned with ethanol followed by distilled water before starting any experiment. The sample cell was filled with FS-DNA solution (approximately 1.9 ml). The syringe was filled with ligand solution (approximately 300 µl) with a concentration usually 12-fold higher than DNA solution (exact ratios depend on individual experiments). The ligand solution was added in 1 injection of 5 µl for the first addition and 19 injections of 15 µl each to the sample cell, injecting every 300 seconds automatically. During the titration the solutions in the sample cell were mixed at a stirring speed of 307 rpm. The heat effects per injection (dh) were calculated using Origin (Microcal, Inc). The integrated heat effects were analysed using IC ITC.[2]

4.13.4 Viscometry

The viscosimetry experiment for **4.2** was carried out in buffer (25 mM MOPS, 50 mM NaCl, pH 7.0). A Cannon-Flenske routine viscometer was placed in a temperature-controlled circulated water bath at 25 °C. The viscometer was filled with a fixed amount of calf thymus DNA (3.0 ml of 0.5 mM) and adding ligand solutions with concentrations, as required, to obtain ratios of ligand / DNA 0.03, 0.06, 0.09, 0.12 and 0.15. The flow time was measured three times for each ligand addition and the results were averaged. The relative viscosity was calculated and plotted as a function of the ratio $[ligand]_{bound}/[DNA]$ where $[ligand]_{bound}$ as calculated using binding parameters from UV-visible spectroscopy.

2.4.5 Docking studies

Molecular docking studies were performed using Auto Dock Vina.[6] The ligand structures were generated using chemdraw and then optimised using Avogadro, using force fields MMFF94 for ligands and GAFF for metal complexes. The rotable bonds in the ligand were assigned using Auto Dock Tools 1.5.6 and the output files were saved in PDBQT format. Our previously developed[9] open-d(ATCGAGACGTCTCGAT)$_2$ was used as a biomacromolecular target. An exhaustiveness of 200 and number modes of 10 were selected. The results of Auto Dock Vina were rendered using Chimera 1.10.2.

References

1- Garbett, N. C.; Ragazzon, P. A.; Chaires, J. B., Nat. Protoc 2007, 2 (12), 3166-3172.

2- Buurma, N. J.; Haq, I., J. Mol. Biol. 2008, 381 (3), 607-621.

3- Ren, J. S.; Chaires, J. B., Biochemistry 1999, 38 (49), 16067-16075.

4- O. Trott, A. J. Olson, AutoDock Vina: improving the speed and accuracy of docking with a new scoring function, efficient optimization and multithreading, Journal of Computational Chemistry 31 (2010) 455-461.

5- Satyanarayana, S.; Dabrowiak, J. C.; Chaires, J. B., Biochemistry 1993, 32 (10), 2573-2584.

6- Jones, J. E.; Amoroso, A. J.; Dorin, I. M.; Parigi, G.; Ward, B.D.; Buurma, N.J. and Pope, S.J., Chemical Communications 2011, 47 (12), 3374-3376.

7- Regan, E. M.; Hallett, A. J.; Wong, L. C.; Saeed, I. Q.; Jones, E. E.; Buurma, N. J.; Pope, S. J. and Estrela, P., Electrochimica Acta 2014, 128, 10-15.

8. Wheelhouse, R. T.; Garbett, N. C.; Buurma, N. J. and Chaires, J. B., Angew. Chem. Int. Ed., 2010, 49, 3207-3210.

9- Spillane, C. B.; Morgan, J. L.; Fletcher, N. C.; Collins, J. G. and Keene, F. R., Dalton Transactions 2006, 25, 3122-3133.

Chapter 5

EPILOGUE

Abstract

This Chapter gives an overview and general conclusions about the DNA binding studies presented in the previous Chapters (2, 3 & 4) and finishes with suggestions for future work.

5.1 General conclusions

The main objective of this project was to explore and advance optoelectronically active DNA-binding compounds for use as sensitisers in sensors for selective detection of genetic biomarkers. The sensitisers bind to DNA and their spectroscopic and electronic properties may change upon interaction with DNA, thus allowing different applications including in biosensors. Additionally, binding of ligands with nucleic acids can be manipulated for the assembly of functional multicomponent structures containing active components.

In this thesis we have described the DNA binding studies for three different groups of compounds using various techniques such as UV-visible and CD spectroscopy, isothermal titration calorimetry, viscometry and molecular docking study. The first group is 1,8-naphthalimide derivatives, which are oligoheteroaromatic compounds having a flat π-conjugated framework attached to different side-groups. In general, based on our results, most compounds of this group show moderate affinity to duplex DNA, however, the anionic compounds of 1,8-naphthalimide derivatives compounds **2.8** and **2.9** do not show any affinity for duplex DNA. This may due to the repulsion arising from the ligand negative charge with negative charge of DNA backbone. Therefore, anionic 1,8-naphthalimide derivatives are not a good element for DNA binding studies. Regarding the sequence selectivity for ds-DNA, most binders of this group show preference to A.T-rich DNA sequences over G.C-rich sequences. Nevertheless, these binders still show considerable affinity toward G.C-rich DNA sequences i.e. they are not completely selective to A.T-rich DNA sequences.

The second group of DNA binders is a family of dendrimeric compounds. These compounds consist of a highly fluorescent flat framework that is attached to small poly(amido amine) side-groups to increase solubility in aqueous medium. The results of our studies show that these compounds bind strongly to duplex DNA in two separate events and the binding is accompanied by change in the optical behaviours of the chromophore. The results of sequence selectivity studies show that these binders also prefer to bind A.T-rich DNA sequences over G.C-rich DNA sequences. The favourable binding mode of this family is intercalation as expected based on their structures. Compounds of this family are promising components for use as sensitisers in genosensors because they carry highly negative charges and still interact with

duplex DNA. In addition, the binding of this group of compounds with DNA usually accompanied by forming precipitation at low DNA concentration, which makes titration data difficult to be analysed, therefore, this problem need to be solved.

The third group of our DNA binders consists of a variety of compounds that have diverse structural frameworks. Most ligands of this group bind to duplex DNA moderately strongly through different binding modes varying from minor-groove binding to intercalation to side-by-side binding in the minor groove. Binding of **4.1** to duplex DNA leads to a change in its optoelectronic properties. Thus, this compound can be used as sensitiser to enhance signals of DNA detection. The binding studies for both ruthenium complexes **4.4** and **4.5** to duplex DNA were carried out using isothermal titration calorimetry. The resulting enthalpograms for diluting **4.4** and **4.5** in Tris buffer (5 mM Tris + DMSO or MeOH (1:1) showed non-reproducibility of the experimental data, we may attribute this non-reproducibility of the experimental data to using high amount of organic solvent as a co-solvent. Therefore, we were unable to analyse the data of dilutions, quantify the heats of dilution and further investigate binding of **4.4** and **4.5** to DNA.

5.2 Suggestions for future work

To confirm and enrich the results of binding studies obtained for our DNA binders, further biophysical studies should be performed such as DNA binding studies using NMR spectroscopy. With regard to the self-aggregation of our ligands in aqueous medium, the aggregation number and the thermodynamic parameters of self-aggregation should be determined. Additionally, some of the our binders are sparingly water soluble, therefore, adding more solubilising groups to their structural frameworks facilitate the solubility and reducing self-aggregation. Furthermore, in order to obtain highly sequence selective DNA-binders, more ligands should be synthesised with new designs and structural properties. DNA binders based (*7H*-benz[*de*]benzimidazo[*2,1-a*]isoquinoline-*7*-one) frameworks are promising components for use as sensitisers in genosensors when detecting DNA hybridization using electrochemical methods, particularly anionic **3.2**. Because they carry highly negative charges and they may act as a signal enhancer by increasing charge transfer resistance when bound to duplex DNA. Furthermore, the family of dendrimeric

compounds are fluorescent, they could be used as fluorochromes in fluorimetry-based biosensors. The 1,8-naphthalimide derivatives are also promising DNA binders, especially compounds **2.1**-**2.3**, they carry significant negative charges. Upon binding of compounds **2.1**-**2.3** with duplex DNA, the negative charges on the duplex DNA increase, thus, these binders can be exploited as signal enhancers in EIS-based biosensors and Field-Effect Transistor (Bio-FET) detections. Additionally, the 1,8-naphthalimide derivatives are fluorescent and they could be useful components in biosensing based on fluorimetry. Compound **4.2** is known to bind to DNA●RNA hybrid duplexes, therefore, compound **4.2** is considered an interesting element to study the interaction of small molecules with other nucleic acid biomarkers such as mRNA. Some of our metal complexes DNA binders, such as compounds **4.1** and **2.4** are redox-active, they could be used as components in biosensors based on coulometry detection. Therefore, we should try these binders in a biosensor with our collaborators.

Finally, in order to determine the affinities of our binders to different nucleic acid structures, competition dialysis is a good technique to achieve this objective and it would be of interest to explore this technique as well.

APPENDIX

A1 Compound 2.1

1.1 Extinction coefficient

A stock solution of **2.1** (1.38 mM) in buffer (25 mM MOPS, pH 7.0, 50 mM NaCl) was prepared. A series of solutions of 0.02, 0.04, 0.05 and 0.07 mM was prepared from the stock solution and UV-visible spectra were recorded for these solutions in a 1.0 cm pathlength cuvette. Ligand absorbances at the λ_{max} of 347 nm were plotted against ligand concentrations and a linear fit (red line) was applied to obtain the extinction coefficient of $(7.45 \pm 0.36) \times 10^3$ dm^3 mol^{-1} cm^{-1} (Figure A1.1).

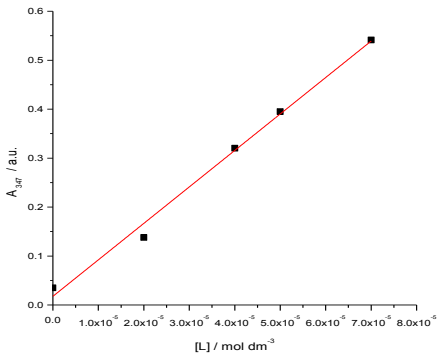

Figure A1.1 Absorbance for **2.1** as a function of concentration.

1.2 Results and error margins for isothermal titration calorimetry of 2.1interacting with DNA.

Table A1.1 Thermodynamic parameters for binding of 2.1 to FSDNA in 25 mM MOPS, 50 mM NaCl, pH 7.0, at 25 °C.

variable	Initial	change?	avoid 0?	Fit value	att. changes
Kagg	1.06E+03	0	n	1.06E+03	0
DHagg	-8.37E+02	0	n	-8.37E+02	0
KA1	5.00E+04	1	y	3.30E+03	98120
DHA1	-5.00E+03	1	y	-3.22E+04	98576
nA1	3.30E-01	1	y	4.08E-02	98296
Hdil1	1.40E+02	1	n.d.	-7.30E+01	98626
Hdil2	1.40E+02	1	n.d.	-1.29E+02	97928
Hdil3	1.40E+02	1	n.d.	-8.38E+01	98454

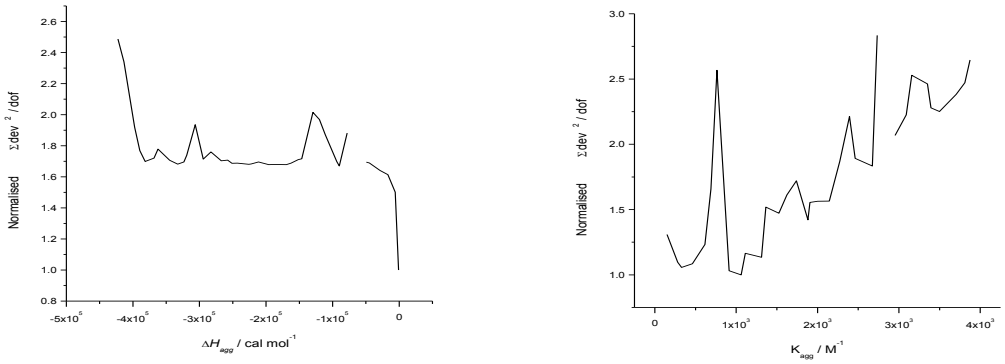

Figure A1.2 Normalised Σdev^2/dof for dilution parameters.

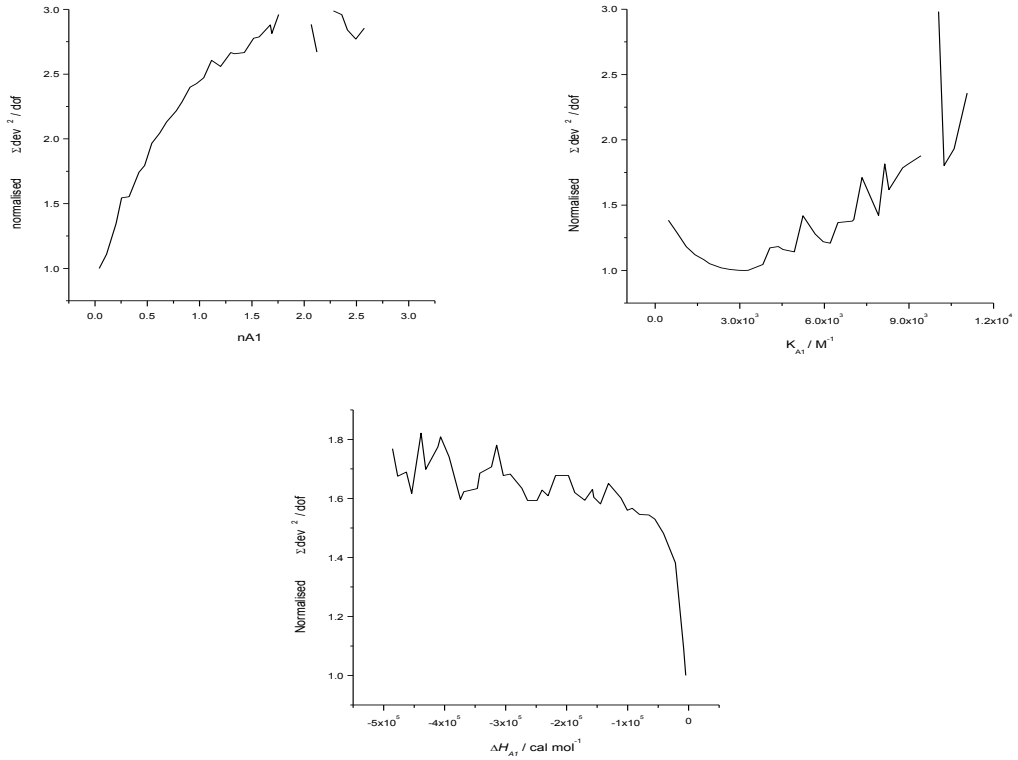

Figure A1.3 Normalised Σdev^2/dof for binding parameters.

A2 Compound 2.2

1.1 Extinction coefficient

A stock solution of **2.2** (3.0 mM) in buffer (25 mM MOPS, pH 7.0, 50 mM NaCl) was prepared. A series of solutions of 0.02, 0.04, 0.06 and 0.08 mM was prepared from the stock solution and UV-visible spectra were recorded for these solutions in a 1.0 cm pathlength cuvette. Ligand absorbances at the λ_{max} of 347 nm were plotted against ligand concentrations and a linear fit (red line) was applied to obtain the extinction coefficient of $(6.0 \pm 0.1) \times 10^3$ dm^3 mol^{-1} cm^{-1} (Figure A2.1).

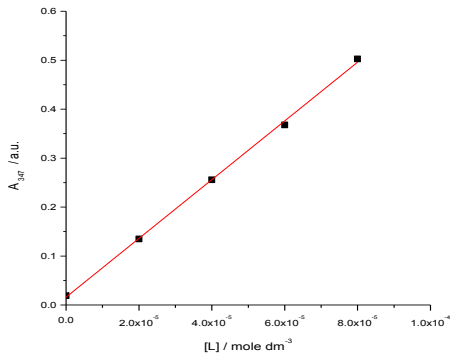

Figure A2.1 Absorbance for **2.2** as a function of concentration.

A3 Compound 2.3

1.1 Extinction coefficient

A stock solution of **2.3** (4.2 mM) in buffer (25 mM MOPS, pH 7.0, 50 mM NaCl) was prepared. A series of solutions of 0.03, 0.05 and 0.07 mM was prepared from the stock solution and UV-visible spectra were recorded for these solutions in a 1.0 cm pathlength cuvette. Ligand absorbances at the λ_{max} of 347 nm were plotted against ligand concentrations and a linear fit (red line) was applied to obtain the extinction coefficient of $(11.7 \pm 0.02) \times 10^3$ dm^3 mol^{-1} cm^{-1} (Figure A3.1).

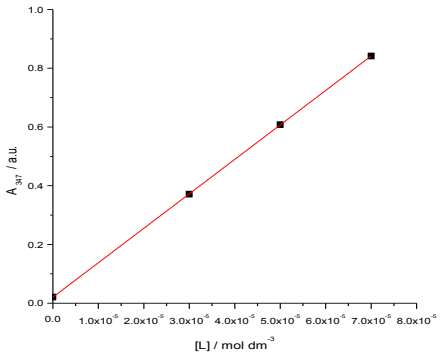

Figure A3.1 Absorbance for **2.3** as a function of concentration.

A4 Compound 2.4

1.1 Extinction coefficient

A stock solution of **2.4** (0.19 mM) in buffer (25 mM MOPS, pH 7.0, 50 mM NaCl) was prepared. A series of solutions of 0.04, 0.049 and 0.062 mM was prepared from the stock solution and UV-visible spectra were recorded for these solutions in a 1.0 cm pathlength cuvette. Ligand absorbances at the λ_{max} of 347 nm were plotted against ligand concentrations and a linear fit (red line) was applied to obtain the extinction coefficient of $(9.55 \pm 0.04) \times 10^3$ dm^3 mol^{-1} cm^{-1} (Figure A4.1).

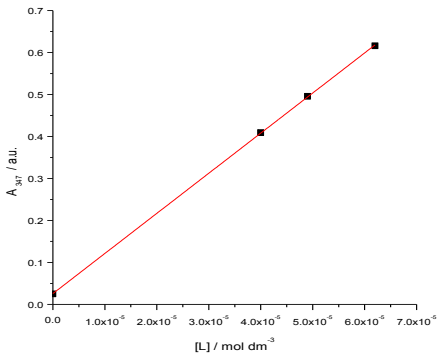

Figure A4.1 Absorbance for **2.4** as a function of concentration.

A5 Compound 2.5

1.1 Extinction coefficient

A stock solution of **2.5** (0.20 mM) in buffer (25 mM MOPS, pH 7.0, 50 mM NaCl) was prepared. A series of solutions of 0.02, 0.04 and 0.06 mM was prepared from the stock solution and UV-visible spectra were recorded for these solutions in a 1.0 cm pathlength cuvette. Ligand absorbances at the λ_{max} of 347 nm were plotted against ligand concentrations and a linear fit (red line) was applied to obtain the extinction coefficient of $(10.13 \pm 0.06) \times 10^3$ dm^3 mol^{-1} cm^{-1} (Figure A5.1).

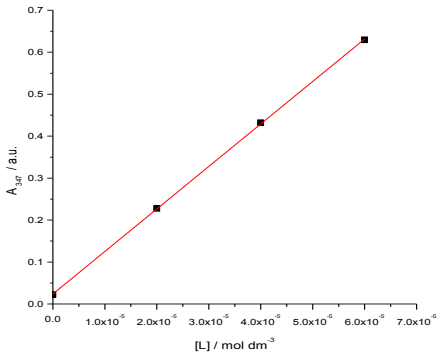

Figure A5.1 Absorbance for **2.5** as a function of concentration.

A6 Compound 2.6

1.1 Extinction coefficient

A stock solution of **2.6** (0.45 mM) in buffer (25 mM MOPS, pH 7.0, 50 mM NaCl) was prepared. Two series of solutions of 0.01, 0.02, 0.04 and 0.05 mM were prepared from the stock solution and UV-visible spectra were recorded for these solutions in a 1.0 cm pathlength cuvette. Ligand absorbances at the λ_{max} of 440 nm were plotted against ligand concentrations and a linear fit (red line) was applied to obtain the extinction coefficient of $(16.5 \pm 0.22) \times 10^3$ dm^3 mol^{-1} cm^{-1} (Figure A6.1).

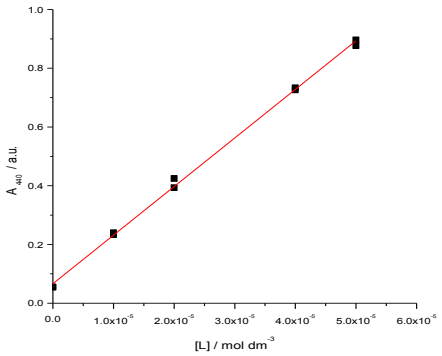

Figure A6.1 Absorbance for **2.6** as a function of concentration.

1.2 Results and error margins for isothermal titration calorimetry of 2.6 interacting with DNA

Table A6.1 Thermodynamic parameters for binding of 2.6 to FSDNA in 25 mM MOPS, 50 mM NaCl, pH 7.0, at 25 °C.					
variable	initial	change?	avoid 0?	fit value	att. changes
KA1	5.00E+04	1	y	8.34E+03	235848
DHA1	-5.00E+03	1	y	-1.74E+05	235880
nA1	3.33E-01	1	y	2.11E-02	235468
Hdil1	1.00E+02	1	n.d.	-8.57E+01	236523
Hdil2	1.00E+02	1	n.d.	3.25E+02	236281

Table A6.1 Thermodynamic parameters for binding of 2.6 to FSDNA in 25 mM MOPS, 50 mM NaCl, pH 7.0, at 25 °C.					
variable	initial	change?	avoid 0?	fit value	att. changes
KA1	5.00E+04	1	y	1.25E+04	294829
DHA1	-5.00E+03	1	y	-9.94E+03	294540
nA1	3.33E-01	0	n	3.33E-01	0
Hdil1	1.00E+02	1	n.d.	3.15E+00	295348
Hdil2	1.00E+02	1	n.d.	3.97E+02	295283

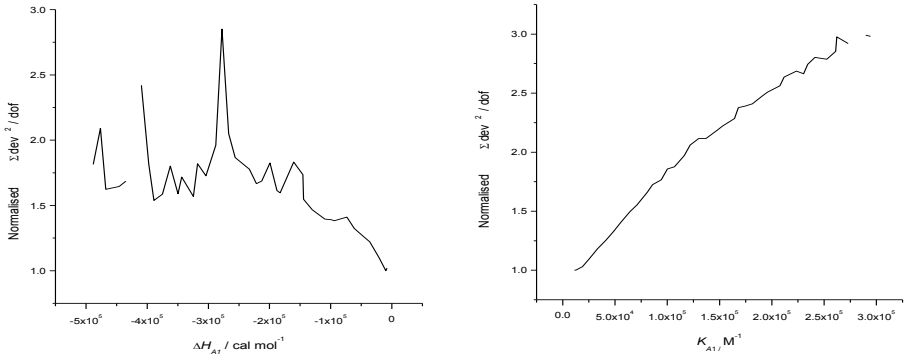

Figure A6.2 Normalised $\Sigma dev^2/dof$ for binding parameters.

A7 Compound 2.7

1.1 Extinction coefficient

A stock solution of **2.7** (1.0 mM) in buffer (25 mM MOPS, pH 7.0, 50 mM NaCl) was prepared. Two series of solutions of 0.02, 0.04, 0.05 and 0.07 mM were prepared from the stock solution and UV-visible spectra were recorded for these solutions in a 1.0 cm pathlength cuvette. Ligand absorbances at the λ_{max} of 434 nm were plotted against ligand concentrations and a linear fit (red line) was applied to obtain the extinction coefficient of $(10.68 \pm 0.20) \times 10^3$ dm^3 mol^{-1} cm^{-1} (Figure A7.1).

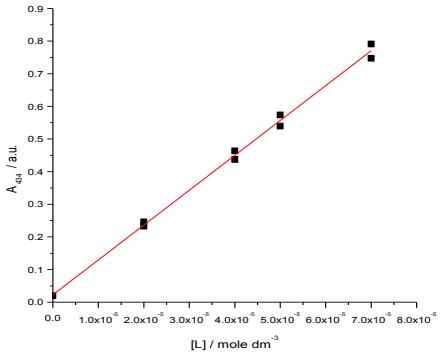

Figure A7.1 Absorbance for **2.7** as a function of concentration.

1.2 Results and error margins for isothermal titration calorimetry of 2.7 interacting with DNA.

Table A7.1 Thermodynamic parameters for binding of 2.7 to FSDNA in 25 mM MOPS, 50 mM NaCl, pH 7.0, at 25 °C.

variable	initial	change?	avoid 0?	fit value	att. changes
Kagg	4.53E+02	0	n	4.53E+02	0
DHagg	-4.68E+03	0	n	-4.68E+03	0
KA1	5.00E+04	1	y	7.99E+03	117794
DHA1	-2.00E+03	1	y	-4.52E+04	118189
nA1	1.66E-01	1	y	1.01E-01	117981
Hdil1	-6.00E+01	1	n.d.	-9.63E+01	117842
Hdil2	-6.00E+01	1	n.d.	-7.53E+01	118194

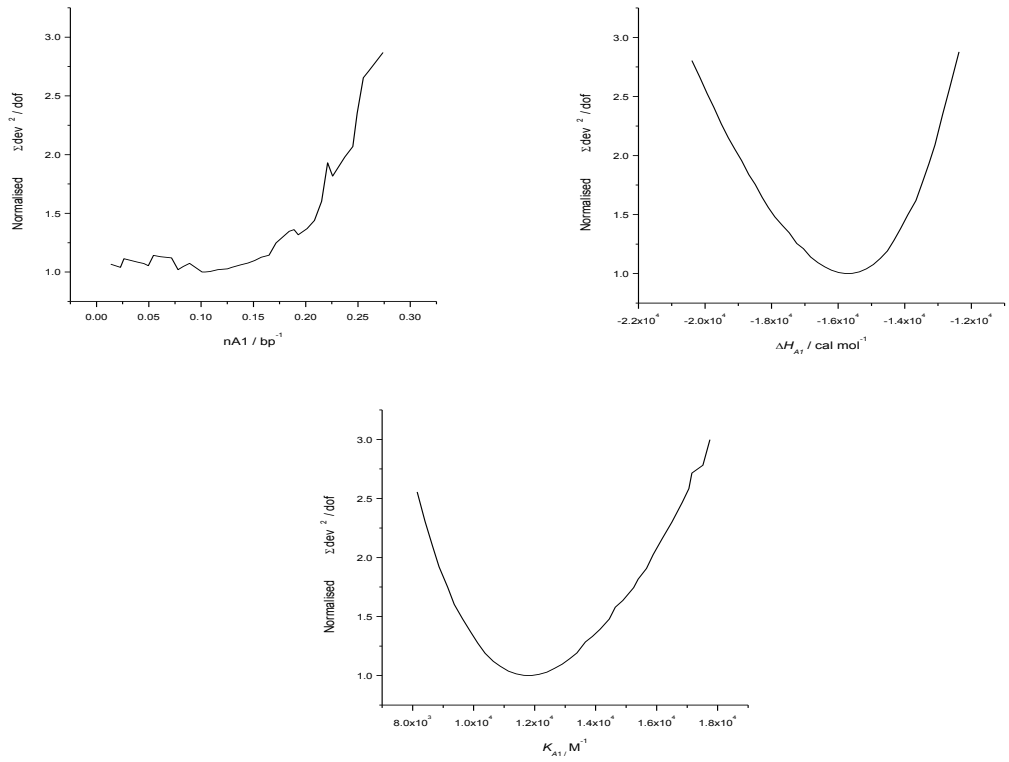

Figure A7.2 Normalised Σdev^2/dof for binding parameters.

A8 Compound 3.2

1.1 Extinction coefficient

A stock solution of **3.2** (0.97 mM) in buffer (25 mM MOPS, pH 7.0, 50 mM NaCl) was prepared. A series of solutions of 0.01, 0.02, 0.03 and 0.04 mM was prepared from the stock solution and UV-visible spectra were recorded for these solutions in a 1.0 cm pathlength cuvette. Ligand absorbances at the λ_{max} of 442 nm were plotted against ligand concentrations and a linear fit (red line) was applied to obtain the extinction coefficient of (12.77 ± 0.35) × 10^3 dm^3 mol^{-1} cm^{-1} (Figure A8.1).

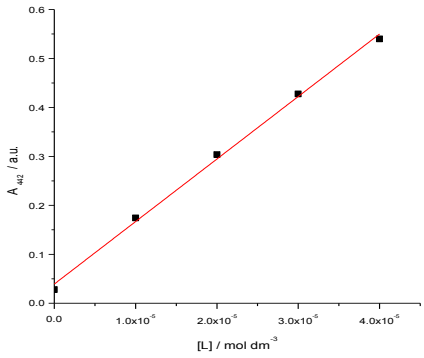

Figure A8.1 Absorbance for **3.2** as a function of concentration.

1.2 Error margins for isothermal titration calorimetry of 3.2.

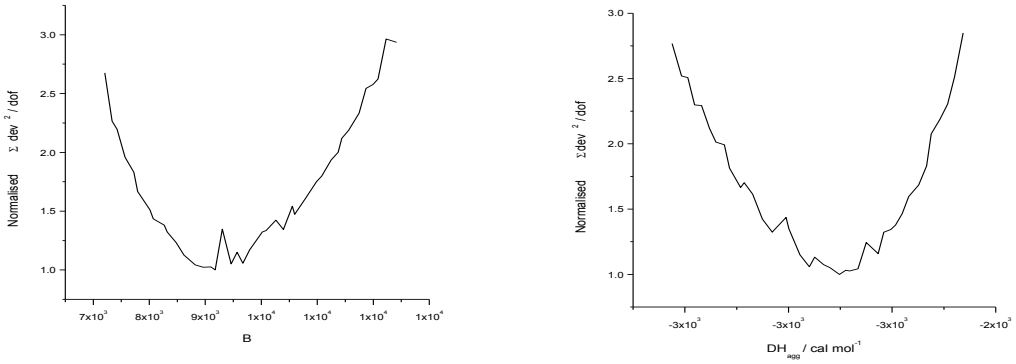

Figure A8.2 Normalised $\Sigma dev^2/dof$ for thermodynamic parameter of interaction of **3.2** to FSDNA. The titration data were analysed in terms of a model accounting only for dilution.

A9 Compound 3.1

1.1 Extinction coefficient

A stock solution of **3.1** (0.24 mM) in buffer (25 mM MOPS, pH 7.0, 50 mM NaCl) was prepared. A series of solutions of 0.02, 0.03, 0.04 and 0.05 mM was prepared from the stock solution and UV-visible spectra were recorded for these solutions in a 1.0 cm pathlength cuvette. Ligand absorbances at the λ_{max} of 444 nm were plotted against ligand concentrations and a linear fit (red line) was applied to obtain the extinction coefficient of $(16.09 \pm 0.30) \times 10^3$ dm^3 mol^{-1} cm^{-1} (Figure A9.1).

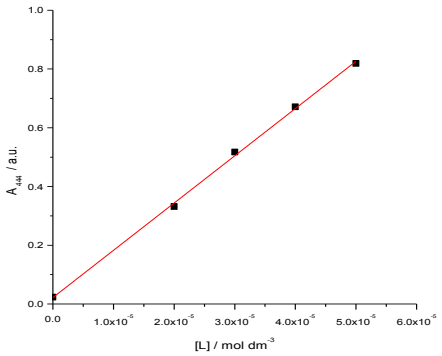

Figure A9.1 Absorbance for **3.1** as a function of concentration.

1.2 Error margins for isothermal titration calorimetry of 3.1.

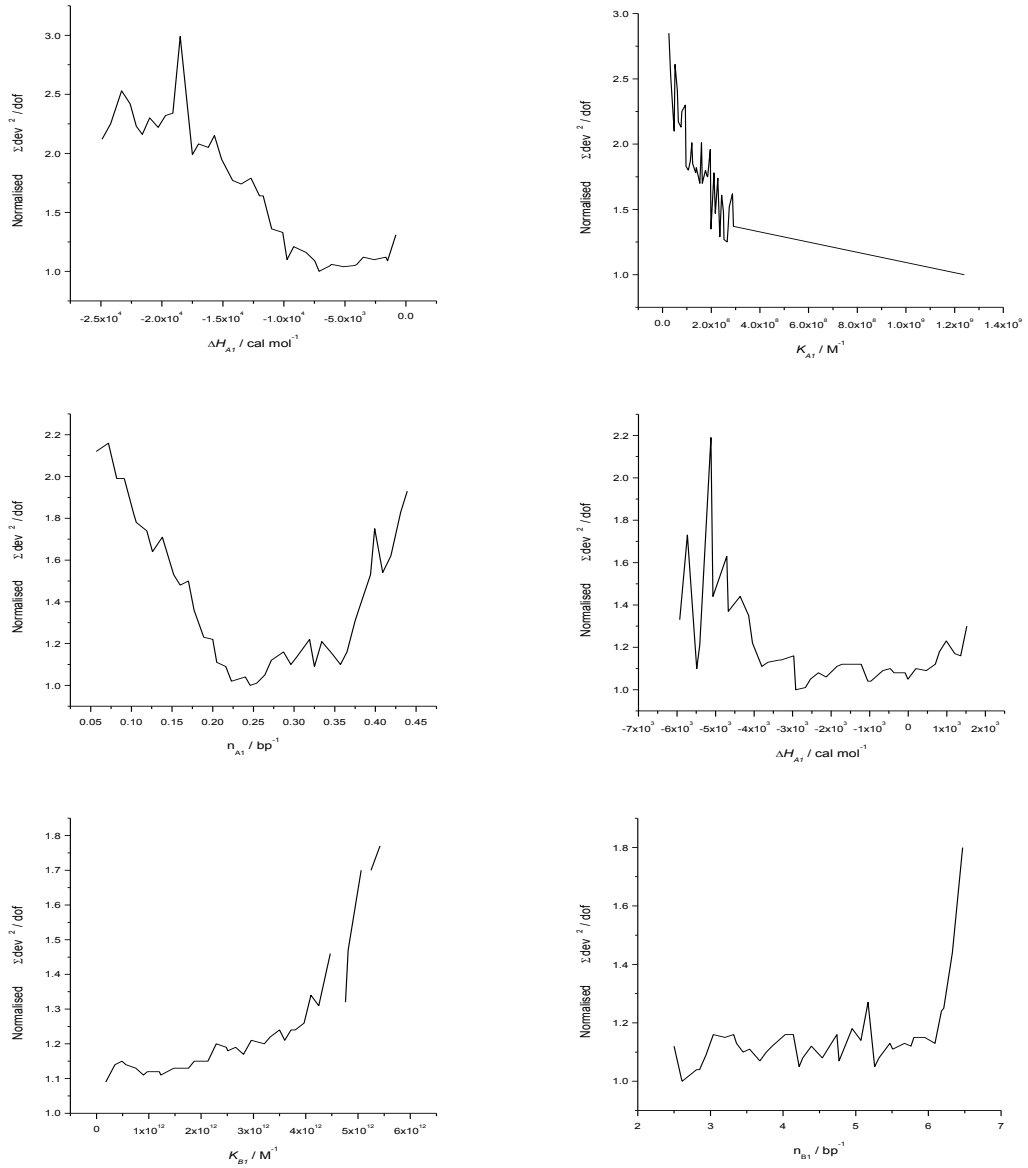

Figure A9.2 Normalised Σdev^2/dof for binding parameters of experiment (a).

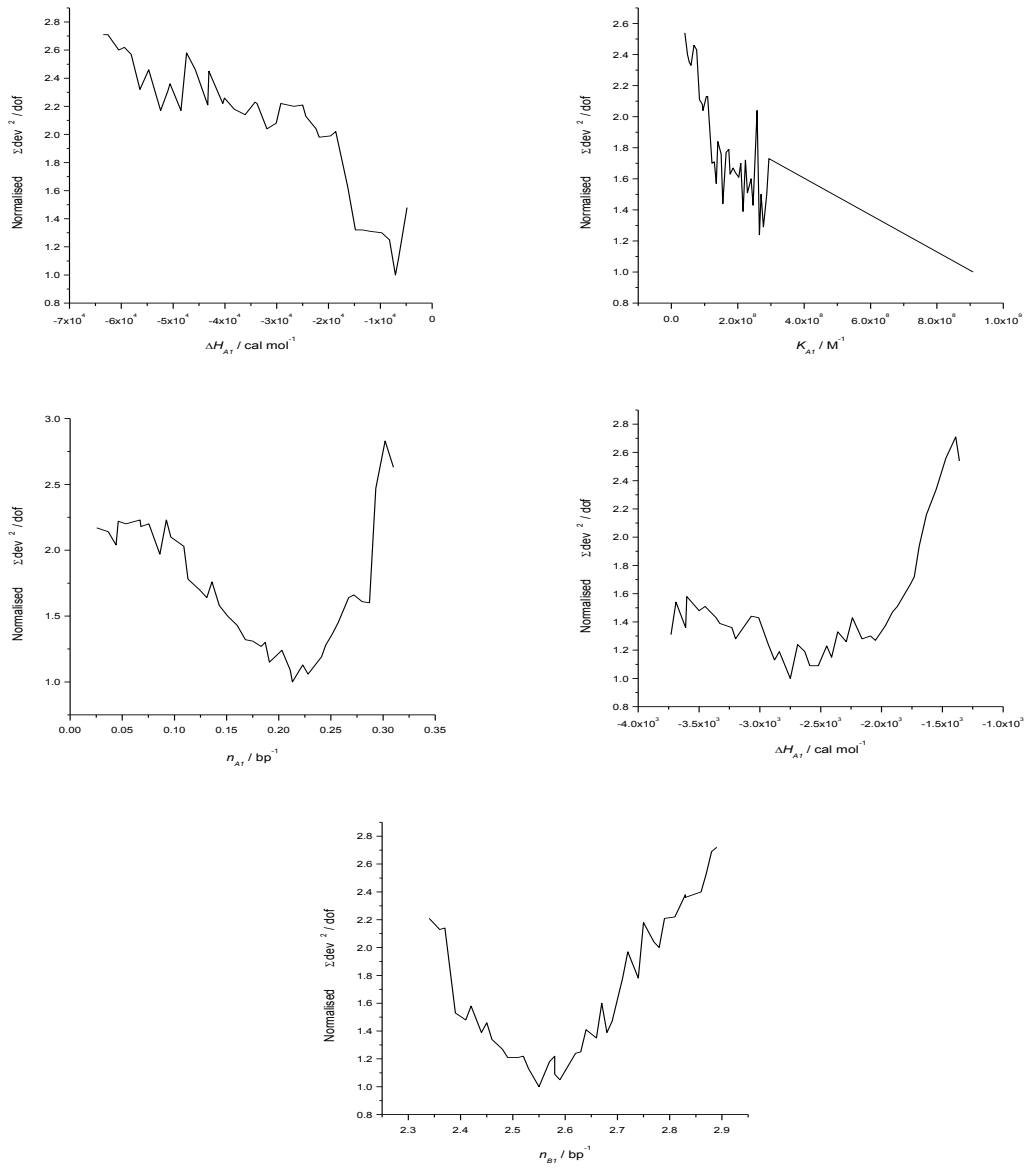

Figure A9.3 Normalised Σdev^2/dof for binding parameters of experiment (b).

A10 Compound 3.3

1.1 Extinction coefficient

A stock solution of **3.3** (0.065 mM) in buffer (25 mM MOPS, pH 7.0, 50 mM NaCl) was prepared. A series of solutions of 0.01, 0.02, 0.03 and 0.04 mM was prepared from the stock solution and UV-visible spectra were recorded for these solutions in a 1.0 cm pathlength cuvette. Ligand absorbances at the λ_{max} of 452 nm were plotted against ligand concentrations and a linear fit (red line) was applied to obtain the extinction coefficient of $(19.57 \pm 0.24) \times 10^3$ dm^3 mol^{-1} cm^{-1} (Figure A10.1).

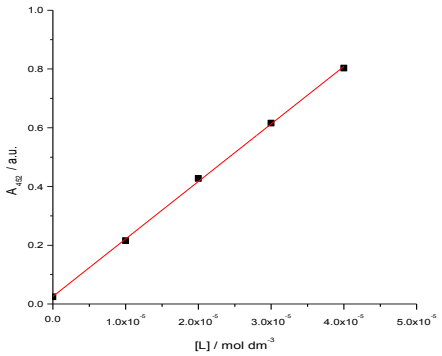

Figure A10.1 Absorbance for **3.3** as a function of concentration.

1.2 Error margins for isothermal titration calorimetry of 3.3.

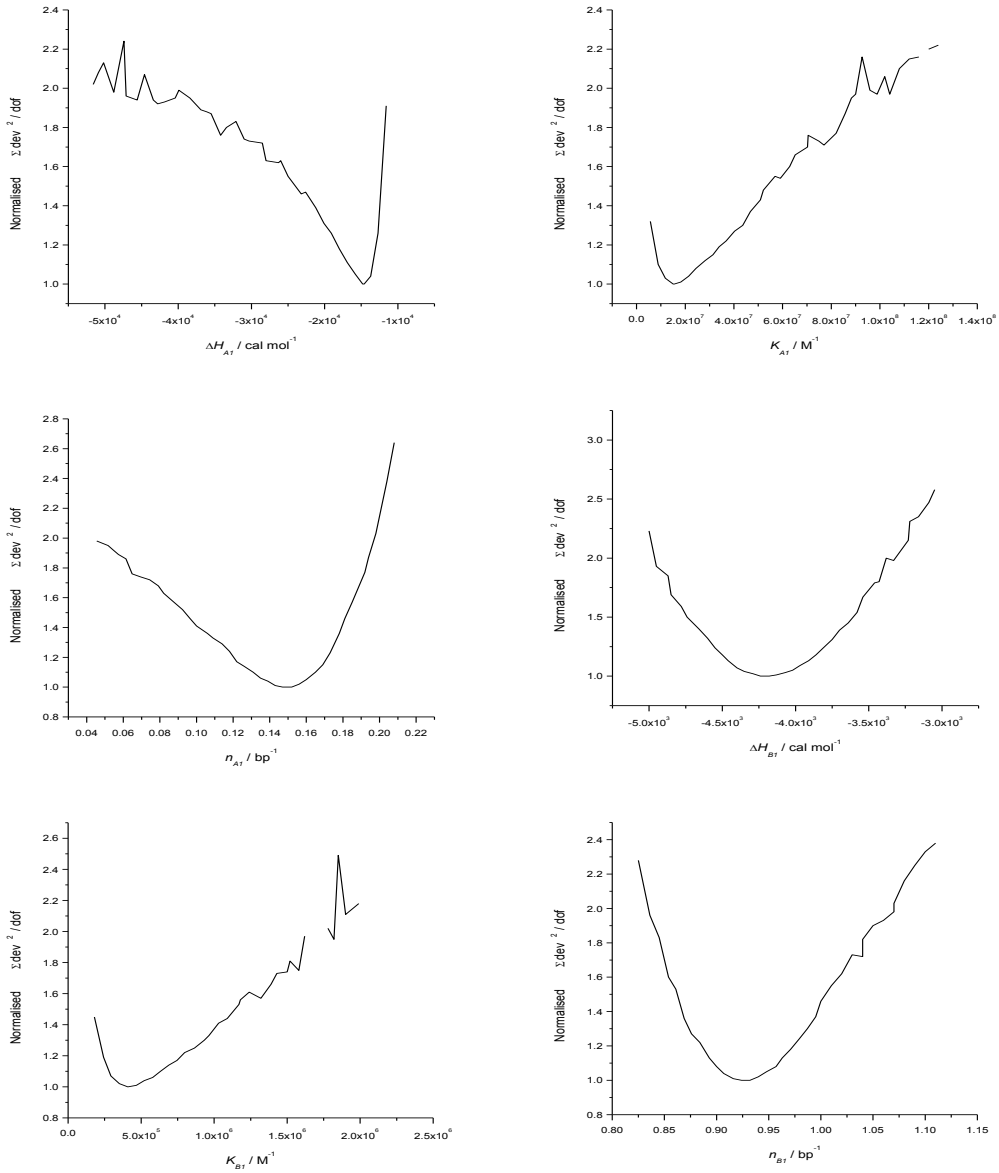

Figure A10.2 Normalised Σdev^2/dof for binding parameters of experiment (a).

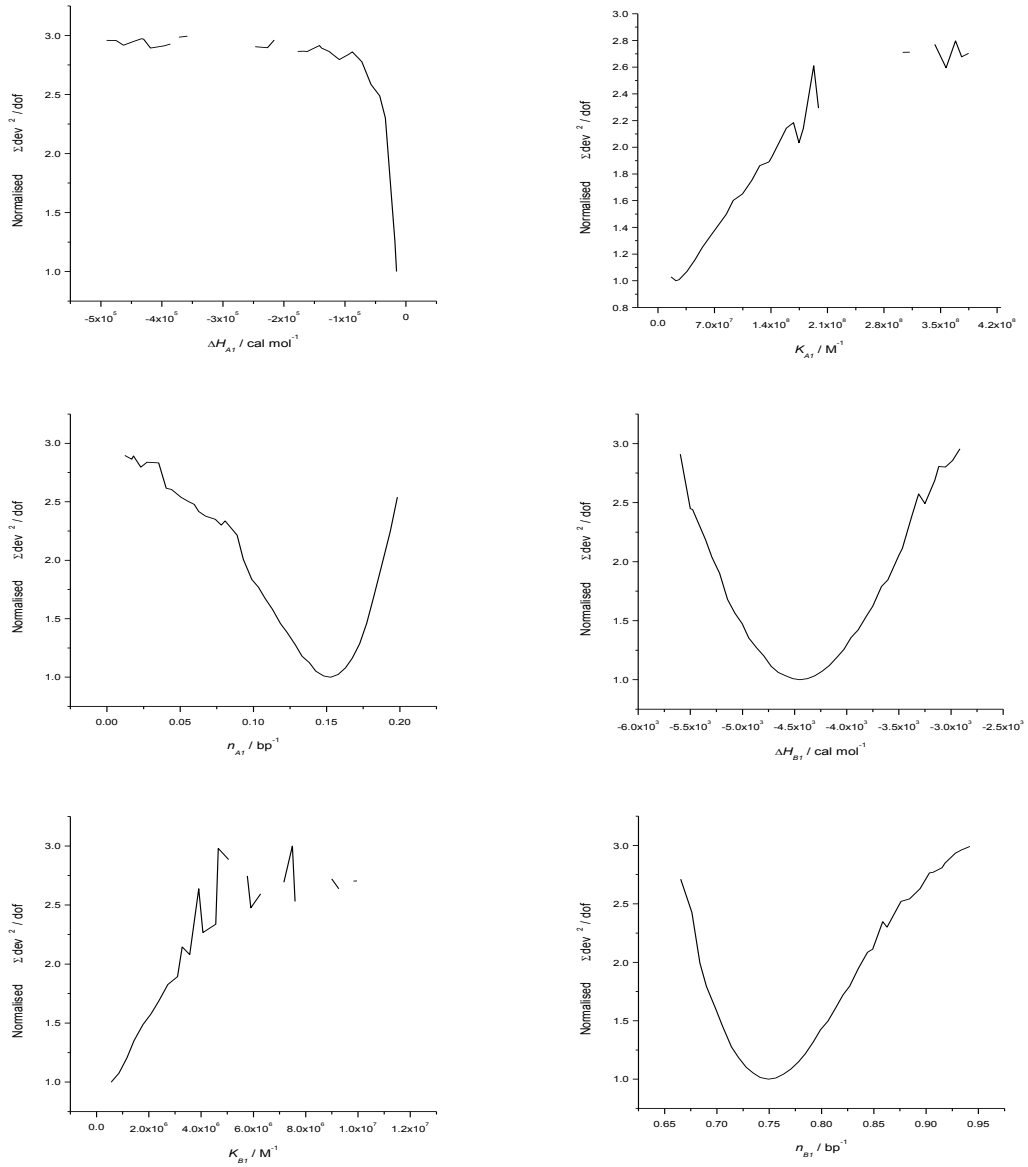

Figure A10.3 Normalised $\Sigma dev^2/dof$ for binding parameters of experiment (b).

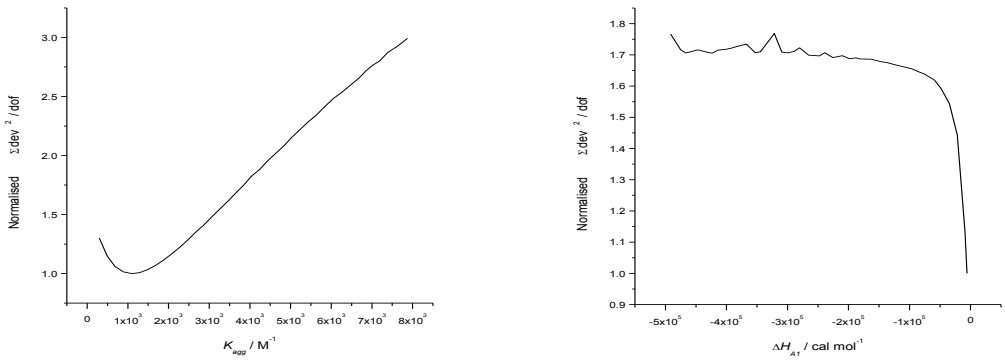

Figure A10.4 Normalised $\Sigma dev^2/dof$ for dilution parameters.

A11 Compound 4.1

1.1 Extinction coefficient

A stock solution of **4.1** (1.0 mM) in DMSO was prepared. Three series of solutions of 0.025, 0.05, 0.075 and 0.1 mM were prepared from the stock solution and UV-visible spectra were recorded for these solutions in a 1.0 cm pathlength cuvette. Ligand absorbances at the λ_{max} of 400 nm were plotted against ligand concentrations and a linear fit (red line) was applied to obtain the extinction coefficient of (13.6 ± 0.2) × 10^3 dm^3 mol^{-1} cm^{-1} (Figure A11.1).

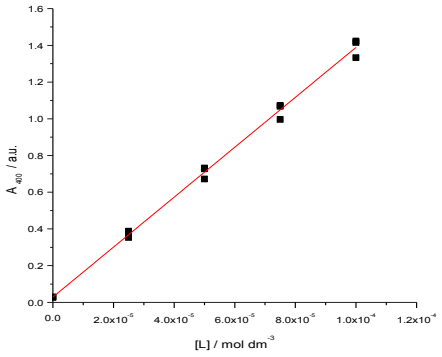

Figure A11.1 Absorbance for **4.1** as a function of concentration.

A12 Compound 4.2

1.1 Extinction coefficient

A stock solution of **4.2** (2.0 mM) in buffer (25 mM MOPS, pH 7.0, 50 mM NaCl) was prepared. A series of solutions of 0.019, 0.029 and 0.039 mM was prepared from the stock solution and UV-visible spectra were recorded for these solutions in a 1.0 cm pathlength cuvette. Ligand absorbances at the λ_{max} of 320 nm were plotted against ligand concentrations and a linear fit (red line) was applied to obtain the extinction coefficient of $(19.63 \pm 0.35) \times 10^3$ dm^3 mol^{-1} cm^{-1} (Figure A12.1).

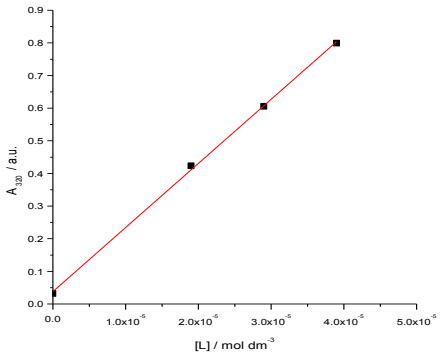

Figure A12.1 Absorbance for **4.2** as a function of concentration.

1.2 Error margins for isothermal titration calorimetry of 4.2.

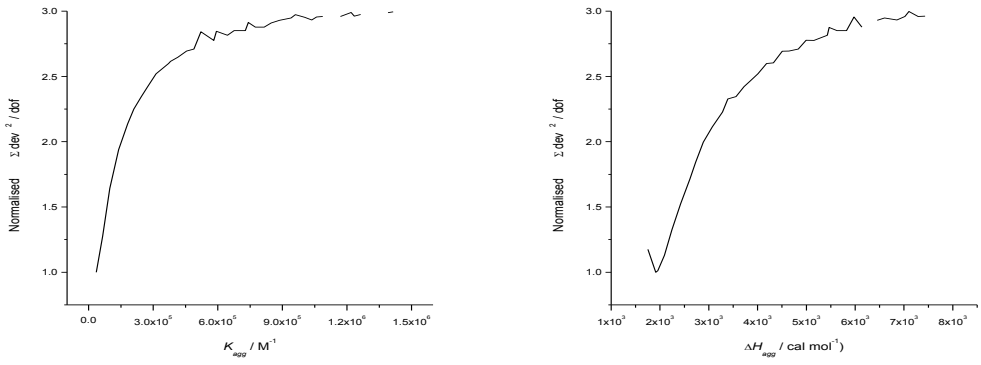

Figure A12.2 Normalised $\Sigma dev^2/dof$ for dilution parameters.

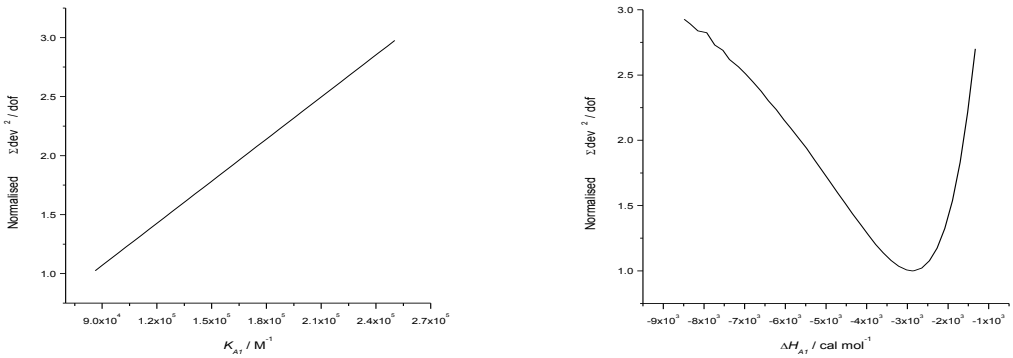

Figure A12.3 Normalised Σdev^2/dof for binding parameters.

A13 Compound 4.3

1.1 Extinction coefficient and UV-visible titrations of 4.3.

Stock solution of **4.3** (0.5 mM) in DMSO was prepared. Series solutions of (0.025, 0.05 and 0.062 mM) in 50 vol-% DMSO-MOPS buffer (25 mM MOPS, pH 7.0, 50 mM NaCl) were prepared from the stock solution and UV-visible spectra were recorded for these solutions in a 1.0 cm pathlength cuvette. Ligand absorbances at the λ_{max} of 362 nm were plotted against ligand concentrations and a linear fit (red line) was applied to obtain the extinction coefficient of (13.51 ± 0.1) × 10^3 dm^3 mol^{-1} cm^{-1} (Figure A13.1).

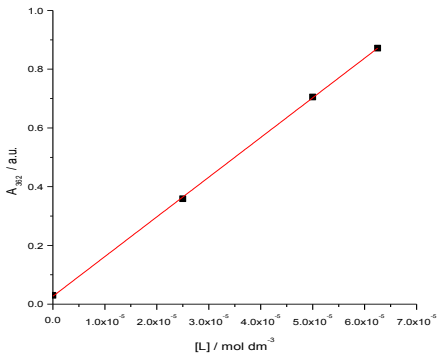

Figure A13.1 Absorbance for 4.3 as a function of concentration.

A14 Sequence selectivity studies of 2.2 and 2.4-2.7

1.1 2.2 binding to $(dAdT)_{12}.(dAdT)_{12}$

The binding of **2.2** to $(dAdT)_{12}.(dAdT)_{12}$ was studied using UV-visible spectroscopy; the changes in absorption of **2.2** upon addition of $(dAdT)_{12}.(dAdT)_{12}$ were measured in buffer (25 mM MOPS pH 7.0 and 50 mM NaCl) at 25 °C (Figure A14.1).

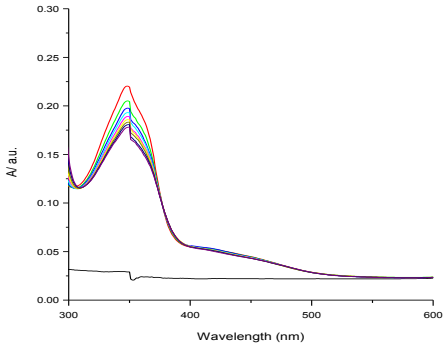

Figure A14.1 UV-visible spectra for 0.031 mM **2.2** upon addition of 0 – 0.26 mM $(dAdT)_{12}.(dAdT)_{12}$ in 25 mM MOPS pH 7.0, 50 mM NaCl, at 25°C.

Figure A14.1 shows a hypochromic shift in absorbance (at the λ_{max} of 347 nm) and hyperchromic shift (at 390 nm) of **2.2** upon addition of $(dAdT)_{12}.(dAdT)_{12}$, this change in UV-visible absorption may occur as a result of geometrical distortion of **2.2** when it interacts with DNA, but it may also be a local medium effect.

To quantify the affinity of **2.2** for $(dAdT)_{12}.(dAdT)_{12}$, the absorbances at 347 were plotted as a function of concentration of $(dAdT)_{12}.(dAdT)_{12}$ (Figure A14.2).

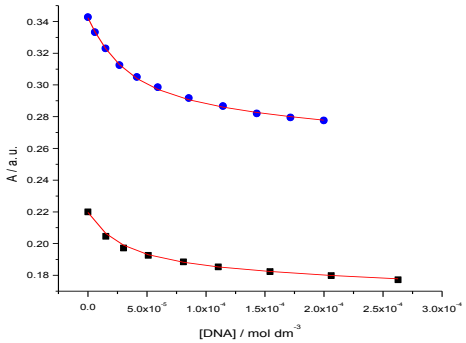

Figure A14.2 Absorbance at 347 nm of a solution of 0.032 mM **2.2** (●) and of a solution of 0.020 mM **2.2** (■), as a function of $(dAdT)_{12}.(dAdT)_{12}$ concentration, in buffer (25 mM MOPS pH 7.0, 50 mM NaCl), at 25 °C. The solid lines represent a global fit of a multiple independent sites model to the data.

The titration curves of Figure A14.2 were analysed globally in terms of a multiple independent binding sites models, which also takes ligand dilution into account, giving an equilibrium constant ($K_{binding}$) of (13.86 ± 6.02) $\times 10^3$ M^{-1} and a binding site size of (0.33 ± 0.10) base pairs. The obtained binding stoichiometry was small therefore the data were reanalysed at fixed binding site size of 3.0 base pairs. Because the fit did not reproduce the experimental data well, therefore we decided to reanalyse the data for a binding site size restricted to 1.0 base pair, giving an equilibrium constant ($K_{binding}$) of (92.49 ± 19.97) $\times 10^3$ M^{-1}.

1.2 2.2 binding to $(dGdC)_{12}.(dGdC)_{12}$

The binding of **2.2** to $(dGdC)_{12}.(dGdC)_{12}$ was studied using UV-visible spectroscopy; the changes in absorption of **2.2** upon addition of $(dGdC)_{12}.(dGdC)_{12}$ were measured in buffer (25 mM MOPS pH 7.0 and 50 mM NaCl) at 25 °C (Figure A14.3).

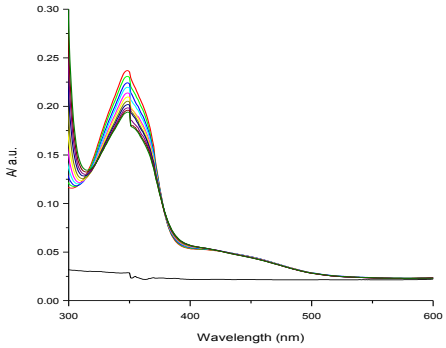

Figure A14.3 UV-visible spectra for 0.034 mM **2.2** upon addition of 0 – 0.33 mM $(dGdC)_{12}.(dGdC)_{12}$ in 25 mM MOPS pH 7.0, 50 mM NaCl, at 25°C.

Figure A14.3 shows a hypochromic shift in absorbance (at the λ_{max} of 347 nm) and hyperchromic shift (at 390 nm) of **2.2** upon addition of $(dGdC)_{12}.(dGdC)_{12}$, this change in UV-visible absorption may occur as a result of geometrical distortion of **2.2** when it interacts with DNA, but it may also be a local medium effect.

To quantify the affinity of **2.2** for $(dGdC)_{12}.(dGdC)_{12}$, the absorbances at 347 were plotted as a function of concentration of $(dGdC)_{12}.(dGdC)_{12}$ (Figure A14.4).

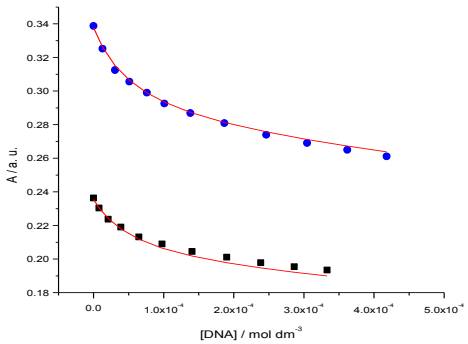

Figure A14.4 Absorbance at 347 nm of a solution of 0.051 mM **2.2** (●) and of a solution of 0.034 mM **2.2** (■), as a function of $(dGdC)_{12}.(dGdC)_{12}$ concentration, in buffer (25 mM MOPS pH 7.0, 50 mM NaCl), at 25 °C. The solid lines represent a global fit of a multiple independent sites model to the data.

The titration curves of Figure A14.4 were analysed globally in terms of a multiple independent binding sites models, which also takes ligand dilution into account to the data, giving an equilibrium constant ($K_{binding}$) of (15 ± 916) $\times 10^{-3}$ M^{-1} and a binding site size of (0.09 ± 5.7) $\times 10^{-6}$ base pairs. The obtained binding constant and stoichiometry were unreasonably small therefore the data were reanalysed at fixed binding site size 3.0 base pairs. Because the fit did not reproduce the experimental data well at n = 3, therefore the data were reanalysed at binding site size 1.0 base pair, giving an equilibrium constant ($K_{binding}$) of (25.45 ± 5.85) $\times 10^{3}$ M^{-1}.

1.3 2.4 binding to (dAdT)12.(dAdT)12

The binding of **2.4** to $(dAdT)_{12}.(dAdT)_{12}$ was studied using UV-visible spectroscopy; the changes in absorption of **2.4** upon addition of $(dAdT)_{12}.(dAdT)_{12}$ were measured in buffer (25 mM MOPS pH 7.0 and 50 mM NaCl) at 25 °C (Figure A14.5).

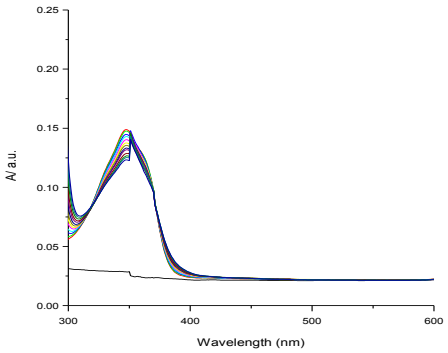

Figure A14.5 UV-visible spectra for 0.012 mM **2.4** upon addition of 0 – 0.44 mM $(dAdT)_{12}.(dAdT)_{12}$ in 25 mM MOPS pH 7.0, 50 mM NaCl, at 25°C.

Figure A14.5 shows a hypochromic shift in absorbance (at the λ_{max} of 347 nm) and hyperchromic shift (at 390 nm) of **2.4** upon addition of $(dAdT)_{12}.(dAdT)_{12}$, this change in UV-visible absorption may occur as a result of geometrical distortion of **2.4** when it interacts with DNA, but it may also be a local medium effect.

To quantify the affinity of **2.4** for $(dAdT)_{12}.(dAdT)_{12}$, the absorbances at 347 were plotted as a function of concentration of $(dAdT)_{12}.(dAdT)_{12}$ (Figure A14.6).

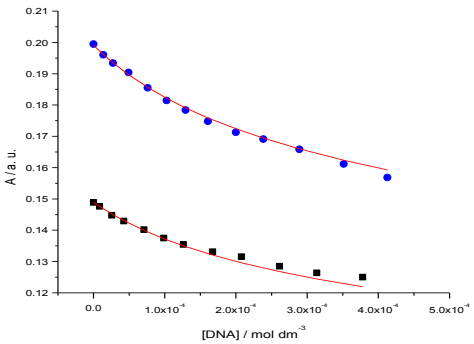

Figure A14.6 Absorbance at 347 nm of a solution of 0.017mM **2.4** (●), Absorbance at 347 nm of a solution of 0.012 mM **2.4** (■), as a function of $(dAdT)_{12}.(dAdT)_{12}$ concentration, in buffer (25 mM MOPS pH 7.0, 50 mM NaCl), at 25 °C. The solid lines represent a global fit of a multiple independent sites model to the data.

The titration curves of Figure A14.6 were analysed globally in terms of a multiple independent binding sites models, which also takes ligand dilution into account to the data, giving an equilibrium constant ($K_{binding}$) of (0.03 ± 3.7) M^{-1} and a binding site

size of (0.08 ± 9.6) $\times 10^{-6}$ base pairs. The obtained binding parameters were unreasonable therefore the data were reanalysed at fixed binding site size 3.0 base pairs, giving an equilibrium constant ($K_{binding}$) of (14.41 ± 3.12) $\times 10^{3}$ M^{-1}.

1.4 2.4 binding to $(dGdC)_{12}.(dGdC)_{12}$

The binding of **2.4** to $(dGdC)_{12}.(dGdC)_{12}$ was studied using UV-visible spectroscopy; the changes in absorption of **2.4** upon addition of $(dGdC)_{12}.(dGdC)_{12}$were measured in buffer (25 mM MOPS pH 7.0 and 50 mM NaCl) at 25 °C (Figure A14.7).

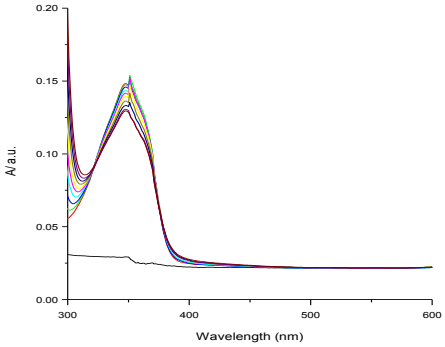

Figure A14.7 UV-visible spectra for 0.012 mM **2.4** upon addition of 0 – 0.26 mM $(dGdC)_{12}.(dGdC)_{12}$ in 25 mM MOPS pH 7.0, 50 mM NaCl, at 25°C.

Figure A14.7 shows a hypochromic shift in absorbance (at the λ_{max} of 347 nm) and hyperchromic shift (at 390 nm) of **2.4** upon addition of $(dGdC)_{12}.(dGdC)_{12}$, this change in UV-visible absorption may occur as a result of geometrical distortion of **2.4** when it interacts with $(dGdC)_{12}.(dGdC)_{12}$, but it may also be a local medium effect.

To quantify the affinity of **2.4** for $(dGdC)_{12}.(dGdC)_{12}$, the absorbances at 347 were plotted as a function of concentration of $(dGdC)_{12}.(dGdC)_{12}$ (Figure A14.8).

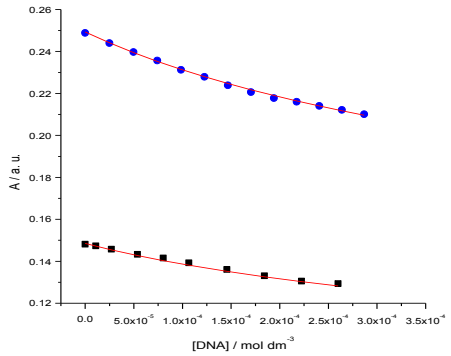

Figure A14.8 Absorbance at 347 nm of a solution of 0.022 mM **2.4** (●) and of a solution of 0.012 mM **2.4** (■), as a function of $(dGdC)_{12}.(dGdC)_{12}$ concentration, in buffer (25 mM MOPS pH 7.0, 50 mM NaCl), at 25 °C. The solid lines represent a global fit of a multiple independent sites model to the data.

The titration curves of Figure A14.8 were analysed globally in terms of a multiple independent binding sites models, which also takes ligand dilution into account, giving an equilibrium constant ($K_{binding}$) of (0.009 ± 1.54) M^{-1} and a binding site size of (0.04 ± 6.4) $\times 10^{-4}$ base pairs. The obtained binding parameters were unreasonably small therefore the data were reanalysed at fixed binding site size 3.0 base pairs, giving an equilibrium constant ($K_{binding}$) of (8.05 ± 2.03) $\times 10^{3}$ M^{-1}.

1.5 2.5 binding to $(dAdT)_{12}.(dAdT)_{12}$

The binding of **2.5** to $(dAdT)_{12}.(dAdT)_{12}$ was studied using UV-visible spectroscopy; the changes in absorption of **2.5** upon addition of $(dAdT)_{12}.(dAdT)_{12}$ were measured in buffer (25 mM MOPS pH 7.0 and 50 mM NaCl) at 25 °C (Figure A14.9).

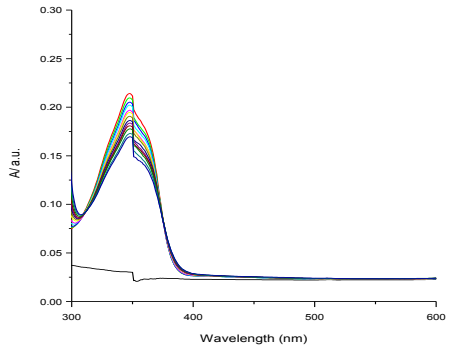

Figure A14.9 UV-visible spectra for 0.018 mM **2.5** upon addition of 0 – 0.47 mM $(dAdT)_{12}.(dAdT)_{12}$ in 25 mM MOPS pH 7.0, 50 mM NaCl, at 25°C

Figure A14.9 shows a hypochromic shift in absorbance (at the λ_{max} of 347 nm) and hyperchromic shift (at 390 nm) of **2.5** upon addition of $(dAdT)_{12}.(dAdT)_{12}$, this change in UV-visible absorption may occur as a result of geometrical distortion of **2.5** when it interacts with DNA, but it may also be a local medium effect.

To quantify the affinity of **2.5** for $(dAdT)_{12}.(dAdT)_{12}$, the absorbances at 347 were plotted as a function of concentration of $(dAdT)_{12}.(dAdT)_{12}$ (Figure A14.10).

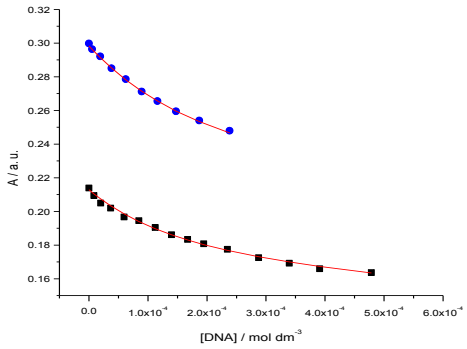

Figure A14.10 Absorbance at 347 nm of a solution of 0.026mM **2.5** (●) and of a solution of 0.018 mM **2.5** (■), as a function of $(dAdT)_{12}.(dAdT)_{12}$ concentration, in buffer (25 mM MOPS pH 7.0, 50 mM NaCl), at 25 °C. The solid lines represent a global fit of a multiple independent sites model to the data.

The titration curves of Figure A14.10 were analysed globally in terms of a multiple independent binding sites models, which also takes ligand dilution into account to the data, giving an equilibrium constant ($K_{binding}$) of (25.61 ± 13.02) $\times 10^3$ M^{-1} and a binding site size of (3.42 ± 1.07) base pairs.

1.6 2.5 binding to $(dGdC)_{12}.(dGdC)_{12}$

The binding of **2.5** to $(dGdC)_{12}.(dGdC)_{12}$ was studied using UV-visible spectroscopy; the changes in absorption of **2.5** upon addition of $(dGdC)_{12}.(dGdC)_{12}$were measured in buffer (25 mM MOPS pH 7.0 and 50 mM NaCl) at 25 °C (Figure A14.11).

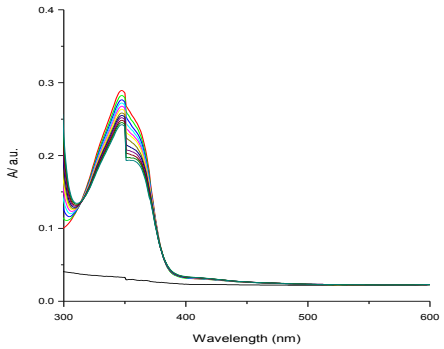

Figure A14.11 UV-visible spectra for 0.025 mM **2.5** upon addition of 0 – 0.27 mM $(dGdC)_{12}.(dGdC)_{12}$ in 25 mM MOPS pH 7.0, 50 mM NaCl, at 25°C.

Figure A14.11 shows a hypochromic shift in absorbance (at the λ_{max} of 347 nm) and hyperchromic shift (at 390 nm) of **2.5** upon addition of $(dGdC)_{12}.(dGdC)_{12}$, this change in UV-visible absorption may occur as a result of geometrical distortion of **2.5** when it interacts with $(dGdC)_{12}.(dGdC)_{12}$, but it may also be a local medium effect.

To quantify the affinity of **2.5** for $(dGdC)_{12}.(dGdC)_{12}$, the absorbances at 347 were plotted as a function of concentration of $(dGdC)_{12}.(dGdC)_{12}$ (Figure A14.12).

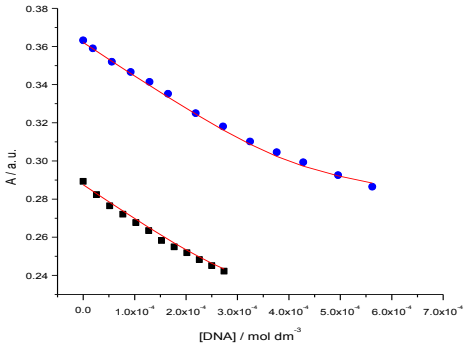

Figure A14.12 Absorbance at 347 nm of a solution of 0.033 mM **2.5** (●) and of a solution of 0.025 mM **2.5** (■), as a function of $(dGdC)_{12}.(dGdC)_{12}$ concentration, in buffer (25 mM MOPS pH 7.0, 50 mM NaCl), at 25 °C. The solid lines represent a global fit of a multiple independent sites model to the data.

The titration curves of Figure A14.12 were analysed globally in terms of a multiple independent binding sites models, which also takes ligand dilution into account to the data, giving an equilibrium constant ($K_{binding}$) of (66.10 ± 52.89) $\times 10^4$ M^{-1} and a binding site size of (12.8 ± 0.7) base pairs. The obtained stoichiometry was big therefore the data were reanalysed at fixed binding site size 3.0 base pairs, giving an equilibrium constant ($K_{binding}$) of (9.30 ± 2.70) $\times 10^3$ M^{-1}.

1.7 2.6 binding to $(dAdT)_{12}.(dAdT)_{12}$

The binding of **2.6** to $(dAdT)_{12}.(dAdT)_{12}$ was studied using UV-visible spectroscopy; the changes in absorption of **2.6** upon addition of $(dAdT)_{12}.(dAdT)_{12}$ were measured in buffer (25 mM MOPS pH 7.0 and 50 mM NaCl) at 25 °C (Figure A14.13).

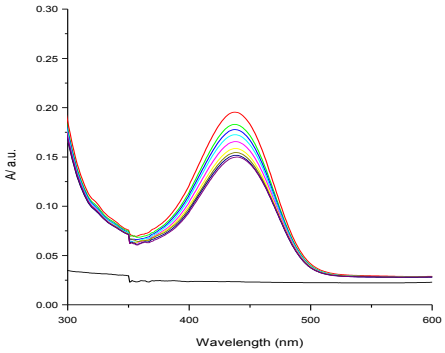

Figure A14.13 UV-visible spectra for 0.010 mM **2.6** upon addition of 0 – 0.016 mM $(dAdT)_{12}.(dAdT)_{12}$ in 25 mM MOPS pH 7.0, 50 mM NaCl, at 25°C

Figure A14.13 shows a hypochromic shift in absorbance (at the λ_{max} of 440 nm) of **2.6** upon addition of $(dAdT)_{12}.(dAdT)_{12}$, this change in UV-visible absorption may occur as a result of geometrical distortion of **2.6** when it interacts with DNA, but it may also be a local medium effect.

To quantify the affinity of **2.6** for $(dAdT)_{12}.(dAdT)_{12}$, the absorbances at 440 were plotted as a function of concentration of $(dAdT)_{12}.(dAdT)_{12}$ (Figure A14.14).

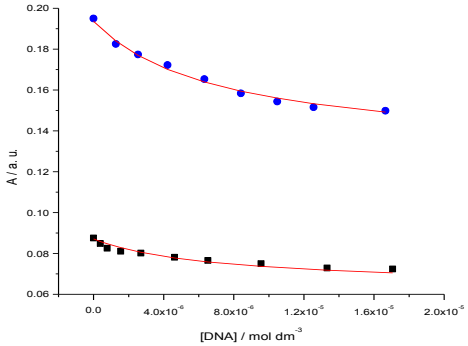

Figure A14.14 Absorbance at 440 nm of a solution of 0.010 mM **2.6** (●) and of a solution of 0.004 mM **2.6** (■), as a function of $(dAdT)_{12}.(dAdT)_{12}$ concentration, in buffer (25 mM MOPS pH 7.0, 50 mM NaCl), at 25 °C. The solid lines represent a global fit of a multiple independent sites model to the data.

The titration curves of Figure A14.14 were analysed globally in terms of a multiple independent binding sites models, which also takes ligand dilution into account to the data, giving an equilibrium constant ($K_{binding}$) of (5.04 ± 36.7) $\times 10^3$ M^{-1} and a binding site size of (0.03 ± 0.22) base pair. The obtained binding site size was small therefore the data were reanalysed at fixed binding site size 3.0 base pairs. Because the fit did not reproduce the experimental data well, therefore we analysed the data again at lower stoichiometry n=1.0 base pair, giving an equilibrium constant ($K_{binding}$) of (74.76 ± 76.62) $\times 10^4$ M^{-1}. Because equilibrium constants cannot be negative, we express the error margin as a confidence interval so that the equilibrium constant is 74×10^4 [0 – 151×10^4].

1.8 2.6 binding to $(dGdC)_{12}.(dGdC)_{12}$

The binding of **2.6** to $(dGdC)_{12}.(dGdC)_{12}$ was studied using UV-visible spectroscopy; the changes in absorption of **2.6** upon addition of $(dGdC)_{12}.(dGdC)_{12}$were measured in buffer (25 mM MOPS pH 7.0 and 50 mM NaCl) at 25 °C (Figure A14.15).

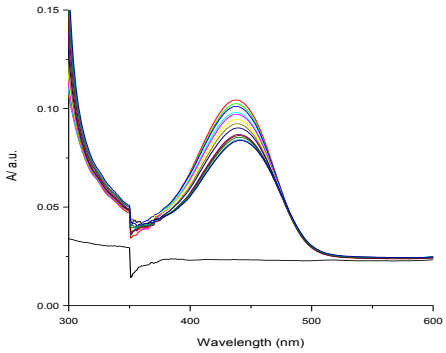

Figure A14.15 UV-visible spectra for 0.0048 mM **2.6** upon addition of 0 – 0.11 mM $(dGdC)_{12}.(dGdC)_{12}$in 25 mM MOPS pH 7.0, 50 mM NaCl, at 25°C.

Figure A14.14 shows a hypochromic shift in absorbance (at the λ_{max} of 440 nm) of **2.6** upon addition of $(dGdC)_{12}.(dGdC)_{12}$, this change in UV-visible absorption may occur as a result of geometrical distortion of **2.6** when it interacts with $(dGdC)_{12}.(dGdC)_{12}$, but it may also be a local medium effect.

To quantify the affinity of **2.6** for $(dGdC)_{12}.(dGdC)_{12}$, the absorbances at 347 were plotted as a function of concentration of $(dGdC)_{12}.(dGdC)_{12}$ (Figure A14.16).

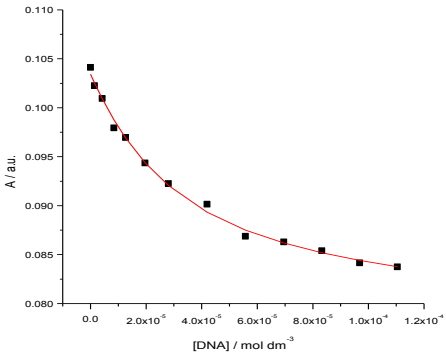

Figure A14.16 Absorbance at 440 nm of a solution of 0.0048 mM **2.6**, as a function of $(dGdC)_{12}.(dGdC)_{12}$ concentration, in buffer (25 mM MOPS pH 7.0, 50 mM NaCl), at 25 °C. The solid lines represent a global fit of a multiple independent sites model to the data.

The titration curve of Figure A14.16 was analysed in terms of a multiple independent binding sites models, which also takes ligand dilution into account to the data, giving

unreasonably small binding parameters, therefore the data were reanalysed at fixed stoichiometry n=3 base pairs, giving an equilibrium constant ($K_{binding}$) of (13.67 ± 1.93) $\times 10^4$ M^{-1}.

1.9 2.7 binding to $(dAdT)_{12}.(dAdT)_{12}$

The binding of **2.7** to $(dAdT)_{12}.(dAdT)_{12}$ was studied using UV-visible spectroscopy; the changes in absorption of **2.7** upon addition of $(dAdT)_{12}.(dAdT)_{12}$ were measured in buffer (25 mM MOPS pH 7.0 and 50 mM NaCl) at 25 °C (Figure A14.17).

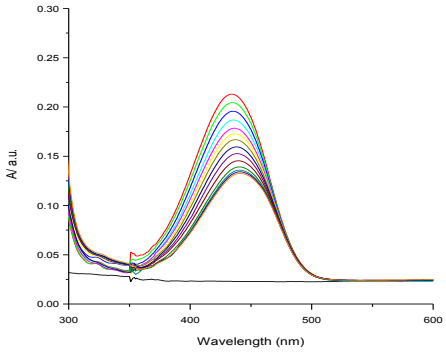

Figure A14.17 UV-visible spectra for 0.018 mM **2.7** upon addition of 0 – 0.28 mM $(dAdT)_{12}.(dAdT)_{12}$ in 25 mM MOPS pH 7.0, 50 mM NaCl, at 25°C

Figure A14.17 shows a hypochromic shift in absorbance (at the λ_{max} of 434 nm) of **2.7** upon addition of $(dAdT)_{12}.(dAdT)_{12}$, this change in UV-visible absorption may occur as a result of geometrical distortion of **2.7** when it interacts with DNA, but it may also be a local medium effect.

To quantify the affinity of **2.7** for $(dAdT)_{12}.(dAdT)_{12}$, the absorbances at 434 were plotted as a function of concentration of $(dAdT)_{12}.(dAdT)_{12}$ (Figure A14.18).

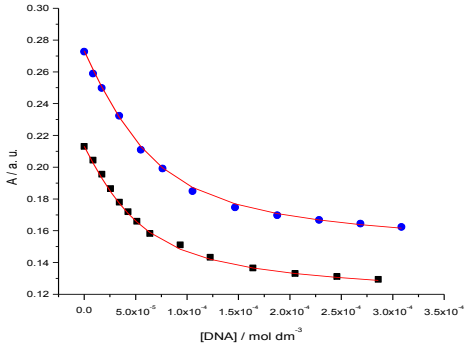

Figure A14.18 Absorbance at 434 nm of a solution of 0.023 mM **2.7** (●), and of a solution of 0.018 mM **2.7** (■), as a function of $(dAdT)_{12}.(dAdT)_{12}$ concentration, in buffer (25 mM MOPS pH 7.0, 50 mM NaCl), at 25 °C. The solid lines represent a global fit of a multiple independent sites model to the data.

The titration curves of Figure A14.18 were analysed globally in terms of a multiple independent binding sites models, which also takes ligand dilution into account to the data, giving an equilibrium constant ($K_{binding}$) of (10.28 ± 2.56) $\times 10^4$ M^{-1} and a binding site size of (2.53 ± 0.28) base pairs.

1.10 2.7 binding to $(dGdC)_{12}.(dGdC)_{12}$

The binding of **2.7** to $(dGdC)_{12}.(dGdC)_{12}$ was studied using UV-visible spectroscopy; the changes in absorption of **2.7** upon addition of $(dGdC)_{12}.(dGdC)_{12}$were measured in buffer (25 mM MOPS pH 7.0 and 50 mM NaCl) at 25 °C (Figure A14.19).

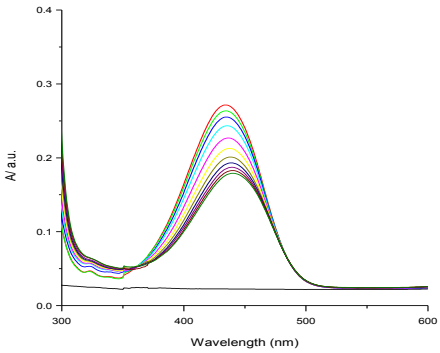

Figure A14.19 UV-visible spectra for 0.023 mM **2.7** upon addition of 0 – 0.21 mM $(dGdC)_{12}.(dGdC)_{12}$in 25 mM MOPS pH 7.0, 50 mM NaCl, at 25°C.

Figure A14.19 shows a hypochromic shift in absorbance (at the λ_{max} of 434 nm) of **2.7** upon addition of $(dGdC)_{12}.(dGdC)_{12}$, this change in UV-visible absorption may occur as a result of geometrical distortion of **2.7** when it interacts with $(dGdC)_{12}.(dGdC)_{12}$, but it may also be a local medium effect.

To quantify the affinity of **2.7** for $(dGdC)_{12}.(dGdC)_{12}$, the absorbances at 434 were plotted as a function of concentration of $(dGdC)_{12}.(dGdC)_{12}$ (Figure A14.20).

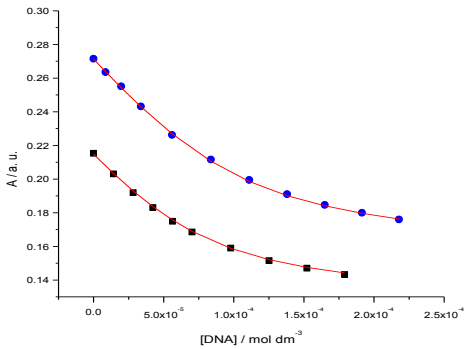

Figure A14.20 Absorbance at 434 nm of a solution of 0.023 mM **2.7** (●) and of a solution of 0.018 mM **2.7** (■), as a function of $(dGdC)_{12}.(dGdC)_{12}$ concentration, in buffer (25 mM MOPS pH 7.0, 50 mM NaCl), at 25 °C. The solid lines represent a global fit of a multiple independent sites model to the data.

The titration curves of Figure A14.20 were analysed globally in terms of a multiple independent binding sites models, which also takes ligand dilution into account to the data, giving an equilibrium constant ($K_{binding}$) of (18.18 ± 3.07) $\times 10^4$ M^{-1} and a binding site size of (4.23 ± 0.17) base pairs.

A15 UV-visible titrations of compounds of 1, 8-naphthalimide derivatives.

Table A15.1 UV-visible titration of 0.066 mM 2.1 upon addition of 0 – 3.33 mM FSDNA in buffer (25 mM MOPS, pH 7.0, 50 mM NaCl), at 25 °C. $[DNA]_{stock}$ = 18.2 mM, $[Ligand]_{stock}$ = 2.68 mM

Cumulative added volume DNA (µL)	Added volume ligand (µL)	Total volume (µL)	[DNA] ($x10^{-6}$ M)	[ligand] ($x10^{-6}$ M)	A347 nm	A390 nm
0	0	1950	0	0	0.027632	0.027265
0	50	2000	0	66.8	0.435931	0.062651
5	50	2005	45.2	66.7	0.421888	0.065224
25	50	2025	224.0	66.0	0.393847	0.07161
55	50	2055	485.7	65.0	0.363846	0.074315
100	50	2100	864.2	63.6	0.342365	0.07741
150	50	2150	1266.2	62.2	0.326849	0.079928
200	50	2200	1650	60.7	0.312306	0.082575
250	50	2250	2016.6	59.4	0.296543	0.078687
300	50	2300	2367.3	58.1	0.287934	0.078798
350	50	2350	2703.1	56.9	0.285368	0.080366
400	50	2400	3025	55.7	0.281174	0.082095
450	50	2450	3333.6	54.5	0.278086	0.082221

Table A15.2 UV-visible titration of 0.093 mM 2.1 upon addition of 0 – 5.18 mM FSDNA in buffer (25 mM MOPS, pH 7.0, 50 mM NaCl), at 25 °C. $[DNA]_{stock}$ = 18.2 mM, $[Ligand]_{stock}$ = 2.68 mM

Cumulative added volume DNA (µL)	Added volume ligand (µL)	Total volume (µL)	[DNA] ($x10^{-6}$ M)	[ligand] ($x10^{-6}$ M)	A347 nm	A390 nm
0	0	1930	0	0	0.027786	0.024696
0	70	2000	0	93.6	0.585879	0.070846
5	70	2005	45.3	93.3	0.569883	0.076091
15	70	2015	135.1	92.9	0.548219	0.077928
30	70	2030	268.2	92.2	0.522634	0.082048
60	70	2060	528.6	90.8	0.491706	0.088094
90	70	2090	781.5	89.5	0.465975	0.087533
130	70	2130	1107.7	87.9	0.443814	0.090592
180	70	2180	1498.6	85.8	0.427986	0.093432
250	70	2250	2016.6	83.2	0.408061	0.09499
320	70	2320	2503.4	80.7	0.393432	0.096321
400	70	2400	3025	78.0	0.378822	0.096355
480	70	2480	3512.9	75.5	0.363442	0.095211
560	70	2560	3970.3	73.1	0.355825	0.097236
640	70	2640	4400	70.9	0.34475	0.095467
720	70	2720	4804.4	68.8	0.339971	0.096234
800	70	2800	5185.7	66.8	0.334898	0.097616

Table A15.3 UV-visible titration of 0.068 mM 2.2 upon addition of 0 – 8.36 mM FSDNA in buffer (25 mM MOPS, pH 7.0, 50 mM NaCl), at 25 °C. $[DNA]_{stock}$ = 22.3 mM, $[Ligand]_{stock}$ = 2.74 mM

Cumulative added volume DNA (µL)	Added volume ligand (µL)	Total volume (µL)	[DNA] ($x10^{-6}$ M)	[ligand] ($x10^{-6}$ M)	A347 nm	A390 nm
0	0	1950	0	0	0.023047	0.024788
0	50	2000	0	68.5	0.438953	0.073699
2	50	2002	22.2	68.4	0.43038	0.073409
7	50	2007	77.8	68.2	0.420197	0.07451
17	50	2017	188.0	67.9	0.413914	0.075619
40	50	2040	437.4	67.1	0.404602	0.077302
80	50	2080	858	65.8	0.392247	0.079189
140	50	2140	1459.5	64	0.376916	0.081599
200	50	2200	2028.1	62.2	0.367003	0.082486
300	50	2300	2910	59.5	0.349798	0.083922
400	50	2400	3718.3	57	0.338344	0.085076
500	50	2500	4462	54.8	0.330875	0.086397
600	50	2600	5148.4	52.6	0.32236	0.086989
700	50	2700	5784	50.7	0.311611	0.086807
800	50	2800	6374.2	48.9	0.302456	0.086982
900	50	2900	6923.7	47.2	0.295426	0.087238
1000	50	3000	7436.6	45.6	0.288329	0.086982
1100	50	3100	7916.4	44.1	0.285218	0.08744
1200	50	3200	8366.2	42.8	0.281465	0.087511

Table A15.4 UV-visible titration of 0.082 mM 2.2 upon addition of 0 – 2.64 mM FSDNA in buffer (25 mM MOPS, pH 7.0, 50 mM NaCl), at 25 °C. $[DNA]_{stock}$ = 22.3 mM, $[Ligand]_{stock}$ = 2.74 mM

Cumulative added volume DNA (µL)	Added volume ligand (µL)	Total volume (µL)	[DNA] ($x10^{-6}$ M)	[ligand] ($x10^{-6}$ M)	A347 nm	A390 nm
0	0	1950	0	0	0.026612 7	0.026461
0	60	2010	0	82.6	0.528632	0.086833
5	60	2015	55.3	82.4	0.518901	0.088661
10	60	2020	110.4	82.2	0.510197	0.090665
20	60	2030	219.8	81.8	0.503451	0.091616
40	60	2050	435.3	81	0.49337	0.095019
60	60	2070	646.6	80.2	0.483417	0.09592
90	60	2100	956.1	79.1	0.470911	0.098251
120	60	2130	1256.9	78	0.465113	0.100438
150	60	2160	1549.3	76.9	0.45531	0.100619
180	60	2190	1833.6	75.8	0.451728	0.10177
210	60	2220	2110.4	74.8	0.442752	0.102961

240	60	2250	2379.7	73.8	0.439894	0.10472
270	60	2280	2641.9	72.8	0.435165	0.105621
300	60	2310	2897.4	71.9	0.433254	0.107851
330	60	2340	3146.2	71	0.429683	0.108092

Table A15.5 UV-visible titration of 0.046 mM 2.2 upon addition of 0 – 0.72 mM FSDNA in buffer (25 mM MOPS, pH 7.0, 50 mM NaCl), at 25 °C. $[DNA]_{stock}$ = 7.91, $[Ligand]_{stock}$ = 1.34 mM

Cumulative added volume DNA (µL)	Added volume ligand (µL)	Total volume (µL)	[DNA] ($x10^{-6}$ M)	[ligand] ($x10^{-6}$ M)	A347 nm	A390 nm
0	0	2200	0	0	0.029406	0.022785
0	80	2280	0	46.8	0.314072	0.059182
5	80	2285	17.3	46.7	0.307997	0.059772
12	80	2292	41.4	46.6	0.303854	0.060504
22	80	2302	75.5	46.4	0.299293	0.060531
35	80	2315	119.5	46.1	0.295389	0.061557
55	80	2335	186.3	45.7	0.292525	0.063465
80	80	2360	268.1	45.2	0.28745	0.063971
110	80	2390	364	44.7	0.281788	0.063883
140	80	2420	457.6	44.1	0.276978	0.063784
170	80	2450	548.8	43.6	0.273351	0.064377
200	80	2480	637.9	43	0.269413	0.064734
230	80	2510	724.8	42.5	0.268436	0.065749

Table A15.6 UV-visible titration of 0.052 mM 2.3 upon addition of 0 – 6.14 mM FSDNA in buffer (25 mM MOPS, pH 7.0, 50 mM NaCl), at 25 °C. $[DNA]_{stock}$ = 22.3 mM, $[Ligand]_{stock}$ = 4.2 mM

Cumulative added volume DNA (µL)	Added volume ligand (µL)	Total volume (µL)	[DNA] ($x10^{-6}$ M)	[ligand] ($x10^{-6}$ M)	A347 nm	A390 nm
0	0	1975	0	0	0.029048	0.025485
0	25	2000	0	52.53	0.634309	0.053235
3	25	2003	33.4	52.45	0.634005	0.054869
13	25	2013	144	52.19	0.626641	0.057612
40	25	2040	437.4	51.50	0.6127	0.059605
60	25	2060	649.8	51	0.60149	0.062083
90	25	2090	960.7	50.27	0.586068	0.063849
120	25	2120	1262.8	49.56	0.573232	0.066581
160	25	2160	1652.5	48.64	0.555958	0.069396
200	25	2200	2028.1	47.76	0.542371	0.071546
250	25	2250	2478.8	46.7	0.527193	0.073638
320	25	2320	3077.2	45.29	0.510831	0.07601
400	25	2400	3718.3	43.78	0.490403	0.077461

480	25	2480	4318	42.36	0.471037	0.078498
560	25	2560	4880.3	41.04	0.456195	0.079494
660	25	2660	5535.5	39.50	0.440688	0.081973
760	25	2760	6143.3	38.07	0.427361	0.082559
860	25	2860	6708.6	36.73	0.417196	0.08361
960	25	2960	7235.6	35.49	0.409591	0.085206
1060	25	3060	7728.3	34.33	0.400954	0.086677
1160	25	3160	8189.7	33.25	0.392412	0.086923
1260	25	3260	8622.8	32.23	0.381338	0.087964

Table A15.7 UV-visible titration of 0.031 mM 2.3 upon addition of 0 – 6.34 mM FSDNA in buffer (25 mM MOPS, pH 7.0, 50 mM NaCl), at 25 °C. $[DNA]_{stock}$ = 22.3 mM, $[Ligand]_{stock}$ = 4.2 mM

Cumulative added volume DNA (µL)	Added volume ligand (µL)	Total volume (µL)	[DNA] ($x10^{-6}$ M)	[ligand] ($x10^{-6}$ M)	A347 nm	A390 nm
0	0	1985	0	0	0.024765	0.024849
0	15	2000	0	31.52	0.392252	0.044218
5	15	2005	55.6	31.44	0.388775	0.046736
15	15	2015	166	31.28	0.383105	0.048289
35	15	2035	383.7	30.98	0.373997	0.05026
110	15	2110	1163	29.87	0.352394	0.055349
160	15	2160	1652.5	29.18	0.341403	0.057655
220	15	2220	2210.9	28.39	0.329947	0.05909
300	15	2300	2910	27.41	0.314648	0.061128
400	15	2400	3718.3	26.26	0.302757	0.063109
500	15	2500	4462	25.21	0.291742	0.064686
600	15	2600	5148.4	24.24	0.283571	0.066708
700	15	2700	5784	23.35	0.27809	0.06792
800	15	2800	6374.2	22.51	0.274685	0.069782

Table A15.8 UV-visible titration of 0.032 mM 2.4 upon addition of 0 – 2.84 mM FSDNA in buffer (25 mM MOPS, pH 7.0, 50 mM NaCl), at 25 °C. $[DNA]_{stock}$ = 22.3 mM, $[Ligand]_{stock}$ = 0.19 mM

Cumulative added volume DNA (µL)	Added volume ligand (µL)	Total volume (µL)	[DNA] ($x10^{-6}$ M)	[ligand] ($x10^{-6}$ M)	A347 nm	A390 nm
0	0	1930	0	0	0.023888	0.02678
0	400	2330	0	32.61	0.333187	0.035034
5	400	2335	47.7	32.54	0.324713	0.036416
20	400	2350	189.8	32.34	0.30818	0.039172
40	400	2370	376.5	32.06	0.298684	0.041821
70	400	2400	650.7	31.66	0.286043	0.044659
110	400	2440	1005.7	31.14	0.277835	0.04702

160	400	2490	1433.5	30.52	0.27249	0.050146
220	400	2550	1924.7	29.80	0.268203	0.053202
280	400	2610	2393.4	29.11	0.265103	0.056557
340	400	2670	2840.9	28.46	0.26055	0.059441

Table A15.9 UV-visible titration of 0.039 mM 2.4 upon addition of 0 – 2.80 mM FSDNA in buffer (25 mM MOPS, pH 7.0, 50 mM NaCl), at 25 °C. $[DNA]_{stock}$ = 22.3 mM, $[Ligand]_{stock}$ = 0.19 mM

Cumulative added volume DNA (µL)	Added volume ligand (µL)	Total volume (µL)	[DNA] ($x10^{-6}$ M)	[ligand] ($x10^{-6}$ M)	A347 nm	A390 nm
0	0	1930	0	0	0.030842	0.02818
0	500	2430	0	39.09	0.397978	0.039056
5	500	2435	45.8	39.01	0.386899	0.040125
10	500	2440	91.4	38.93	0.373891	0.041094
20	500	2450	182.1	38.77	0.360386	0.042303
35	500	2465	316.7	38.53	0.350881	0.044647
55	500	2485	493.7	38.22	0.341798	0.049063
80	500	2510	711	37.84	0.337937	0.052284
110	500	2540	966.1	37.40	0.325524	0.052049
200	500	2630	1696.5	36.12	0.313236	0.057526
250	500	2680	2081.1	35.44	0.309597	0.060593
300	500	2730	2451.6	34.79	0.307366	0.063353
350	500	2780	2808.8	34.17	0.301015	0.064268

Table A15.10 UV-visible titration of 0.027 mM 2.5 upon addition of 0 – 2.64 mM FSDNA in buffer (25 mM MOPS, pH 7.0, 50 mM NaCl), at 25 °C. $[DNA]_{stock}$ = 22.3 mM, $[Ligand]_{stock}$ = 0.20 mM

Cumulative added volume DNA (µL)	Added volume ligand (µL)	Total volume (µL)	[DNA] ($x10^{-6}$ M)	[ligand] ($x10^{-6}$ M)	A347 nm	A390 nm
0	0	1930	0	0	0.033529	0.028969
0	300	2230	0	26.90	0.320386	0.042414
5	300	2235	49.9	26.84	0.313233	0.044746
10	300	2240	99.5	26.78	0.304809	0.04707
20	300	2250	198.3	26.66	0.292607	0.052492
30	300	2260	296.1	26.54	0.28827	0.052277
50	300	2280	489.2	26.31	0.278384	0.055375
80	300	2310	772.6	25.97	0.268272	0.058643
110	300	2340	1048.7	25.64	0.263449	0.060291
150	300	2380	1406	25.21	0.253099	0.062493
200	300	2430	1836.2	24.69	0.249063	0.064686
250	300	2480	2248.9	24.19	0.244124	0.065632
300	300	2530	2645.4	23.71	0.245754	0.068818

Table A15.11 UV-visible titration of 0.034 mM 2.5 upon addition of 0 – 3.12 mM FSDNA in buffer (25 mM MOPS, pH 7.0, 50 mM NaCl), at 25 °C. $[DNA]_{stock}$ = 22.3 mM, $[Ligand]_{stock}$ = 0.20 mM						
Cumulative added volume DNA (µL)	Added volume ligand (µL)	Total volume (µL)	[DNA] ($x10^{-6}$ M)	[ligand] ($x10^{-6}$ M)	A347 nm	A390 nm
0	0	1930	0	0	0.052546	0.031363
0	400	2330	0	34.33	0.406359	0.047333
5	400	2335	47.7	34.26	0.390551	0.050145
20	400	2350	189.8	34.04	0.362305	0.055136
30	400	2360	283.6	33.89	0.347741	0.05603
50	400	2380	468.6	33.61	0.33154	0.058862
80	400	2410	740.5	33.19	0.327251	0.064988
120	400	2450	1092.7	32.65	0.313787	0.066648
160	400	2490	1433.5	32.12	0.306317	0.069176
220	400	2550	1924.7	31.37	0.30214	0.071634
300	400	2630	2544.8	30.41	0.296365	0.074513
380	400	2710	3128.3	29.52	0.295583	0.077883

Table A15.12 UV-visible titration of 0.039 mM 2.6 upon addition of 0 – 0.172 mM FSDNA in buffer (25 mM MOPS, pH 7.0, 50 mM NaCl), at 25 °C. $[DNA]_{stock}$ = 8.82 mM, $[Ligand]_{stock}$ = 0.453 mM					
Cumulative added volume DNA (µL)	Added volume ligand (µL)	Total volume (µL)	[DNA] ($x10^{-6}$ M)	[ligand] ($x10^{-6}$ M)	A440 nm
0	0	1825	0	0	0.064903
0	175	2000	0	39.63	0.722703
5	175	2005	21.9	39.53	0.601699
10	175	2010	43.8	39.44	0.557855
15	175	2015	65.6	39.34	0.515106
20	175	2020	87.2	39.24	0.478175
25	175	2025	108.8	39.14	0.469029
30	175	2030	130.2	39.05	0.465279
35	175	2035	151.6	38.95	0.469551
40	175	2040	172.8	38.86	0.472086

Table A15.13 UV-visible titration of 0.017 mM 2.6 upon addition of 0 – 0.11 mM FSDNA in buffer (25 mM MOPS, pH 7.0, 50 mM NaCl), at 25 °C. $[DNA]_{stock}$ = 0.882 mM, $[Ligand]_{stock}$ = 0.088 mM

Cumulative added volume DNA (µL)	Added volume ligand (µL)	Total volume (µL)	[DNA] ($x10^{-6}$ M)	[ligand] ($x10^{-6}$ M)	A440 nm
0	0	2000	0	0	0.026758
0	500	2500	0	17.7	0.314793
10	500	2510	3.5	17.62	0.298538
20	500	2520	6.9	17.55	0.285953
30	500	2530	10.4	17.49	0.272431
50	500	2550	17.2	17.35	0.25026
70	500	2570	24.0	17.21	0.232741
90	500	2590	30.6	17.08	0.22819
120	500	2620	40.3	16.88	0.223655
160	500	2660	53.0	16.63	0.215173
210	500	2710	68.3	16.32	0.207669
260	500	2760	83.0	16.03	0.206074
310	500	2810	97.2	15.74	0.204175
360	500	2860	110.9	15.47	0.202484

Table A15.14 UV-visible titration of 0.050 mM 2.7 upon addition of 0 – 2.42 mM FSDNA in buffer (25 mM MOPS, pH 7.0, 50 mM NaCl), at 25 °C. $[DNA]_{stock}$ = 8.82 mM, $[Ligand]_{stock}$ = 1.0 mM

Cumulative added volume DNA (µL)	Added volume ligand (µL)	Total volume (µL)	[DNA] ($x10^{-6}$ M)	[ligand] ($x10^{-6}$ M)	A434 nm
0	0	2375	0	0	0.026722
0	125	2500	0	50	0.576419
10	125	2510	35.1	49.80	0.534488
20	125	2520	69.9	49.60	0.500561
40	125	2540	138.8	49.21	0.455751
80	125	2580	273.3	48.44	0.42202
120	125	2620	403.7	47.70	0.381122
180	125	2680	592.1	46.64	0.352162
250	125	2750	801.4	45.45	0.333512
350	125	2850	1082.6	43.85	0.317715
450	125	2950	1344.8	42.37	0.306221
550	125	3050	1589.7	40.98	0.296742
650	125	3150	1819.1	39.68	0.28738
750	125	3250	2034.4	38.46	0.279759
850	125	3350	2236.8	37.31	0.273626
950	125	3450	2427.5	36.23	0.266191

Table A15.15 UV-visible titration of 0.070 mM 2.7 upon addition of 0 – 3.91 mM FSDNA in buffer (25 mM MOPS, pH 7.0, 50 mM NaCl), at 25 °C. $[DNA]_{stock}$ = 8.82 mM, $[Ligand]_{stock}$ = 1.0 mM

Cumulative added volume DNA (µL)	Added volume ligand (µL)	Total volume (µL)	[DNA] ($x10^{-6}$ M)	[ligand] ($x10^{-6}$ M)	A434 nm
0	0	1860	0	0	0.041577
0	140	2000	0	70	0.790216
20	140	2020	87.2	69.30	0.679863
40	140	2040	172.8	68.62	0.607376
100	140	2100	419.	66.66	0.503345
150	140	2150	615.0	65.11	0.469667
200	140	2200	801.4	63.63	0.451018
300	140	2300	1149.9	60.86	0.426156
400	140	2400	1469.3	58.33	0.407444
600	140	2600	2034.4	53.84	0.379523
800	140	2800	2518.8	50	0.356633
1000	140	3000	2938.6	46.66	0.337084
1200	140	3200	3306	43.75	0.320481
1400	140	3400	3630.1	41.17	0.305826
1600	140	3600	3918.2	38.88	0.29323

Table A15.16 UV-visible titration of 0.055 mM 2.8 upon addition of 0 – 1.84 mM FSDNA in buffer (25 mM MOPS, pH 7.0, 50 mM NaCl), at 25 °C. $[DNA]_{stock}$ = 7.90 mM, $[Ligand]_{stock}$ = 1.29 mM

Cumulative added volume DNA (µL)	Added volume ligand (µL)	Total volume (µL)	[DNA] ($x10^{-6}$ M)	[ligand] ($x10^{-6}$ M)	A400 nm
0	0	2200	0	0	0.029839
0	100	2300	0	55.95	0.589737
100	100	2400	329.1	53.62	0.568852
200	100	2500	632	51.48	0.549938
300	100	2600	911.5	49.5	0.532331
400	100	2700	1170.3	47.66	0.514968
500	100	2800	1410.7	45.96	0.500165
600	100	2900	1634.4	44.37	0.488542
700	100	3000	1843.3	42.9	0.474469

Table A15.17 UV-visible titration of 0.017 mM 2.9 upon addition of 0 – 1.17 mM FSDNA in buffer (25 mM MOPS, pH 7.0, 50 mM NaCl), at 25 °C. $[DNA]_{stock}$ = 7.90 mM, $[Ligand]_{stock}$ = 0.40 mM

Cumulative added volume DNA (µL)	Added volume ligand (µL)	Total volume (µL)	[DNA] ($x10^{-6}$ M)	[ligand] ($x10^{-6}$ M)	A445 nm
0	0	2200	0	0	0.025621
0	100	2300	0	17.65	0.202416
50	100	2350	168.0	17.27	0.199916
100	100	2400	329.1	16.91	0.197534
150	100	2450	483.6	16.57	0.195182
200	100	2500	632	16.24	0.193083
250	100	2550	774.5	15.92	0.190992
300	100	2600	911.5	15.61	0.189019
350	100	2650	1043.3	15.32	0.187018
400	100	2700	1170.3	15.03	0.185181

A16 UV-visible titrations of a family of dendrimeric compounds.

Table A16.1 UV-visible titration of 0.030 mM 3.1 upon addition of 0 – 1.72 mM FSDNA in buffer (25 mM MOPS, pH 7.0, 50 mM NaCl), at 25 °C. $[DNA]_{stock1}$ = 0.88 mM, $[DNA]_{stock2}$ = 8.8 mM, $[Ligand]_{stock}$ = 0.24 mM

Cumulative added volume DNA (µL)	Added volume ligand (µL)	Total volume (µL)	[DNA] ($x10^{-6}$ M)	[ligand] ($x10^{-6}$ M)	A446 nm
0	0	1750	0	0	0.025593
0	250	2000	0	30	0.50648
2	250	2002	0.879	29.97	0.493582
5	250	2005	2.19	29.92	0.466583
10	250	2010	4.37	29.85	0.425542
17	250	2017	7.41	29.74	0.386106
25	250	2025	10.8	29.63	0.350095
35	250	2035	15.1	29.48	0.341056
55	250	2055	23.5	29.19	0.33125
3	250	2058	12.8	29.15	0.337398
10	250	2065	42.6	29.05	0.356346
30	250	2085	126.6	28.77	0.397427
60	250	2115	249.6	28.36	0.440075
120	250	2175	485.5	27.58	0.466323
200	250	2255	780.4	26.60	0.470562
300	250	2355	1121	25.47	0.467293
500	250	2555	1722.1	23.48	0.452551

Table A16.2 UV-visible titration of 0.030 mM 3.3 upon addition of 0 – 0.69 mM FSDNA in buffer (25 mM MOPS, pH 7.0, 50 mM NaCl), at 25 °C. $[DNA]_{stock}$ = 8.44 mM, $[Ligand]_{stock}$ = 0.065 mM

Cumulative added volume DNA (µL)	Added volume ligand (µL)	Total volume (µL)	[DNA] ($x10^{-6}$ M)	[ligand] ($x10^{-6}$ M)	A452 nm
0	0	1077	0	0	0.025038
0	923	2000	0	29.99	0.574101
5	923	2005	21	29.92	0.54774
10	923	2010	41.9	29.84	0.508703
15	923	2015	62.8	29.77	0.468969
20	923	2020	83.5	29.70	0.44068
25	923	2025	104.1	29.62	0.448753
30	923	2030	124.7	29.55	0.457968
35	923	2035	145.1	29.48	0.464445
40	923	2040	165.4	29.40	0.473138
50	923	2050	205.8	29.26	0.476097
60	923	2060	245.8	29.12	0.479285
70	923	2070	285.4	28.98	0.483075

80	923	2080	324.6	28.84	0.485389
90	923	2090	363.4	28.70	0.486509
100	923	2100	401.9	28.56	0.487495
110	923	2110	440	28.43	0.487879
120	923	2120	477.7	28.29	0.488603
130	923	2130	515.1	28.16	0.487556
140	923	2140	552.1	28.03	0.486759
150	923	2150	588.8	27.90	0.486494
160	923	2160	625.1	27.77	0.485927
180	923	2180	696.8	27.52	0.485055

Table A16.3 UV-visible titration of 0.040 mM 3.4 upon addition of 0 – 0.18 mM FSDNA in buffer (25 mM MOPS, pH 7.0, 50 mM NaCl), at 25 °C. $[DNA]_{stock}$ = 0.84 mM, $[Ligand]_{stock}$ = 0.29 mM

Cumulative added volume DNA (µL)	Added volume ligand (µL)	Total volume (µL)	[DNA] ($x10^{-6}$ M)	[ligand] ($x10^{-6}$ M)	A454 nm
0	0	1724	0	0	0.024984
0	276	2000	0	40.02	0.576088
5	276	2005	2.1	39.92	0.572607
10	276	2010	4.1	39.82	0.569453
20	276	2020	8.3	39.62	0.567421
30	276	2030	12.4	39.42	0.567702
40	276	2040	16.5	39.23	0.569631
50	276	2050	20.5	39.04	0.567449
70	276	2070	28.5	38.66	0.567275
100	276	2100	40.1	38.11	0.558772
150	276	2150	58.8	37.22	0.55986
200	276	2200	76.7	36.38	0.515736
230	276	2230	87	35.89	0.495073
260	276	2260	97	35.41	0.472145
300	276	2300	110	34.8	0.418326
330	276	2330	119.5	34.35	0.390231
350	276	2350	125.7	34.05	0.377664
370	276	2370	131.7	33.77	0.376748
390	276	2390	137.7	33.48	0.379635
410	276	2410	143.5	33.21	0.380514
450	276	2450	155	32.66	0.381929
490	276	2490	166	32.14	0.37966
550	276	2550	182	31.38	0.374827

Table A16.4 UV-visible titration of 0.040 mM 3.4 upon addition of 0 – 0.18 mM FSDNA in buffer (25 mM MOPS, pH 7.0, 50 mM NaCl), at 25 °C. $[DNA]_{stock}$ = 0.84 mM, $[Ligand]_{stock}$ = 0.29 mM

Cumulative added volume DNA (µL)	Added volume ligand (µL)	Total volume (µL)	[DNA] ($x10^{-6}$ M)	[ligand] ($x10^{-6}$ M)	A(454 – 530) nm
0	0	1724	0	0	0.001823
0	276	2000	0	40.02	0.542694
5	276	2005	2.1	39.92	0.536365
10	276	2010	4.1	39.82	0.530002
20	276	2020	8.3	39.62	0.519134
30	276	2030	12.4	39.42	0.502283
40	276	2040	16.5	39.23	0.484283
50	276	2050	20.5	39.04	0.463229
70	276	2070	28.5	38.66	0.429676
100	276	2100	40.1	38.11	0.377043
150	276	2150	58.8	37.22	0.318118
200	276	2200	76.7	36.38	0.289899
230	276	2230	87	35.89	0.29274
260	276	2260	97	35.41	0.304341
300	276	2300	110	34.8	0.314157
330	276	2330	119.5	34.35	0.324013
350	276	2350	125.7	34.05	0.330823
370	276	2370	131.7	33.77	0.334887
390	276	2390	137.7	33.48	0.34072
410	276	2410	143.5	33.21	0.342795
450	276	2450	155	32.66	0.345223
490	276	2490	166	32.14	0.344062
550	276	2550	182	31.38	0.342382

A17 UV-visible titrations of miscellaneous compounds.

Table A17.1 UV-visible titration of 0.041 mM 4.1 upon addition of 0 – 0.25 mM FSDNA in deionised water, at 25 °C. $[DNA]_{stock}$ = 1.93 mM, $[Ligand]_{stock}$ = 1.04 mM					
Cumulative added volume DNA (µL)	Added volume ligand (µL)	Total volume (µL)	[DNA] ($x10^{-6}$ M)	[ligand] ($x10^{-6}$ M)	A394 nm
0	0	2400	0	0	0.028274
0	100	2500	0	41.68	0.32393
10	100	2510	7.6	41.51	0.304186
20	100	2520	15.3	41.34	0.317852
40	100	2540	30.3	41.02	0.33568
80	100	2580	59.8	40.38	0.347837
120	100	2620	88.3	39.77	0.358118
200	100	2700	142.9	38.59	0.367925
280	100	2780	194.3	37.48	0.364969
380	100	2880	254.6	36.18	0.360931

Table A17.2 UV-visible titration of 0.084 mM 4.1 upon addition of 0 – 0.28 mM FSDNA in deionised water, at 25 °C. $[DNA]_{stock1}$ = 0.193 mM, $[DNA]_{stock2}$ = 1.93 mM, $[Ligand]_{stock}$ = 1.40 mM					
Cumulative added volume DNA (µL)	Added volume ligand (µL)	Total volume (µL)	[DNA] ($x10^{-6}$ M)	[ligand] ($x10^{-6}$ M)	A394 nm
0	0	2350	0	0	0.026489
0	150	2500	0	84	0.467068
10	150	2510	0.76	83.66	0.466843
30	150	2530	2.2	83.0	0.466147
50	150	2550	3.7	82.35	0.442464
100	150	2600	7.4	80.76	0.441871
150	150	2650	10.9	79.24	0.407051
200	150	2700	14.2	77.77	0.371592
10	150	2710	21.3	77.49	0.428337
30	150	2730	35.3	76.92	0.430722
70	150	2770	62.7	75.81	0.455761
140	150	2840	108.7	73.94	0.464585
240	150	2940	170.6	71.42	0.48508
340	150	3040	228.5	69.07	0.485247
440	150	3140	282.7	66.87	0.475217

Table A17.3 UV-visible titration of 0.01 mM 4.2 upon addition of 0 – 0.44 mM FSDNA in buffer (25 mM MOPS, pH 7.0, 50 mM NaCl), at 25 °C. $[DNA]_{stock}$ = 7.60 mM, $[Ligand]_{stock}$ = 2.0 mM

Cumulative added volume DNA (µL)	Added volume ligand (µL)	Total volume (µL)	[DNA] ($x10^{-6}$ M)	[ligand] ($x10^{-6}$ M)	A338 nm	A320 nm
0	0	2000	0	0	0.032674	0.034264
0	10	2010	0	9.95	0.095902	0.231002
1	10	2011	3.7	9.94	0.098611	0.22531
2	10	2012	7.5	9.94	0.102374	0.223906
4	10	2014	15.0	9.93	0.106114	0.219161
6	10	2016	22.6	9.92	0.110148	0.215982
10	10	2020	37.6	9.90	0.116609	0.211459
15	10	2025	56.2	9.87	0.121613	0.206956
25	10	2035	93.3	9.82	0.128873	0.203655
40	10	2050	148.2	9.75	0.136158	0.202099
55	10	2065	202.4	9.68	0.140632	0.20151
85	10	2095	308.3	9.54	0.142368	0.199076
125	10	2135	444.9	9.36	0.145055	0.19918

Table A17.4 UV-visible titration of 0.014 mM 4.2 upon addition of 0 – 0.56 mM FSDNA in buffer (25 mM MOPS, pH 7.0, 50 mM NaCl), at 25 °C. $[DNA]_{stock}$ = 7.60 mM , $[Ligand]_{stock}$ = 2.0 mM

Cumulative added volume DNA (µL)	Added volume ligand (µL)	Total volume (µL)	[DNA] ($x10^{-6}$ M)	[ligand] ($x10^{-6}$ M)	A338 nm	A320 nm
0	0	2000	0	0	0.034140	0.035223
0	15	2015	0	14.88	0.123671	0.318755
0.5	15	2015.5	1.8	14.88	0.12467	0.316741
1.5	15	2016.5	5.6	14.87	0.126793	0.311712
4	15	2019	15.0	14.85	0.133725	0.303991
8	15	2023	30.0	14.82	0.14444	0.296364
15	15	2030	56.1	14.77	0.156894	0.287784
25	15	2040	93.1	14.70	0.169268	0.281667
40	15	2055	147.9	14.59	0.179958	0.279563
70	15	2085	255.1	14.38	0.184334	0.273049
110	15	2125	393.7	14.11	0.188484	0.269579
160	15	2175	559.0	13.79	0.188726	0.265784

Table A17.5 UV-visible titration of 0.02 mM 4.3 upon addition of 0 – 0.96 mM FSDNA in buffer (25 mM MOPS, pH 7.0, 50 mM NaCl), at 25 °C. $[DNA]_{stock}$ = 10.7 mM, $[Ligand]_{stock}$ = 0.5 mM

Cumulative added volume DNA (µL)	Added volume ligand (µL)	Total volume (µL)	[DNA] ($x10^{-6}$ M)	[ligand] ($x10^{-6}$ M)	A362 nm	A390 nm
0	0	1920	0	0	0.038211	0.034337
0	80	2000	0	20	0.267499	0.150274
2	80	2002	10.6	19.98	0.259499	0.149548
4	80	2004	21.2	19.96	0.257543	0.153484
8	80	2008	42.4	19.92	0.252968	0.155526
15	80	2015	79.2	19.85	0.246963	0.158812
25	80	2025	131.4	19.75	0.245708	0.163802
45	80	2045	234.3	19.55	0.244132	0.167995
80	80	2080	409.6	19.23	0.241058	0.169113
120	80	2120	602.8	18.86	0.240878	0.16902
160	80	2160	788.8	18.51	0.239512	0.169497
200	80	2200	968.1	18.18	0.237382	0.168298

Table A17.6 UV-visible titration of 0.02 mM 4.3 upon addition of 0 – 0.5 mM FSDNA in buffer (25 mM MOPS, pH 7.0, 50 mM NaCl), at 25 °C. $[DNA]_{stock}$ = 10.7 mM, $[Ligand]_{stock}$ = 0.5 mM

Cumulative added volume DNA (µL)	Added volume ligand (µL)	Total volume (µL)	[DNA] ($x10^{-6}$ M)	[ligand] ($x10^{-6}$ M)	A362 nm	A390 nm
0	0	1920	0	0	0.035040	0.033779
0	80	2000	0	20	0.263413	0.148956
0.5	80	2000.5	2.6	19.99	0.259557	0.148183
1	80	2001	5.3	19.99	0.255524	0.147416
2	80	2002	10.6	19.98	0.252617	0.14959
4	80	2004	21.2	19.96	0.248849	0.15051
6	80	2006	31.8	19.94	0.245508	0.152216
8	80	2008	42.4	19.92	0.245933	0.155936
13	80	2013	68.7	19.87	0.242976	0.159106
20	80	2020	105.4	19.80	0.242603	0.161735
35	80	2035	183.1	19.65	0.240558	0.167197
60	80	2060	310.1	19.41	0.238452	0.167174
100	80	2100	507.1	19.04	0.234535	0.164241